

NGU Report 2006.018

**Interpretation of aeromagnetic data
along the Jan Mayen Fracture Zone
JAS-05**

| | | | | |
|--|-------------------------------|--|---|-------|
| Report no.: 2006.018 | | ISSN 0800-3416 | Grading: Confidential to 17.02.2011 | |
| Title: Interpretation of aeromagnetic data along the Jan Mayen Fracture Zone, JAS-05 | | | | |
| Authors: Odleiv Olesen, Laurent Gernigon, Jörg Ebbing, John Olav Mogaard, Christophe Pascal & Suzann Wienecke | | | Clients: NGU, Norske Shell, Oljedirektoratet & Statoil | |
| County: | | | Commune: | |
| Map-sheet name (M=1:250.000) | | | Number of pages: 161 Price (NOK): Map enclosures: | |
| Fieldwork carried out: August-October, 2005 | Date of report: 17.02.2006 | Project no.: 3108.00 | Person responsible: | |
| <p>Summary:</p> <p>Aeromagnetic data from the Jan Mayen Fracture Zone (JAS-05) were acquired and processed during the autumn of 2005 and compiled with neighbouring data-sets. Data processing comprised spike removal and data editing, IGRF correction, statistical levelling of tie lines and profiles. The new JAS-05 survey has been merged with more than 40 other surveys including the mainland of Norway, Svalbard and East-Greenland. A compilation of the existing gravity data in the area has also been carried out. Potential field modelling has been constrained by available data on density, magnetic properties and reflection and refraction (OBS) seismics. New features have been revealed by the interpretation of the Jan Mayen Aeromagnetic Survey 2005 (JAS-05). The Aegir Marginal High (AMH) represents an inverted structure, uplifted during late Oligocene-early Miocene time. The thickening of the oceanic crust is syn-accretion and is not necessarily related to a Late Miocene underplaying (post-accretion), as previously assumed. The magnetic anomaly map shows also evidences of earlier deformation and block rotation linked with a propagator system along the Aegir through. A late Eocene displacement of the magnetic chrons suggests a progressive plate reorganisation leading to a major pulse in Oligocene. The major pulse coincides with two main unconformities seismically observed along the Jan Mayen Corridor (PM and MU) and could explain the main uplift phase of the AMH as well. We propose also a new challenging model for the Mid-Norwegian breakup system. Our tectonic analysis suggests that a triple junction Ridge-Ridge-Fracture Zone was initiated during the Late Paleocene-Early Eocene breakup between Greenland-Jan Mayen and Norway. Our interpretation infers also that the north Atlantic breakup probably started earlier at C24R or C25 time south of the EJMFZ. Spreading rates between the Aegir and Mohns ridges appear on the new magnetic compilation to differ by ~2 mm/yr for much of the period ranging from continental break up to extinction of the Aegir Ridge. The contrasting spreading rates of either side of the Jan Mayen Fracture Zone (JMFZ) resulted in dextral strike-slip along the JMFZ. Preliminary modelling suggests that such a minor difference in spreading rates could have led to significant shortening in the Vøring Basin. This model can explain why most of the mid-Norwegian domes are located to the north of the Jan Mayen Lineament.</p> | | | | |
| Keywords: Geofysikk | | Kontinentalsokkel | Tolkning | |
| Berggrunnsgeologi | | Magnetometri | Forkastning | |
| NGU Report 2006.018 Interpretation of Petrofysikk | | aeromagnetic data along the Jan Mayen Fracture Gravimetri | Zone, JAS-05. | 1/161 |
| | | | Fagrapport | |

CONTENTS

| | | |
|-----|---|----|
| 1 | INTRODUCTION | 5 |
| 2 | DATA SETS | 8 |
| 2.1 | Jan Mayen aeromagnetic survey | 8 |
| 2.2 | Aeromagnetic data compilation..... | 14 |
| 2.3 | Bathymetric and topographic data..... | 23 |
| 2.4 | Seismic studies | 24 |
| 2.5 | Data presentation | 25 |
| 3 | MAIN STRUCTURAL ELEMENTS OF THE NORWEGIAN-GREENLAND SEA | 26 |
| 3.1 | Outer Vøring Basin and the Vøring Marginal High | 29 |
| 3.2 | Island of Jan Mayen and the Jan Mayen microcontinent..... | 29 |
| 3.3 | The Jan Mayen Ridge..... | 30 |
| 3.4 | Mohns Ridge..... | 33 |
| 3.5 | Iceland Plateau and the Kolbeinsey Ridge..... | 34 |
| 3.6 | Aegir Ridge..... | 36 |
| 4 | INTERPRETATION METHODS..... | 38 |
| 4.1 | Euler Deconvolution..... | 38 |
| 4.2 | Forward modeling | 39 |
| 4.3 | Depth to magnetic sources | 43 |
| 4.4 | Transect 1: the southern NW-SE line..... | 43 |
| 4.5 | Transect 2: the central NW-SE line..... | 43 |
| 4.6 | Transect 3: the cross-line..... | 44 |
| 4.7 | Transect 4: The northern NW-SE line..... | 44 |
| 4.8 | Discussion and conclusion | 53 |
| 5 | THE JAN MAYEN FRACTURE ZONE: COMPLEX MORPHO- STRUKTURE, GRAVITY AND MAGNETIC SIGNATURE | 54 |
| 5.1 | Fracture zones, transform faults and JMFZ | 54 |
| 5.2 | Internal physiography and segmentation | 55 |
| 5.3 | The Jan Mayen Fracture Zone: New magnetic picture of the Norwegian Sea..... | 67 |
| 6 | THE JAN MAYEN FRACTURE ZONE AND SURROUNDING AREAS: STRUCTURE, MAGMATISM AND TECTONICS | 72 |
| 6.1 | Vøring Marginal High and breakup features | 72 |
| 6.2 | The SDRS system along the Jan Mayen Microcontinent: Are they really volcanic features? | 79 |
| 6.3 | Breakup south of the EJMFZ | 79 |

| | | |
|----|---|-----|
| 7 | THE AEGIR MARGINAL HIGH (AMH): ARCHITECTURE, DEEP STRUCTURES AND DEFORMATION | 81 |
| | 7.1 Shallow structure and sedimentary sequences | 81 |
| | 7.2 Deep structures and origin of the inversion(s) | 88 |
| | 7.3 Uplift, overcrusting and tectonic model for the Aegir Marginal High | 93 |
| | 7.4 Quantitative analysis..... | 96 |
| 8 | TECTONOSTRATIGRAPHIC FRAMEWORK OF THE JMFZ AND COMPARISON AT THE SCALE OF THE ADJACENT MARGIN | 101 |
| | 8.1 Plate reconstructions..... | 102 |
| | 8.2 Tectonic evolution from continental extension to seafloor spreading..... | 106 |
| | 8.3 Early to mid-Eocene deformation of the AMH and relationship with a probable propagating oceanic rift..... | 107 |
| | 8.4 The late Eocene–early Oligocene..... | 111 |
| | 8.5 Late Oligocene to mid-Miocene..... | 114 |
| 9 | STRUCTURAL INHERITANCE AND MAGMATISM | 116 |
| | 9.1 The JMFZ and its relation to inheritance | 116 |
| | 9.2 Inheritance and magmatism..... | 117 |
| 10 | IMPACT OF DIFFERENTIAL SPREADING RATES ON THE STRUCTURAL EVOLUTION OF THE MID-NORWEGIAN MARGIN | 122 |
| | 10.1 Rationale..... | 122 |
| | 10.2 Modelling strategy..... | 122 |
| | 10.3 Results..... | 123 |
| | 10.4 Conclusions and recommendations..... | 125 |
| 11 | CONCLUSIONS | 126 |
| 12 | RECOMMENDATIONS FOR FURTHER WORK | 128 |
| 13 | REFERENCES | 129 |
| 14 | FIGURES | 139 |
| 15 | Tables | 146 |
| 16 | APPENDIX A, TECHNICAL REPORT JAN MAYEN AEROMAGNETIC SURVEY 2005 (JAS-05)..... | 147 |
| 17 | APPENDIX B Start-up report, August 2005, Jan Mayen Aeromagnetic Survey..... | 159 |

1 INTRODUCTION

The present report documents the results from the Jan Mayen Aeromagnetic Survey 2005 (JAS-05) financed by the Geological Survey of Norway, Norske Shell, the Norwegian Petroleum Directorate and Statoil. The new survey covers the Jan Mayen Fracture Zone and adjacent areas.

Before our new survey, marine magnetic profiles along the Jan Mayen Fracture Zone have been sparse and unevenly spaced. There is therefore all reason to believe that the existing interpretation of the Jan Mayen Fracture Zones is rudimentary. The new survey was expected to reveal the exact location of both the oceanic spreading anomalies and the exact offset of these anomalies along the fracture zones. The new interpretations form the basis for identifying the date and rate of movements along the individual segments of the East and Central Jan Mayen Fracture Zones (CJMFZ and EJMFZ).

High-resolution aeromagnetic measurements can aid in the study of the following geological features in the outer Vøring-Jan Mayen area:

- Mapping of oceanic spreading anomalies and oceanic fracture zones
- Tertiary magmatism - intrusives and volcanic centres affecting paleotemperature
- Continent – ocean boundary
- Propagating Aegir and Kolbeinsey ridges?
- Cenozoic compression (domes – paleostress)

The RAS-03 survey (Olesen et al. 2004) revealed that some of the aeromagnetic anomalies that previously were interpreted as spreading anomalies, were in fact younger igneous complexes cutting across the spreading anomalies at a low angle. The new survey provides us with the necessary tool to trace analogous intrusions along the CJMFZ and EJMFZ where similar broad and high-amplitude anomalies occur on the existing data-set.

The new magnetic survey stretches from Jan Mayen Ridge NW to the Vøring Marginal High, which defined the continental-oceanic transition of the Mid-Norwegian continental margin. The survey is approximately 400 km long and 200 km wide. It lies across a complex domain involving several structural features, which include continental margin, active and aborted spreading ridges, microcontinent, transform faults and fault zones.

The new data of the Jan Mayen Aeromagnetic Survey 2005 have been used to study the magnetic sources and the crustal structure in the study area. We applied Euler deconvolution to the new survey data, and carried out 2.5 D density and magnetic modelling along three northwest-southeast transects and gravity modelling along one cross line.

Potential field data, new bathymetric grids and available 2D seismic lines have been compiled over the Norwegian and Greenland Sea, with a special interest along the western part of the JMFZ itself. The compilation builds on new unpublished data and allows us to better constrain the seismostratigraphic, the structural and crustal characteristics of this atypical oceanic feature in order to re-evaluate the tectonic environment in which this part of the oceanic crust, off Norway has evolved during the Cenozoic. Particularly, the transition zone between the two accretion segments is investigated at both basin and crustal scales, including the reinterpretation of the magnetic anomalies and fractures zone. The early stage of the continental breakup and the different stage of the JMFZ initiation were studied in detail. Then, the influence of the magmatism as well as the role of the inheritance during the breakup and the drift evolutions of the conjugate continental margin system is discussed. Finally, since authors suggested that an accurate spreading history of the JMFZ is of direct relevance for petroleum and dome formation on the NW European margins (Boldreel & Anderson 1993; Doré & Lundin 1996; Vågnes et al. 1998; Lundin & Doré 2002), we correlate the main tectonic movement of the Cenozoic crust with the basin evolution in the adjacent areas.

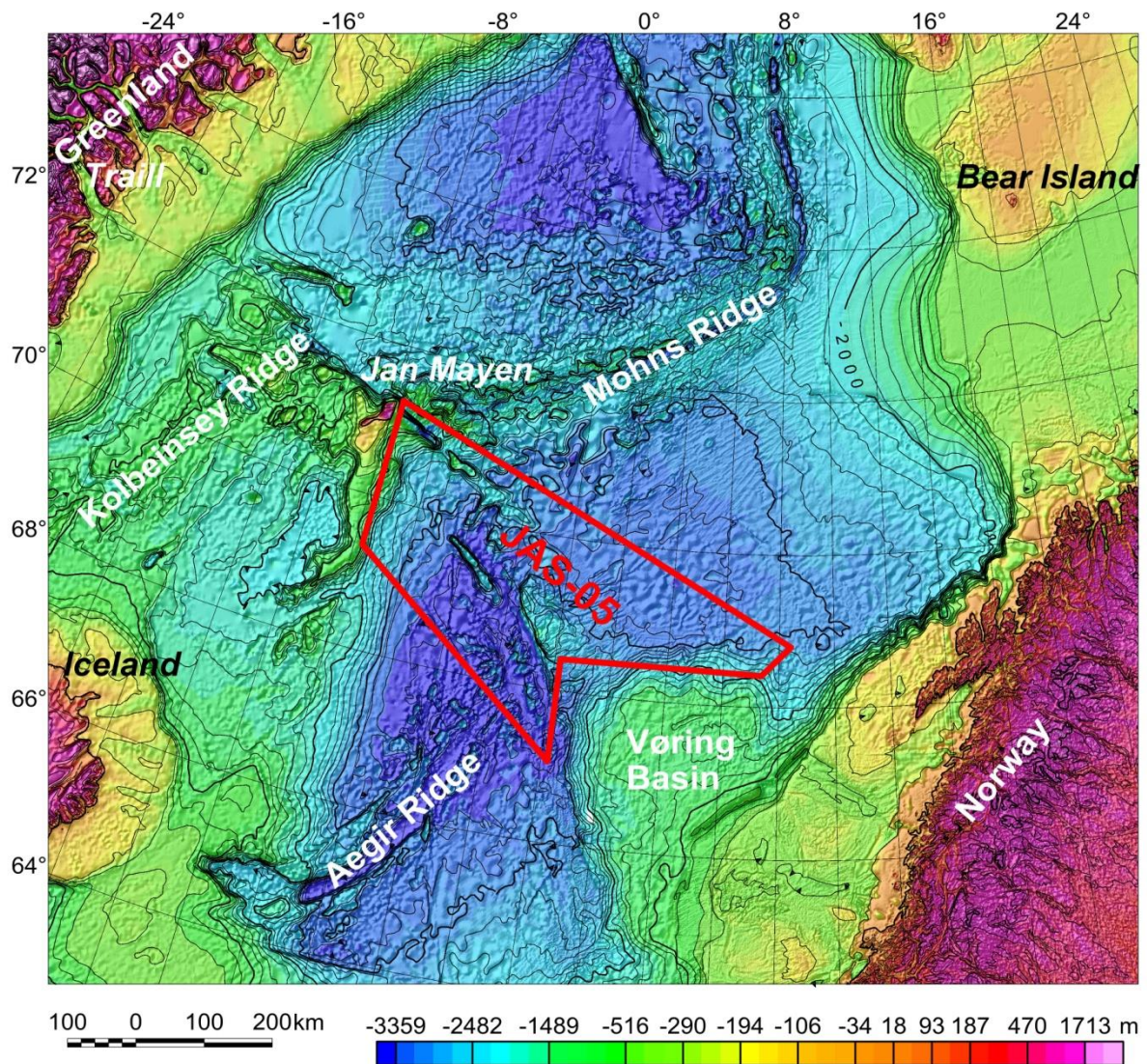


Figure 1.1 Bathymetry and topography, Norwegian-Greenland Sea, 100 and 500 m contour intervals. The red frame shows the JAS-05 survey area.



Figure 1.2 The Navajo PA31 LN-NPZ operated by Blom Geomatics was hired by TGS NOPEC for the data acquisition.

2 DATA SETS

Odleiv Olesen

2.1 Jan Mayen aeromagnetic survey

Data acquisition was carried out by TGS-NOPEC during the period 1 August to 10 October. The company was awarded the contract after a bidding round with three other companies. Hiring of aeroplane with crew was further sub-contracted to Blom Geomatics. The survey area was located southeast of Jan Mayen in the Norwegian-Greenland Sea (Fig. 1.1). The south-easterly extreme of the survey area lies at approximately 8°25'E, 68° 48'N whilst the north-westerly extreme lies at approximately 7° 40'W, 71°18'N. The crews from Blom Geomatics and TGS-NOPEC were based on Jan Mayen.

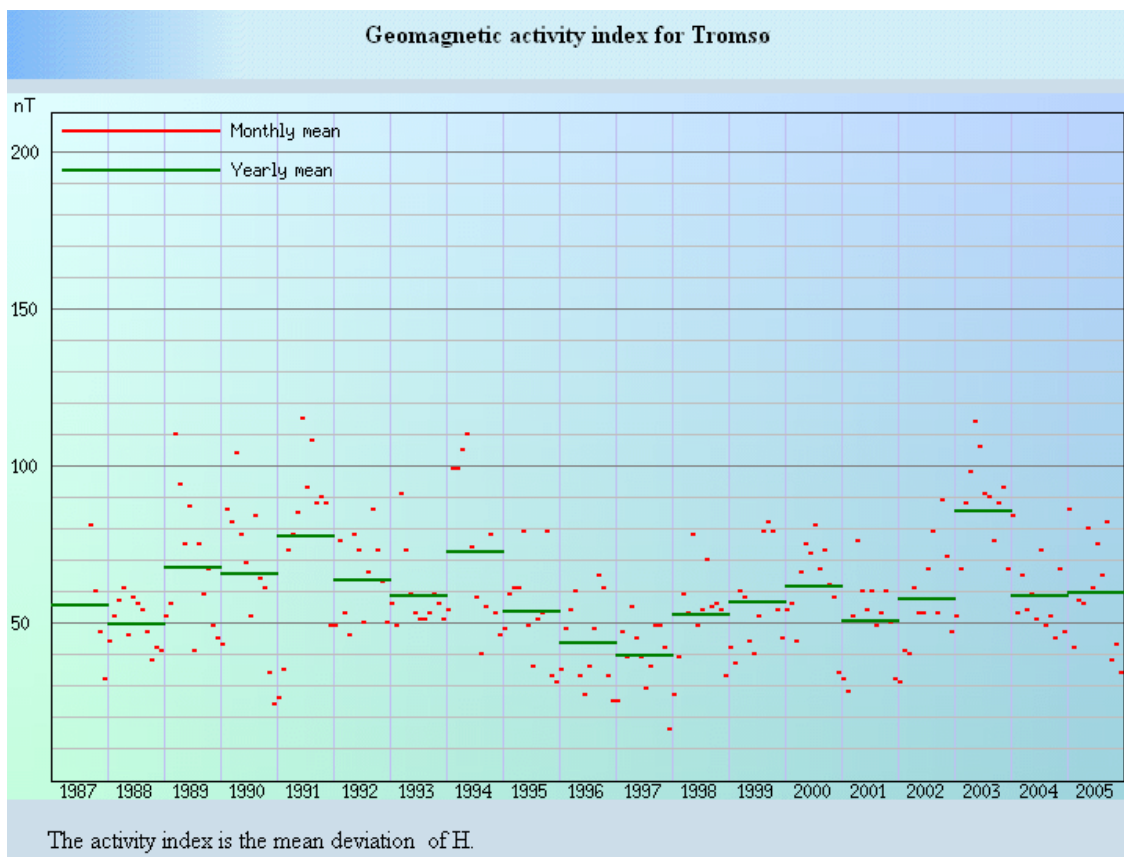


Figure 2.1 Diagram from the Tromsø Geophysical Observatory (<http://www.tgo.uit.no/aix>) showing the magnetic disturbances in Tromsø during the time period 1987-2005. The JAS-05 survey was carried out during August and September 2005, a period with intermediate to high geomagnetic activity.

The survey period was extended 2-3 weeks because of poor weather conditions and magnetic disturbances. The profile and tie-line spacing were 5 and 20 km, respectively. The total flying distance of 32,600 km was acquired during 54 flights. The survey covered an area of c.120.000 km². The flight altitude of was c. 230 m. The JAS-05 data-set has been merged with more than 40 additional surveys containing a total of more than 1 million profile km.

Appendices A and B show the technical report and start-up report, respectively, from TGS-NOPEC. The results from the tests in the 'JAS-05 Start up report' (Appendix B) were compared with the specifications in the bidding documents to make sure that the acquisition system had the necessary sensitivity. Weekly operation reports and list of profiles and diurnals are not included in the present report but can be found in the JAS-05 archive CD as Appendices C and D, respectively.

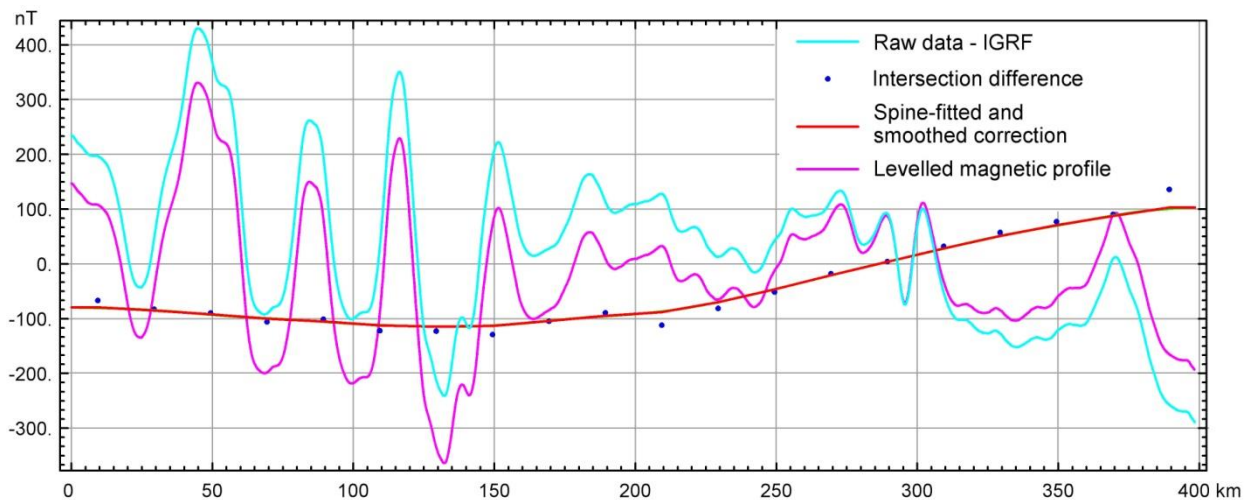


Figure 2.2 Example of statistical levelling (Geosoft 2005a) of line 170 in the JAS-05 survey. 'Outliers' of intersection differences have been removed manually from the lines.

The quality control of the data is described in Appendix A. The final editing of the flight pattern was carried out at NGU. The reflight parts of previous lines were removed from the database. We subsequently deleted manually spikes in the final dataset before removing heading errors. The heading error was 1.5 nT between the tie-lines in the NE- and SW-direction and 15 nT along the profiles in the NW and SE direction (Appendix B). The survey was levelled at NGU using the standard Geosoft (2005a) statistical levelling method of the tie-lines followed by a statistical levelling of the profiles utilising the levelled tie-lines. We used a first order (linear) trend removal in the levelling of the tie-line. 'Suspicious' tie line values (outliers) were removed manually before levelling of the tie lines. The linearly trended tie lines were then used in a full levelling of the survey lines using an Akima spline algorithm. Extreme tie points (outliers) were again removed manually before calculating the spline corrections that were subsequently lowpass filtered using a 50 km Gaussian high-pass filter and subtracted from the observed magnetic field. The IGRF field was calculated and subtracted from the levelled survey lines to produce the magnetic anomalies of the survey area.

We did also test the more sophisticated moving median filtering methods (Mauring et al. 2002; Mauring & Kihle 2006) but there were no observable improvements in the grid. This is most likely due to the high-amplitude anomalies (in the order of several hundred nanoTeslas). The moving median levelling technique has shown its advantages in microlevelling

NGU Report 2006.018 Interpretation of aeromagnetic data along the Jan Mayen Fracture Zone, JAS-05. 9/161

processing, where a few nanoTesla errors have been removed. This kind of anomalies arises within the sedimentary column in the basins on the shallower continental shelf. The moving median levelling technique is especially advantageous for processing of surveys with very few or no tie-lines (Mauring & Kihle 2006). The 0.1 sec. sampling interval (< 8 m) was resampled to 50 m. No smoothing has been applied to profiles or grids during the processing. Fig. 2.4 shows the total magnetic field referred to DGRF-05 of the JAS-05 survey while the Gaussian 20 km high-pass filtered grid is shown in Fig. 2.5. The contour interval of the total magnetic field map is 50 nT.

The information of the JAS-05 profile- and grid-files is included on the readme.txt file on the JAS-05 archive CD.

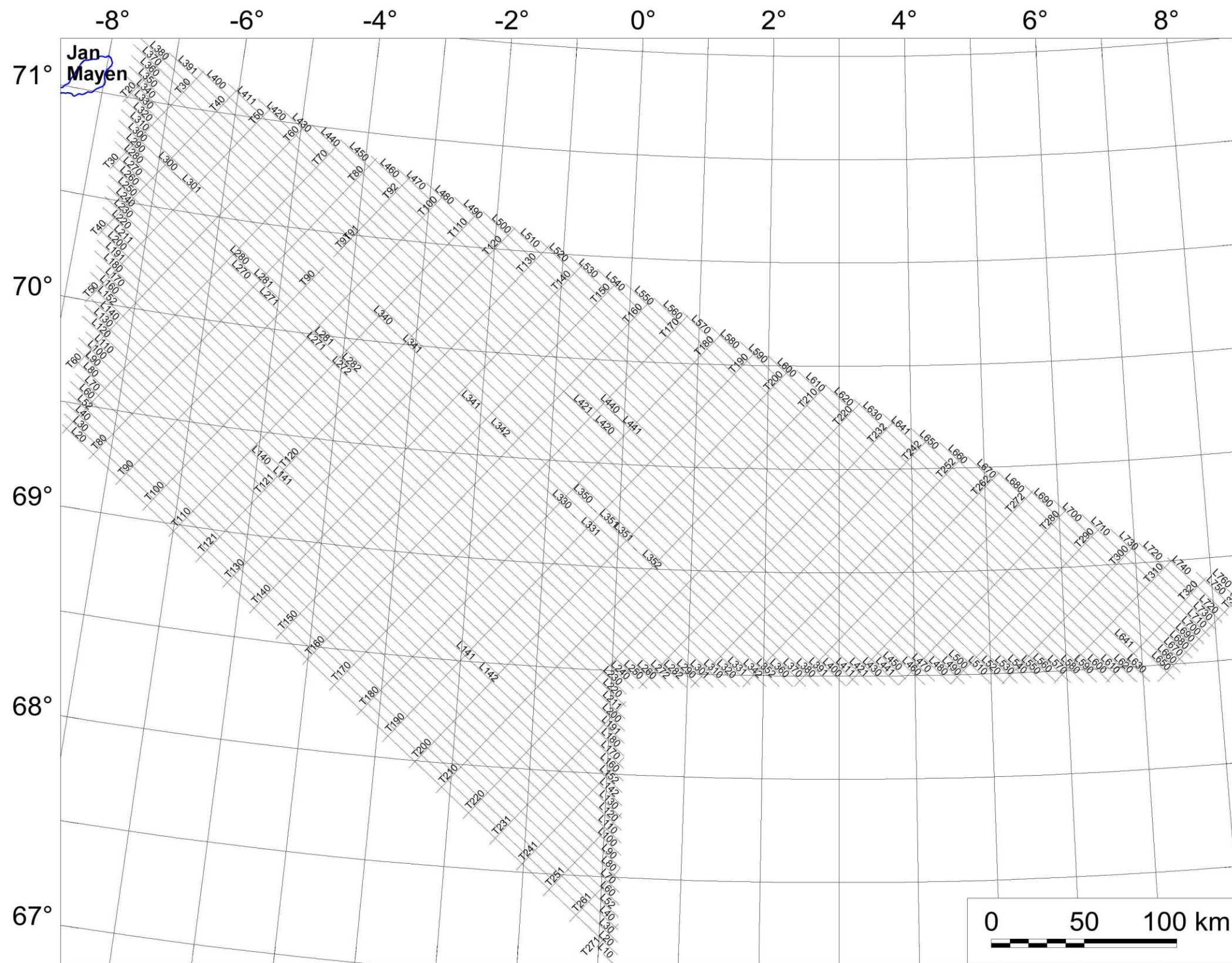


Figure 2.3 JAS-05 flight pattern.

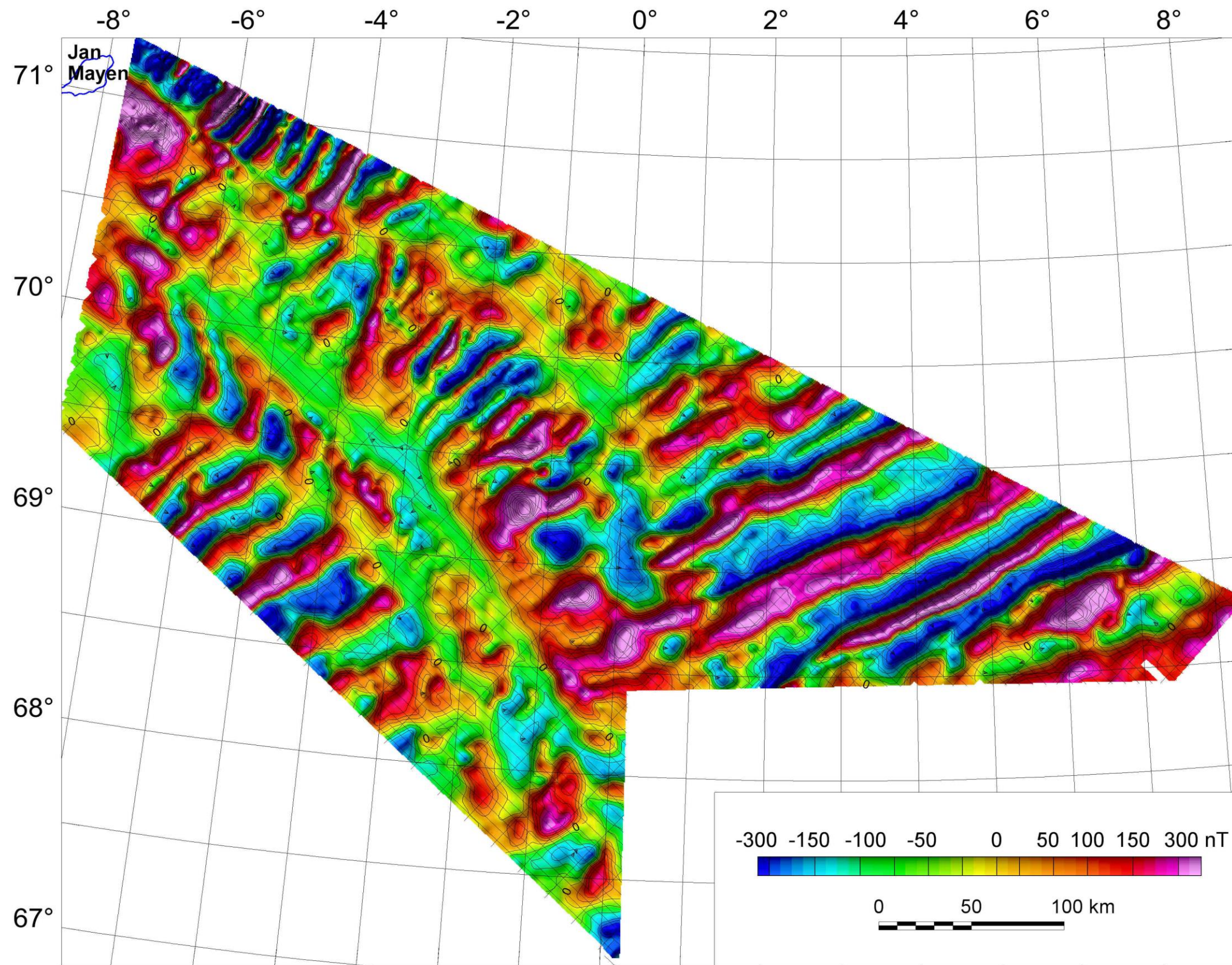


Figure 2.4 Total magnetic field of the JAS-05 survey referred to DGRF-05. The contour interval is 50 nT.

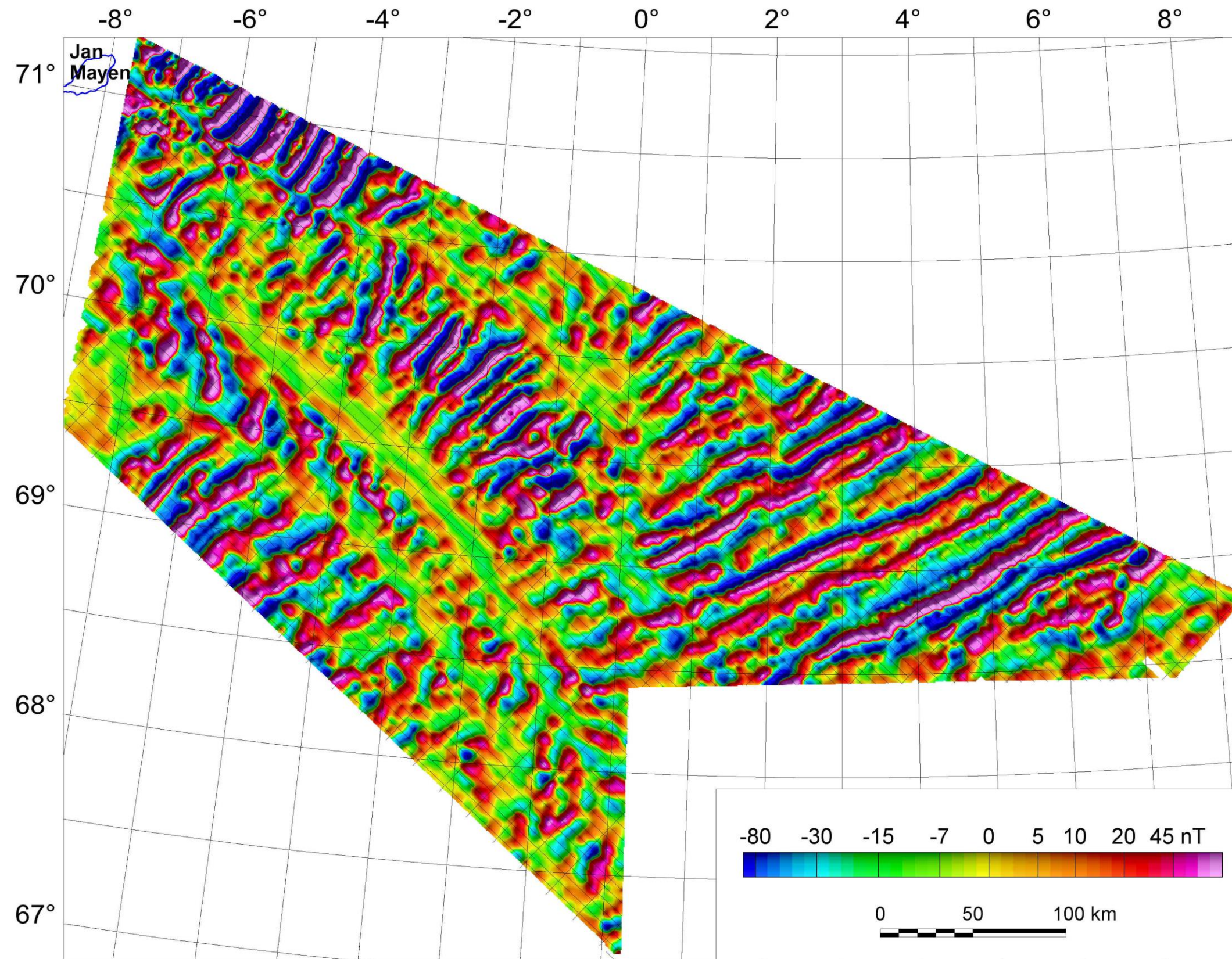


Figure 2.5 Gaussian 20 km high-pass filtered magnetic field.

2.2 Aeromagnetic data compilation

Aeromagnetic data from Norway and the adjacent continental margin have been compiled earlier (Skilbrei et al. 1991; Olesen et al. 1997). The pre-1996 surveys were reprocessed during the periods of 1999-2001 and 2003-2004 using the median levelling and loop closure methods (Mauring et al. 2002, 2003) and these new versions of the NGU-69/-70/-73/-74/-75, Fairey-71, TAMS-84, BAMS-85, Hunting-86, BSA-87, SPA-88, LAS-89, Viking-93 and NAS-94, have been included in the present compilation. Statoil financed parts of this reprocessing within the Dragon database project (DiRect Access to Geophysics On the Net) in 1999/2000. Reprocessed data from the mid-Norwegian continental margin have been published by Olesen et al. (2002, 2004) and Skilbrei et al. (2002, 2005) but the North Sea and Barents Sea data-sets remain unpublished. The more recent surveys SAS-96, VGVB-94, MBAM-97, VAS-97, VBE-AM-00 and RAS-03 are also included in the new data compilation.

A total of 10 additional offshore aeromagnetic surveys (Fig. 2.1) have been gridded to 500 x 500 m cells and added to the regional data compilation (Figs. 2.6 & 2.7). Specifications for these surveys are shown in Table 2.1. The CGG-76 survey (Compagnie Générale de Géophysique 1977) from the Jan Mayen Ridge was provided by the Norwegian Petroleum Directorate to the JAS-05 Project. This survey has not been included in any of the previous data compilations from the region. The nine other surveys have been provided by the Atlantic Geoscience Centre, which is part of the Canadian Geological Survey in Halifax (Gordon Oakey, pers. comm. 2004). All these surveys were reprocessed for the Gammaa5 grid of the Arctic and North Atlantic area by Verhoef et al. (1996).

The mainland of Norway grid has previously been digitised into a 500x500 m matrix from manually drawn contour maps and the Definite Geomagnetic Reference Field (DGRF) has been subtracted (Nor. geol. unders. 1992). The mainland area was flown at different flight altitudes and line spacing dependent on the topography.

We have also included Verhoef et al. (1996) grid-versions (5 x5 km) of the ship-magnetic data, including the Aegir Ridge NRL-90 data-set (Jong & Vogt 1997) and the aeromagnetic GEUS-74 and Fairey-71/72/73 (west of Shetland) surveys. These three datasets represent 25.000, 10.400 and 64.000 line-km, respectively, and are adding to the survey-list in Table. 2.1. Fig. 2.9 is also including the aeromagnetic data from Great Britain incorporated in Verhoef et al. (1996) 5x5 km grid.

The 5 x 5 km grids were regridded to 500 x 500 m cells before merging with the regional compilation. The new grid merging has been produced using the minimum curvature GRIDKNIT software from Geosoft (2005b).

**Table 2.1. Offshore aeromagnetic surveys compiled for the present study (Figs. 2.6, 2.7, 2.9 & 2.10).
CGG - Compagnie Générale de Géophysique; GEUS – Geological Survey of Denmark and Greenland; NOO - Naval Oceanographic Office; NGU – Geological Survey of Norway; NPD – Norwegian Petroleum Directorate; NRL - Naval Research Laboratory**

| Year | Area | Operator | Survey name | Sensor elevation m | Line spacing km | Length km |
|-------|--------------------------------|---------------------------|-------------|--------------------|-----------------|-----------|
| 1969 | SW Barents Sea | NGU | NGU-69 | 200 | 4 | 26.200 |
| 1970 | SE Barents Sea | NGU | NGU-70 | 200 | 4-8 | 22.800 |
| 1971 | Viking Graben | Fairey | Fairey-71 | 300 | 2 | 11.100 |
| 1973 | Vøring Basin | NGU | NGU-73 | 500 | 5 | 35.000 |
| 1972 | North Norwegian-Greenland Sea | NRL (Vogt et al. 1979) | NRL-72 | 300 | 7.5 | 38.500 |
| 1973 | South Norwegian-Greenland Sea | NRL (Vogt et al. 1979) | NRL-73 | 300 | 10 (20) | 50.600 |
| 1973 | Denmark Strait | NOO (Vogt et al. 1980) | NOO-73 | 160 | 5.5 | 60.400 |
| 1974 | Norwegian Sea, east of Iceland | NOO | NOO-74a | 160 | 10 | 5.500 |
| 1974 | Norwegian Sea, SE of Iceland | NOO | NOO-74b | 160 | 10 | 2.000 |
| 1974 | NE Atlantic, south of Iceland | NOO | NOO-74c | 160 | 5 | 22.200 |
| 1974 | Norwegian North Sea | NGU | NGU-74 | 300 | 2-7 | 23.000 |
| 1975 | Norwegian North Sea | NGU | NGU-75 | 300 | 1-6 | 19.000 |
| 1976 | Jan Mayen Ridge | CGG/NPD | CGG-76 | 700 | 5 | 11.600 |
| 1979 | East Greenland shelf | GEUS | GEUS-79 | 600 | 8 | 63.500 |
| 1983 | Greenland Sea | NRL | NRL-83 | 300 | 20 | 13.000 |
| 1984 | SW Barents Sea | CGG | TAMS-84 | 200 | 2 | 11.800 |
| 1985 | SW Barents Sea | CGG | BAMS-85 | 200 | 4 | 16.900 |
| 1985 | S of Faroe Islands | NOO | NOO-85 | 230 | 3 | 18.100 |
| 1986 | Trøndelag Platform | Hunting | Hunting-86 | 200 | 2 | 57.000 |
| 1987 | Vøring Plateau | NOO | NOO-87 | 230 | 5 | 16.900 |
| 1987 | NW Barents Sea | NGU | BSA-87 | 250 | 4-8 | 34.000 |
| 1988 | Spitsbergen | NGU | SPA-88 | 1550 | 5.5 | 13.300 |
| 1989 | Lofoten | NGU | LAS-89 | 250 | 2 | 30.000 |
| 1991 | Svalbard | Amarok/TGS-Nopec | SVA-91 | 900 | 7.5 | 27.800 |
| 1993 | N. Viking Graben | NGU | Viking-93 | 150 | 0.5-2 | 28.000 |
| 1993 | Hel Graben- Nyk High | World Geoscience | SPT-93 | 80 | 0.75 | 19.000 |
| 1994 | Vøring Basin | Amarok/TGS-Nopec | VGVB-94 | 140 | 1-3 | 31.800 |
| 1994 | Nordland Ridge-Helgeland Basin | NGU | NAS-94 | 150 | 2 | 36.000 |
| 1994 | S. Viking Graben | Amarok/TGS-Nopec | VGVG-94 | 160 | 0.2 | 44.800 |
| 1996 | Skagerrak | NGU | SAS-96 | 150 | 2 | 42.000 |
| 1997 | Møre Basin | Amarok/TGS-Nopec | MBAM-97 | 220 | 1-2 | 46.600 |
| 1998 | Vestfjorden | NGU | VAS-98 | 150 | 2 | 6.000 |
| 2000 | Vøring Basin | TGS-Nopec | VBE-AM-00 | 130 | 1-4 | 17.300 |
| 2003 | Røst Basin | NGU | RAS-03 | 230 | 2 | 30.000 |
| 2005 | Jan Mayen FZ | NGU | JAS-05 | 230 | 5 | 32.600 |
| Total | | | | | | 964.300 |

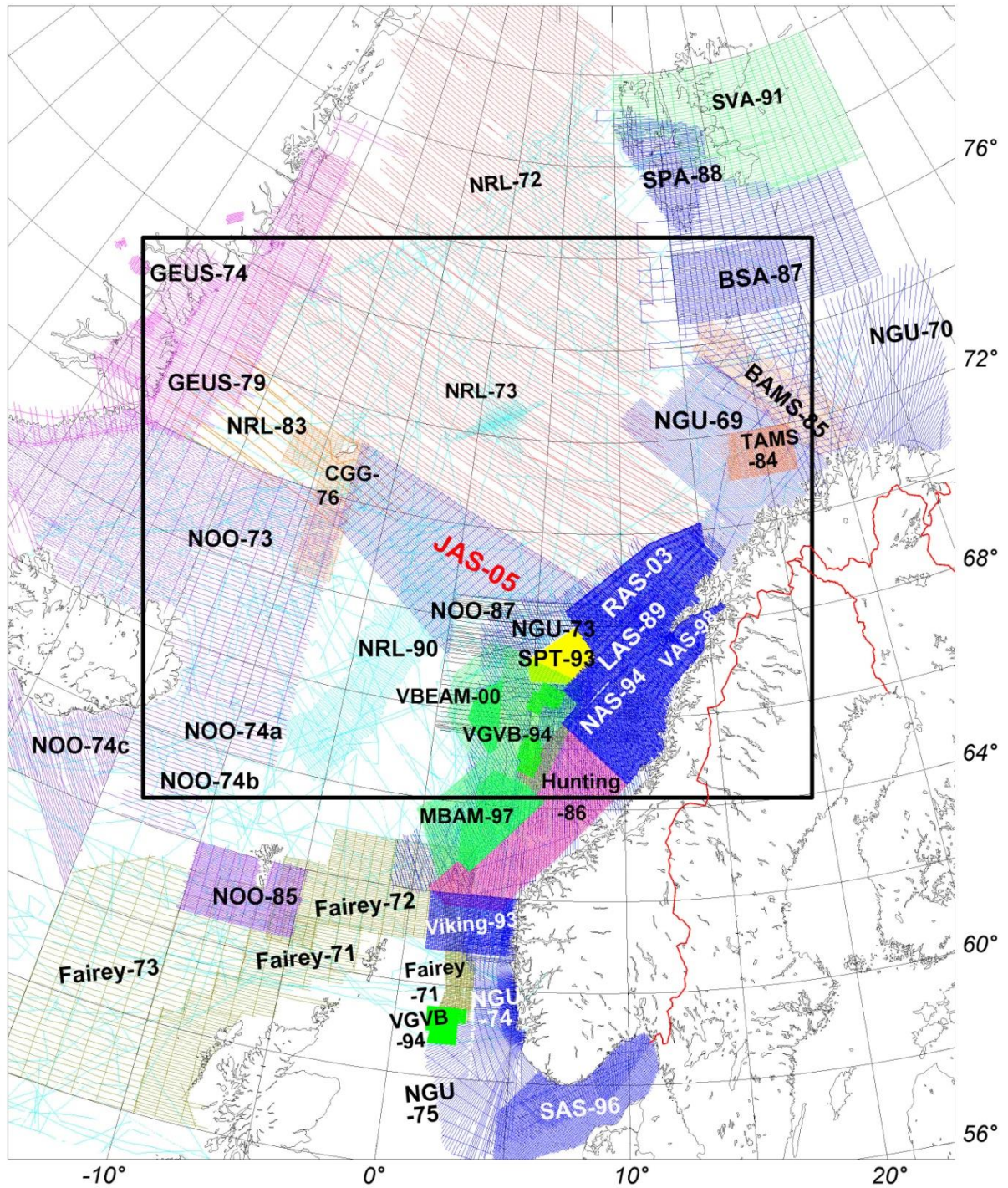


Figure 2.6 Compilation of magnetic surveys in the NE Atlantic area. The sub-grids from the 35 aeromagnetic surveys listed in Table 2.1 are produced from original profile data. The marine magnetic survey (pale blue), Fairey surveys to the west of Shetland (olive green lines) and the GEUS-survey on mainland Greenland (GEUS-74) are adapted from the Verhoef et al. (1996) Gammaa5 compilation and added to the regional data-set.

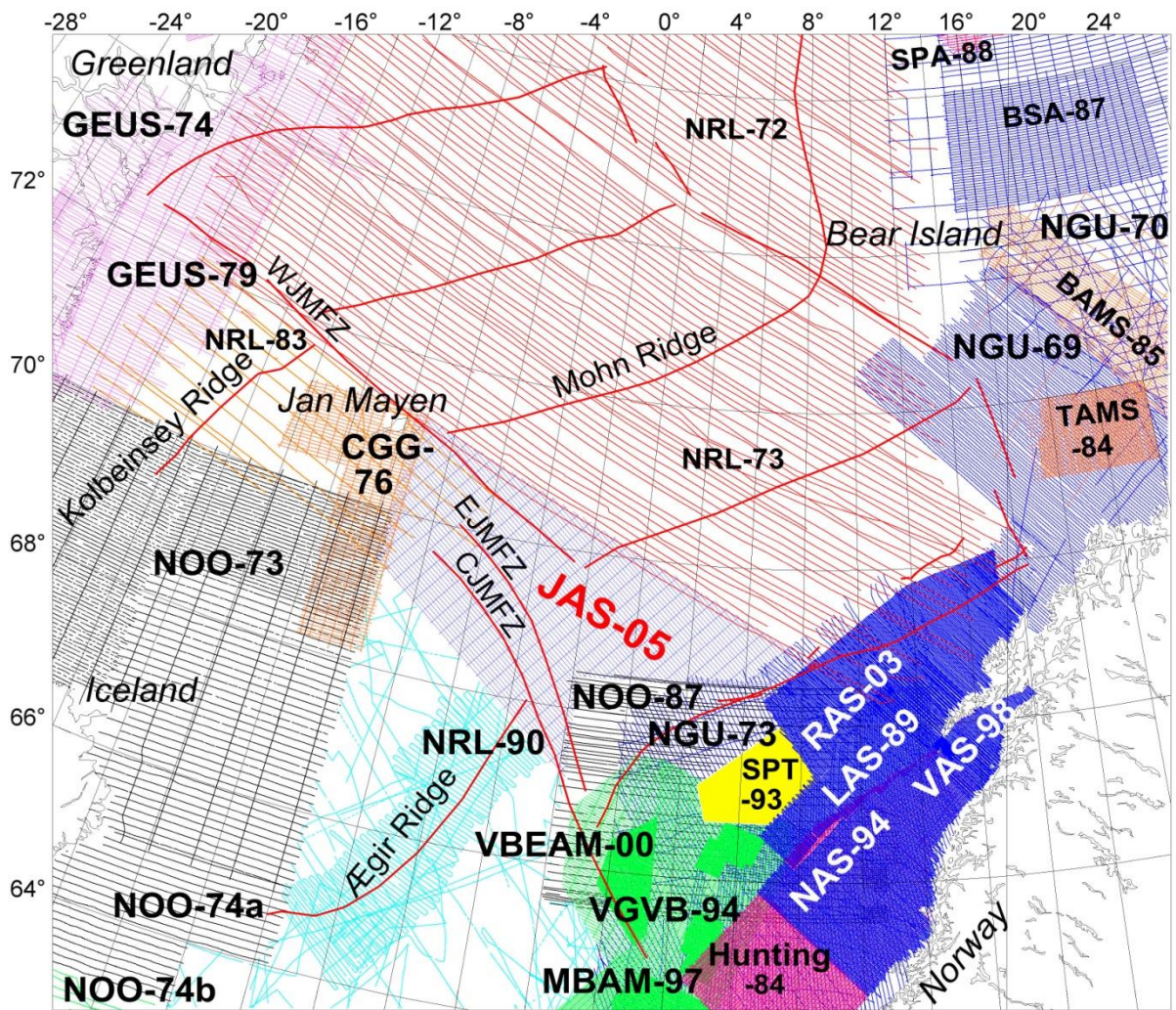


Figure 2.7 Compilation of aeromagnetic surveys in the Norwegian-Greenland Sea (subset of NE Atlantic compilation in Fig. 2.4)..

Specifications for the different sub-areas are given in Table 2.1. The grids were trimmed to c. 10 km overlap and merged using a minimum curvature algorithm, GRIDKNIT, developed by Geosoft (2005b). The final grid shown in Figs. 2.9 & 2.10 was displayed using the shaded-relief technique with illumination from the southeast. To enhance the high frequency component of the regional compilation a 20 km Gaussian high pass filtered map of the compiled data-set has been produced. A grey tone shaded relief version of a 20 km high-pass filtered grid is superimposed on the coloured total field map (Figs. 2.9 & 2.10). The location of flow basalts and sills are more visible on this map than on the total field map.

Gravity and petrophysical data

The gravity grid was compiled by Skilbrei et al. (2000) from gravity stations on mainland Norway in addition to marine gravity data from the Geological Survey of Norway, the Norwegian Mapping Authority, the Norwegian Petroleum Directorate and Norwegian and foreign universities and commercial companies. The compiled grid was merged with gravity data from satellite altimetry in the deep-water areas of the Norwegian-Greenland Sea (Andersen & Knudsen 1998; Laxon & McAdoo 1994). The compiled free-air dataset has been interpolated to a square grid of 2 km x 2 km using the minimum curvature method (Geosoft 2005). The simple Bouguer correction at sea (Mathisen 1976) was carried out using the bathymetry data in Fig. 1.1 and a density of 2200 kg/m³. The International Standardization Net 1971 (I.G.S.N. 71) and the Gravity Formula 1980 for normal gravity have been used to level the surveys. The location of the gravity stations and the marine profiles are shown in Fig. 2.8 while Fig. 2.12 shows the free air gravity at sea and Bouguer gravity on land in the Greenland-Norwegian Sea area.

An Airy-Heiskanen 'root' (Heiskanen & Moritz 1967) was calculated from a compiled topographic and bathymetric data-set (see Fig. 1.1 and section 2.4 below). The gravitational attraction from the 'root' was calculated using the AIRYROOT algorithm (Simpson *et al.* 1983). The isostatic residual (Fig. 2.13) was achieved by subtracting the gravity response of the Airy-Heiskanen 'root' from the observed Bouguer gravity data. Shaded relief versions (in grey tones) of the 100 km high-pass filtered grid is superimposed on the gravity maps in Figs. 2.13 and 2.14. The contour interval is 10 mGal.

The magnetic properties used in the magnetic modelling are adapted from measurements on drill cores acquired within the DSDP and ODP projects (Table 2.2).

Table 2.2. Magnetic properties of igneous rocks from drilling in the Vøring area within the Deep Sea Drilling Project (DSDP) and Ocean Drilling Program (ODP) in 1974 and 1985, respectively (¹Kent & Opdyke 1978, ²Eldholm et al. 1987). The ODP susceptibility data are claimed to be cgs-units, but they are most likely in SI-units, because a corresponding magnetite content of 30-40 % in the volcanics is highly unlikely. A log diagram of the 642E well in Schönharting & Abrahamsen (1989) supports this conclusion.

| Site | Penetration | Number samples | of NRM (A/m) | Suscept. (SI) | Polarity | Mean inclination |
|-------------------|-------------|----------------|--------------|---------------|----------|------------------|
| 338 ¹ | 437 m | 7 | 3.1 | 0.016 | Normal | 70.4° |
| 342 ¹ | 170 m | 3 | 1.4 | 0.015 | Reversed | -81.0° |
| 642E ² | 1229 m | 221 | 5.0 | 0.030 | Reversed | -63° |

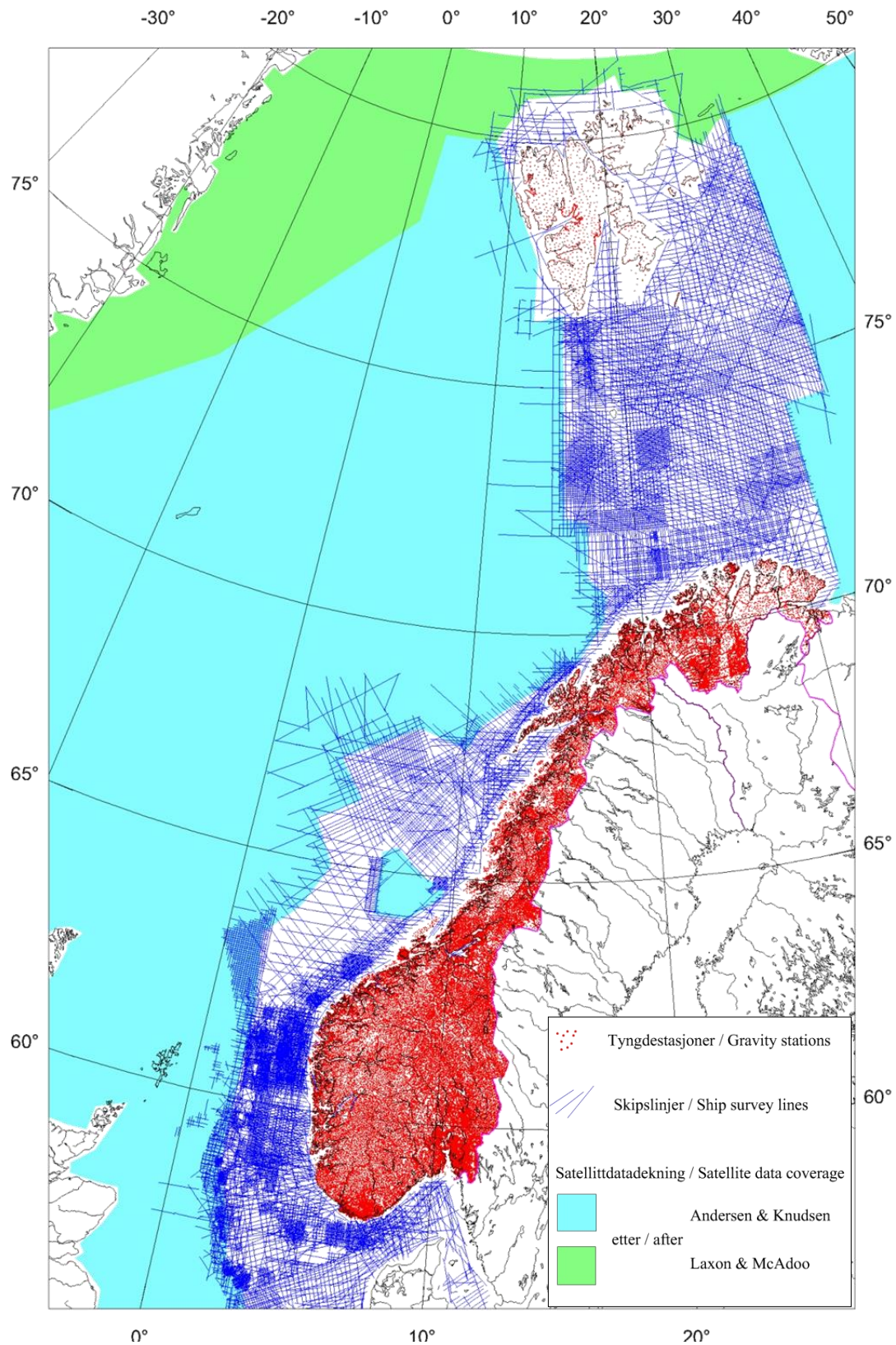


Figure 2.8 Compilation of gravity surveys in the NE Atlantic (Skilbrei et al. 2000).

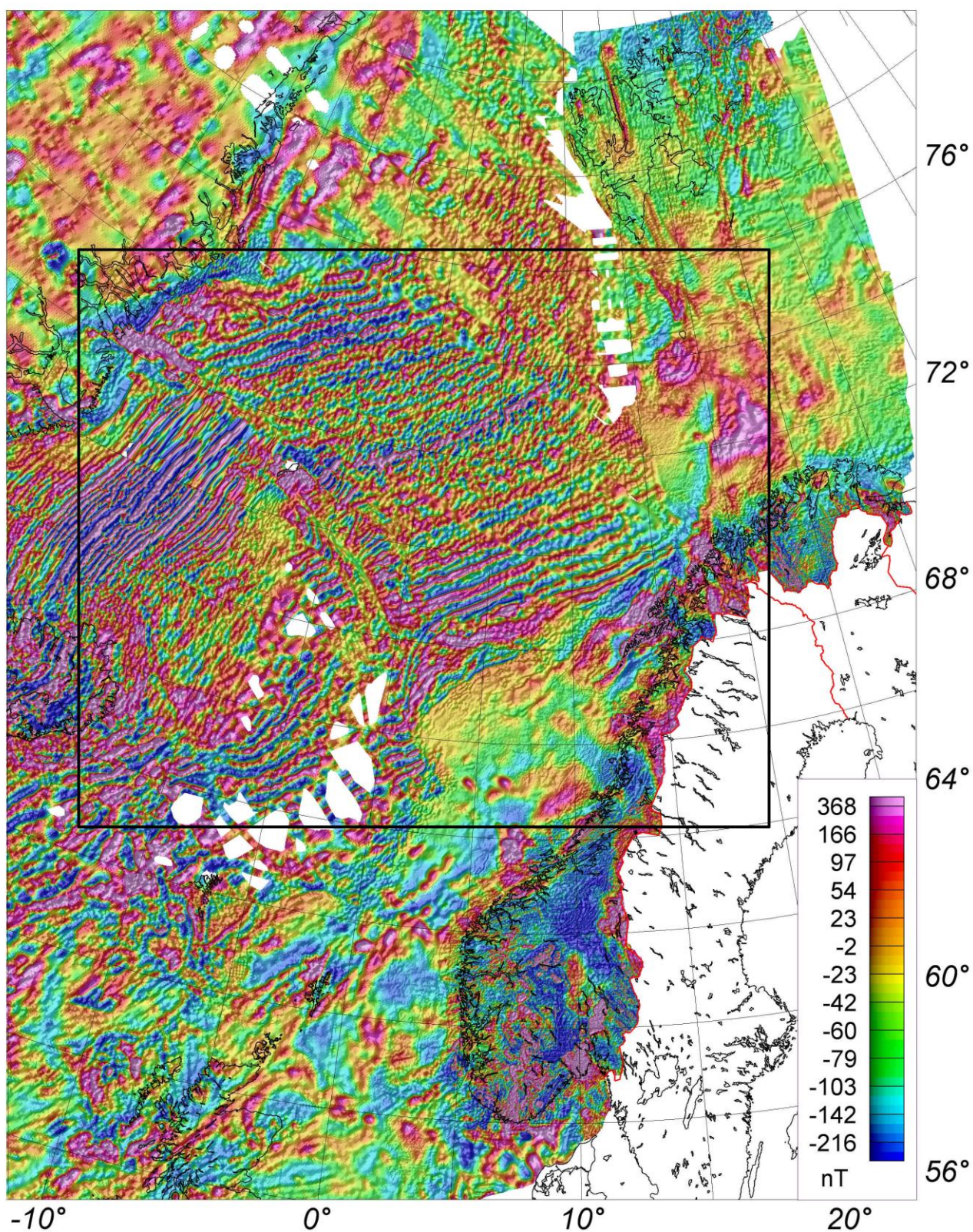


Figure 2.9 Magnetic compilation of the NE Atlantic. Total magnetic field referred to DGRF.

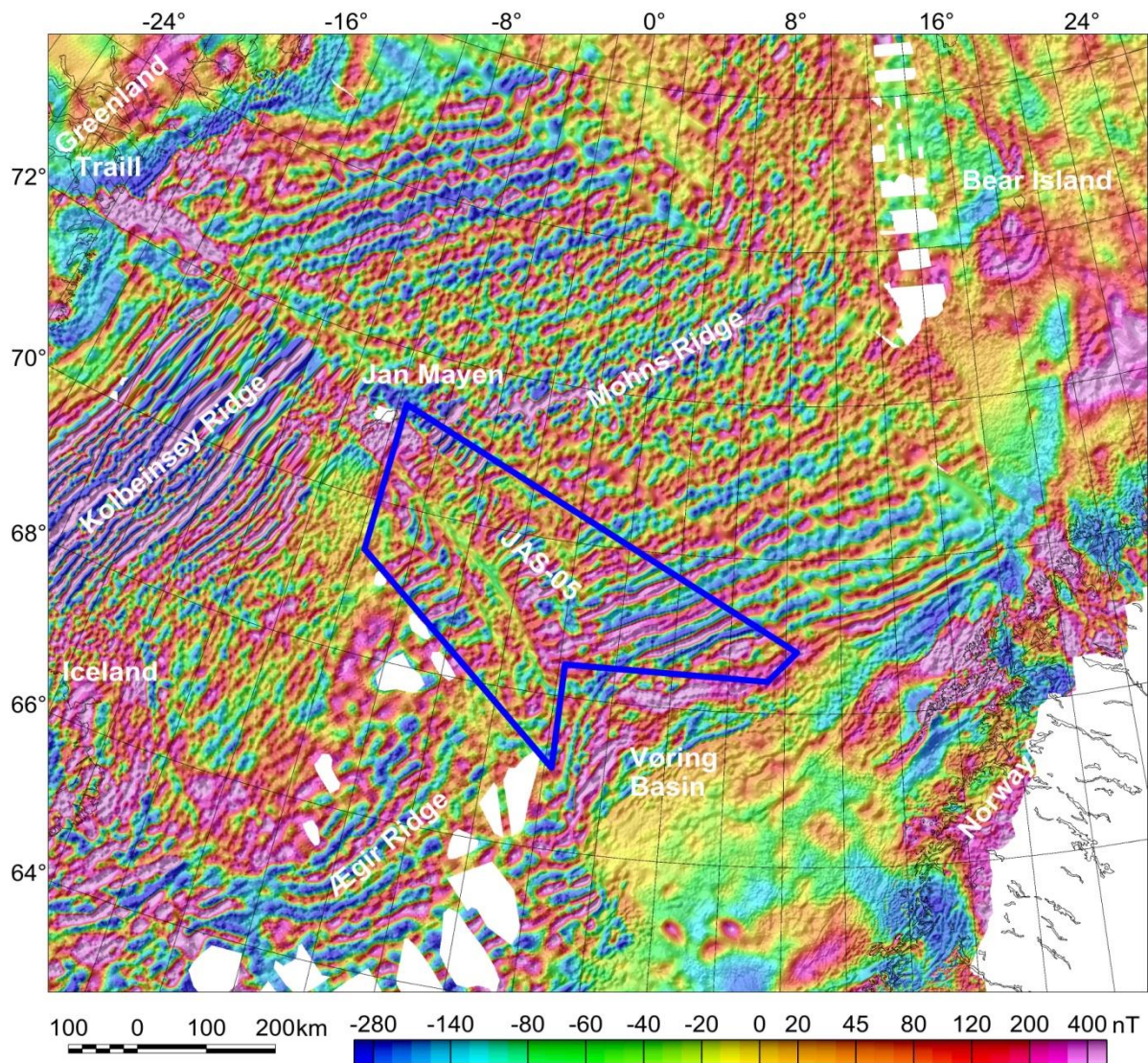


Figure 2.10 Magnetic compilation of the Norwegian-Greenland Sea. Total magnetic field referred to DGRF.

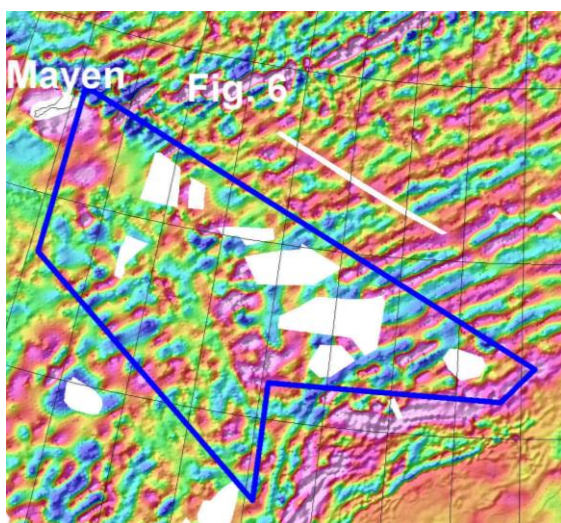


Figure 2.11 Pre JAS-05 magnetic map (Olesen et al. 2004) of the Jan Mayen fracture Zone.

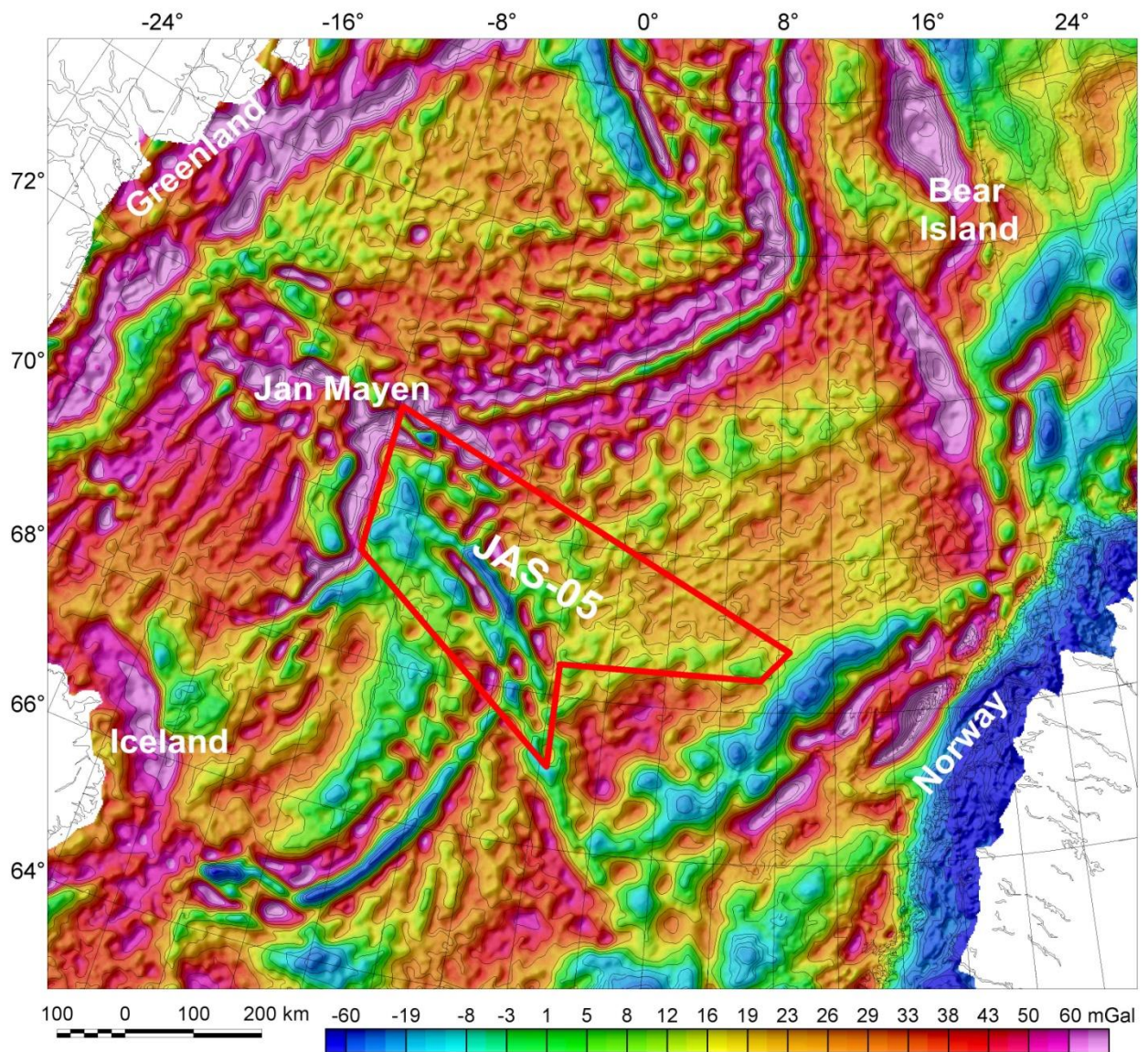


Figure 2.12 Free air gravity at sea and Bouguer gravity on land in the Greenland-Norwegian Sea area (Skilbrei et al. 2000). The contour interval is 10mGal. The red frame shows the JAS-05 area.

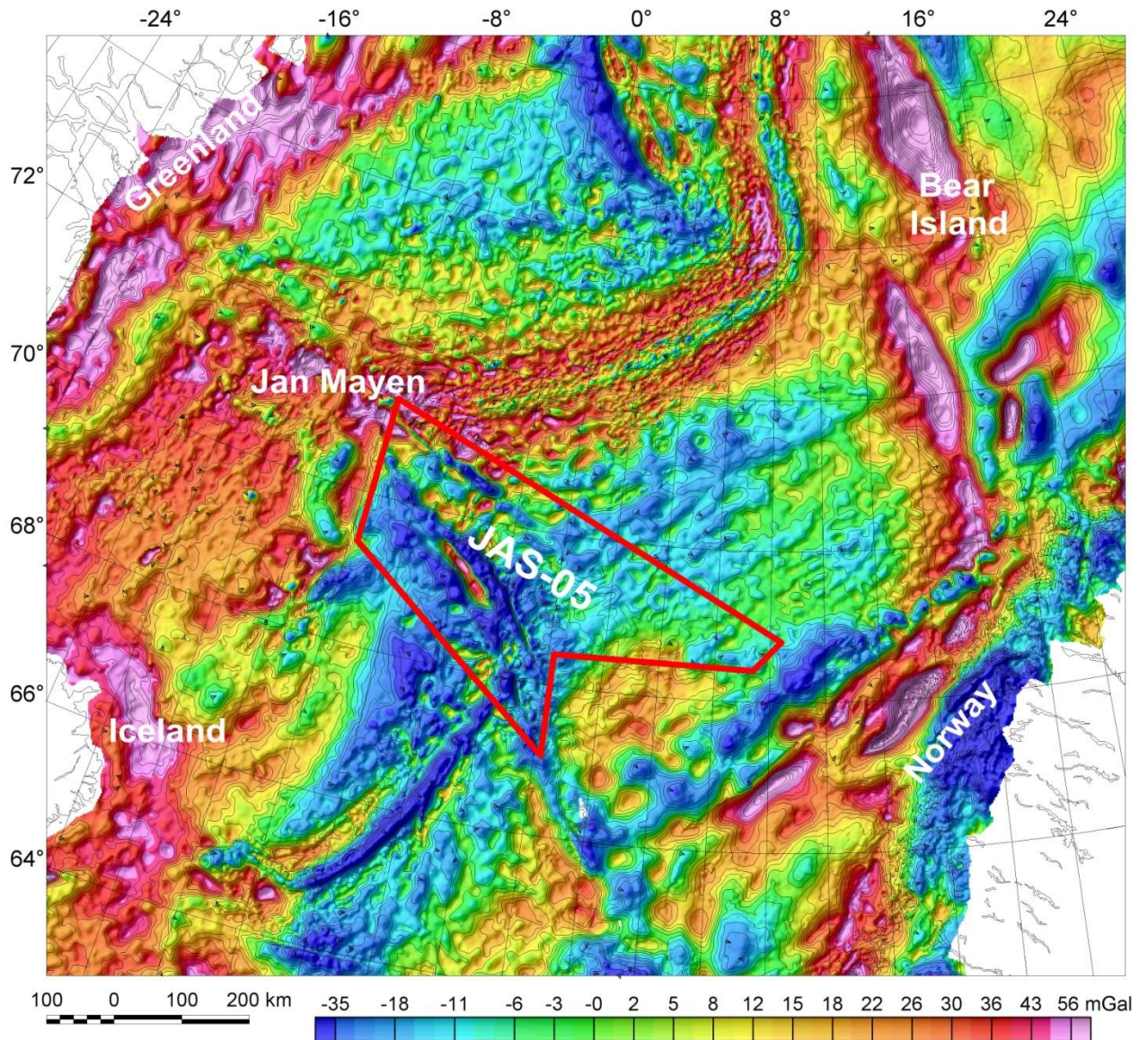


Figure 2.13 Residual gravity after isostatic correction of Bouguer gravity data from the Greenland and Norwegian Seas and adjacent areas. The isostatic correction has been calculated applying the AIRYROOT algorithm (Simpson et al. 1983) to the topography/bathymetry in Fig. 1.1 (rock density 2670 kg/m^3 on land, 2200 kg/m^3 at sea and a crust/mantle density contrast of 300 kg/m^3). The contour interval is 10 mGal . The red frame shows the JAS-05 area.

2.3 Bathymetric and topographic data

The bathymetry data for the deep-water part of the map (Fig. 1.1) come from satellite altimeter data released by Smith and Sandwell (1997). The bathymetric data from the shallow water areas were compiled by The Norwegian Mapping Authority, Marine Department in Stavanger. This data set has three different sources; 1) modern multi-beam echo sounder in the Vestfjorden area, 2) digitised naval maps in areas adjacent to the coast and 3) depth data collected during seismic surveys in areas further offshore. The quality of these data varies

considerably. Data set 1 has the highest quality while data set 3 is poorest. The cell size of the combined grid is 1 km x 1 km.

Very coarse data to fill in the gaps in coverage were extracted from a global data set supplied with the ER-Mapper software. High-resolution topography data (100m x 100m) for Norway were supplied by the Norwegian Mapping Authority. Topography for Sweden was downloaded from the GTOPO30 data set (<http://edcwww.cr.usgs.gov/landdaac/topo30/topo30.html>). The final grid shown in Fig. 1.1 was displayed using the shaded-relief technique with illumination from the southeast. The grey tone part of the maps is calculated from a 20 km high pass filtered grid and is superimposed on the coloured elevation model.

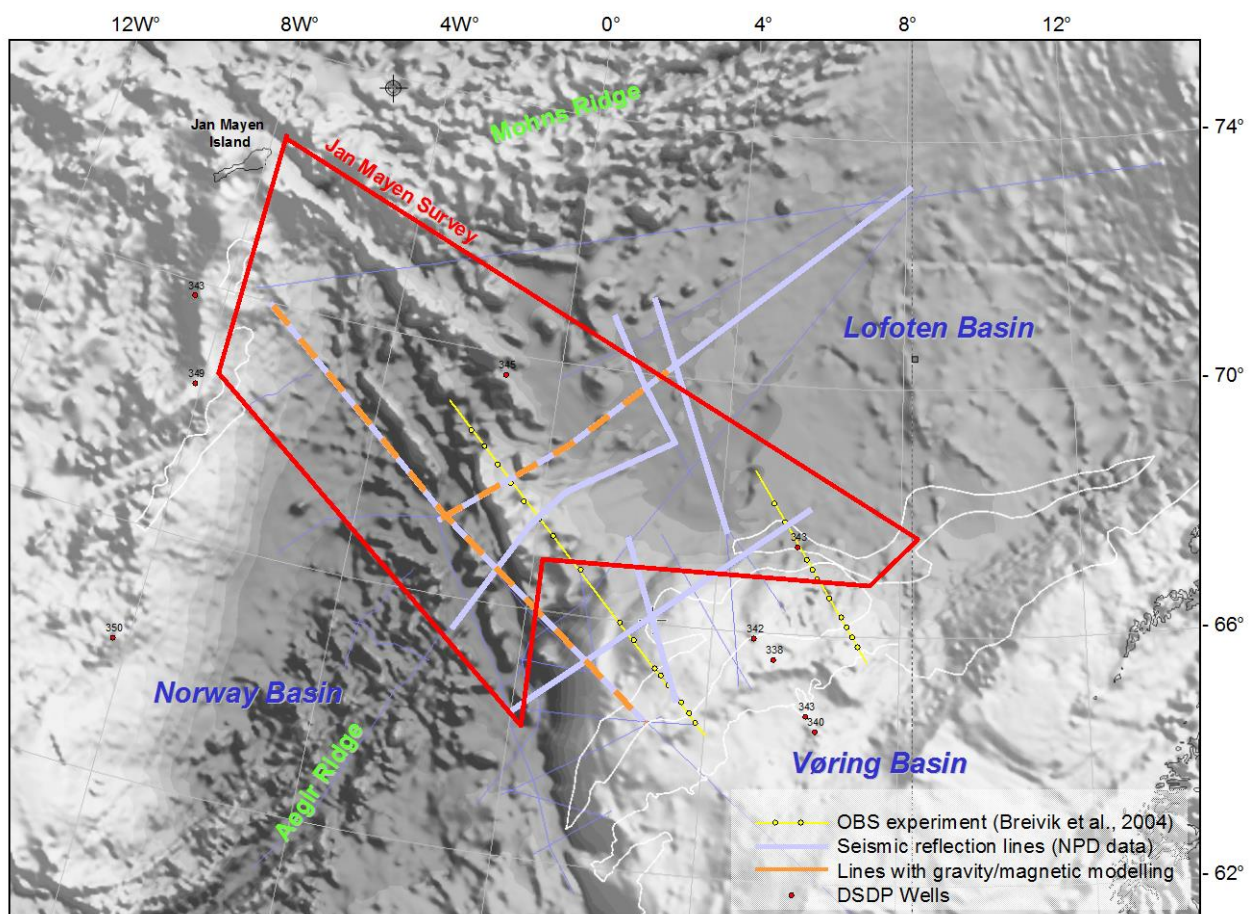


Figure 2.14 Seismic database for the interpretation of the JAS-05 data. The OBS and reflection seismic data have been provided by Breivik et al. (2004) and NPD, respectively. The information from the Deep Sea Drilling Project is adapted from Talwani et al. (1978).

2.4 Seismic studies

Interpretations of Ocean Bottom Seismograph (OBS) arrays from the Vøring-Jan Mayen area are available from the studies of Breivik et al. (2004) and Mjelde et al. (1997, 1998, 2003, 2005). OBS lines, reflection seismics and Deep Sea Drilling Project wells within the JAS-05 area are shown in Fig. 2.14.

Structural interpretations from the Vøring – Jan Mayen area have been published by Blystad et al. (1995). Brekke (2000), Eldholm et al. (2002), Berndt et al. (2000, 2001a, 2001b), Lundin & Doré (1997) and Skogseid et al. (1992) present additional interpretations from reflection seismic profiles along the margin. The information of these studies was considered, wherever possible, to constrain the modelling and analysis results.

2.5 Data presentation

Histogram-equalised colour (i.e. each colour cover the same area on the map), high-frequency filtered and shaded-relief images have been used to enhance the information of the regional data-sets. Shaded-relief presentations, which treat the grid as topography illuminated from a particular direction, have the property of enhancing features that do not trend parallel to the direction of illumination. These maps are presented in Figs. 2.4, 2.5 and 2.9-2.12, the two former maps are in A3 format. The separation of the residual field on the magnetic and gravity datasets is carried out in the frequency domain using 20 and 100 km Gaussian filters, respectively. A shaded relief version in black/white of the high-pass filtered aeromagnetic and gravity grids are superimposed on the coloured total field aeromagnetic and gravity grids (Figs. 2.4, 2.11 & 2.12).

The grid data-sets were analysed with the Oasis Montaj software (Geosoft 2004, 2005c,d). Fault zones within the basement and partly within the sediments are interpreted from the aeromagnetic map.

3 MAIN STRUCTURAL ELEMENTS OF THE NORWEGIAN-GREENLAND SEA

Laurent Gernigon

The Jan Mayen Fracture Zone (JMFZ) is probably the most atypical expression of the Norwegian-Greenland Sea and its complexity and profound nature are clearly mirrored in contrasting spreading configurations visible in the North Atlantic oceanic domain (Sykes 1965; Johnson and Heezen 1967; Skogseid and Eldholm et al. 1987; Lundin & Doré, 2002; Scott 2005). The JMFZ is defined in the bathymetry as a prominent NW-SE escarpment lying in the southern part of the Vøring Basin and as a complex structural zone in the oceanic domain of the Norwegian-Greenland Sea. During Paleocene times, the JMFZ strongly influenced the breakup of the Mid-Norwegian continental margin, hence resulting in the development of a transform margin between the Møre and Vøring margin segments, offshore Norway (Berndt et al., 2001). Progressively, the JMFZ played an important role during the development of the North Atlantic as controlling the evolution of the Jan Mayen Microcontinent progressively dislocated from the Mid-Norwegian margin during the accretion of the Aegir Ridge at 54-55 Ma (Unternehr 1982; Scott et al. 2005).

In the central part of the Mid-Norwegian continental shelf, the Jan Mayen Lineament lies in the prolongation of the JMFZ and is referred to a possible continuation of the JMFZ that separates the deep Møre Basin to the southwest from the Vøring Basin and Halten Terrace to the northeast (Fig. 3.1) (Blystad et al. 1995; Brekke et al. 2000).

Despite the number and range of investigation over the Mid-Norwegian continental shelf, the junction and transition from the JMFZ in the continental domain are poorly understood. Most of the authors have previously suggested that the JMFZ was controlled by the pre-existing structure of the Mid-Norwegian continental margin characterized by the sinistral shift in the basin axis and basins margins (Blystad et al. 1995; Grunnaleite & Gabrielsen 1995).

Most of previous studies highlight the fact that the JMFZ is influenced by the pre-breakup configuration of the Mid-Norwegian continental margin. However, the structural relationship between the pre-breakup sedimentary basins and the JMFZ, especially during the breakup initiation, is poorly documented in the literature. Jongepier et al., (1996), Grunnaleite and Gabrielsen (1995) investigated the inner part of the Møre Basin whereas Skogseid et al. (1992), Ren et al. (1998) and Lundin and Doré (1997) investigated the outer Vøring Basin but their studies were mainly focused in the central and northern parts of the Vøring Basin. Based on potential field observations Doré et al. (1997); Fichler et al. (1999) noted also a possible relation of the JMFZ with Proterozoic or Caledonian NW-SE trends. Recently, Berndt (2001b) investigated the nature of the Early Tertiary magmatism along the transform segment of the Mid-Norwegian margin and show that the breakup magmatism was extremely reduced along this area compared to the Møre and Vøring marginal highs, where thick basaltic lava piles are known to form Seaward Dipping Reflectors (SDRS). In a regional synthesis dealing with the along strike variability of the structural style along the outer Vøring Basin,

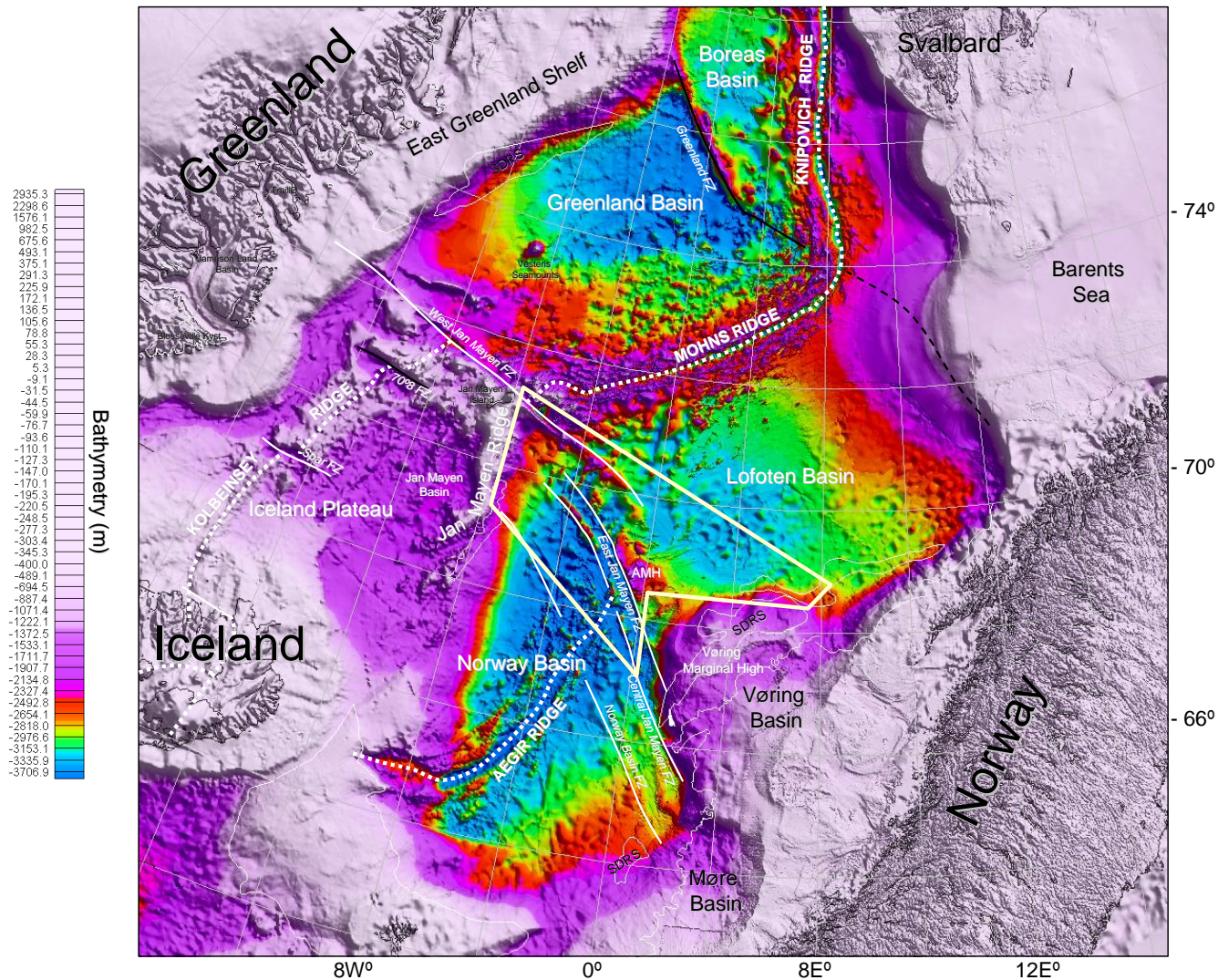


Figure 3.1 Bathymetry of the Norwegian-Greenland Sea and location of the Jan Mayen survey area.

Gernigon et al. (2003) note the structure of the Vøring Basin changes markedly at the latitude of the JMFZ. A relationship with the JMFZ was suggested, but no detailed studies were performed at this stage.

In the oceanic domain, the JMFZ itself is usually divided in two entities defined by a difference in bathymetric trend of appreciatively 30° between the East Jan Mayen Fracture Zone (EJMZF) and the West and Central Jan Mayen Fracture Zone (WJMFZ and CJMFZ) (Fig. 3.1). North of the JMFZ, the Mohns Ridge, which is the current oceanic spreading ridge, divides the Lofoten Basin from the Greenland Basin to the West. South of the JMFZ, the Kolbeinsy Ridge is located far closer to Greenland. This observation led several authors to postulate a fossil spreading axis in the Norway Basin (Johnson and Heezen 1967). The existence of this extinct ridge was confirmed by subsequent studies and named Aegir Ridge after the Norse sea god (Vogt et al. 1970; Talwani & Eldholm 1977; Grønlie et al. 1978; Nunns 1983; Jung & Vogt 1997).

Two important geological events are usually invoked in the literature for the present location and configuration of the study area (Talwani and Eldholm 1977; Lundin & Doré, 2002).

- The first was the opening of the Norwegian Sea by the splitting apart of Greenland and Norway in Early Eocene, 54 Ma ago. It is also now well established that the Early Tertiary opening of the Norwegian-Greenland Sea was affected by a significant volcanic activity along the breakup axis which is well document along the Vøring Marginal High. Following White et al. (1987) and White (1988) most of the workers explain the Early Tertiary volcanism of the North Atlantic Igneous Province (NAIP) in terms of lithospheric impingement of the proto-Iceland “mantle plume” but challenging and convincing alternatives, including small-scale convection and mantle heterogeneities have also been proposed (Foulger & Anderson 2004). Soon after the breakup, sea-floor spreading occurred simultaneously along the Mohns and Aegir spreading axis, connected to the south with the Reykjanes Ridge spreading axis between SE Greenland and Rockall. During this period, accretion along the Aegir Ridge and the Mohns Ridge was accommodated along the JMFZ acting as a transform zone between the two spreading systems.

- The second main geodynamic event happens in Oligocene times. During this stage, the Aegir Ridge, where the opening was actively taking place became extinct and the spreading axis "jumped" westwards to form the Kolbeinsy Ridge, still active at present. At this time, a major rotation of the opening direction took place in the North Atlantic, changing from NNW-SSE to NW-SE (Lundin & Doré 2002). Accurate timing of the ridge jump between Aegir and Kolbeinsey is not perfectly constrained but most of previous authors agree that it happened after the formation of magnetic chrons C13 and C7, approximately between 32 and 25 Ma according to the CK95 time scale of Cande and Kent (1995).

The opening at the new ridge axis resulted in separating a thin, long continental fragment away from Greenland. This long sliver is the Jan Mayen microcontinent, the missing piece between the outer Vøring Basin and the Faeroes Plateau (Gudlaugsson et al. 1988; Kodaira et al. 1998)

3.1 Outer Vøring Basin and the Vøring Marginal High

During the last 30 years, numerous seismic studies and commercial and scientific drilling showed that magmatism is particularly well developed along the breakup axis of the Mid-Norwegian continental margin. As part of a polyrifted system, the outer Vøring Basin was particularly affected by Early Campanian-Paleocene rifting leading to breakup in Late Paleocene-Early Eocene along the Vøring Marginal High. The same system is not clearly expressed in the outer Møre Basin, where no significant faulted structures are observed.

The Mid-Norwegian continental margin is usually classified as a "Volcanic rifted margin" (Mutter et al. 1984; White & McKenzie 1989; Planke et al. 1991; Planke & Eldhom 1994; Mjelde et al. 1997, 2005). It is characterised by huge volumes of magma formed during the early stages of crustal accretion along the future spreading axis, typically expressed seismically as seaward dipping reflector sequences, (i.e SDRS) and by lower crust with anomalous high seismic P-wave velocities (7.1-7.8 km/s) so-called lower crustal bodies (i.e LCBs) (Mutter et al. 1984; Planke et al. 1991; Eldholm et al. 2000; Mjelde et al. 1996, 1997, 2002), whose nature is still debated (Gernigon et al. 2003, 2004; Ebbing et al. 2005). SDRS and LCBs have long been recognized along the Vøring Marginal High but only the volcanic nature of the SDRS is now well proved by the Deep Sea Drilling Legs 38 and the Ocean Drilling Program Leg 81 (Talwani et al. 1978; Eldholm et al. 1987).

3.2 Island of Jan Mayen and the Jan Mayen microcontinent

Jan Mayen Island

The western part of the survey is bounded by the Jan Mayen Island and the Jan Mayen Ridge. Jan Mayen is situated 550 km NE of Iceland and 500 km east of Greenland, between 75° 5'N and 72° N, and between 7° 5'W and 8° 5'W. The island is 53 km long and covers 377 km². Some historians believe that an Irish monk, Brendan, who was known as a good sailor, was the first to discover Jan Mayen early in the 6th century before the Dutchman Jan Jacobs May van Schellinkhout, who visited and named the island in 1614. When Brendan came back, he reported that he had been close to a black island, which was on fire, and that there was a terrible noise. He thought that he might have found the entrance to hell. This is probably the first historical testimony of any volcanic activity on Jan Mayen Island.

The Jan Mayen locates in a fairly unusual tectonic setting near the intersection of the WJMF and the Mohns Ridge. The Kolbeinsey Ridge is shifted 170 km to the east by the WJMFZ. The Jan Mayen Island is seismically active (Zobin 1993) and the main volcano of the island (i.e Beerenberg, 2277 m) is also active present day (Imsland 1986). The Beerenberg is the world's northernmost volcano above sea level, and Norway's only active volcano with a constant threat

of new eruptions and earthquakes. There were at least five active craters.

The first modern eruption witnessed in modern times was in 1970 (Gjelsvik, T. 1970; Havskov & Atakan 1991). The eruption was large, erupting at least 0.5 km³ of basalt from a 6 km long fissure that stretched from sea-level to an elevation of 1000 m. The eruption started again in 1985. In that brief time about 7 million m³ of lava were erupted. Earthquakes, with magnitudes up to 5 occurred during the eruption. The eruption was thought to be from a leaky fracture zone, not the Jan Mayen magma system proper (Imsland 1986).

Trace element and Nd-Sr-Pb isotope systematic suggest that the recent basaltic rocks formed near Jan Mayen Island from an enriched mantle source but low ³He/⁴He isotope do not favour a mantle plume origin for the magmatism (Svellingén & Pedersen 2003). There is no evidence of continental contamination either. This suggest that the Jan Mayen Island could be entirely oceanic and slightly different from the rest of the Jan Mayen Ridge



Figure 3.2 Picture of the active Beerenberg volcano, northern Jan Mayen during its eruption in 1985 (<http://www.jan-mayen.no/>). The Beerenberg has erupted six times between 1732 and 1985. All of these eruptions were on flank vents and produced lava flows and scoria cones. The most recent eruptions were in 1970, 1973, and 1985.

3.3 The Jan Mayen Ridge

The Jan Mayen Ridge is a roughly N-S trending feature with water depths between 0-1000 m subdivided by a depression, situated between latitudes 68° and 69° N, into a northern plateau like area and a southern zone (Figs. 3.1 and 3.3). Although the ridge is not uniform through the entire area lying between Jan Mayen Island and Iceland, the region is often referred to as the Jan Mayen Microcontinent (Kuvaas & Kodaira 1997). Geologically speaking, the Jan Mayen Ridge is a microcontinent that predates both Jan Mayen and Iceland, which are composed of younger volcanics.

Surprisingly, this piece of “continent” did not stay above sea level and it is likely that it has been so far below sea level. It was part of a shallow sedimentary basin in Mesozoic times, and later in, the Early Tertiary, part of the East Greenland margin. The northern part subsided less and stayed relatively shallow; it also remained a single block-like feature while the southern part broke into several fragments that subsided deeper (Scott et al. 2005).

It is generally agreed that the Jan Mayen Microcontinent contain continental rocks whose age predates the opening of the Norwegian Sea. Recent discovery of Lewisian and Jurassic zircon xenocrysts from eastern Iceland lavas (Schlatterger et al. 2002) suggest also that some continental fragments could be present below Iceland, commonly interpreted as a purely oceanic feature.

Sedimentary patterns and structure of the Jan Mayen Microcontinent have been detected by seismic reflection profiling and wide-angle survey (Gairaud et al. 1978; Skogseid & Eldholm 1987; Gudlaugsson et al. 1988; Kuvaas & Kodaira 1997; Alvestad 1997).

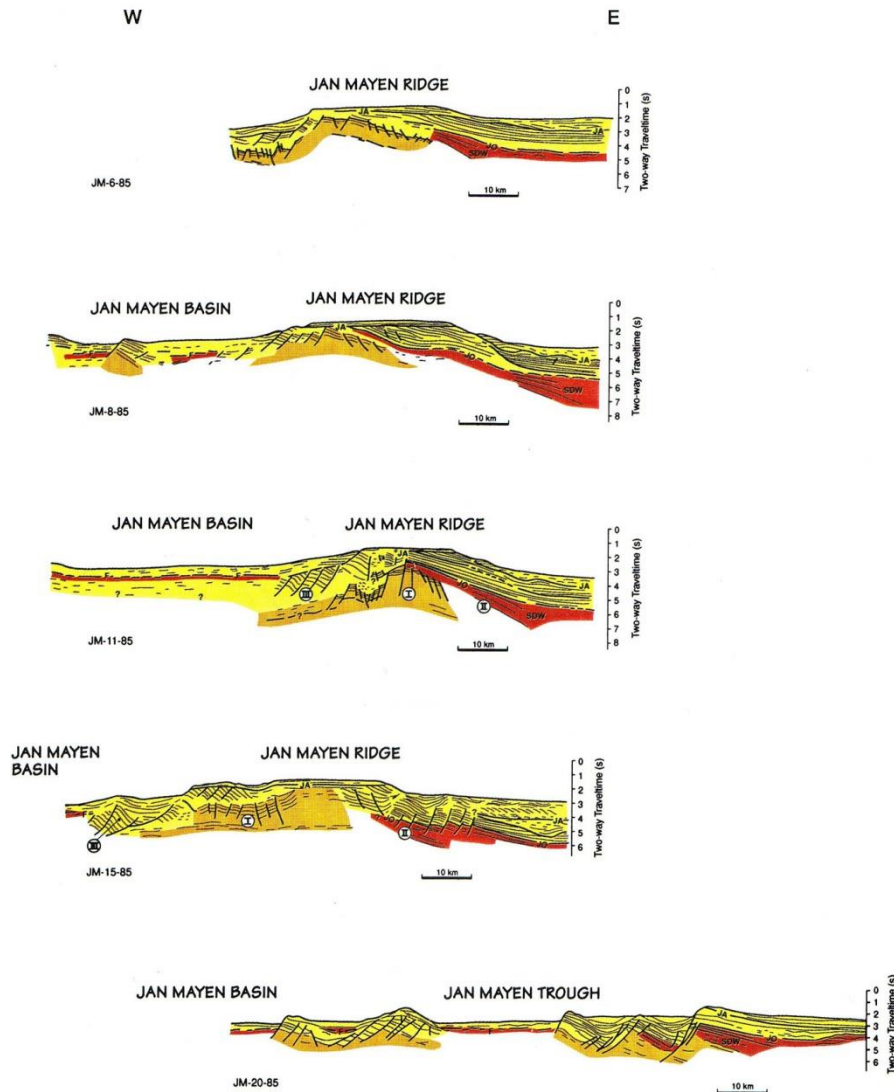


Figure 3.3 Interpreted line-drawings of seismic reflection profiles across the Jan Mayen Ridge and the Jan Mayen Basin (Kuvaas & Kodaira 1997). SDW=Seaward dipping wedge (referred as SDRS in our report). The sediments lying above JA are Miocene or younger in age: The sediments below JA are Oligocene or older. Rocks below Horizon O have not been drilled but may represent Palaeozoic to Mesozoic faulted Ridges. Red sequences represent volcanic rocks. Reflectors F in the western Jan Mayen Margin masks the underlying structures and is interpreted as Early Miocene lava flows. Note also that crustal extension occurs during Eocene?-Oligocene time in the western part of the Jan Mayen Ridge.

Two important unconformities are readily seen in the seismic records. The lower unconformity (O), is believed to be associated with the first episode of breakup that started between the Mid-Norwegian margin and the Jan Mayen Microcontinent 55-54 Ma ago. It has not been reached by drilling, and the estimate of its age is based in part on the Vp-waves provided by Ocean Bottom Seismometer experiment (Kuvaas & Kodaira 1998) and partly on its juxtaposition with basaltic rocks outpourings formed during the early Tertiary opening. The second unconformity (JA) is believed to be associated with a second episode of opening (in Oligocene times).

DSDP scientific drilling has been carried out at four sites, 346, 347, 349 and 350, in the survey area (Talwani et al. 1976). At sites 346, 347, and 349 the drilling penetrated through horizon A.

The sediments lying above JA are Miocene or younger in age, and are believed to have been deposited after initiation of the second opening stage. The underlying sediments are Oligocene or older and have a larger terrigenous component than the sediments overlying JA. They are believed to have been deposited when Jan Mayen Ridge was still part of Greenland and formed part of its eastern margin. Rocks below Horizon O have not been drilled. Hole 350 was drilled down to the seismically opaque layer (F), which was determined to represent Eocene basalts.

The crustal structures from the centre of the Jan Mayen Ridge to the Jan Mayen Basin have been better documented by means of Ocean Bottom Seismograph (OBS) acquisitions (Kodaira et al. 1998). The OBS data indicate that a continental upper crust ($V_p=5.8-6.1$ km/s) and lower crust ($V_p=6.7-6.8$ km/s) underlie the deep sedimentary basin. The thickness of the continental lower crust varies significantly from 12 km beneath the Jan Mayen Ridge to almost zero thickness beneath the northwestern part of the Jan Mayen Basin.

The eastern margin of the Jan Mayen Microcontinent has been formed during initiation of spreading in the Norwegian Basin. Skogseid and Eldholm, (1987), Gudlaugsson et al. (1988); Kuvaas and Kodaira (1997) and Alvestad (1997) identified SDRS along the eastern margin. The "SDRS" were later faulted, probably when the Jan Mayen Ridge separated from East Greenland during the mid-Tertiary (Gudlaugsson et al. 1988). Landward-dipping reflector segments below the SDRS, similar to those found in the Møre Margin, have been interpreted as a feeder dike system on the Jan Mayen Ridge (Alvestad 1997). This SDRS interpretation (eg. SDRS=volcanic feature) can be however partly challenged. We will see later that the Jan Mayen aeromagnetic survey contributes to new challenging interpretations.

The western margin of the Jan Mayen Microcontinent is different. First this margin was formed later during a rifting phase leading to oceanic spreading between East Greenland and the microcontinent during Oligocene times. No SDRS are observed but Early Miocene volcanic activity is interpreted (marker "F" of Kuvaas and Kodaira 1997). There is, however, no clear calibration and the underlying formation are not imaged, due to sub-basalt imaging problem. Globally, the onset of rifting and the structure of the margin in this part of the Jan Mayen Microcontinent is still unclear. Jan Mayen has probably been affected by a rifting phase in Oligocene time but could have been affected by an older Cretaceous-Paleocene phase. The Jan Mayen Basin, to the west of the Jan Mayen Ridge, is probably underlain by highly attenuated continental crust, which agrees with pre-breakup rifting event(s) (Kodaira et al. 1998).

3.4 Mohns Ridge

The Mohns Ridge is located north of the JMFZ corridor between the northern part of the Mid-Norwegian margin (Lofoten and Vøring margin segment) and the Northeast Greenland Margin. The Mohns Ridge has been formed since the breakup between the two conjugate systems (Figs. 3.1 and 3.4). The spreading ridge is still active now. The rift-drift transition occurred in Early

Eocene usually characterized by the C24 magnetic anomalies usually divided in two sub-chrons C24A (52.5 Ma) and C24B (53.3 Ma), also named C24n1r and C24n2r (Cande & Kent 1995). Before C24A, the reverse C24R (53.3-55.9 Ma) represent the continental-ocean boundary (COB) (Skogseid and Ehldohm 1987; Mosar et al. 2002). The C24 anomalies are well defined along the continent-ocean transition (COT) of the Lofoten Margin and to its conjugate but not so well defined to the south.

Compared to the Norway Basin the magnetic anomalies are pretty well defined on either side of the Mohns Ridge (Fig. 3.4). The magnetic anomalies are relatively linear, with few gaps and interruption.

Mosar et al. (2000) estimated the spreading rate on either side of the Mohns Ridge. Initial spreading rate were high and estimated between 1.4 to 1.8 cm.a⁻¹, when the C24 anomaly is well defined. A systematic decrease in velocity toward anomalies C13 (33.5 Ma) and C7 (25 Ma) is observed from 1.8 cm.a⁻¹ to 0.5 cm.a⁻¹ during this intermediate period. Between C7 (25 Ma) and C6 (20 Ma), a sudden increase of the spreading rate is observed and could coincide with the positioning of the Iceland anomaly (plume ?) below the ridge. This impingement could have increased the ridge push and the NE shift of Eurasia in the absolute motion direction (Torsvik et al. 2001).

Since C6 (20 Ma) the spreading rates stayed more or less constant around 0.7-0.75 cm.a⁻¹ for the last 10.3 Ma.

3.5 Iceland Plateau and the Kolbeinsey Ridge

There is no general agreement regarding the tectonic history of the Icelandic Plateau and the formation of the Kolbeinsey Ridge between anomaly C7?-6C and C5 (Fig. 3.4). Grønlie et al., (1979) proposed an extinct spreading axis to the west of the Jan Mayen Ridge where oceanic spreading continued until prior to magnetic anomaly C5, before spreading jumped westward to the present day active Kolbeinsey Ridge.

Unternehrl (1982) shows seismic evidence to support this extinct axis and confirm this interpretation. Vogt et al., (1980), however, argued against the existence of this extinct axis. They proposed a continuous spreading along the Kolbeinsey Ridge after anomaly C7?-C6, with an increase in full spreading rate from 15 to 20 mm/year at magnetic anomaly C5.

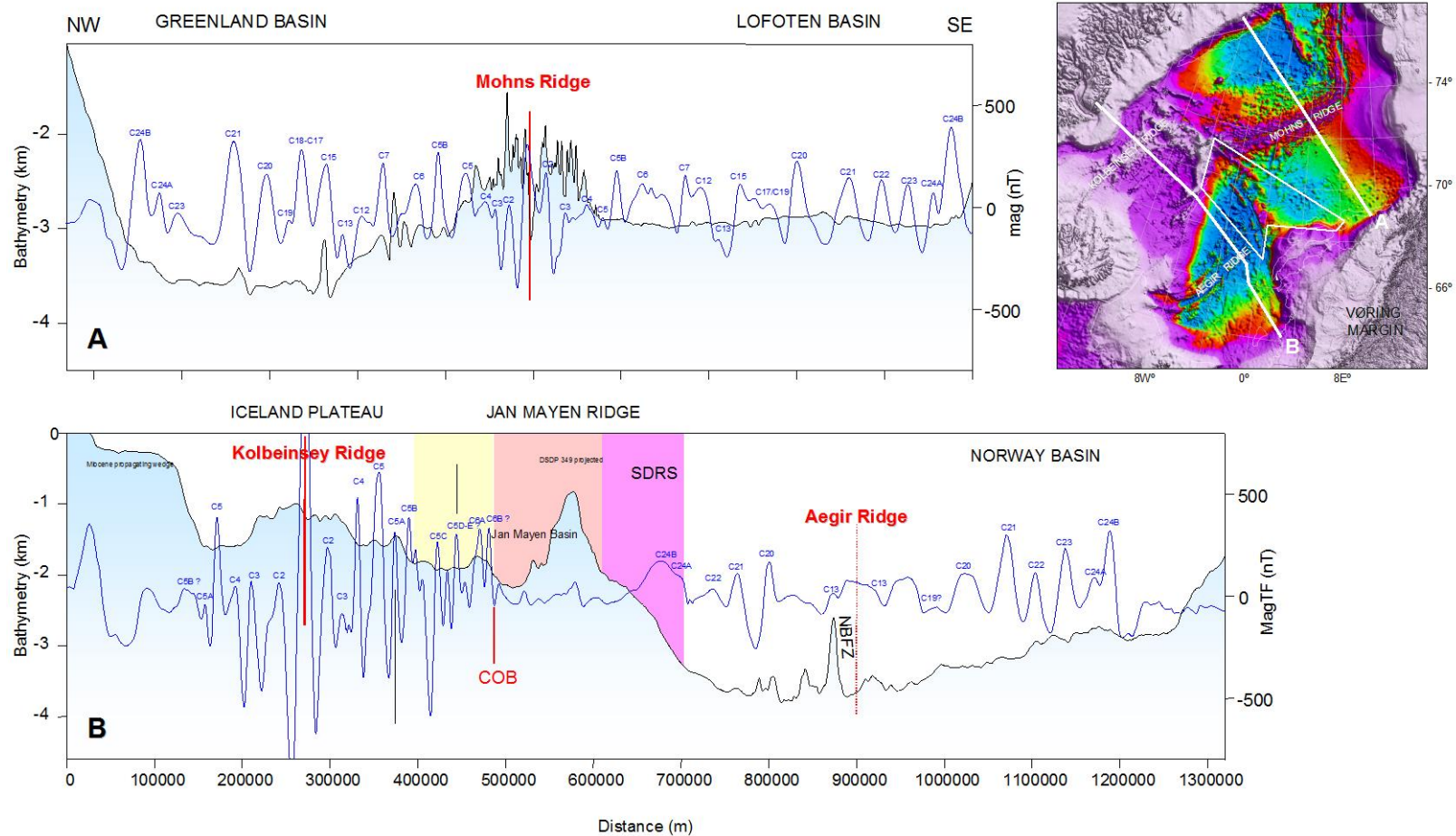


Figure 3.4 Regional bathymetric transects between the main spreading systems located on both side of the JMFZ corridor. Blue curves represent the magnetic anomalies with the interpreted magnetic chronos from C24 to the current or extinct spreading Ridges. The oceanic crust between Norwegian and Greenland Seas can be subdivided into four domains: 1) The Mohns Ridge spreading system along the Greenland Basin and the Lofoten Basin and 2) the aborted Aegir Ridge spreading system, situated west of the Møre Margin and delimited to the west by 3) the Jan Mayen Microcontinent. The microcontinent separates 4) the currently active Kolbeinsey Ridge from the extinct Aegir Ridge. A ridge jump between Aegir Ridge and the Kolbeinsey Ridge occurred progressively between C13 (33.3 Ma) and C6-C7(20-25 Ma).

A fundamental problem about this interpretation is the asymmetry on either side of the Kolbeinsey Ridge. The existence of anomalies 5A and 6C east of the median ridge requires similar anomalies and oceanic crust on the Greenland side. These anomalies are however reduced in amplitude or may be nonexistent (Fig. 3.4). Vogt et al. (1980) attribute the “suppressed amplitudes” of these lineations to crustal heating or erasure of primary magnetization, triggered by deep subsidence and the thick Plio-Pleistocene deltaic accumulation, documented seaward of the mouth of Scoresby Sund (Vogt and Perry 1978).

Between C5 and the current spreading axis C1, the oceanic spreading system is well documented by a clear symmetric magnetic pattern (Fig. 3.4). However, north of the 70°40' Fracture Zone, low magnetic coverage and local artefacts due to interpolation do not allow for accurate calibration of magnetic anomalies.

Kodaira et al. (1998) defined the ocean-continent transition using OBS modelling at the western edge of the Jan Mayen Basin. This ocean-continent transition defined by OBS coincides with the C7?-C6 magnetic anomaly. Within the 10 km wide transition zone, crustal velocities increase towards the west and approach the velocities of the oceanic crust obtained along the Iceland Plateau, that is 3.8–5.1 km/s (oceanic layer 2A), 5.9–6.5 km/s (oceanic layer 2B) and 6.8–7.3 km/s (oceanic layer 3). The crustal model indicates thin oceanic crust (5 km) immediately oceanwards of the ocean/continent transition zone. Beneath the Iceland Plateau, the oceanic crust is thicker (11 km) than the typical thickness of normal oceanic crust (usually around 6-7 km). This might imply that the oceanic crust at the Iceland Plateau has been generated by anomalous accretion (over-accretion) or late underplating.

3.6 Aegir Ridge

The Aegir Ridge should be considered as the equivalent of the modern Reykjanes or Kolbeinsey Ridge in relation to the paleo-Iceland mantle anomaly (Figs. 3.1 and 3.4). The Aegir Ridge lies from the Greenland-Iceland-Ridge to the south to the CJMFZ in the north. To the north, the ridge is obliquely (~60°) truncated by the CJMFZ (Fig. 3.1). However, the interaction between the spreading ridge and the fracture zone is not clear. The rift valley could have formed a complex “en échelon” spreading system between the CMFZ and the EMFZ.

Opening rates along the Aegir Ridge ranged from 8 mm/a near Iceland to 13 mm/a in the northern Norway Basin during the period 55-36 Ma (C24-C16), but must have decreased to lower rates and then down to zero at around 25 Ma (C7), the probable time for ridge extinction. This differential accretion rate could explain the fan-shaped pattern of the Norwegian Basin (Vogt et al. 1970).

The Aegir Ridge rift valley ranges from 40 to 50 km in width, somewhat wider than most active slow-spreading ridges. Partially sediment-filled, the basement valley is up to 2500-3000 m

deeper than the adjoining ridge flanks and has also a greater relief than usually seen at slow-spreading active ridges (Jung & Vogt 1997). Jung and Vogt (1997) attribute the wide, deep valley to slow spreading and possible slow extension after spreading ceased. The southern Aegir Ridge is oblique to the opening direction, but individual rift valley wall escarpments are normal to the calculated opening direction.

4 INTERPRETATION METHODS

Jörg Ebbing

4.1 Euler Deconvolution

The Euler 3-D deconvolution method (Reid et al. 1990; Geosoft 2005) was used to estimate the depth to magnetic rocks within the oceanic basement. The depths to the magnetic sources can constrain the interpretation of the basement anomalies and aid in the separation of anomalies (e.g. Olesen et al. 2003).

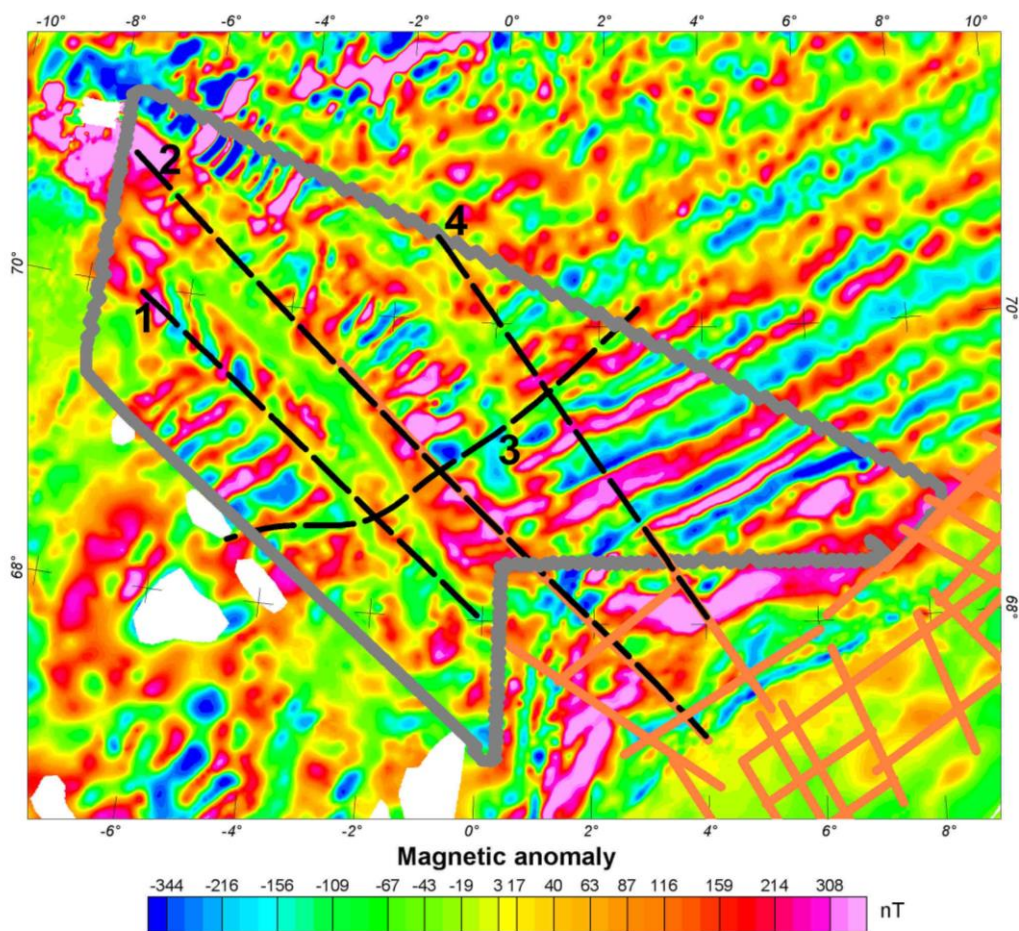


Figure 4.1 The study area: Total magnetic field anomaly and the location of the three interpreted transects. The orange line denote the location of OBS lines in and adjacent to the study area (Mjælde et al. 2005 and references therein).

Euler's homogeneity equation relates the potential field (either magnetic or gravity) and its orthogonal derivative components to the location of the source, given an assumed rate of change of the field with distance. This rate of change (degree of homogeneity) can be interpreted as a

structural index describing the form of the source structure (Thompson 1982). The method is applicable to anomalies caused by a wide variety of geological structures and being independent of remanent magnetisation and ambient field direction.

We applied the 'Located Euler 3D method' to resolve the source depth of the magnetic field making use of the analytic signal to locate edges of the magnetic field sources. The Blakely & Simpson (1986) grid peak-picking algorithm locates the crest of the analytic signal anomalies improving the location of the depth estimates. The window size for this analysis is determined from the location of the adjacent anomaly inflection points. The Located Euler method produces fewer solutions than the Standard Euler method and the spray-pattern of source positions commonly observed in Euler depth solutions is avoided.

We calculated the Located Euler Deconvolution for SI of -0.5 (thick step), -1 (sill/dyke), -1.5, -2 (pipe) and -3 (sphere). For the thick step geometry most of the solutions are located in the seawater or the sediments. In Figs. 4.2 and 4.3 the depth solutions for SI=-1 are presented. The depth of the solutions varies between 3 and 7 km. The shallow solutions are mostly present, where the magnetic anomalies are not clearly observable, while the deep solutions (>6 km) correlate with clear reversal anomalies.

4.2 Forward modeling

The 2.5 modelling was carried out with an Interactive Gravity and Magnetic Application System (IGMAS; <http://www.gravity.uni-kiel.de/igmas>). The three transects, which have been modelled are shown in Figs. 4.1-4.4. For all the transects we decided to use a start density structure as shown in Table 1.

Table 4.1 Densities for structures in the 2.5D models. The water density is used in modelling the Free-Air/Bouguer anomaly, respectively.

| Structure | Density [Mg/m ³] |
|----------------|------------------------------|
| Water | 1.03/2.2 |
| Sediments | 2.1 |
| Upper basement | 2.75 |
| Lower Basement | 2.9 |
| Mantle | 3.3 |

In addition to the crustal structure we discuss below, we did also consider the density variation in

the mantle with distance to the continent-ocean boundary and the spreading ridge, respectively. This result could certainly be refined by removing the long-wavelength gravity signal in respect to the age of the oceanic floor (e.g. Chapell and Kusznir et al. 2005). We did not apply the method in the present study, as the analysis of the magnetic sources was the main focus of our interpretation.

To model the magnetic signature we introduced blocks of normal and inverse remanent magnetisation in the upper basement with varying susceptibilities and Q-ratios, as described for the four profiles in the reminder. The underlying lower basement has a constant susceptibility of 0.01 and a Q-ratio of 2, while the water is nonmagnetic and the sediments low-magnetic (susceptibility 0.0002). The depth to Curie temperature is calculated to be at a depth of 12.5 km, implying that the mantle is in general not contributing to the magnetic signal.

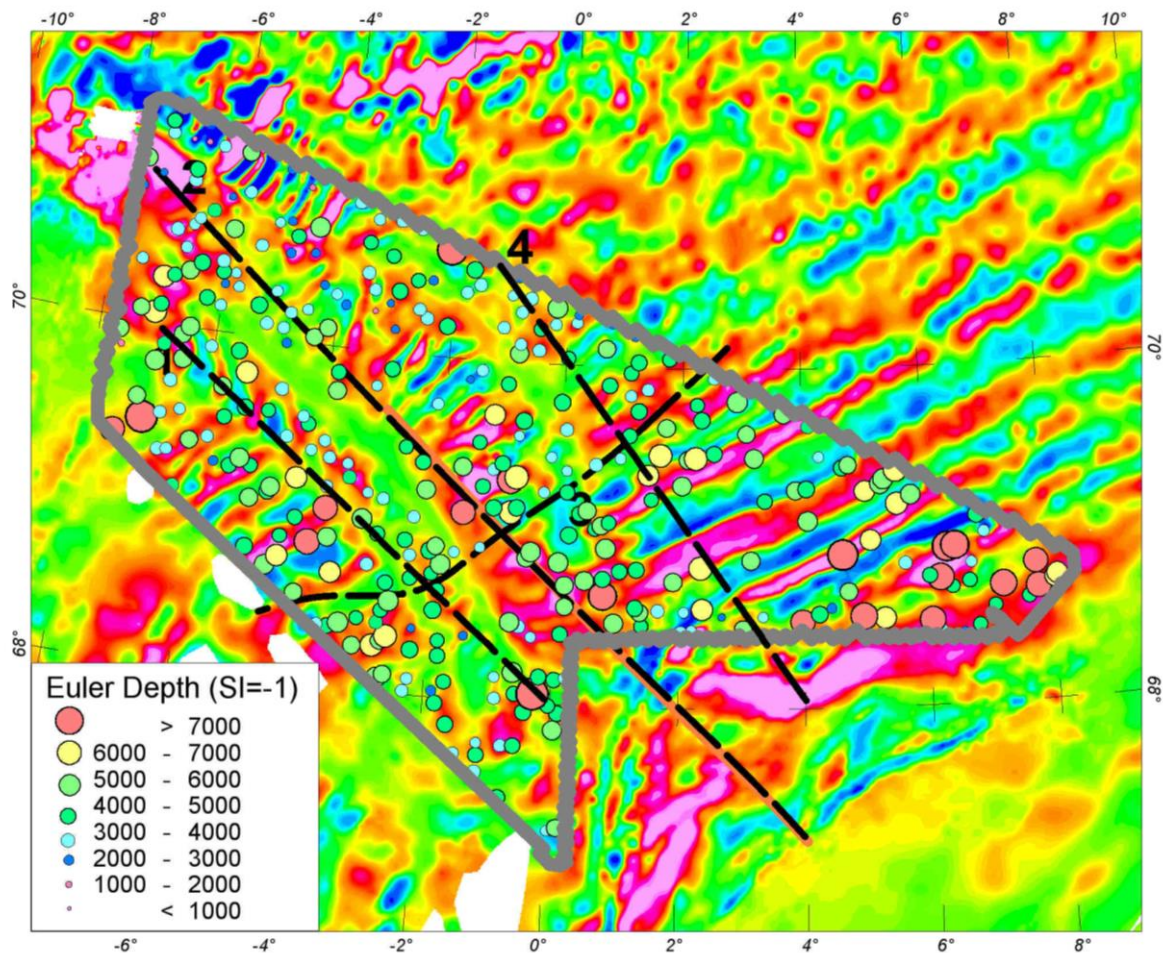


Figure 4.2 Source depth of Located Euler deconvolution for $SI=-1$ (dyke). The deep solutions are mainly located in areas with clear observable magnetic reversals, pointing to a source at the boundary between inverse and normal polarised magnetic domains. The solutions have been limited to solutions with a horizontal and vertical uncertainty less than 15 %.

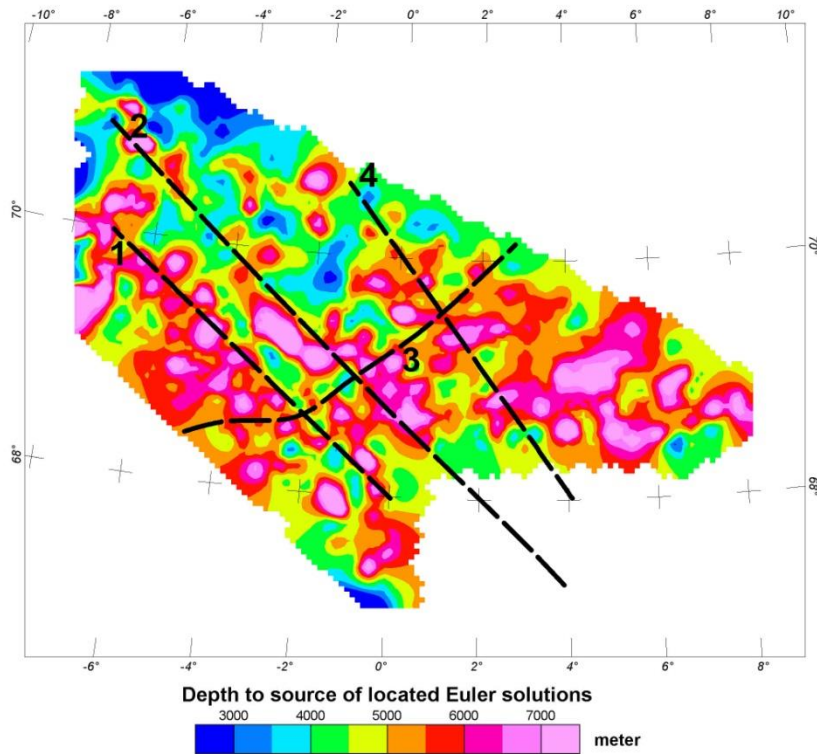


Figure 4.3 Gridded source depth Located Euler deconvolution for $SI=-1$ (dyke). The depth map is based on the source depth solutions in Fig. 4.2.

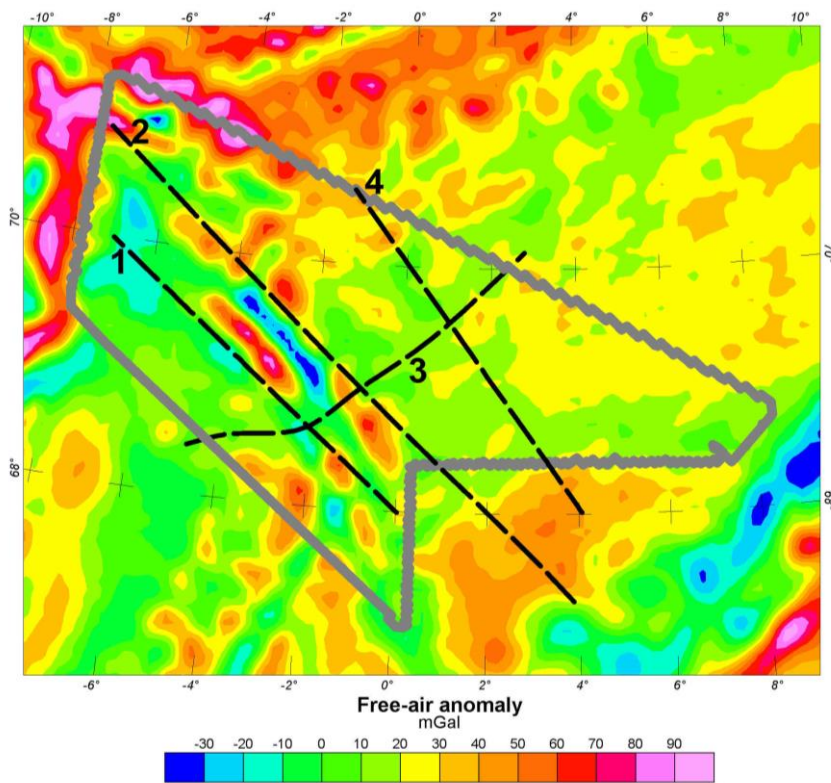


Figure 4.4 Free-air anomaly of the Jan Mayen Survey area.

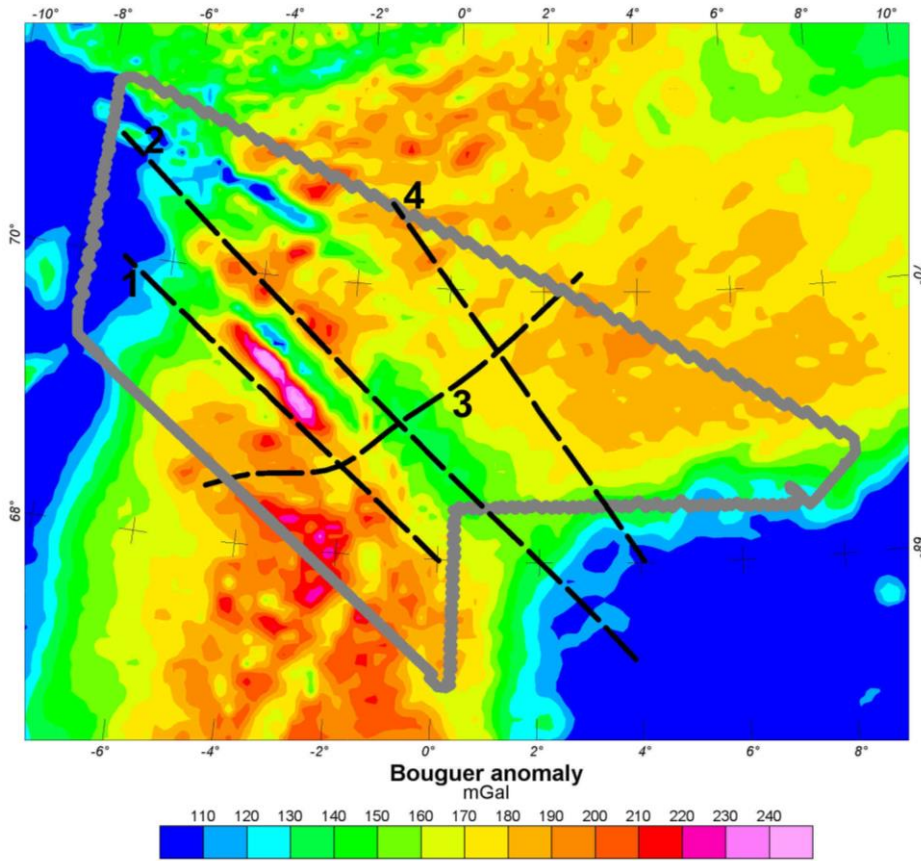


Figure 4.5 Bouguer anomaly of the Jan Mayen Survey area. For the Bouguer plate reduction a density of 2.200 Mg/m³ has been used.

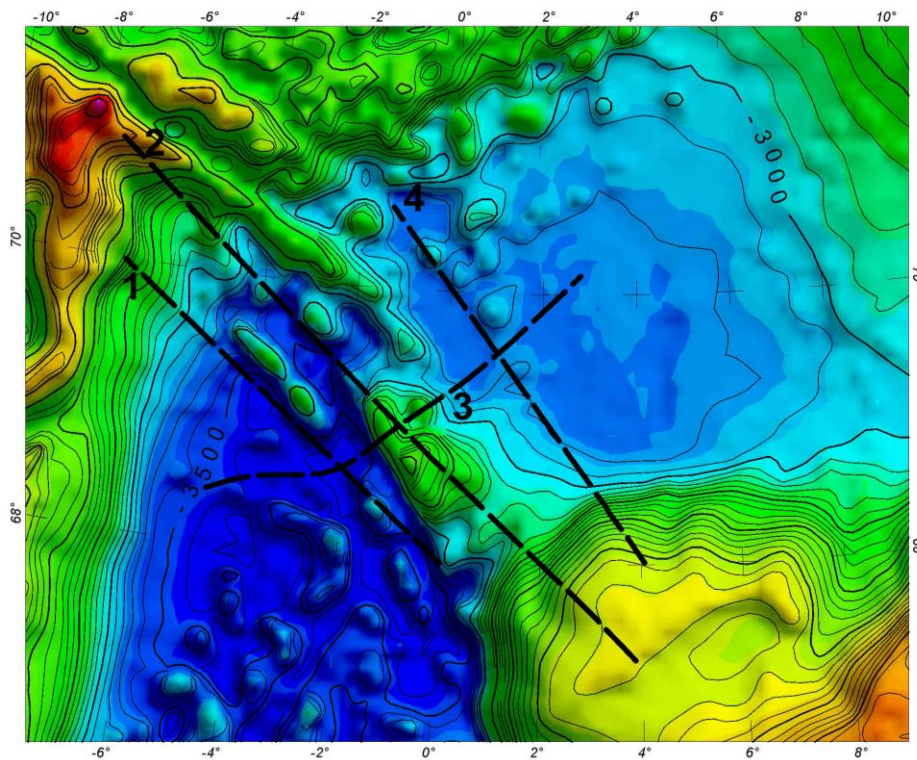


Figure 4.6 Bathymetry (IBCAO) and profile location.

4.3 Depth to magnetic sources

As the modelled profiles will show, one problem of using the Euler deconvolution in the oceanic domains is, that the reversed polarisation of remanent magnetisation in the basement is causing the main magnetic signals. The sequence of changing polarisation causes the main change in magnetic properties to occur at the side at the crustal blocks and not at the top. Therefore, the depth solutions of the Euler Deconvolution give relatively shallow results at the top and relatively deep results at the side of the magnetic blocks. However, without knowledge of the geometry of the crustal blocks the different sources cannot be distinguished. Where the reversal pattern is not preserved, the deep solutions disappear and the solutions focus more on the top of the basement. However, using Euler Deconvolution depth in interpreting the top basement for the oceanic crust gives less well-defined results than for the continental crust. We have performed 2.5D modelling of the density and magnetic structure to gain further insights into the crustal properties in the study area.

4.4 Transect 1: the southern NW-SE line

Along the southern transect seismic interpretation of the top basement and the faults have been used to model the upper crustal density structure. To explain the differences between the gravity effect of the sediments and the Bouguer anomaly, the crust-mantle boundary and the density distribution in the mantle has to be modelled. The modelled geometry (Fig. 4.7) adjusts the Bouguer anomaly and leads to an isostatically compensated model.

The modelled faults and the polarity changes in the magnetic field have then been used to introduce the magmatic blocks in the upper basement (Fig. 4.8). The magnetic susceptibility of the upper basement varies in the blocks between 0.01 and 0.02 SI with Q-ratios from 1 to 4. The modelled values are in agreement with the magnetic properties of igneous rocks in the Vøring area from the Deep Sea Drilling Project (DSDP) and Ocean Drilling Project (ODP) in 1974 and 1985 (Kent & Opdyke 1978, Eldholm et al. 1987).

In the central part of the profile the Moho is located at a depth of 12.5 km and is deepening either side. To the west of the shallow Moho the reversals in the polarisation can be clearly identified. To the east the magnetic signal is less clear and consequently more difficult to interpret.

4.5 Transect 2: the central NW-SE line

The central northwest-southeast line we modelled is located along the OBS Line11 presented in Breivik et al. (2005). The interpretation of the OBS experiments provides some control on the geometry of the Moho and the top basement (Fig. 4.9). While modelling the free-air anomaly it is obvious that certain offsets can only be explained by 3D side effects of the bathymetry (see

also profile location and bathymetry in Fig 4.6). Therefore, the model adjustment was done relative to the Bouguer anomaly. The top basement is generally located in a depth of 4-5 km, with 1.5 to 2.5 km overlying sediments. An area of thick crust can be observed at the northwestern end of the profile, bounded by two local highs in the Bouguer anomaly.

The area of the thick crust is the area where the magnetic signature shows the most variations in amplitude and reversals (Fig. 4.10). Here the spreading anomalies have persisted, despite the interpretation of large-volume magmatic underplating in the lower crust (Breivik et al. 2005) Further to the northwest the spreading anomalies are less distinct and secondary processes might have demagnetised the upper basement.

To model the magnetic signature we introduced blocks of normal and inverse remanent magnetization in the upper basement. The magnetic susceptibility of the upper basement varies in the blocks between 0.01 and 0.02 SI with Q-ratios from 2 to 5.

Correlating the blocks of normal and reverse polarisation between the cross-sections is difficult as no continuous features between the two lines can be identified in the potential field data. Also the bathymetry shows a clear change between the two lines. The third line illustrates this problem.

4.6 Transect 3: the cross-line

The third line is a southwest-northeast oriented line crossing the other lines and illustrates the changes from south to north in the study area. We concentrated on the modelling the density structure, as the profile is located parallel to the magnetic anomalies. Therefore, 2D or 2.5D magnetic modelling would certainly not lead to reasonable results. The density model we present is also constrained by the cross-points with the other interpreted sections (Fig. 4.11).

The free-air gravity is first of all affected by the bathymetry, which is c. 100 m deeper in the south, than in the north. The step in bathymetry is also correlating with a prominent signal in the Bouguer anomaly, indicating isostatic compensation. In the modelled section the area of shallow bathymetry shows a deep Moho (~16 km). This area of deep Moho between profile km 40 and 140 certainly is an important tectonic feature.

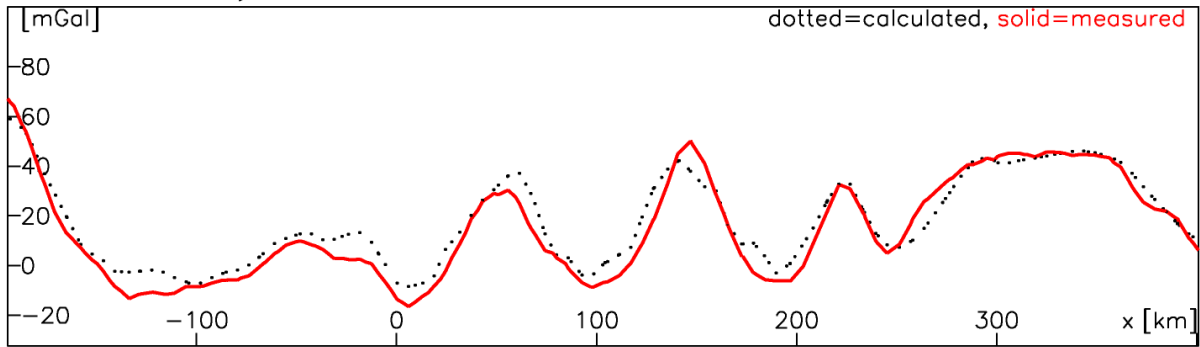
4.7 Transect 4: The northern NW-SE line

The last interpreted line is located in the northern part of the study area, where the sea-floor spreading anomalies can be clearly observed. Hence, less secondary tectonics overprinted the magnetic signal. The south-easternmost part of the profile is constrained by the results of the OBS line 2-96 (Fig. 4.12; Mjelde et al. 2003): on the magnetic anomaly map (Fig. 4.1) the area is visible with a broad positive magnetic anomaly. However, on the profile the magnetic anomaly

looks similar to the sea-floor spreading anomalies along the rest of the profile, only with a higher base-level (Fig. 4.13).

First we modelled the Bouguer anomaly, which is rather flat before it decreases smoothly from 160 mGal to 100 mGal, correlating with the increase of depth to Moho as observed in the OBS study. The magnetic model takes again the geometry of the density model and applies magnetic parameters to the structures. Most of the anomalies can be modelled with a simple series of blocks with normal and reversed magnetization. However, the anomaly at the eastern end of the profile cannot be modelled with such a simple structure. The overall positive anomaly requires a broad block of normal magnetization. However, the central minimum requires an additional reversed magnetized body on top of the structure. The reversed magnetized body cannot be explained by magnetization during the opening, but can be explained by magnetization related to a complex of seaward dipping reflectors or secondary intrusion of magnetic material.

Free-air anomaly



Bouguer anomaly

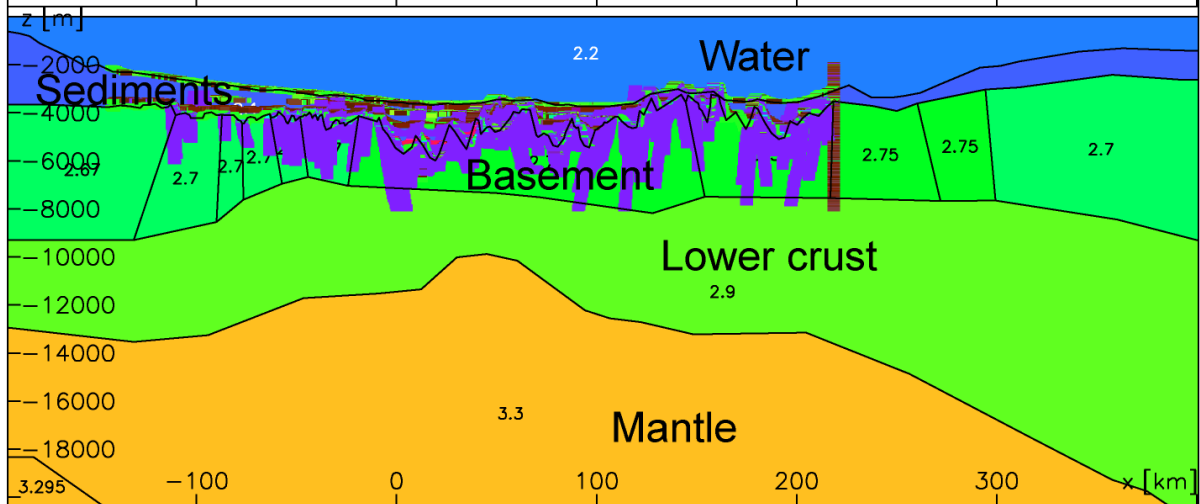
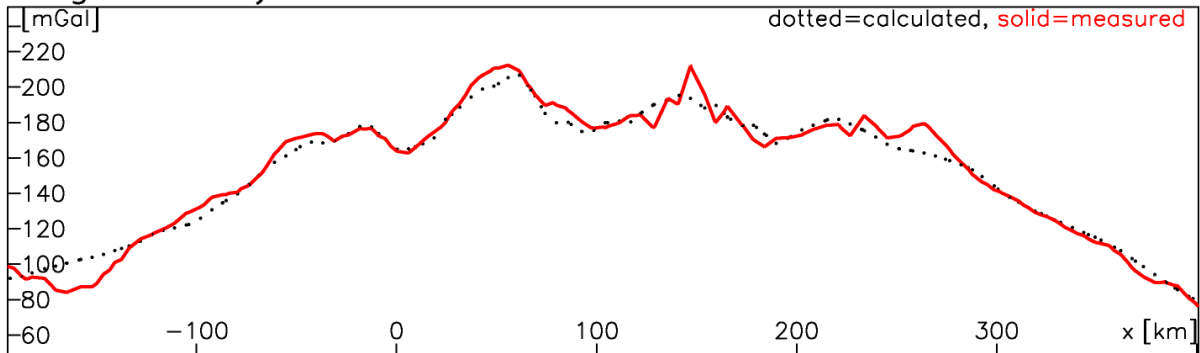


Figure 4.7 Density structure along Line 1. The upper panels show the modelled and observed Free-air and Bouguer anomaly. The lower panel shows the density model (densities in Mg/m^3) and the depth-converted shallow seismic interpretation.

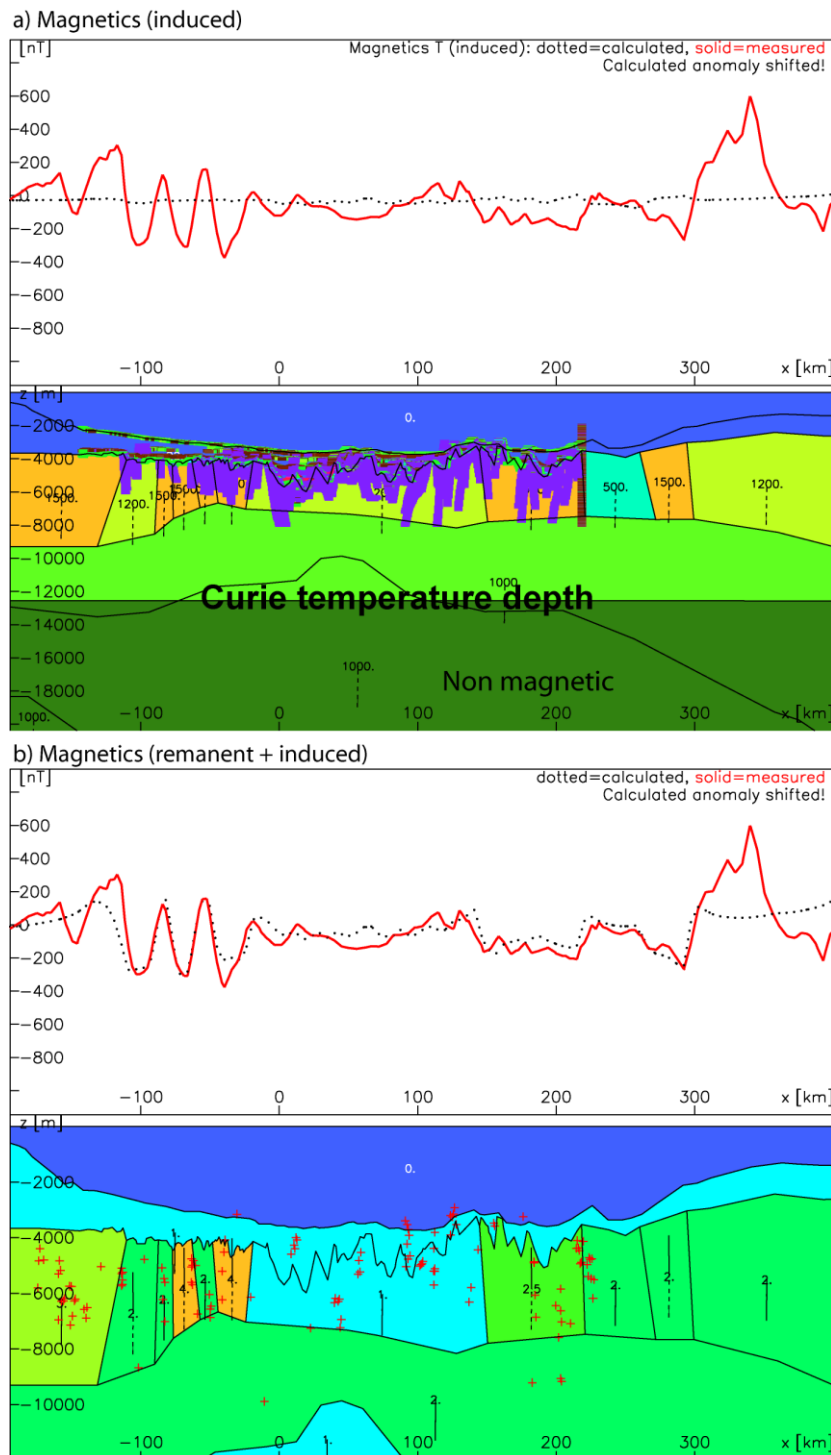


Figure 4.8 Magnetic model along Line 1. a) The upper panels shows the modelled induced and observed total magnetic field anomaly. The lower panel shows magnetic susceptibilities in 10^{-5} SI. Below the drawn depth to Curie temperature the model is featuring non-magnetic material. b) The upper panels shows the modelled induced + remanent and observed total magnetic field anomaly. The modelled field is generated by the geometry and Q -ratios shown in the lower panel and the susceptibilities shown in (a). Arrows next to the magnetic properties indicate the directions of induced and remanent magnetisation. In addition shown are the located Euler-depth solutions (red-crosses).

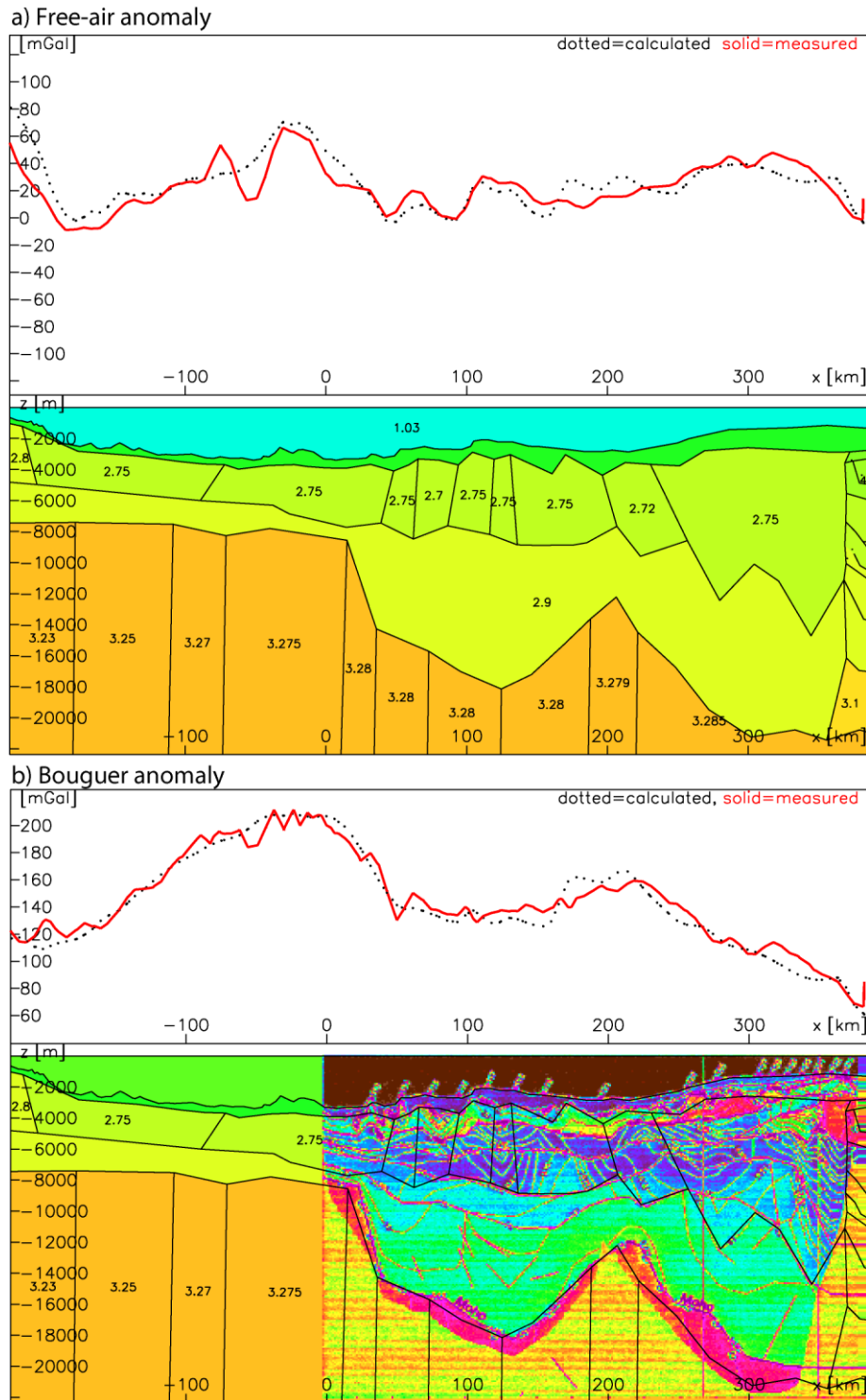


Figure 4.9 Density structure along Line 2. a) The upper panels show the modelled and observed free-air and the lower panel the density structure (densities in Mg/m³). b) The upper panels show the modelled and observed free-air and the lower panel the same density structure as in (a) and the colour-coded OBS velocity model by Breivik et al. (2005) as an overlay.

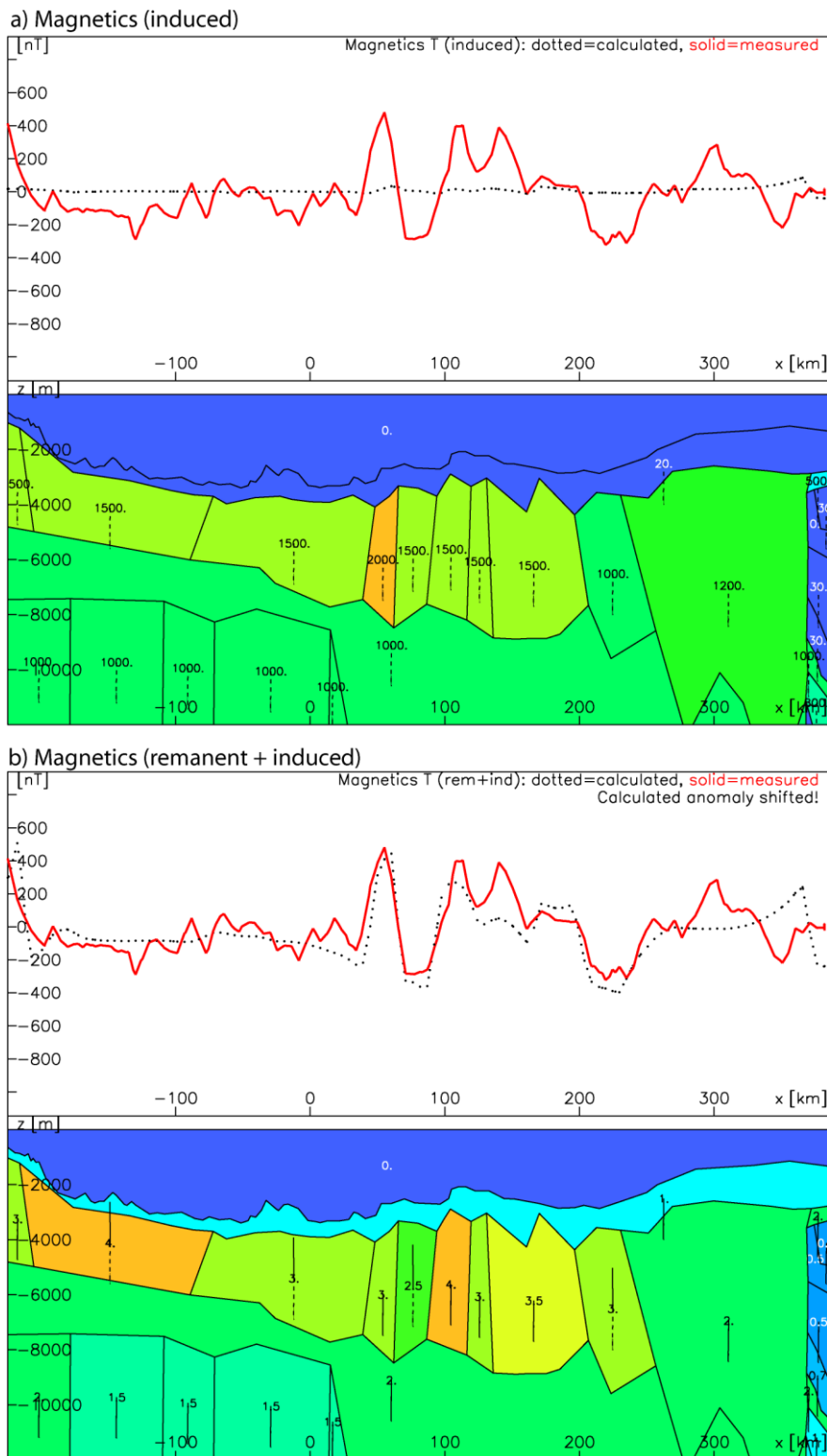
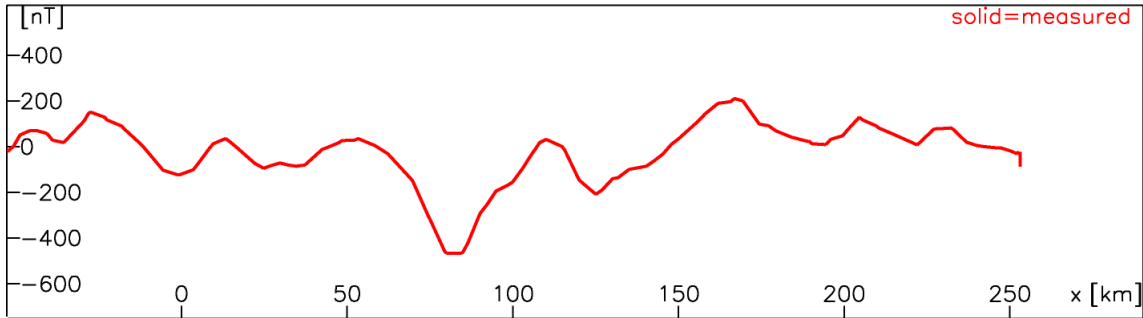
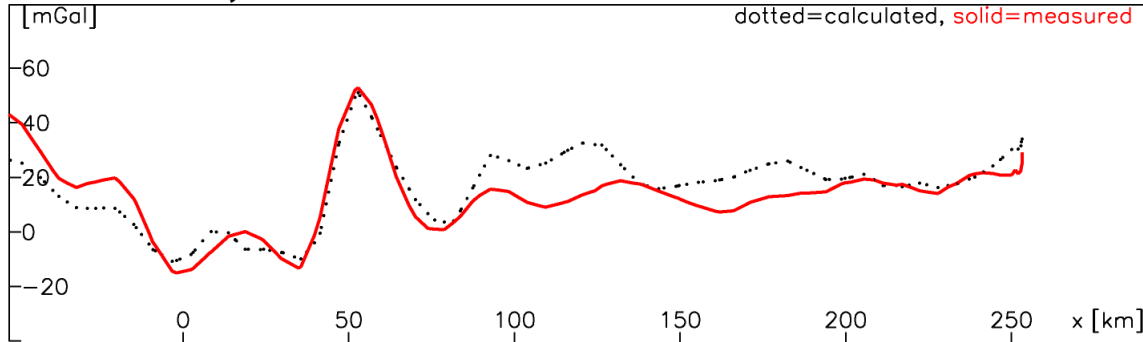


Figure 4.10 Magnetic model along Line 2. a) The upper panels shows the modelled induced and observed total magnetic field anomaly. The lower panel shows magnetic susceptibilities in 10^{-5} SI. Below the drawn depth to Curie temperature the model is featuring non-magnetic material. b) The upper panels shows the modelled induced + remanent and observed total magnetic field anomaly. The modelled field is generated by the geometry and Q -ratios shown in the lower panel and the susceptibilities shown in (a). Arrows next to the magnetic properties indicate the directions of induced and remanent magnetisation.

Magnetic anomaly



Free-air anomaly



Bouguer anomaly

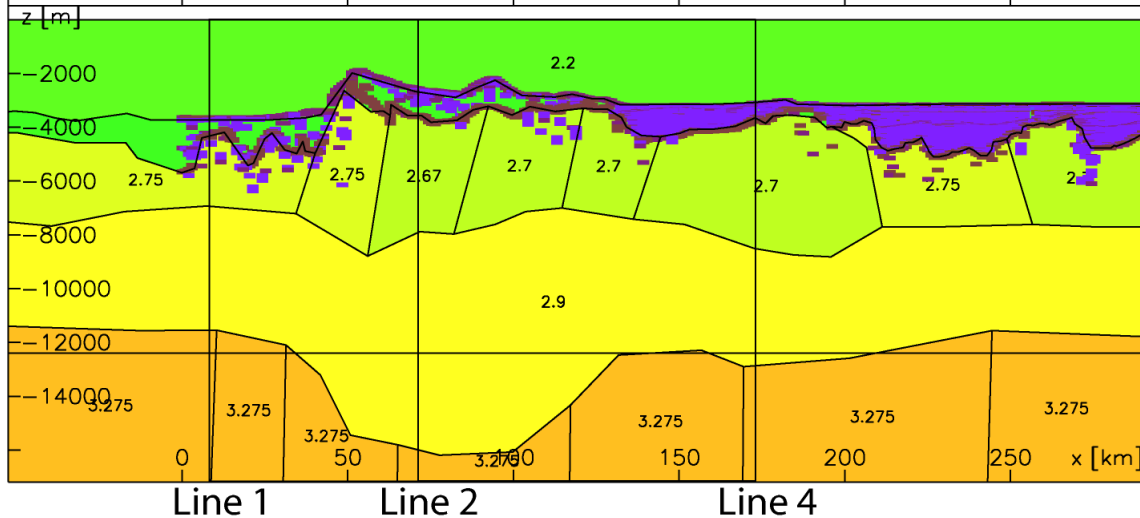
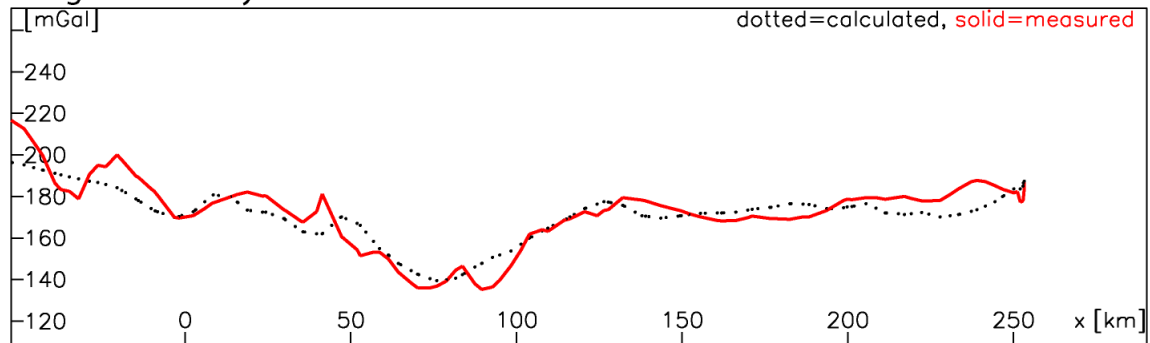
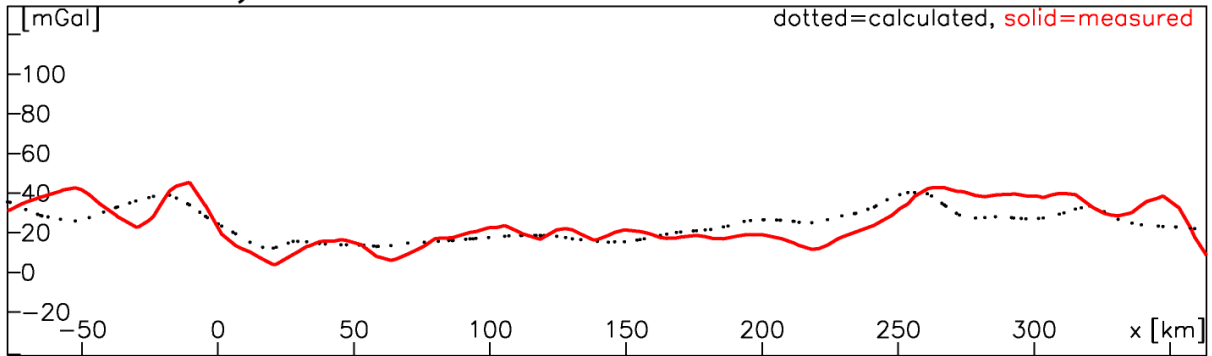


Figure 4.11 Density structure along the Cross-line 3. The upper panels show the observed magnetic anomaly, and the central ones the modelled and observed free-air and Bouguer anomaly. Lower panel shows density structure (densities in Mg/m^3) and depth-converted shallow seismic interpretation.

Free-air anomaly



Bouguer anomaly

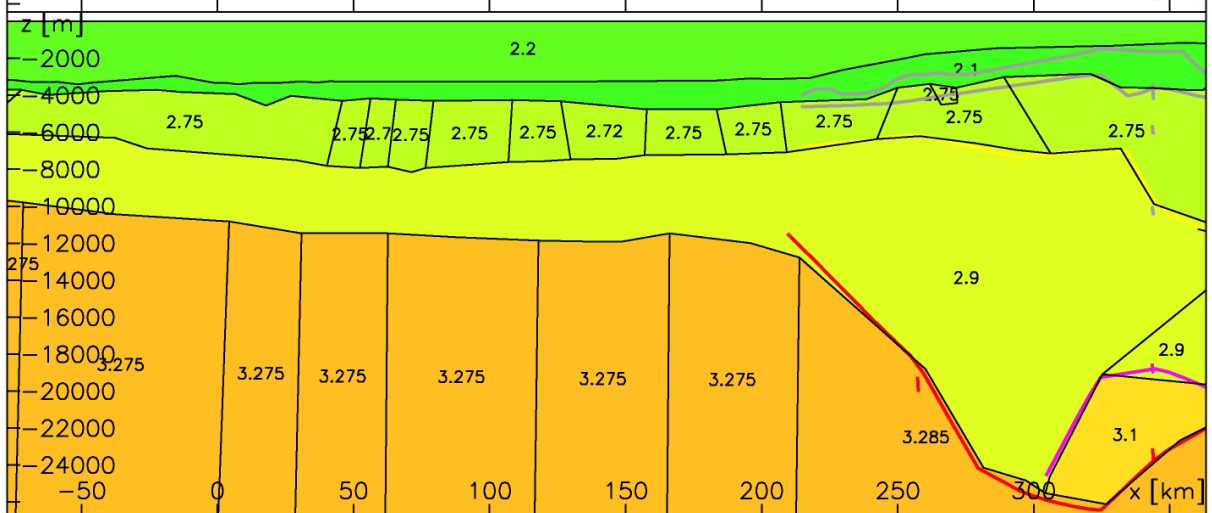
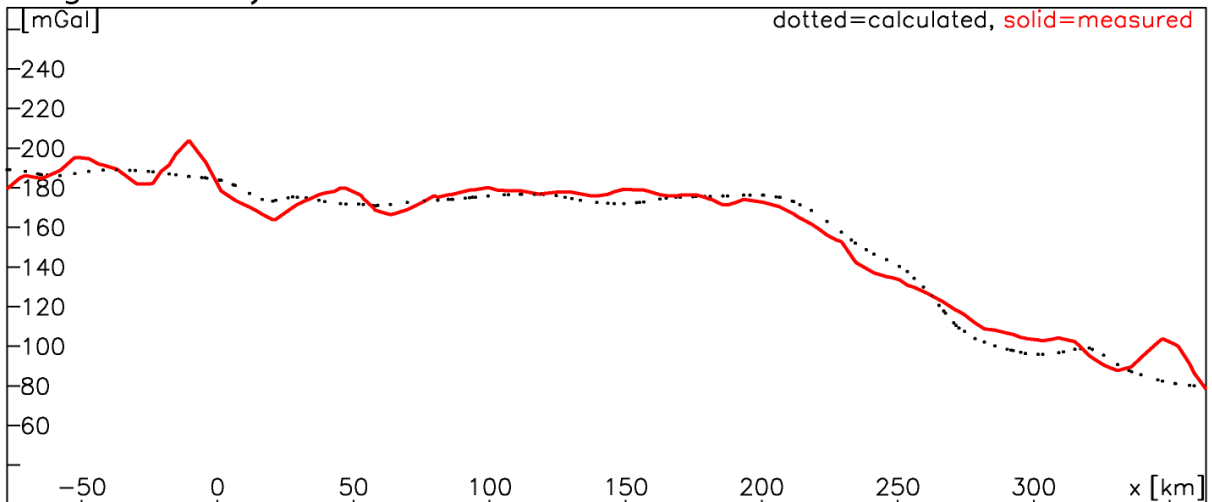


Figure 4.12 Density structure along Line 4. The upper panels show the modelled and observed Free-air and Bouguer anomaly. The lower panel shows the density model (densities in Mg/m³) and the coloured lines refer to the OBS model L2-96 (Mjelde et al. 2003).

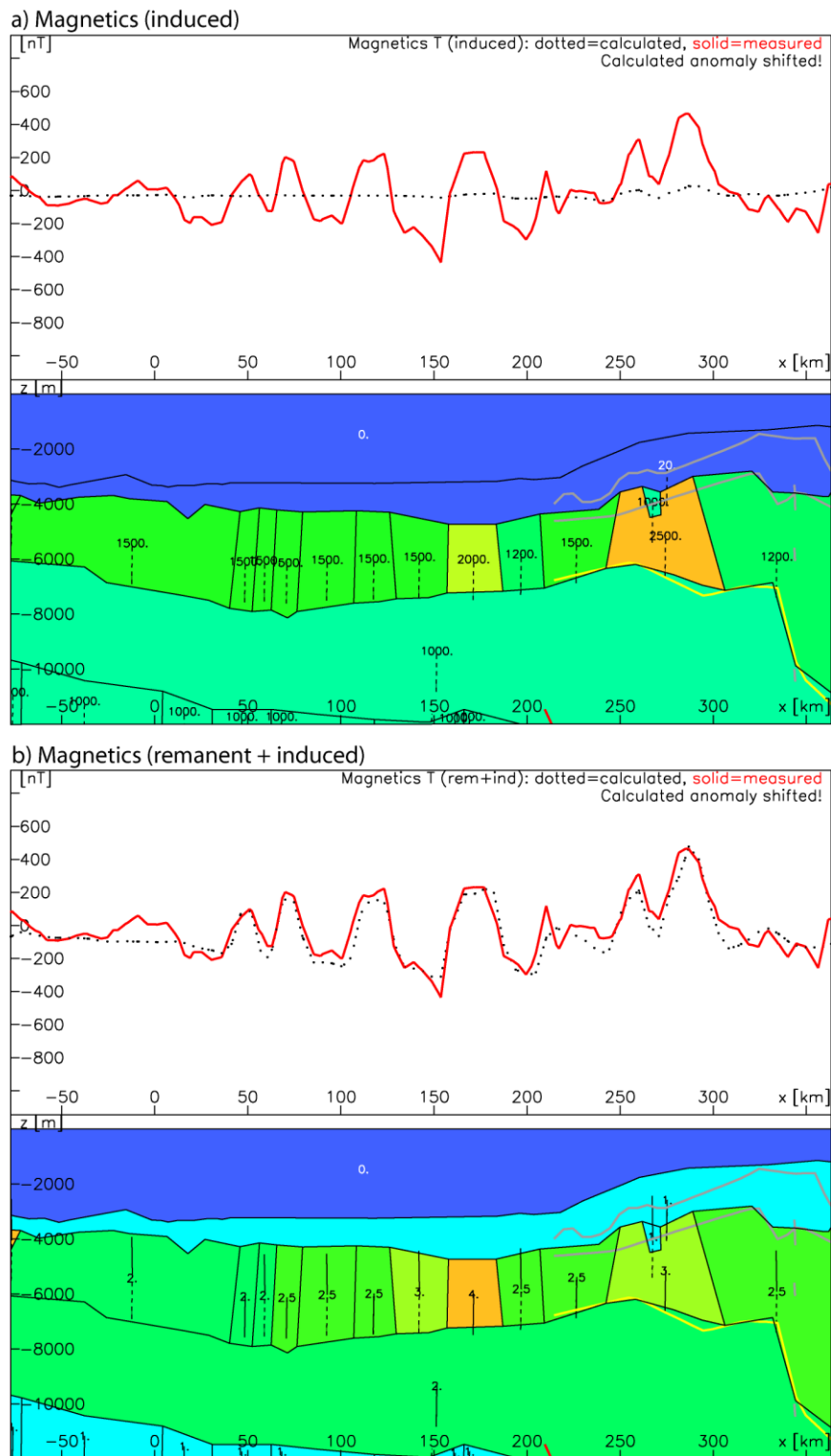


Figure 4.13 Magnetic model along Line 4. a) The upper panels shows the modelled induced and observed total magnetic field anomaly. The lower panel shows the magnetic part of the model with magnetic susceptibilities in 10^{-5} SI. b) The upper panels shows the modelled induced + remanent and observed total magnetic field anomaly. The modelled field is generated by the geometry and Q -ratios shown in the lower panel and the susceptibilities shown in (a). Arrows next to the magnetic properties indicate the directions of induced and remanent magnetisation.

4.8 Discussion and conclusion

The forward potential field modelling of the area of the Jan Mayen Survey is limited, because of the few constraints available. Gravity and bathymetry show already that lateral inhomogeneities exist in the area, indicating later tectonic events in addition to the general opening of the North Atlantic. However, as only OBS results along one line through the study area and to the east exist, the interpretation of the density structure is ambiguous. We decided to model only the known topography and adjust an inner basement horizon for intermediate wavelength and the Moho for long-wavelength in the gravity field. Afterwards we tested the isostatic state of the cross-sections, which lead to satisfying results.

However, focus was given to the magnetic modelling with the assumption that the main magnetic field can be related to sea-floor spreading. The modelling shows that the series of blocks with reversed and normal magnetization with minor changes in susceptibility or Q-ratio is sufficient to explain the observed magnetic field. In addition to the direction of magnetisation the geometry of the top basement is important. Correlation with shallow seismics can help to model the top basement and the location of the main faults, bordering the blocks. Inverse methods like Euler-deconvolution do however, not lead to satisfying results, as the main contrast is located at the side of the sources and not at the top or base. This makes the proper use of Euler-Deconvolution for marine magnetic anomalies difficult.

Evidence for a secondary influence on the magnetic field is only given for the northernmost line 4 (Figs. 4.12 & 4.13). Here, a vertical superposition of different magnetized bodies is necessary to explain the magnetic anomaly. Hence, here a secondary effect as (sill?) intrusion must be found to match our observations.

5 THE JAN MAYEN FRACTURE ZONE: COMPLEX MORPHO-STRUKTURE, GRAVITY AND MAGNETIC SIGNATURE

Laurent Gernigon

In this chapter, we describe the preliminary interpretation of the Jan Mayen Fracture Zone (JMFZ) based on bathymetric, gravity and magnetic and available seismic dataset. Particularly, the description and interpretation focus on the eastern part of the system lying along JMFZ aeromagnetic survey area. The main faults zones and the magnetic anomalies have been interpreted using a systematic comparison between bathymetry, gravity, magnetic patterns and available seismic data. The interpretation is however limited due to poor magnetic coverage in the Norway Basin, south of the Jan Mayen Survey. Structural analysis is also relatively speculative after C13 since we don't have any seismic data across this area.

5.1 Fracture zones, transform faults and JMFZ

North Atlantic oceanic ridges (and their associated spreading centres) are usually offset along their trend by fracture zones. These are ridges and valleys on the order of tens of kilometers wide that cut across the crests of the ridges at approximately right angles and offset their trend. Typically, a regional depth offset is present across a fracture zone, owing to the juxtaposition of crust of different ages (and, therefore, depth and subsidence) across it.

Strictly speaking, a portion of a fracture zone between different offset spreading centers constitutes a transform fault (Fig. 5.1). Faults of this kind are the only segments of fracture zones that are seismically active. Morgan (1968) was one of the first to propose that opposing plates along an oceanic ridge crest offset by fracture zones are divided by the spreading centres and transform faults. The inactive portions of the fracture zone on the ridge flanks (so called inactive fracture zones) are scars on the ocean floor created in the transform faults.

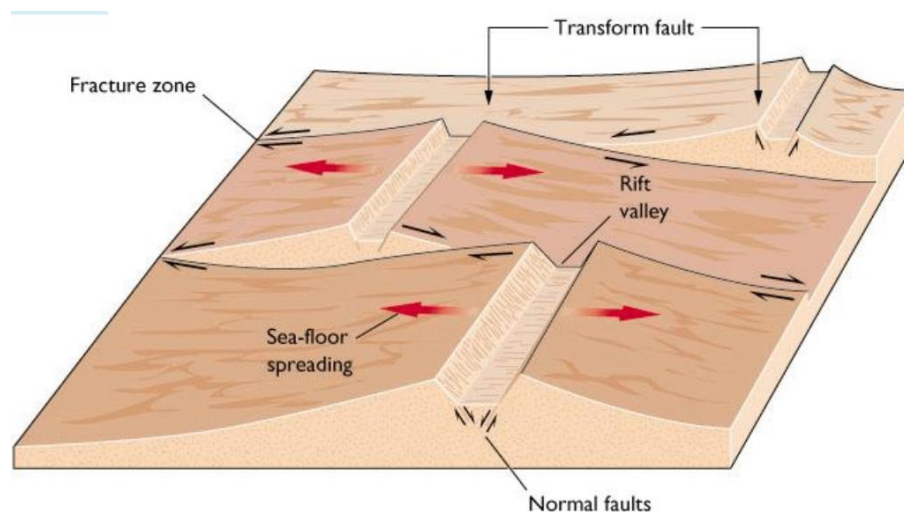


Figure 5.1 Schematic diagram illustrating the concepts of transform fault and fracture zone in the strict sense.

The JMFZ represents such a complex zone including both active transform faults offsetting the mid-oceanic spreading axis (active now between the Mohns and Kolbeinsey Ridges) and inactive fracture zones.

The JMFZ includes 3 major bathymetric segments informally named western, eastern and central Jan Mayen Faults Zones (WJMFZ, EJMFZ, CJMFZ) by Skogseid and Eldholm et al. (1989). This system defines an oceanic "tectonic corridor" between the Lofoten Basin and the Greenland Basin to the north and the Icelandic Plateau and the Norwegian Basin to the south (Fig. 3.1 and 5.2).

A southern fracture zone, the Norwegian Basin Fracture Zone is also expected in the Norwegian Basin (Skogseid & Eldholm 1989) but could be part of a more complex fault system described near the Aegir Ridge (Jung & Vogt 1997). Mapping of this fracture is not so obvious because the magnetic data in this area are extremely sparse and misinterpretations can be easily made.

Rates

5.2 Internal physiography and segmentation

Large scale segmentation

Regional maps (Fig. 5.2) and a set of cross-sections suggest a number of regional patterns. According to bathymetry and gravity, recompiled in this study, the JMFZ corridor can be divided in two main lateral segments :

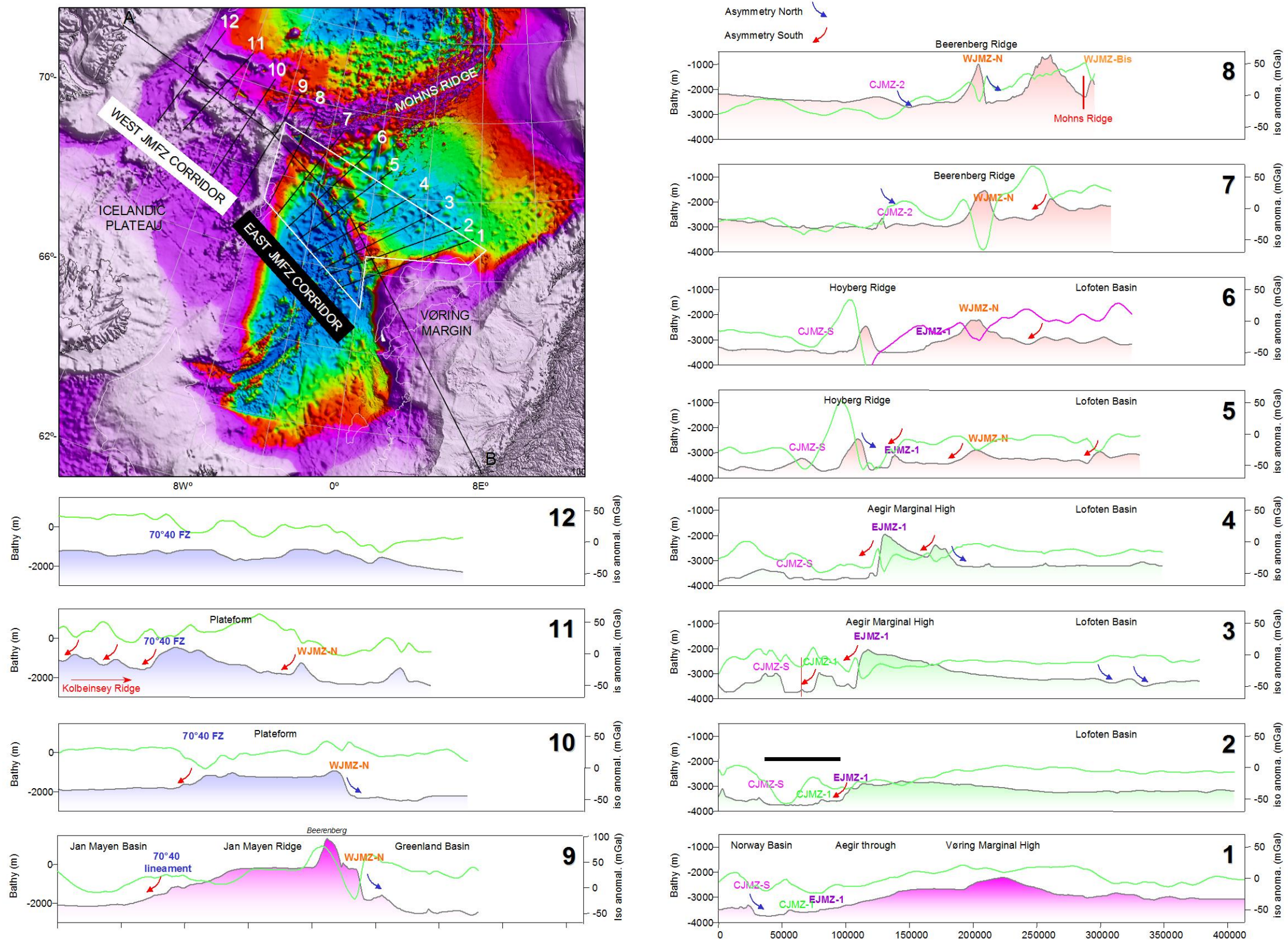


Figure 5.2 Bathymetric and gravity transects (isostatic anomalies) along the whole Jan Mayen Fracture Zone. CJMFZ: Central Jan Mayen Fracture Zone; EJMZF: East Jan Mayen Fracture Zone; WJMZ: West Jan Mayen Fracture Zone. The transects illustrate the complex physiography of JMFZ corridor divided in two main segments (West JMFZ corridor and East JMFZ corridor) at the level of Jan Mayen. The aeromagnetic survey covers most of the East JMFZ corridor). Inside the East JMFZ corridor, both symmetric or asymmetric bathymetric feature can be observed and suggest lateral sub-segmentation of the corridor.

1) The *East JMFZ corridor* between the Vøring Marginal High and the Jan Mayen Ridge. Bathymetry varies appreciatively from 2000 m to the east to 3500 m in the western part of the segment. The Jan Mayen Aeromagnetic Survey 2005 (JAS-05) covers most of this area, which is mainly described in the following description.

2) The *West JMFZ corridor* between the Jan Mayen Ridge and the Greenland Margin. Here, bathymetry is shallower ranging from 0 m (Jan Mayen Iceland coastline) to 1700 m across the Kolbeinsey spreading system.

Sub-segmentation

Inside the two segments, the bathymetry suggests a complex oceanic pattern and a sub-segmentation as well (Figs. 5.2 and 5.3):

-Along the *West JMFZ corridor*, the bathymetry reflects morphological changes between the East Greenland margin, the Jan Mayen Ridge and the Kolbeinsey spreading system. The shallowest bathymetry coincides with the coastline of the Jan Mayen Island, lying at the intersection between the Mohns Ridge and the active transform fault. Compared to the East JMFZ corridor, it represents a shallow platform, where the Kolbeinsey Ridge develops in the central part. The platform is clearly bounded by the WJMFZ and the 70°40' Fracture Zone.

- Along the *East JMFZ corridor*, bathymetry and gravity reveals a more complex pattern. Close to the Jan Mayen Ridge, the bathymetry is characterized by large-scale NW-SE elongated ridges and troughs with associated free-air anomalies (Figs. 5.4, 5.5 and 5.6). These elongated ridges, 50-200 km wide, are mostly symmetric or slightly asymmetric to the northeast. The ridges coincide with the location of the main fault zones. We named the two main ridges the Beerenberg Ridge to the north and the Høyberg Ridge to the south (Fig. 5.4). The Beerenberg Ridge forms a continuous ridge in the trend of the WJMFZ from longitude 2°W to the Jan Mayen Island. The Høyberg Ridge is not so continuous and terminates at 2°W as well. Similar elongated, but no continuous features, are observed to the southeast, in close relationship with the CJMFZ. Between the two ridges, the bathymetric pattern suggests N°25-N°35-oriented bathymetric highs and lows, oblique to the main fault zones. Similar trend is observed on the gravity grids. They probably reflect underlying oceanic horsts and grabens.

Southeast of longitude 2°W bathymetry and gravity patterns change a lot. Instead of elongated ridges, a broad bathymetric high is observed. We informally named this bathymetric high, the Aegir Marginal High (AMH). Compared to bathymetry values of the adjacent oceanic basins (Norway and Lofoten Basins), the AMH is extremely shallow and lies at a depth of between 2 and 3 km (Figs. 5.3 and 5.4). The AMH is appreciatively 150 km long, 75 km wide and is bounded to the south by the EJMFZ. This structure is

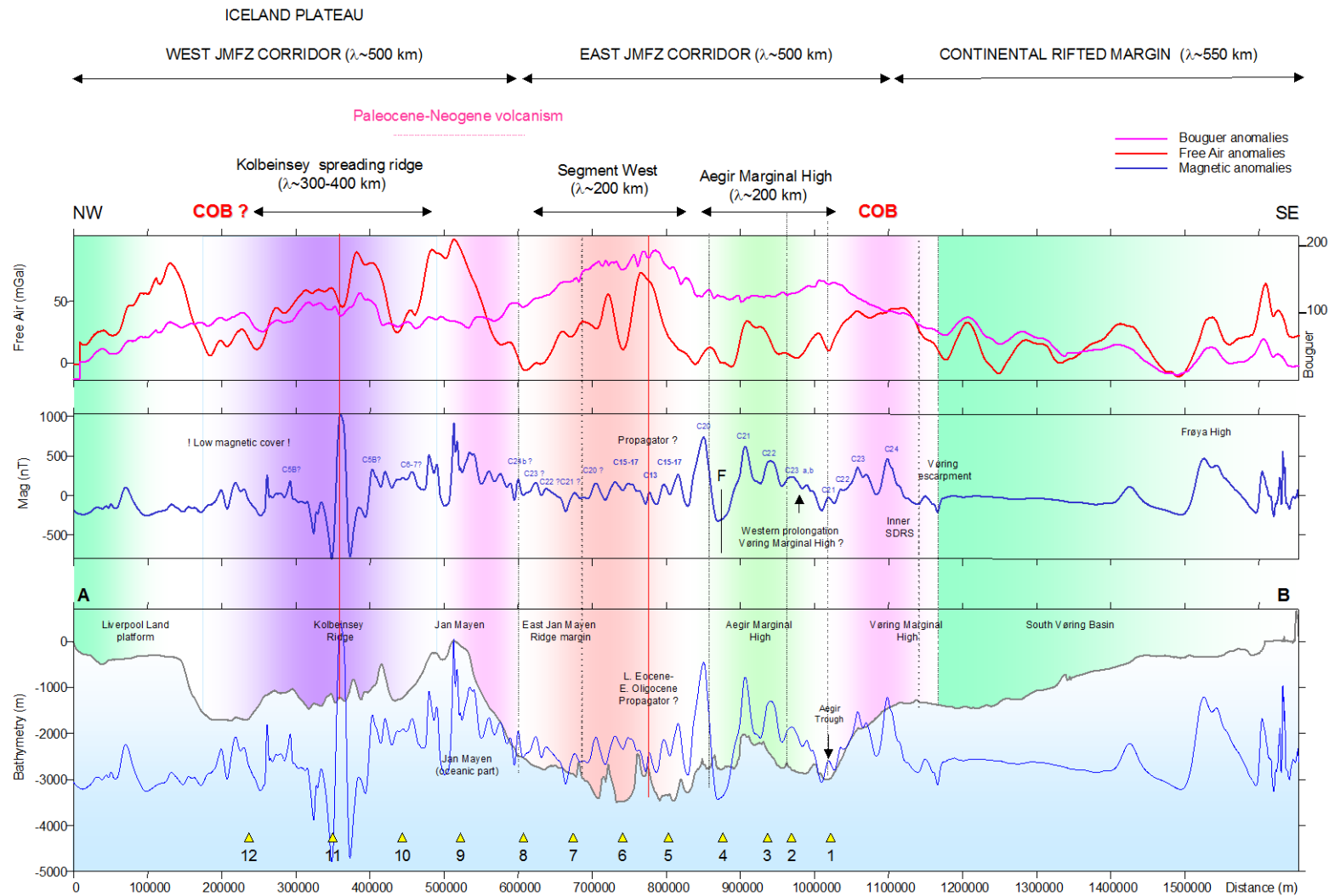


Figure 5.3 Longitudinal transect across the Jan Mayen Fault Zone Corridor (location A-B) on previous map (Fig. 5.2). Interpolated gravity (Free-Air and Bouguer anomalies) and interpreted magnetic profiles along the bathymetry illustrate the complexity of the corridor. Yellow triangles indicate the intersection with the previous profiles.

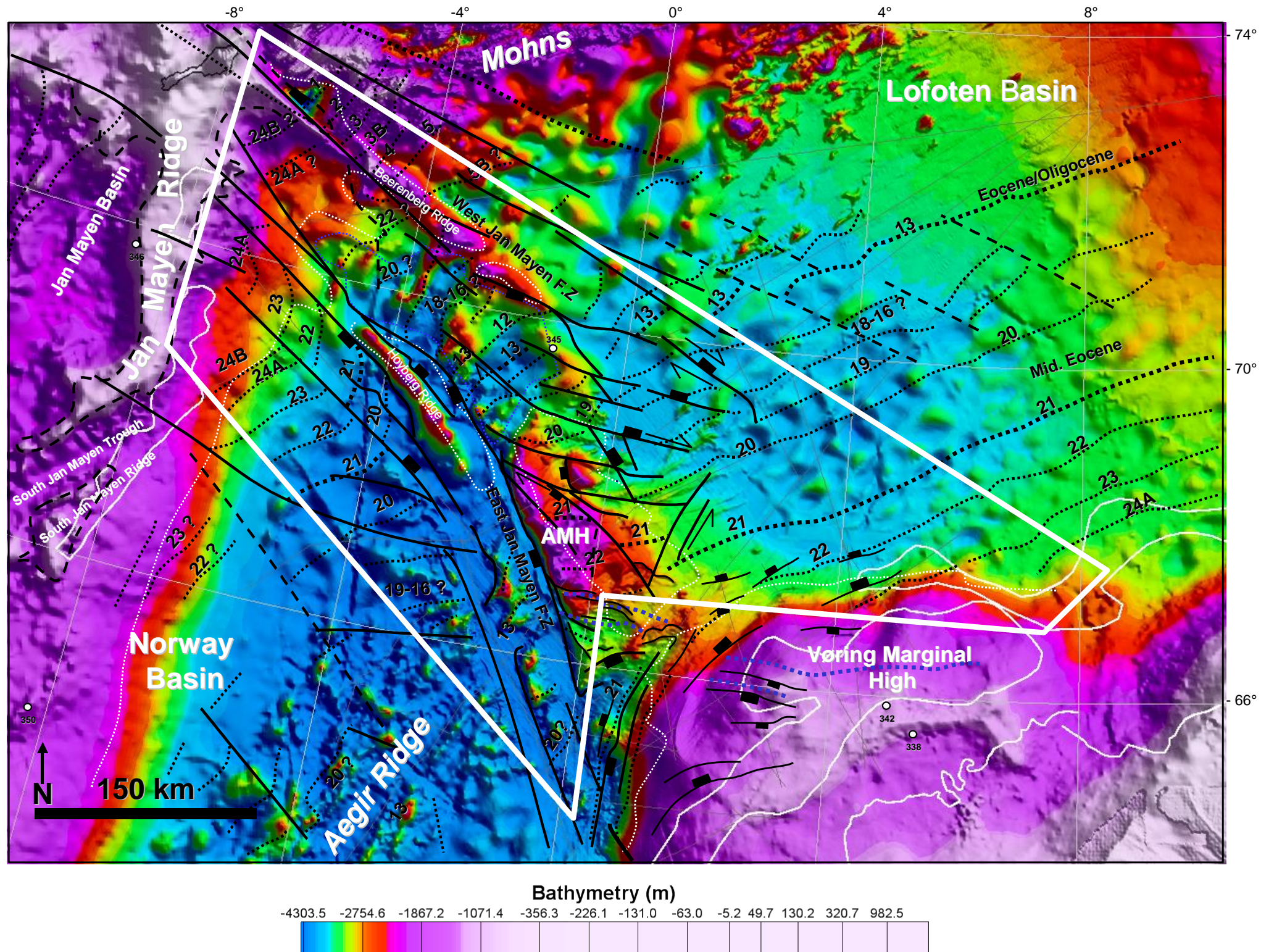


Figure 5.4 Map of gridded bathymetry along the East JMFZ corridor, constructed using high-resolution ship-track and satellite-derived data set. The main fracture zones and magnetic anomalies have been re-interpreted using a systematic comparison between bathymetry, gravity, magnetic patterns and available seismic data. The white frame represents the location of the Jan Mayen aeromagnetic survey located between the Jan Mayen Ridge (to the west) and the Vøring Marginal High (to the east). Note that the Norway Basin is deeper than the Lofoten Basin. The JMFZ corridor delimits these two subsiding oceanic domain. Across the Norway Basin, the Aegir Ridge represents a fossil-spreading axis. Close to the Jan Mayen Island, the Mohns Ridge is still active. NW-SE elongated troughs and elongated ridges characterise CJMFZ, EJMZF and WJMF. North of the EJMZF, the Aegir Marginal High (AMH) represents a broad and anomalous bathymetric high. This bathymetric feature is atypical and shallower than surrounding areas. Dashed curved represent the Bouguer lows.

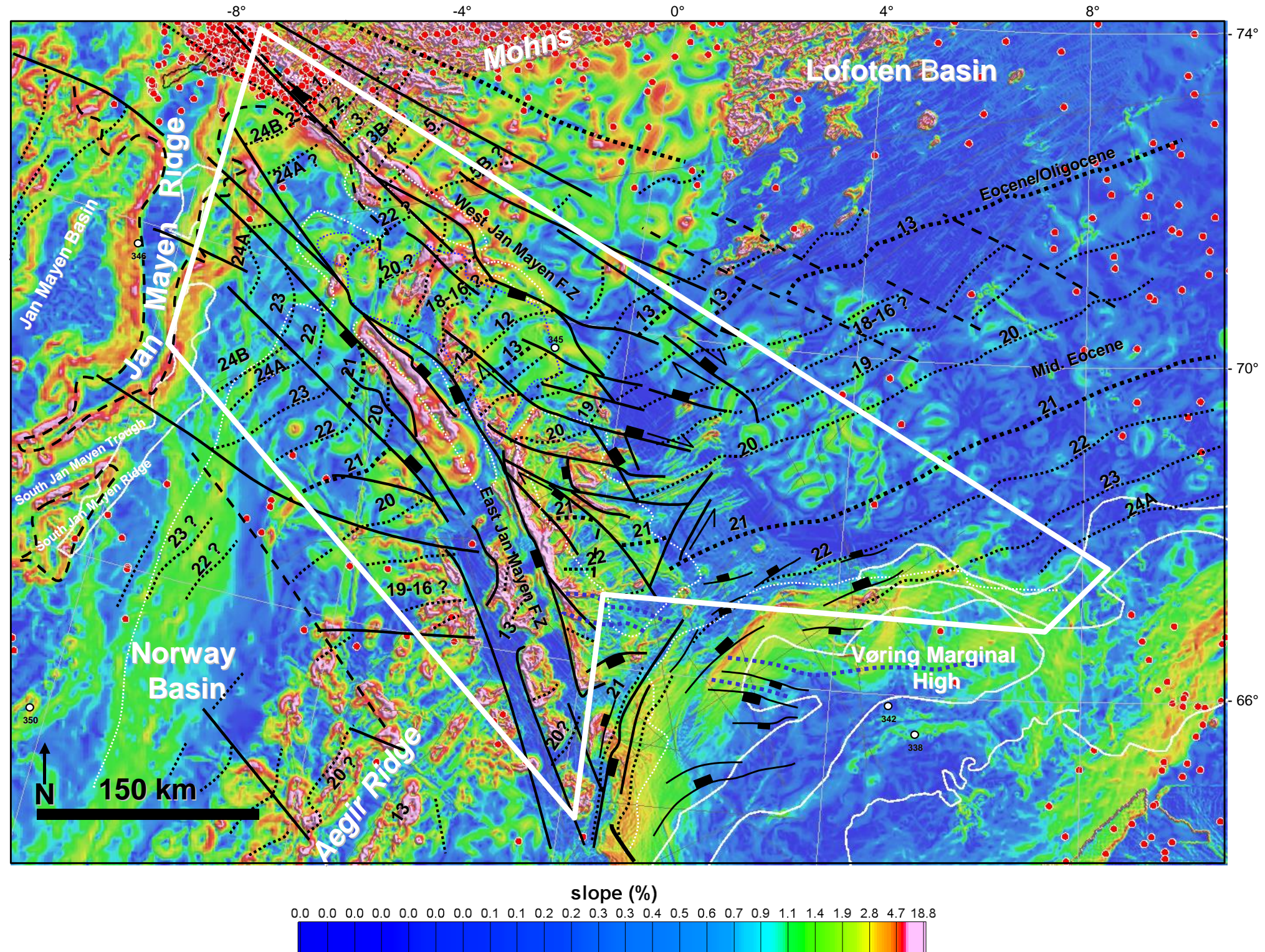


Figure 5.5 Map of terrain slope along the East JMFB corridor. The map is overlain with fault zones and magnetic anomalies. The slope has been calculated at any bathymetric grid node on the surface. Terrain slope is reported in percentage from zero (horizontal) to 90 (vertical). For a particular point on the surface, the terrain slope is based on the direction of steepest descent or ascent at that point. This means that across the surface, the gradient direction can change. This filter was extremely useful to constrain the fault pattern. This map illustrates also the asymmetry or asymmetry of the main structures identified along the survey area. Red circles represent the seismicity recorded by USGS in this area between 1973 and 2005. Only the northern part of the Jan Mayen Island is extremely active now.

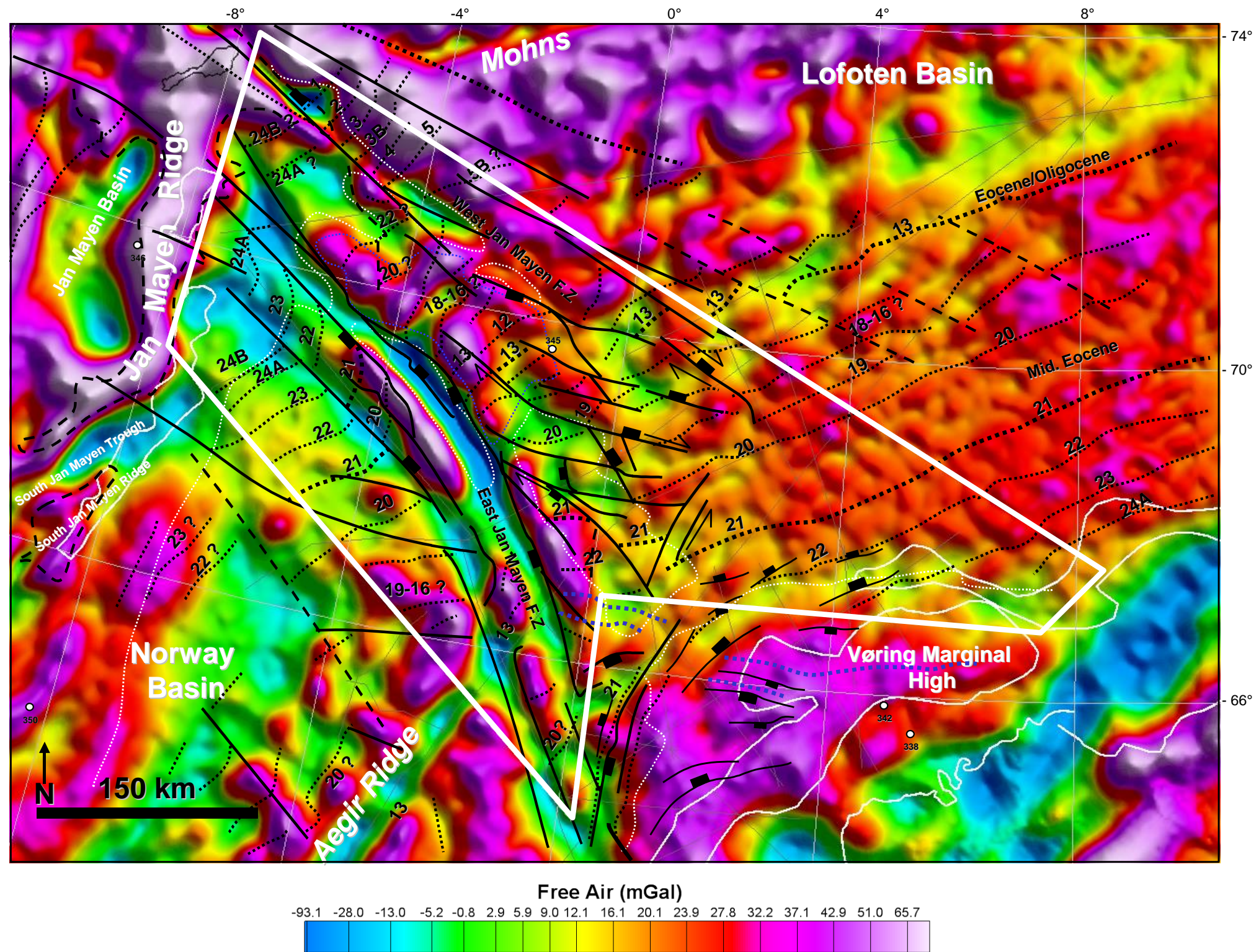


Figure 5.6 Map of gridded Free-Air anomalies along the East JMFZ corridor overlain with fault zones and magnetic anomalies. The anomalies show trends and structure resembling those of bathymetry, although short-wavelength gravity features are subdued. The map is overlain with magnetic anomalies and faults zones. Note that the EJMFZ is characterized by lower free air anomalies compared to the WJMFZ.

clearly asymmetric with a steep slope along the EJMfZ side and a smooth slope towards the Lofoten Basin (Figs. 5.4 and 5.5). At this stage, we point out that the symmetry and asymmetry of the JMFZ corridor features are closely connected to the location of the spreading ridges (Mohns, Aegir and Kolbeinsey). When the fault zones intersect (or are close) to spreading ridges (profiles 3, 4, 9 and 11 in Fig. 5.2), an asymmetry of the corridor is usually observed. The main fault scarps usually dip towards the spreading centers and the shallowest bathymetry occurs near the intersection.

Between the AMH and the Vøring Marginal High, a V-shaped trough is clearly observed on the new high-resolution bathymetric grid (Fig. 5.7). Its width is around 50-70 km to the south and narrows northwards until disappears before reaching the Lofoten Basin. Around this V-shaped structure, a few collapse structures and gravity slope features can be identified and round-shaped features observed in the northeastern part of this trough may represent some volcanic vents. We informally named this V-shaped bathymetric feature the Aegir trough.

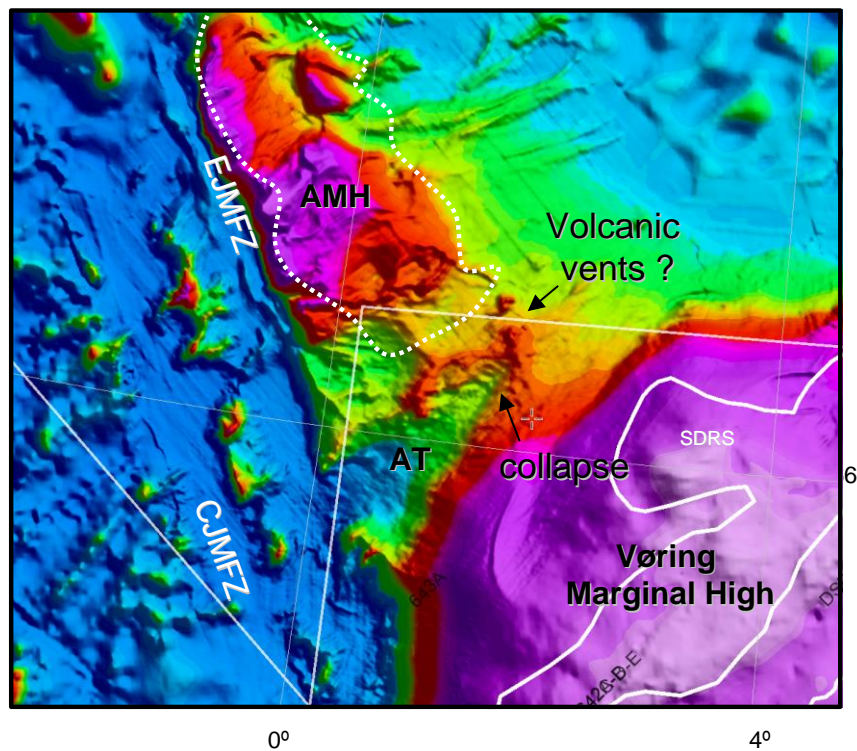


Figure 5.7 High-resolution bathymetry between the Vøring Marginal High and the Aegir Marginal High (AMH). The Aegir trough (AT) represents a V-shaped bathymetric low and a bathymetric hinge between the two shallow highs.

5.3 The Jan Mayen Fracture Zone: New magnetic picture of the Norwegian Sea

The new Jan Mayen aeromagnetic survey provides new insights along the East JMFZ corridor. New magnetic features are highlighted by the new dataset (Figs. 5. 8). In oceanic domain, when basalt lava flows cools and solidify magnetic iron minerals align themselves with the direction of Earth's magnetic field at the location where they form. From sequences of age-dated lava flows in continents, it has been concluded that the Earth magnetic field has reversed itself many times in the past. That is, north and south magnetic poles swapped positions. The duration of those intervals of "normal" polarity (like today) and "reverse" polarity range from 0.1 to about 3 Ma along the Jan Mayen survey. The most likely explanation is that the magnetic anomalies are due to the continuous creation of ocean crust during magnetic reversals. But demagnetisation can be produced by late magmatic events of hydrothermal alterations of the initial crust.

Those variations, so called chrons (abbreviation from C25 to C1 in this study), are symmetrical on either side of the Mohns and Aegir Ridge spreading system and interfered together along the East JMFZ corridor (Figs 5.9). The new magnetic picture allows us to better identified the magnetic chrons between the Lofoten Basin and the Norway Basin and the fault pattern along the survey area is also better constrained as well (Figs. 5.8 and 5.9). Combined with other potential field data, all these new elements are useful to refine the tectonic model for this part of the Greenland-Norwegian Sea (see next chapters).

Normal and reversal magnetic strip are now better imaged (Fig. 5.8):

- north of the Jan Mayen Island the spreading system from C5 (10-12 Ma) to C1 (actual spreading Mohns Ridge chron) is perfectly defined.
- north of the WJMFZ, between C23 (51 Ma) and C18-C16 (40- 36Ma)
- between the Aegir Marginal High (AMH) and the Jan Mayen Island from C23 (51 Ma) to C13 (33.3 ma) (or C12 ?)
- Between the Aegir Ridge and the Jan Mayen Ridge from C24 to C13. C25 and C24r can be observed along the eastern margin of the Jan Mayen Microcontinent. Same anomaly C25B is interpreted in the conjugate system (Figure x)
- The C19 anomaly (43.5 Ma) is now well identified with the new survey. It is shifted to the northwest in the northern part of the AMH.
- A complex and atypical overlapping and shift of the C21 (47 Ma) is observed along the AMH and suggest faulting as well.
- In the northwestern part of the survey, magnetic chrons with different orientations are observed and probably reflects local structural reorganization during sea-floor spreading. North of the WJMFZ, trends change between C5B (?) and C5.
- In the western part of the East JMFZ corridor, identification of the magnetic

chrons is relatively uncertain. This area probably represents a spreading interaction between the two accretion ridges from C24B (53Ma) to C13-C12 (33.3-30.5).

- East of the Jan Mayen Island, the magnetic pattern is interpreted as the prolongation of the C24B-C20 chrons observed south of the EJMFZ (according to Skogseid and Eldholm, 1987). Close to the AMH, however, the magnetic pattern represents the southern prolongation of the magnetic strips observed in the Lofoten Basin. Ambiguous changes of trends are also observed between the two magnetic domains. To explain these features we propose a propagating system, linked with the Mohns Ridge interacting with the ongoing spreading axis initially linked with the Aegir Ridge spreading system (Figs.5.8 and 5.9). The propagator probably migrates southward during C18-C16 (40-36 Ma) and stop near C13-C12 (33.3-30.5 Ma). Seismic lines across this structure are however required to valid such a model.

The major fracture zones (WJMFZ, EJMFZ and CJMFZ) are immediately obvious on inspection of the new map and a good correlation exists with other datasets. The fault zones usually coincide with low magnetic values and area characterized by NW-SE elongations, also seen on gravity and bathymetry maps (Figs. 5.4, 5.5 and 5.6). Close to the Jan Mayen Island, the WJMFZ is well defined between C5 and the current spreading ridge. To the southeast, the presence of the fault is suggested by the observed shift of the magnetic chrons from C5 to C13 and could be expected up to C19. To the south, a broad, elongated low magnetic strip observed from the Jan Mayen Island to the Aegir trough, defines the EJMFZ. The low magnetic signature is probably due to seawater alteration of the crust favoured by the faults. West of the extinct Aegir Ridge, the CJMFZ is suggested by the dextral shift of the magnetic chrons from C24 to C19-18.

Between the EJMFZ and the CJMFZ, curved magnetic anomalies from C24B to C16 are observed. They likely represent the passive effects of local deviatoric stress reorientation close to the main fault zone. Alternatively they may represent riedel fractures due to dextral strike slip displacement between EJMFZ and the CJMFZ.

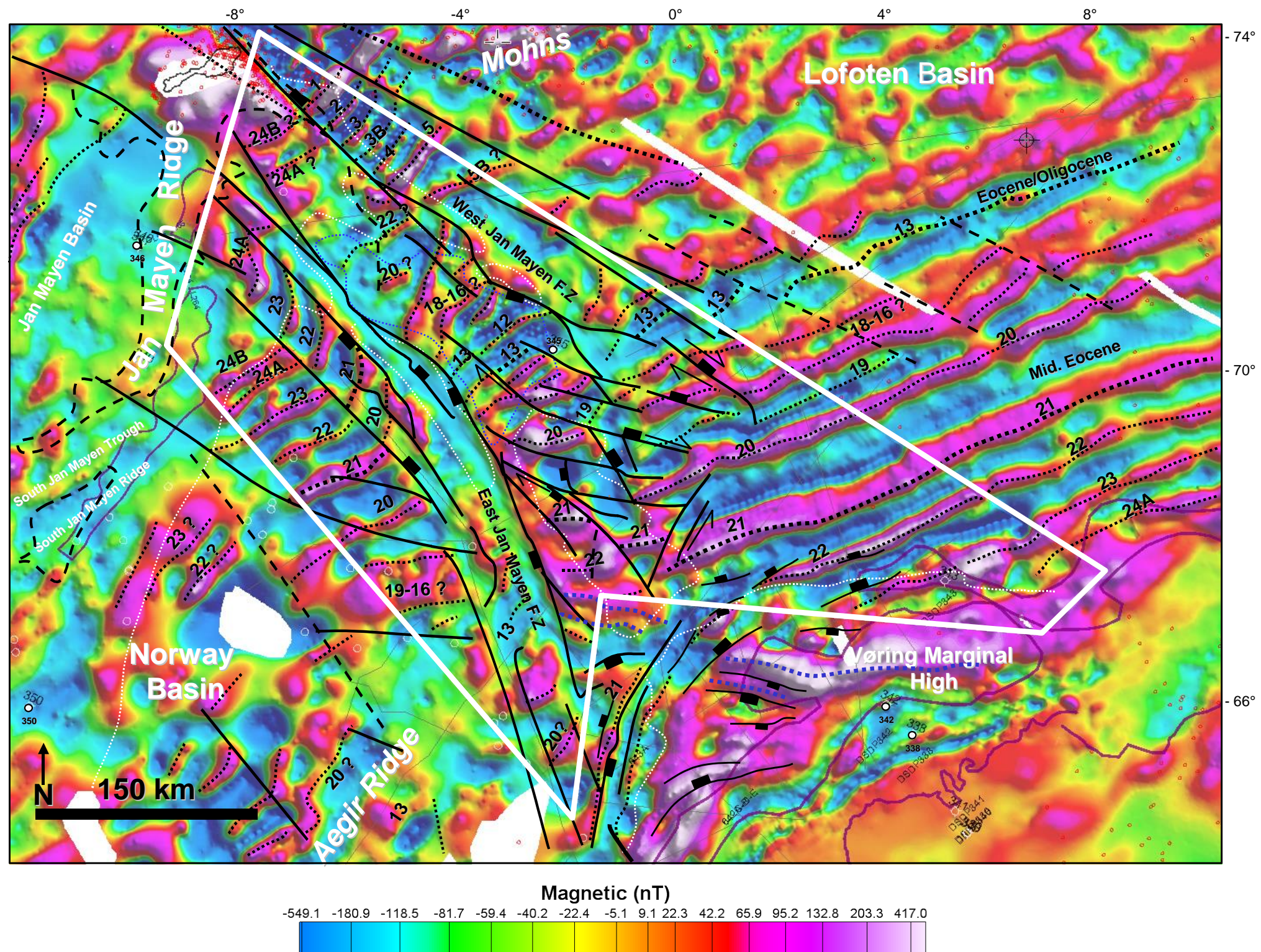


Figure 5.8 Magnetic anomaly map (Gridded magnetic anomalies) along the East JMFZ corridor overlain with the identified and interpreted magnetic anomalies (C24 to C1) between the Lofoten Basin and the Norway Basin. The main fracture zones have been re-interpreted using a systematic comparison between bathymetry, gravity, magnetic patterns and seismic data.

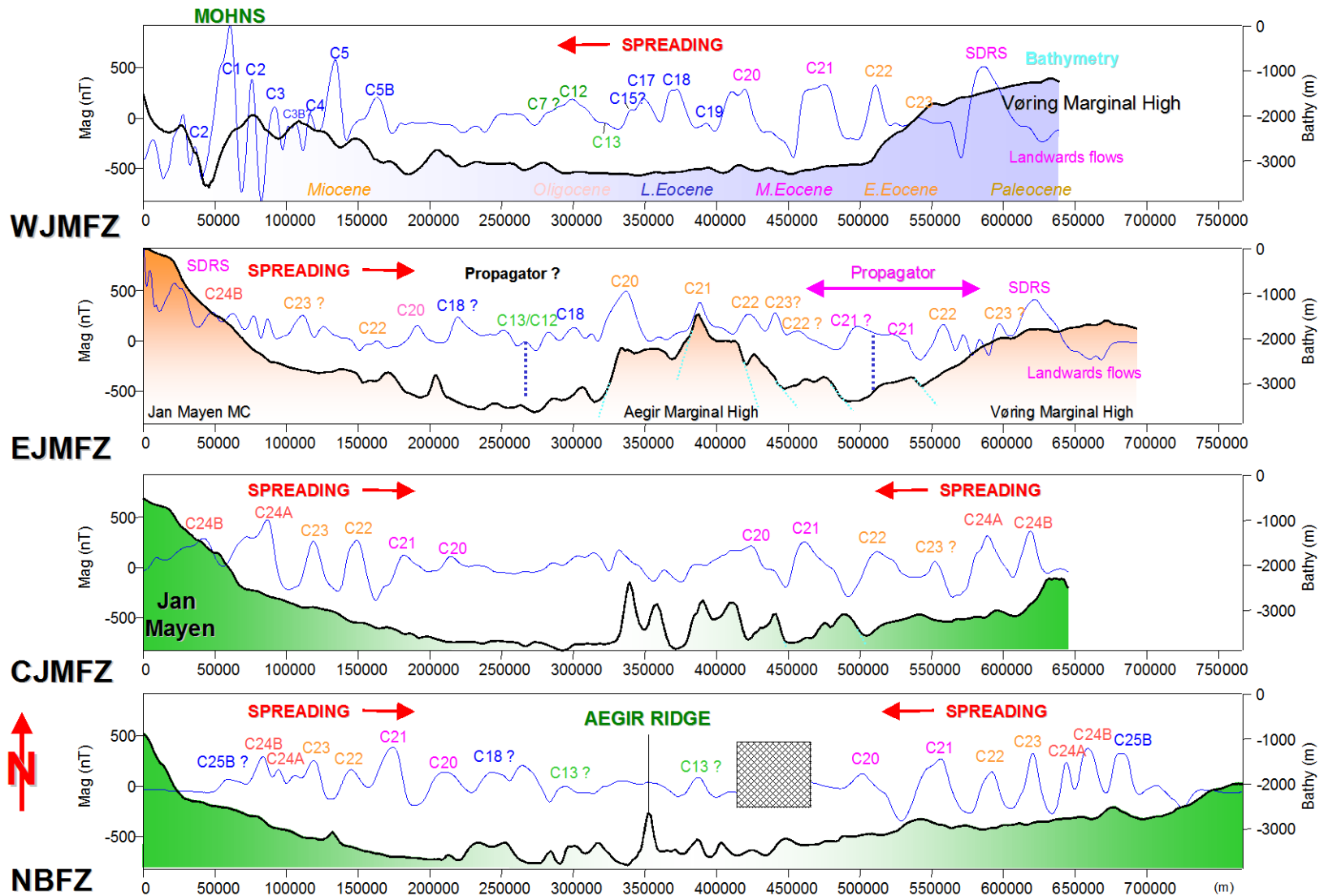


Figure 5.9 Magnetic and bathymetric profiles along the Jan Mayen survey. The main magnetic chronos have been interpreted. CJMFZ: Central Jan Mayen Fracture Zone; EJMFZ: East Jan Mayen Fracture Zone; WJMFZ: West Jan Mayen Fracture Zone.

6 THE JAN MAYEN FRACTURE ZONE AND SURROUNDING AREAS: STRUCTURE, MAGMATISM AND TECTONICS

Laurent Gernigon

6.1 Vøring Marginal High and breakup features

The process of initial opening in Late Paleocene-Early Eocene along the Vøring Marginal High (first breakup) was associated with the extrusion of large amounts of lava. The lava flows covered the newly created ocean floor and the Mid-Norwegian margin (Fig. 6.1). Along the ocean-transition zone, there is some uncertainties in the areas covered by lava flows whether the underlying rocks are oceanic or continental. Along the Vøring Marginal High, the magnetic signature is strongly influenced by the Late Paleocene-Early Eocene magmatism and the volcanic traps emplaced all along the Vøring Marginal High (Fig. 6.1). Skogseid and Eldholm (1987) proposed a model from the pre-anomaly 23 time evolution of the area which includes a double C24B and C24A magnetic system (ridge jump) slightly parallel to the C23 and later magnetic anomalies, pretty was defined in the oceanic Lofoten Basin. In our reinterpretation of the new magnetic compilation, we do not confirm previous interpretation from Skogseid and Eldholm (1987). The magnetic trends along the Vøring Marginal High are not strictly parallel to the clear oceanic trends but the magnetic trends appear to vary between N°45 and N°90. We also rise some concerns regarding the interpretation of these magnetic trends as real oceanic anomalies and analogues of the C24. Alternative interpretation of the pre-Anomaly 23 magnetic lineation could be dike swarms feeding SDRS prisms in the transitional crust.

East of 3°W, the southern part of the JMFZ is defined by a brutal slope (~1500m of vertical offset), which delimits a sharp continental-oceanic transition parallel to the CJMFZ and EJMFZ (Figs. 6.1 or 3.1). This area between the Møre and Vøring marginal highs defined a transform margin (Berndt et al. 2001). We point out, for later discussion that Berndt et al. (2001a, 2001b) do not report any SDRS along this relatively "amagmatic" segment.

The SDRS and LCB represent the most typical expression of the deep offshore magmatism related to the breakup along the Mid-Norwegian volcanic margin (Figure x and y). SDRS are seismically imaged as strongly reflective seaward dipping reflectors sequences. The SDRS have been drilled during ODP Leg 104 on the Vøring Marginal High (Eldholm et al. 1987). These drillings have provided a wealth of information regarding their structure. The drilling proves that the upper part of the SDRS represents a wedge of volcanic material emplaced in a sub-aerial or shallow marine environment. This suggests an absence of initial subsidence associated with

the final phase of rifting, that left the margin emergent during breakup. In addition, comparison between seismic reflectors and borehole data suggests that the reflectors are slightly parallel to the individual lava flows, although seismic data fail to image particular lava or volcanoclastic level by themselves (Planke & Eldholm 1994).

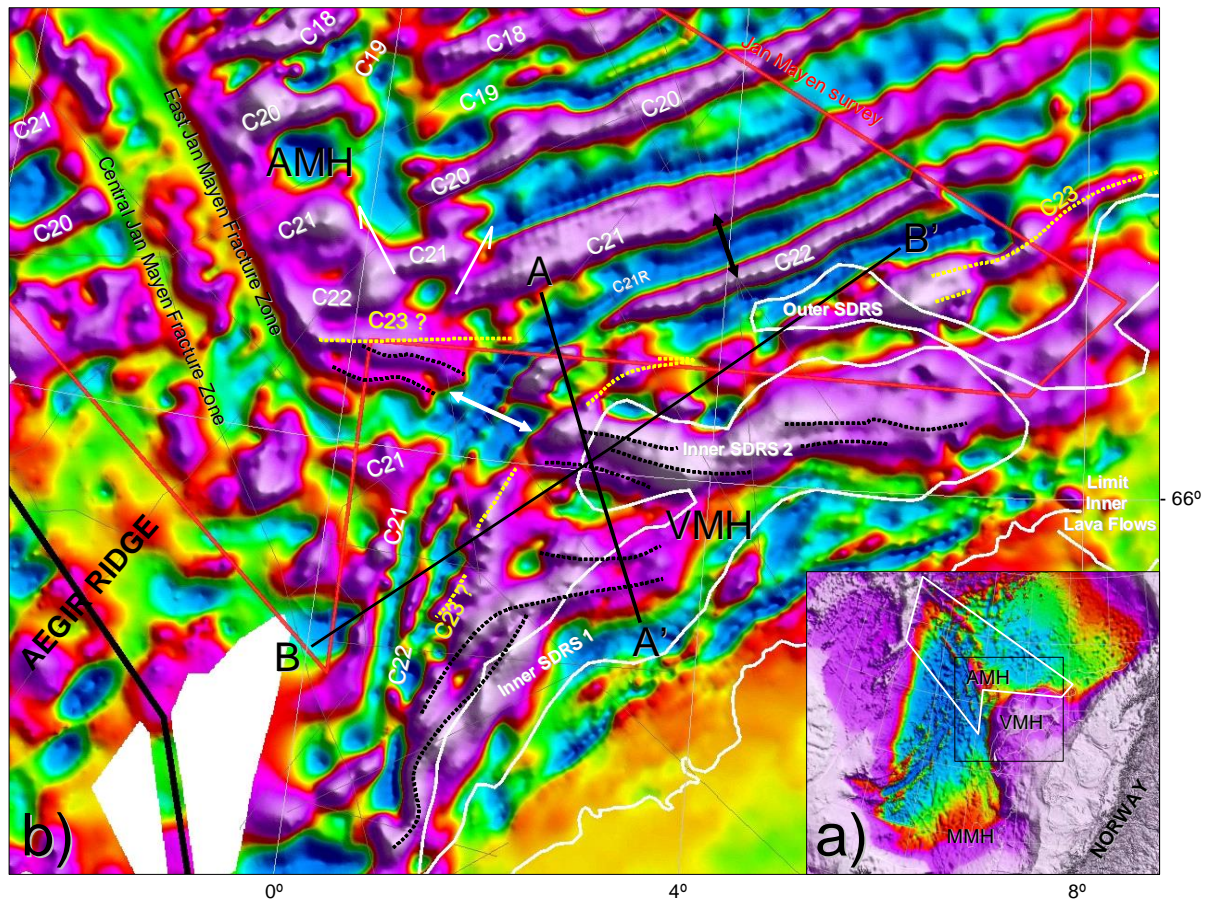


Figure 6.1 a) General bathymetry of the Mid-Norwegian margin and b) detail of the magnetic map between the Vøring Marginal High (VMH) and the Aegir Marginal High (AMH). The broad high positive anomalies along the VMH coincide with the main SDRS wedges. There is no clear identifiable magnetic chronos along the two distinct branches. However, some EW-oriented magnetic lineaments are observed and could suggest a link between the SDRS and the AMH. AMH: Aegir Marginal High; MMH: Møre Marginal High; VMH: Vøring Marginal High. Outline of the Inner SDRS and Outer SDRS (white contours) and the limit of the Inner Lava flows are from Berndt et al. (2001a).

Recent seismic investigations show that the SDRS are part of a more complex and detailed volcano-stratigraphic sequence including respectively Landward flows, Inner SDRS, outer High and outer SDRS in the distal part of the margin (Planke et al. 2000; Berndt et al. 2001a). The Inner SDRS (Fig. 6.2) present wedge-shaped units in the oceanward prolongation of the Landward Flows, which characterize a

thick sub-horizontal seismic sequence. Prograding features, interpreted as lava deltas, sometimes characterize the internal part of the Landward Flows. Intra-wedges reflections are fairly weak, discontinuous with a divergent, arcuate or sometimes a divergent planar pattern. Internal sub-sequences can be observed in the inner SDRS wedges, with small angular unconformities suggesting syn-volcanic growth of the wedge. In the deeper part of the Inner SDRS, strong amplitude continentward dipping reflections can be observed locally. They might be artefacts; deep rotated faulted blocks, dike swarms or other intrusions. Outer Highs represent mounded features with chaotic seismic facies between the Inner and Outer SDRS. Secondary sets of SDRS are documented along the Mid-Norwegian margin (Fig. 6.3). The Outer SDRS are smaller with weaker, less prominent internal reflection.

Planke et al. (2000) propose a general model to explain the development of these shallow structures, also imaged along most of the volcanic margins. Their model (Fig. 4) evolves in five stages, including:

- 1) The onset of explosive volcanism in an aquatic or wet sediment environment forming basalt-sediment complexes poorly imaged on seismic data.
- 2) The onset of effusive sub-aerial volcanism including the development of the Landward Flows, locally terminated by prograding lava deltas near the shoreline.
- 3) The continuing effusive subaerial volcanism, infilling rapidly the rift system along the breakup and forming the Inner SDRS wedge. The Inner SDRS mostly represent flood basalts and fluvial sediment emplaced in a subaerial setting. The distal part of the wedge probably represents subaquatic volcanics.
- 4) During the relative subsidence of the margin, explosive shallow marine volcanism occurs forming shallow marine build-ups (surtseyien type), imaged as the Outer High. The High could represent hyaloclastic flows and volcanoclastics and fragmented basalts emplaced in shallow marine to subaerial environment.
- 5) The last wedges (so-called outer SDRS) form in the oceanic part of the system.

Berndt et al. (2001a) suggest that the outer SDRS may represent flood basalts mixed with pillow basalts, sediment and sills emplaced in a deeper marine environment.

A recent discussion (Geoffroy et al. 1998; Callot et al. 2001; Geoffroy 2004) suggests, however, that SDRS formation could be influenced by syn-magmatic tectonic flexure controlled by major continentward detachment accommodating the seaward flexure of the igneous crust about the necking zone (Gibson & Love 1989). Although these features are extremely difficult to image, some seismic

interpretations along the Mid-Norwegian margin agree with this "roll-over" model (Gernigon et al. 2006). However, this 'detachment' is not observed everywhere. By means of analog modelling, Callot et al. (2001) show that the distribution of magmatic reservoirs inside the lithosphere can exert a strong control on the SDRS geometry. Onshore East Greenland, the crust beneath the Inner SDRS is particularly well exposed. This area documents an exceptional coast-parallel dike swarm system exposed along the outermost Greenland coast. The dike swarm and associated intrusive centers were emplaced between a few million years before and 7 My after breakup. The progressive rotation of the dike swarm during the onset of breakup witnesses the seaward flexure of the crust and SDRS (Nielsen & Brooks 1981).

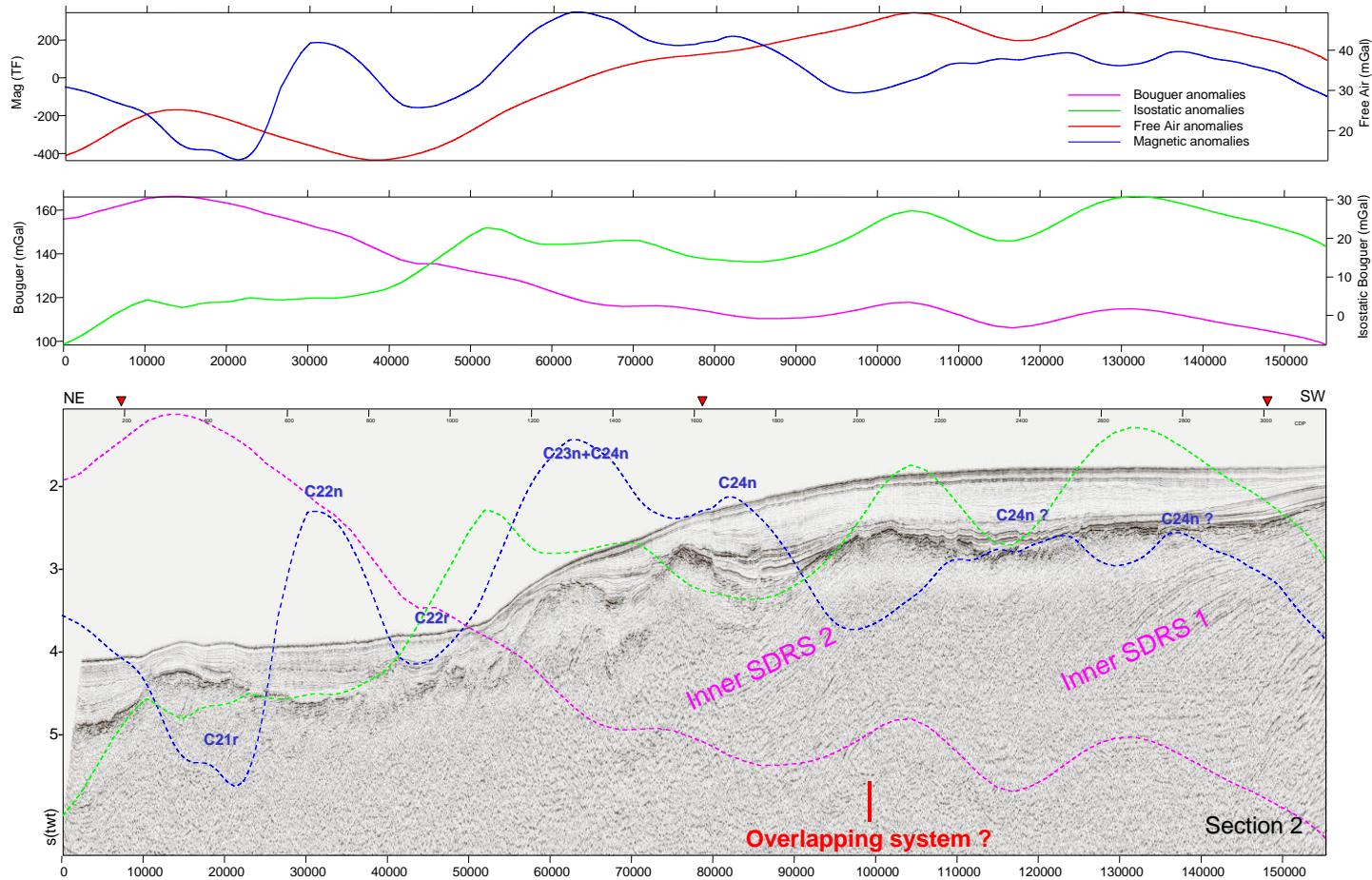


Figure 6.2 Seismic transect AA' across the Vøring Marginal High, combined with gravity and magnetic signatures. The transect crosscut the two high-amplitude magnetic branches observed along the volcanic plateau. Two Inner SDRS (1 and 2) represent wedge-shaped units interpreted as lava piles emplaced during the breakup. Intra-wedges reflections are fairly weak, discontinuous with a divergent-arcuate pattern. The top basalt is characterised by strong amplitude reflections. Small angular unconformities suggest syn-volcanism growth of the SDRS. Unclear magnetic trends may represent “real C24” anomalies or dike swarms. Two Inner SDRS wedges can be observed and may reflect an overlapping spreading system along the Vøring Marginal High.

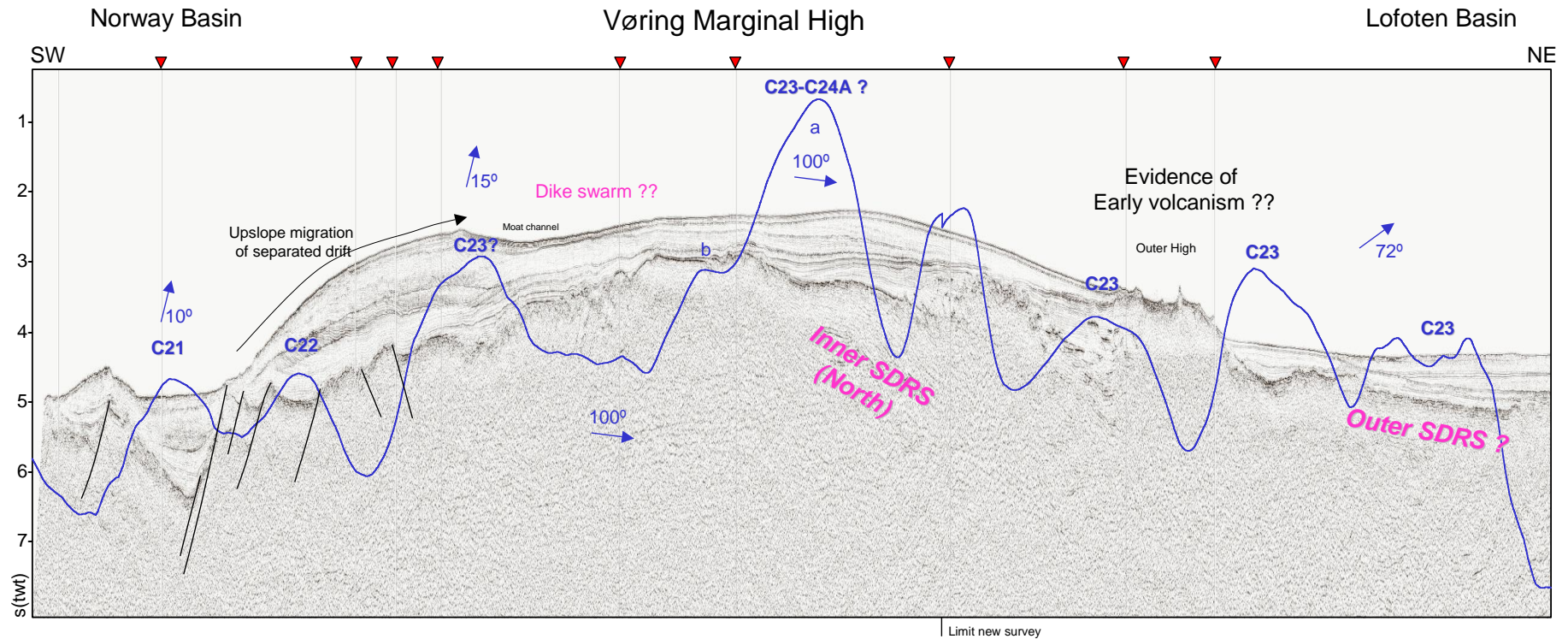
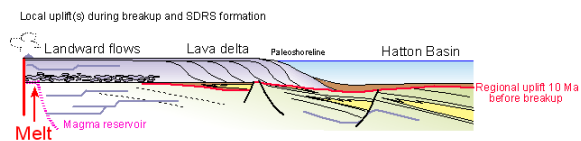


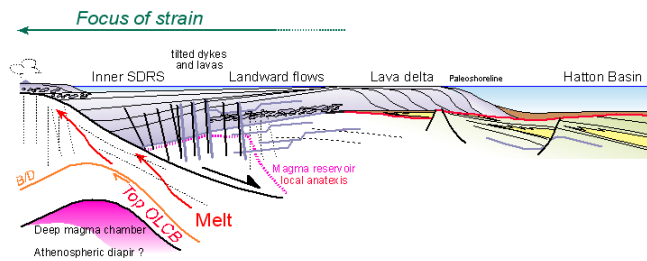
Figure 6.3 Seismic transect BB' from the Norway Basin to the Lofoten Basin. The seismic line crosses the Vøring Marginal High, the Inner SDRS 2 and the Outer SDRS observed near the C23 magnetic anomalies. The Inner SDRS are characterised by the highest magnetic anomalies. Some strong reflections and small plugs between the Vøring Marginal High and the Lofoten Basin suggest some kind of post-breakup (may be?) volcanic mound and sills. Alternatively, it could represent the syn-breakup Outer High defined by Planke et al. (2001). Note also the thick sedimentary section (contourite drift) overlying the volcanic plateau. This kind of drift sedimentation could explain the thick sedimentary section atypically observed on top of the AMH, located in the trend of the structure illustrated above. Arrows indicates the different orientations of the magnetic trends.

The EW magnetic trends, which are very different from the major NW-SE trends observed after C23 (Figs 6.1 and 6.3) could reflect the magnetic signature of underlying dike swarms, the angular difference could be explained by local effects of underlying intrusive complexes interacting with the regional tensional field. The same complexes may also explain the SDRS geometries controlled by an overlapping necking system at depth

1) Late Paleocene



2) Latest Paleocene/Early Eocene



3) Early Eocene

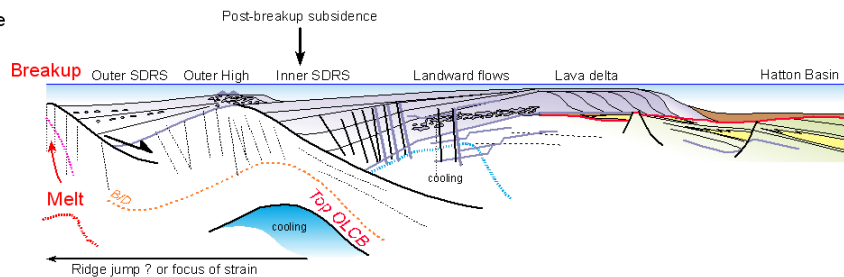


Figure 6.4 From rift to breakup-evolution of the volcanic margin and formation of the main volcano-stratigraphic sequences. (modified after Planke et al. 2000). The geometry of the wedge is not only controlled by lava flows loading but could also be controlled by the structure of the underlying necking system, controlled by the distribution of magmatic underplating. OLCB: Oceanic high velocity lower crustal body.

6.2 The SDRS system along the Jan Mayen Microcontinent: Are they really volcanic features?

The Northwestern part of the aeromagnetic survey cover part of the East Jan Mayen margin (Fig. 6.5). There, Gudlaugsson et al., (1988) described the structural style of the Jan Mayen Ridge and interpret a system of rotated blocks and seaward-dipping reflectors features. The wedge structure on the eastern flank of the Jan Mayen Microcontinent was interpreted as SDRS by Skogseid and Eldholm 1987; Gudlaugsson et al. (1988); Kuvås and Kodaira (1997) and Alvestad (1997) (see also chapter 3.3).

The new JAS-05 data-set shows also that the seaward dipping wedges along the east Jan Mayen margin are located to the east of the C24A and C24B, which represent, in time, the onset of the main volcanic event (Fig. 6.5). According to the observations, the seaward dipping wedges, mapped by the previous authors should be older in this area. However, it does not really agree with the timing of the main volcanic phase (late Paleocene-early Eocene, C24). In addition to the fact that real volcanic SDRS are missing along the conjugate system (Berndt et al. 2001), we believe that some of the seaward dipping wedges, along the eastern margin of the Jan Mayen, are not necessarily volcanic SDRS, otherwise the conjugate system should be asymmetric.

At this stage we do not have access to further seismic data along Jan Mayen but we think that the dipping wedges observed between the Norway Basin Fracture Zone and the EJMFZ could be mostly sedimentary and could represent the prolongation of the Rån Ridge (southwest Vøring Basin), redefined at the Base Cretaceous unconformity level and interpreted to be Triassic to Jurassic in age (Gernigon et al. 2004). Currently, sufficient information is not available on the Jan Mayen Microcontinent to test such hypothesis and well data (DSDP sites 346-347-349) do not penetrate deeper than Oligocene sediment (Talwani et al. 1976). However, OBS data from Kuvås and Kodaira (1997) suggests that ~10 km of Mesozoic and Palaeozoic sediments may be present below the Jan Mayen Ridge.

6.3 Breakup south of the EJMFZ

Close to the EJMFZ and the CJMFZ, some magnetic anomalies are observed to the east of the C24A magnetic anomalies. Tentatively, the positive anomalies observed in the domain 2 may represent C25 magnetic chrons (56 Ma). These anomalies are oblique to the C24A. Further to the south it is difficult to identify similar trends due, once again to a low magnetic dataset along this area.

Along the Jan Mayen transform margin, south of the Vøring Basin, Gernigon et al. (2002)

described similar pattern and already suggested that this C25 anomalies could agree with an earlier phase of breakup south of the EJMfZ. Similar observation on the conjugate system confirms such a hypothesis. Breakup could have been already initiated in Thanetian time (late Paleocene), south of the Vøring Margin. This hypothesis is supported by recent plate reconstructions at the North Atlantic scale (C. Gaina, personal communication).

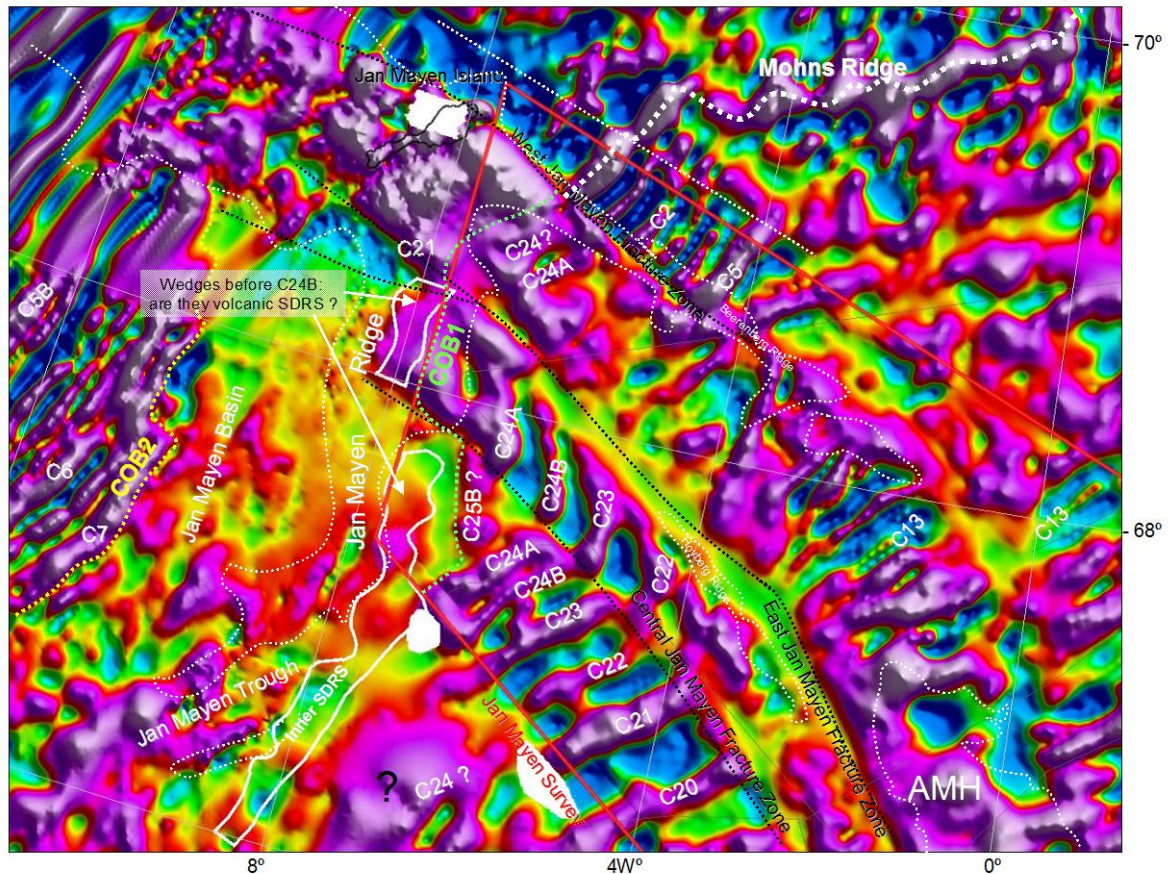


Figure 6.5 Magnetic pattern (gridded anomalies) near the Jan Mayen microcontinent. At the northeastern margin, the "SDRS" are surprisingly located before the C24B. However, SDRS are not observed at the conjugate margin, between the East Jan Mayen Fracture Zone and the Norway Fracture Zone according Berndt et al. (2001). In this part of the Jan Mayen, all wedges are not necessarily volcanic features but could also represent the southern prolongation of the Rån Ridge located to the north before the opening of the Norway Basin. Positive anomaly before C24B probably represents C25 anomalies. This suggests an early phase of breakup in Thanetian time. Same observation has been made in the Norwegian part by Gernigon, (2002).

7 THE AEGIR MARGINAL HIGH (AMH): ARCHITECTURE, DEEP STRUCTURES AND DEFORMATION

Laurent Gernigon

7.1 Shallow structure and sedimentary sequences

Previous observations show that the AMH is an anomalous bathymetric high feature of the East JMFZ corridor (Figs. 7.1). The AMH is oceanic and lies in the trend of magnetic anomalies C18n-16n to C21n/C22n, well defined in the Lofoten Basin. These magnetic anomalies represent geological ages between early Mid. Eocene to Late Eocene (48- 36 Ma) according to the scale of Cande and Kent (1995). In the Norway Basin, the AMH is located in the northern prolongation of the two C20n (43Ma) magnetic anomalies observed on either side of the Aegir Ridge.

We had access to two seismic lines across the AMH (Figs. 7.1b and 7.2). One line has been converted to depth in order to support the gravity modelling of this anomalous bathymetric feature (Figure 4.11, chapter 4). Figures 7.1 and 7.2 (converted in depth) illustrate both the structure and seismic sequences of the AMH. The western part of the AMH is characterized by a steep slope with an apparent displacement of ~1500 meters, from the top of the ridge to the sea floor of the EJMfZ valley. The AMH itself could be divided between a narrow (75 km) main ridge (section A-B, Fig. 7.1) and an adjacent terrace, 100 km long, linking the ridge with the Lofoten Basin (section B-C).

Internal seismic facies are quite difficult to interpret along the main ridge due to numerous fault and poor seismic resolution decreasing from SE to NW. The top oceanic basement is, however, constrained by strong amplitude reflections and underlying transparent facies. The top basement has an irregular morphology, with "whitening" effects, characteristic of an igneous nature. Some rough, discontinuous and transgressive reflections, observed locally along the main ridge may represent igneous sills emplaced close to the top basement.

The top basement is controlled by the development of normal faults with small to significant offset in the range between 500 and 1000 meters. The most significant fracture zones coincide with the boundaries of the main structural features of the AMH (transitions main ridge/terrace and terrace /Lofoten Basin).

The sedimentary basin between the AMH to the Lofoten Basin may be grouped into two major seismic units, separated by a significant regional unconformity (MU), which extend along most of the Lofoten Basin (Figs. 7.3 and 7.4):

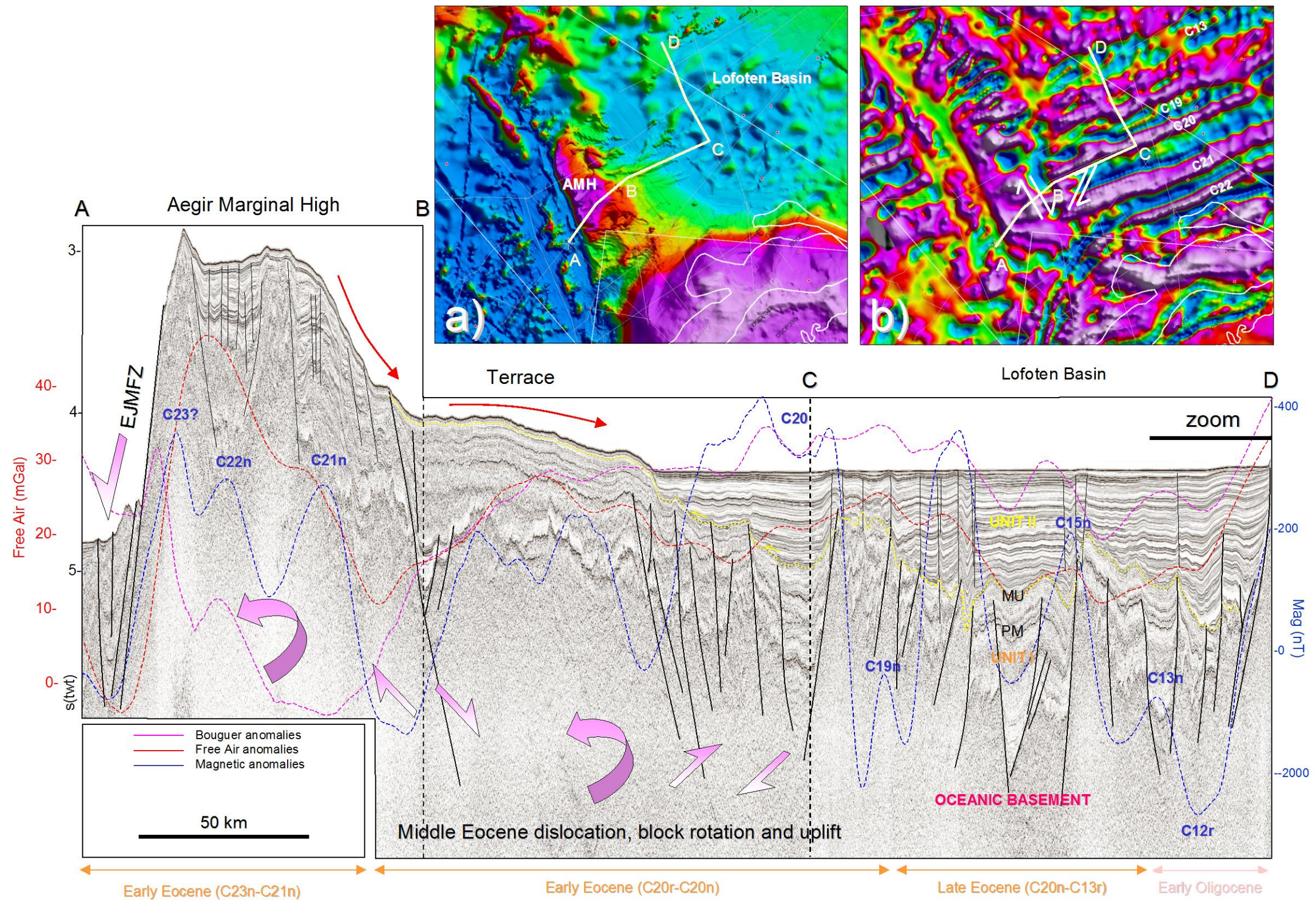


Figure 7.1 Composite seismic transect from the Aegir Marginal High (AMH) to the Lofoten Basin. Section A-B illustrates the main ridge bounded to the west by the East Jan Mayen Fracture Zone (EJMFZ). Section B-C illustrates the transition between the AMH and the Lofoten Basin. This transition is characterised by an intermediate terrace, clearly defined by the main unconformity MU (yellow curve). Section CD represents the oceanic crust accreted between Chrons C20n (43 Ma) and C12n (31 Ma), underlined by the magnetic total field anomalies. C13n marks the Eocene-Oligocene transition according to the geomagnetic polarity time scale of Cande and Kent (1995). Two main sedimentary units (Unit I and Unit II) are defined (see text for description). Unit II pinch-out the northern flanks of the AMH, at the terrace level. Units II and I are divided by the major erosional unconformity (MU) assumed to be Late Oligocene (?) to intra-Miocene in age. This significant seismic unconformity, overlaying the C12 anomaly, formed during the inversion of the AMH, which represents a former Eocene-Oligocene depocentre uplifted during Late Oligocene (?) - Miocene time.

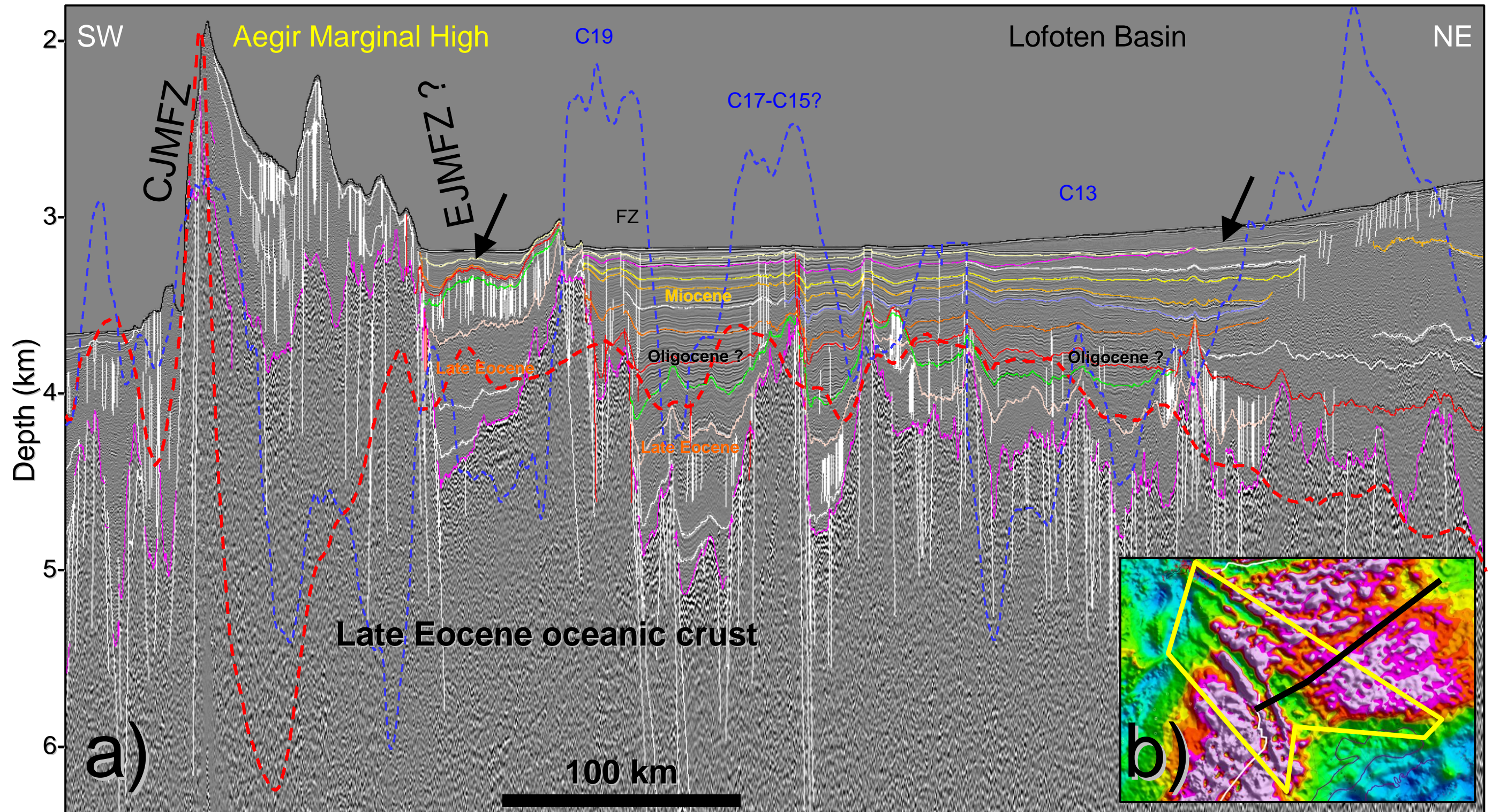


Figure 7.2 a) Depth-converted seismic transect from the Aegir Marginal High (AMH) to the Lofoten Basin. The main ridge is bounded to the southwest by the East Jan Mayen Fracture Zone (EJMFZ) and probably by the prolongation of the West Jan Mayen Fracture Zone (WJMFZ) to the northeast. MU represent the major erosional unconformity (MU) assumed to be Late Oligocene (?) to intra-Miocene in age. PM is the prominent marker (Late Eocene-mid-Oligocene?). The dotted red curve represents the Bouguer anomalies along the transect, and the blue dotted curve the magnetic signature. This depth profile has been used to constrain the gravity modelling along the AMH and Lofoten Basin (see Potential field modelling chapter). b) Location of the seismic line draped on the Bouguer anomaly map. The figure shows clearly that AMH coincides with a gravity low, which is not observed in the western part of the West JMFZ corridor, covered by the Jan Mayen survey.

- Between the top basement (=top oceanic crust) and the main unconformity MU, the first main seismic units (Unit I) represents a seismic sequence with variable, semi continuous low amplitude markers. The thickness of Unit I varies between 500 and 1000 meters. Close to the main fault zones, the facies is locally disorganised, discontinuous and sometimes chaotic. A prominent amplitude marker (PM) observed from the Lofoten Basin to the AMH terrace is easily distinguishable in the middle part of the unit and defines a boundary between the subsequence I-A and I-B (Fig. 7.3). PM represents a major discordant unconformity. On top of this thin layer, more continuous low to high amplitudes facies are observed. Unit I has been clearly inverted during the formation on the MU unconformity but the lower part of the sequence has been uplifted during the formation of the PM unconformity as well. This first inversion coincides with a major fault reactivation phase and fault block rotation. Faulting affects also the Unit I but most of the faults are cut by the PM unconformity.

Between the main unconformity MU and the sea floor, the second main unit (Unit II) represent a relatively uniform seismic unit. This unit onlaps the main unconformity and is characterised dominantly by continuous sub-parallel high amplitude reflections. A chaotic sequence is locally observed in the middle part of the unit between magnetic chrons C21n and C18n. The thickness can reach 1000 meters in the Lofoten Basin but clearly thins and pinches out the AMH. This sequence disappears on top of the AMH, where only Unit I is observed. Minor faulting affects Unit II. Recent minor movements and reactivation of deeper faults are observed and seem to accommodate growth wedges, which defines unit II-B (Figs 7.3 and 7.4). The growth wedge suggests that minor inversion and faulting were still continuous during and after the formation of the unconformity.

Obviously, the sediment and the oceanic basement are post-breakup in age and post-Ypresian (Early Eocene). Precise ages of the sequences are more ambiguous and direct calibration with ODP or commercial wells are not possible in this study due to low seismic coverage and the pinch-out of the sequences near the Vøring Marginal High. However, the seismic lines, together with the magnetic data, help to constrain the geometry and age of the oceanic blocks and overlying sediments. The seismic features can be easily correlated with the magnetic signature of the AMH, then providing an interesting shrewdness to constrain the 4D evolution of the oceanic basin.

The main unconformity (MU) can be followed to oceanic crust at least up to C12n (31 Ma). The sediments of the Unit II clearly overlap the C12r (32 Ma) and C12n (30.5 Ma) (Fig. 7.3). This means that Unit II is post-mid-Oligocene and probably mostly Miocene in age. Since the main unconformity is erosional and records a prolonged

inversion, its age is assumed to spread between Late Oligocene to intra-Miocene.

The prominent marker (PM) seems to pinch-out along the eastern flank of a significant oceanic horst near C12n (30.5 Ma). Due to low seismic coverage after C12n, we were not able to determine if these markers are present after chron C12. Then, it could be older than Oligocene. In this part of the oceanic basin and according to the geomagnetic polarity time scale of Cande and Kent (1995), the PM unconformity could represent a Late Oligocene horizon. The sequence underneath thins from east to west and is interpreted to represent Eocene to Oligocene sediments. Eocene sediments disappear progressively to the west and after C13 (33.3 Ma).

The sequence between the top basement and the MU and PM unconformity is mostly Oligocene in age. Usually the main unconformities climb over inverted highs, controlled by significant fault reactivation. The main inversion is defined by the AMH itself, which represents an Eocene-Oligocene (?) depocentre. The depocentre started to be inverted after early-Oligocene and recorded prolonged inversion locally. A better timing is still a challenging task but since this event witnesses a regional phenomenon, it is certainly recorded at the adjacent margin. We will compare our observations with the tectonostratigraphic framework of the Cenozoic at a larger regional scale later.

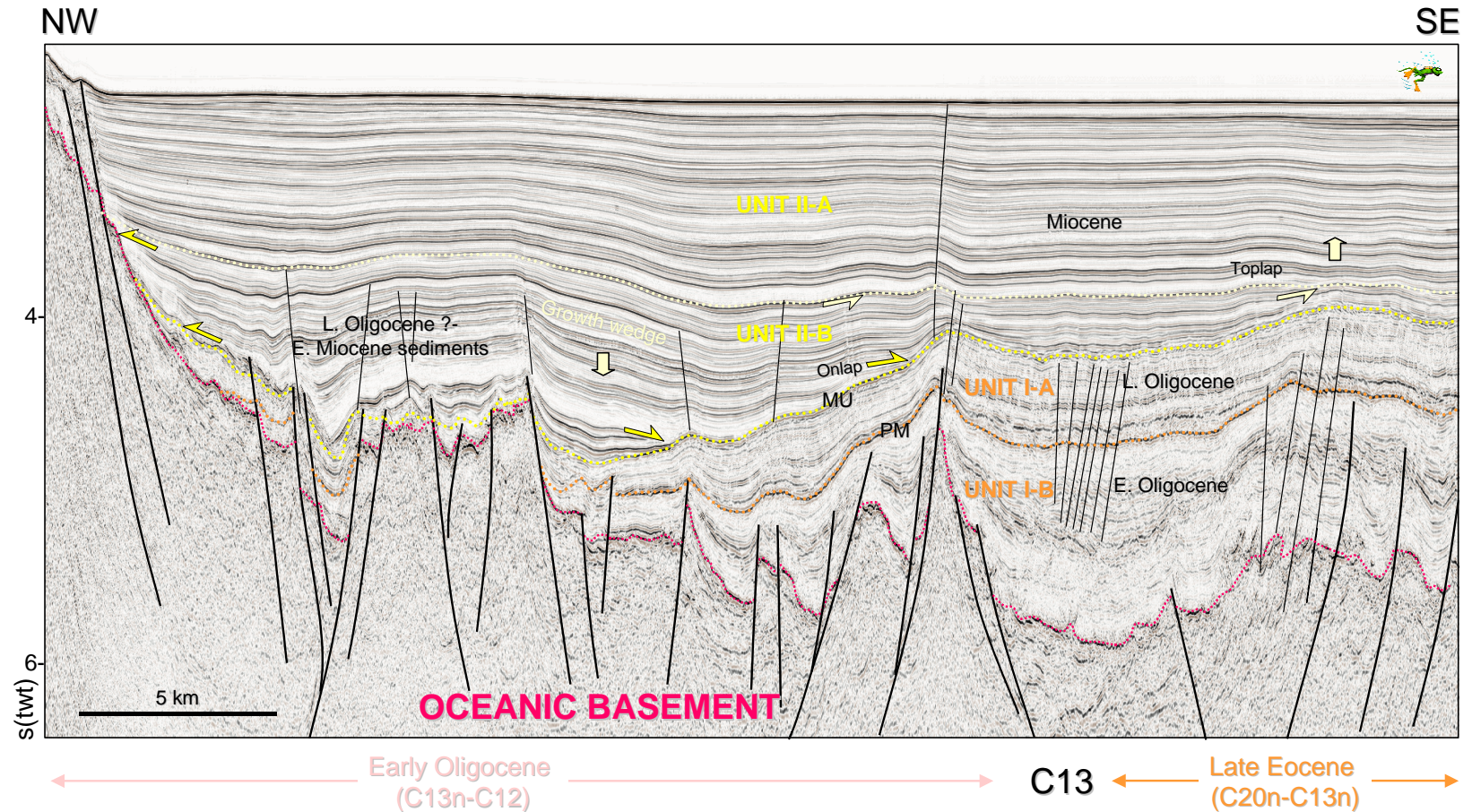


Figure 7.3 Details of the seismic interpretation on the eastern flank of a major oceanic horst situated close to the transition between Eocene and Oligocene (the C13n magnetic chron). This example illustrates the main seismic units (Units I and II) and their sub-sequences (I-A, I-B, II-A, II-B). MU represents the main unconformity between Unit I and Unit II and PM represents the prominent marker and unconformity between sub-sequences I-A and I-B. After C13, sediments between the top oceanic basement (Early Oligocene in age) is obviously post-early Oligocene. The growth wedge observed to the east of the C12 oceanic horst represents probably a late Oligocene (?)–Early Miocene sequence. Onlaps suggest that the growing wedge has been formed during the inversion of the underlying Unit I.

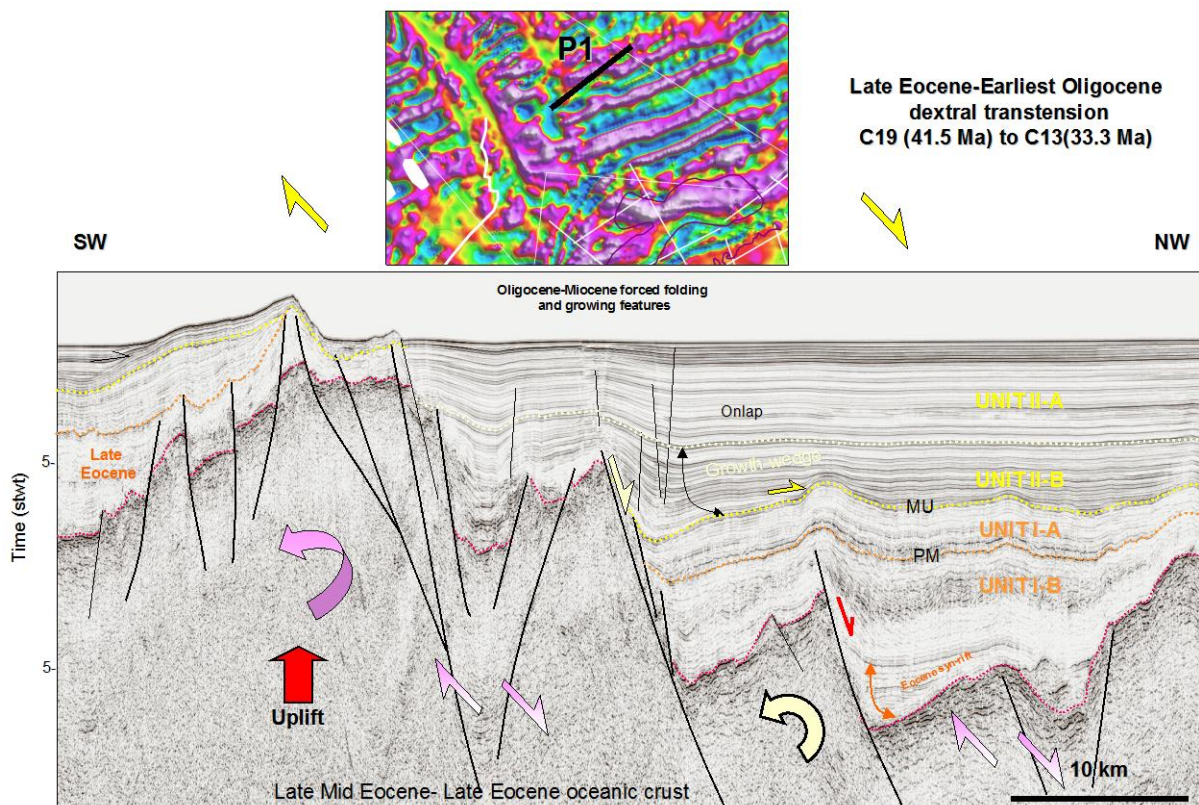


Figure 7.4 Details of the seismic interpretation on the northern part of the AMH. This example illustrates the seismic sequences and the relationships with the main faults. This section suggests a long-live period of fault activity. Comparison with magnetic data suggests dextral transtension between C19 (41.5 Ma) and C13 (33.3 ma). Faulting probably started before the main inversion between Unit I-A and II-B. A forced folding feature can be observed in Unit II-B and suggests late reactivation (Miocene) and rotation of pre-existing hanging-wall. Deep wedges suggest faulting during Late Eocene time as well.

7.2 Deep structures and origin of the inversion(s)

We suggest also that the long magnetic and long Bouguer wavelength anomalies observed along the AMH (Figs. 7.2 and 7.5) could reflect the atypical structure of the AMH (shallow magnetic basement and existence of the deep crustal root). The AMH represents a Bouguer low compared to the surrounding areas (Fig. 7.5). The resulting Bouguer map has removed the bathymetry-sourced anomalies but not the Moho-sourced anomalies. An isostatic correction continues the process of removing as many as known effects as possible from the gravity field (Fig. 7.6). Calculation of the isostatic residual involves additional assumptions, among which are the choice of crust/mantle density contrast. The isostatic residual map shows the low density of the AMH and indicates an atypical nature of the AMH within the oceanic crust. 2D- Gravity modeling (previous chapter) shows that

the bathymetric high coincides also with a deep root, observed up to 17 km. This is rather atypical for a normal oceanic crust.

In 2003, an Ocean Bottom Seismometer (OBS) survey was acquired from the Vøring Marginal High and the AHM by the Universities of Oslo and Bergen (See seismic database description, Chapter I). First results of the modelling were presented by Breivik et al. (2004; 2005) and we only got access to released information (Fig. 7.7). This experiment confirms our hypotheses. We point out also that the transect is located close to one of the major shear zone interpreted between the main ridge and the AMH terrace.

Similar to earlier results on the Vøring Marginal High, the new OBS model shows an abrupt continent-ocean transition under the SDRS. Maximum igneous crustal thickness was found to be 17.5 km, with a thickness in general 5 km lower than found by previous studies. As a matter of fact, geophysical evidences of a lower crust with anomalous high seismic P-wave velocities (7.1-7.8 km/s) so-called lower crustal bodies (LCBs) has for a long time been recognised along the Vøring Marginal High (Mutter et al. 1984; Planke et al. 1991; Eldholm et al. 2000; Mjelde et al. 1997, 2002, 2005).

The most popular interpretation of LCBs, underlying the SDRS is the magmatic underplating hypothesis. Underplating represent both ponded magmatic material trapped beneath the Moho and magmatic sills injected into the lower crust (White and McKenzie 1989). Strong evidences of underplating occurring during the rifting comes from petrological indications of both fractionation at lower crustal pressures, temperatures, and crustal contamination occurring during the melt migration into shallow or deep magma chambers (Cox 1993). Although the underplating hypothesis sounds quite reasonable along the transitional and oceanic domain, there are not so many constrains on its petrophysical nature and its chronology in the continental domain and beneath the Vøring Basin and other non-magmatic interpretation can be advanced as well (Gernigon et al. 2003, 2004; Ebbing et al. 2005).

From the COT, defined by the inner SDRS, the igneous crustal thickness decreases from 17.5 to 9 km over a distance of ~90 km, indicating decrease of melt production over 4-5 Ma after continental breakup. This “thin” portion coincides with the V-shaped Aegeir Trough between the Vøring Marginal High and the AMH (Fig 7.1a).

The crustal thickness increases again to the west below the AMH to 12-17 km (Fig. 7.7). The thick crust coincides with the Bouguer and isostatic gravity signature and gravity modelling done during this work and is confirmed by the crustal architecture deduced from the OBS experiment (see section potential field modelling). Vp velocity is constrained to be 7-7.25 km in the lower crust of the AMH indicating a mafic-gabbroic

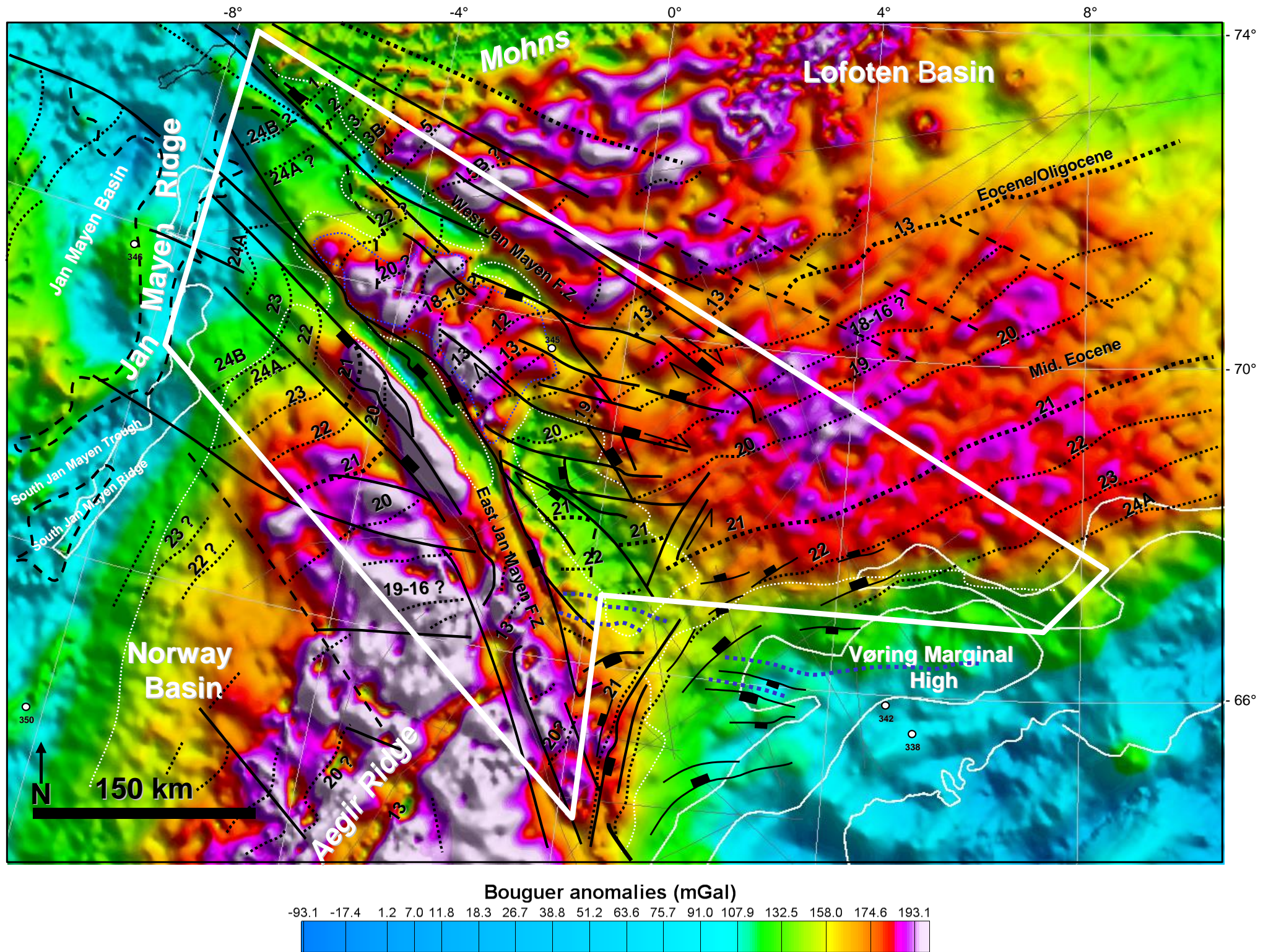


Figure 7.5 Map of Bouguer anomalies along the East JMFZ corridor overlain with fault zones and magnetic anomalies. This map reflects the crustal anomalies along the East JMFZ corridor. The Aegir Marginal High represents a clear gravity low (green color) compared to the surrounding oceanic domain (red-purple).

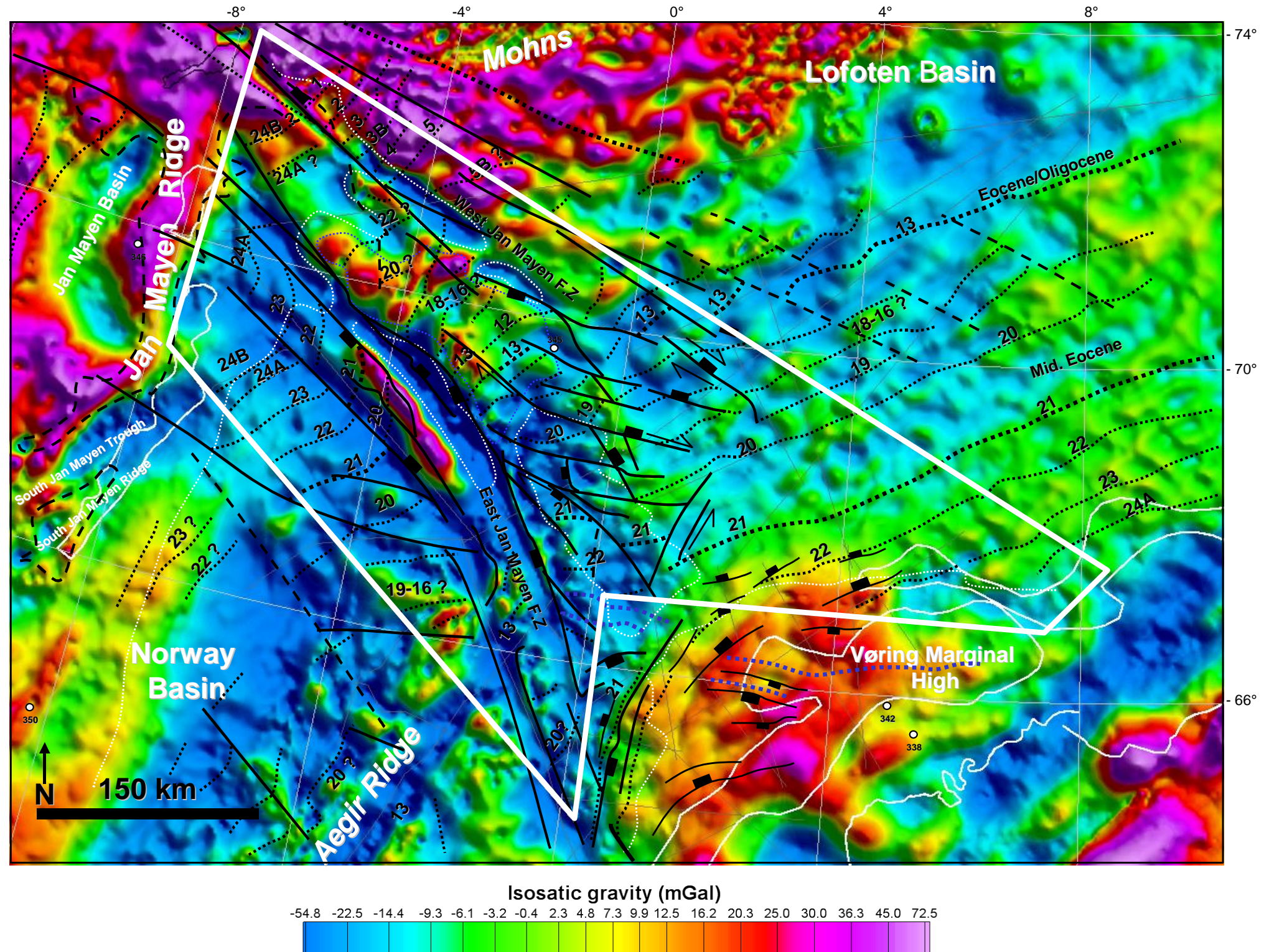
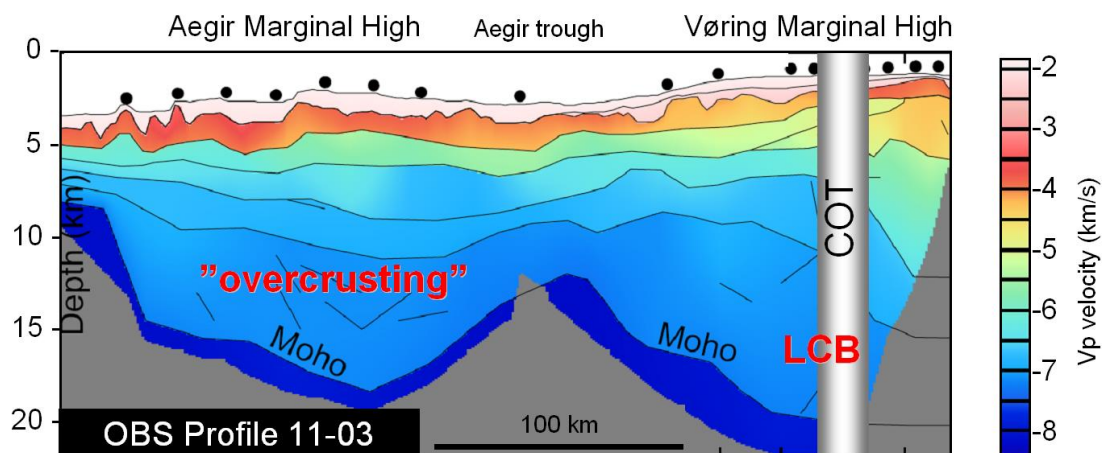


Figure 7.6 Map of isostatically corrected Bouguer anomalies along the East JMFZ corridor overlain with the identified and interpreted magnetic anomalies. Isostatic residual gravity anomaly maps are produced by subtracting long-wavelength anomalies, produced by masses deep within the crust or mantle, from the Bouguer anomaly map. Isostatic residual gravity anomaly maps therefore reveal more clearly than Bouguer anomaly maps the density distributions within the upper crust.

composition. Breivik et al. (2004, 2005) suggest that the thick crust is due to a late Miocene underplating beneath the pre-existing crust.

This result is significant and shows a genetic relationship between the anomalous bathymetry, the deep oceanic crustal root and the gravity signature.



A. Breivik, 2004, 2005

Figure 7.7 Ocean Bottom Seismometer (OBS) velocity transect across the Vøring Marginal High and across the Aegir Marginal High (AMH) to the west (from Breivik et al. 2004, 2005, Euromargins experiment 2003). A thick anomalous crust is observed underneath the AMH. The thickening is similar in size with the lower crustal body (LCB), lying underneath the Vøring Marginal High and is generally interpreted as mafic underplating formed during the breakup and of the Norwegian-Greenland Sea. The V-shaped Aegir Through coincides with a shallow Moho between the two highs. COT: continent-ocean transition.

7.3 Uplift, overcrusting and tectonic model for the Aegir Marginal High

The nature and the meaning of the anomalous thick crust beneath the AMH have been previously described by Breivik et al. (2004, 2005) but some points are unclear.

Breivik et al. (2004, 2005) interpreted the deep root as late Miocene underplating emplaced beneath the pre-existing Eocene oceanic crust. Breivik et al. (2004, 2005) suggest a complex interaction between the Aegir Ridge and the Iceland plume to explain the underplating emplacement. The conceptual model of Breivik et al. (2004, 2005) considers a northeastward transport of asthenospheric flow from the Iceland hot spot to the AMH after extinction of the Aegir Ridge in late Oligocene (~25 Ma). Before this event, Breivik et al. (2004, 2005) suggest that the spreading along the Aegir Ridge prevented such lateral flow before Late Oligocene because buoyancy and advection created by the active spreading system were too active during this period to allow spreading of deep lateral flows.

We agree with the anomalous melt production beneath the AMH but the age of this event is still unclear and relatively ambiguous. Post-breakup anomalous melt production is not surprising. However, there are no evidences of Late Miocene volcanism in the Norwegian and Greenland Sea. Post-breakup volcanism is well known in East Greenland and in the Greenland Basin but is mostly Eocene to Oligocene in age. Late Eocene to Oligocene rocks outcrop out in the TraillØ Basin, onshore East Greenland, along the trend of the JMFZ (Upton et al. 1995; Price et al. 1997; Torske and Prestvik 1991; Lundin & Doré 2002). Middle Miocene basaltic lava (13-14 Ma) has been identified in the Kangerlussuaq area to the south (Storey et al. 2004).

Concerning the plume hypothesis, Nd-Sr-Pb isotope systematics and low $^3\text{He}/^4\text{He}$ recorded on basaltic rocks on the Jan Mayen Island do not favor a mantle plume origin of the recent magmatism (Svellingén and Pedersen 2003). However alternative explanation involving a metasomatised mantle originating from the primitive Iceland Plume could also explain the same geochemical characteristics (Storey et al. 2004). The validity of a mantle plume beneath Iceland is also another controversial debate, which is beyond the scope of this report. For many authors, The potential temperature of the mantle is obviously one factor that may explain anomalous melt production but alternative non-plume models involving high extension rates, differential stretching, leaky transform, small-scale convection or fertile patches in the upper mantle may however explain significant partial melting as well (McKenzie and Bickle 1988; Wilson 1993; Boutillier and Keen 1999; Korenaga 2004; Buck 1986, Pedersen and van der Beek 1994; Van Wijk et al. 2001; Nilsen and Hopper 2002; Foulger and Anderson 2005; Gernigon et al. 2006).

A challenging point against a late Miocene underplating beneath the AMH is the apparent lack of major igneous intrusions or lava flows in the sedimentary record. If such a

magmatic event was emplaced in Late Miocene time, then numerous sill intrusions and lava flows would have been expected in the sedimentary basin. It is clearly the case 100 km to the East, where the thick lower crustal body (Late Paleocene-Eocene in age) is clearly associated with thick lava flows (SDRS) and numerous sill intrusions in the Vøring Basin. Unfortunately, it is not obvious on the few seismic lines we got across the AMH.

We believe that the thick crust beneath the AMH could be better an anomalous oceanic crust simply formed by "overcrusting" during the early Eocene accretion of the AMH from C22 to C19 (Fig. 7.8).

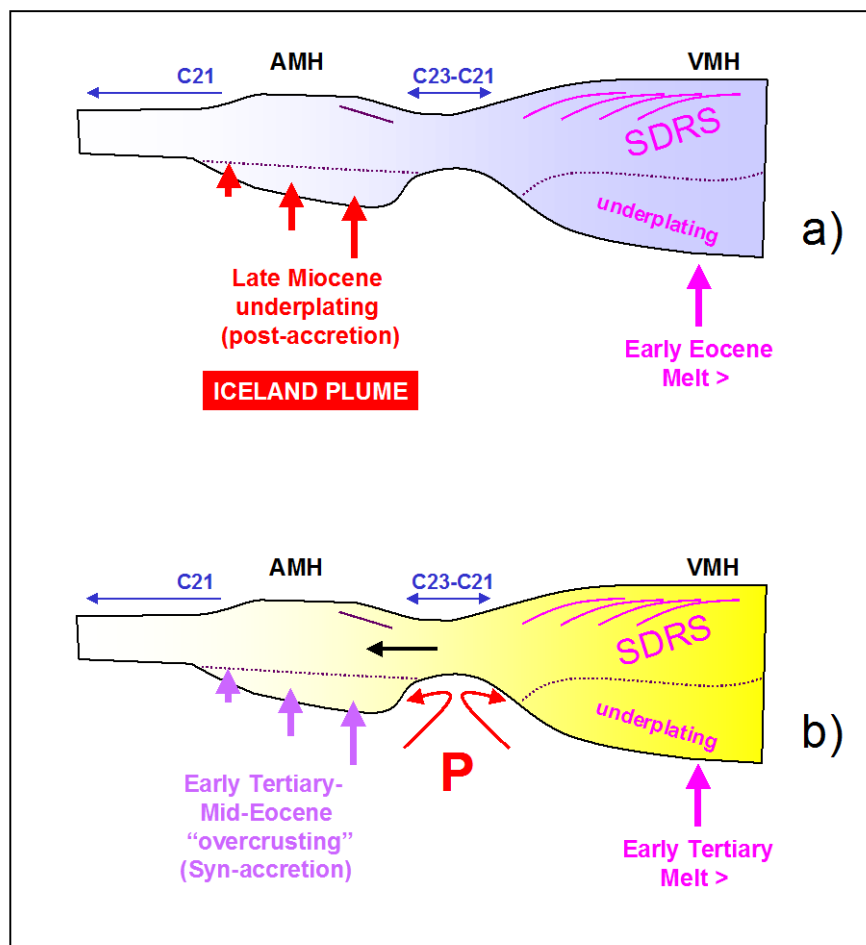


Figure 7.8 Two hypotheses to explain the anomalous thick crust beneath the Aegir Marginal High (AMH). a) A late Miocene magmatic underplating added to the preexisting oceanic crust (underplating model from Brevik et al. 2004, 2005). b) anomalous melt production generated during the oceanic accretion of the AMH in Eocene (overcrusting model, proposed by NGU). P: Aegir through propagating system. AMH: Aegir Marginal High; VMH: Vøring Marginal High.

According to the OBS model of Brevik et al. (2004, 2005) the highest magmatic rate expected (thicker crust) would be located at the level of C22 (49 Ma) to C21 (47Ma), representing an Early Eocene age.

A major argument for the Late Miocene underplating hypothesis is the relationship between the underplate and the main uplift of the AMH, proposed by Breivik et al. (2004, 2005). A late Miocene age for the uplift could have been caused by this late magmatic event. At this stage, we cannot confirm that the main uplift is Late Miocene in age but we clearly show that it happened after Early Oligocene (main unconformity MU event). Seismic sequences suggest that the uplift could be a prolonged event initiated in late Oligocene and still persistent in Miocene time.

In a global way, we believe that the uplift history along the AMH is probably more complex and not triggered by the buoyancy effects of the deep root only. Based on other observations, significant uplift associated with transform faults is commonly recognized in several other places. When transform faults connect divergent plate boundaries, a narrow and elongated valley and an adjacent marginal ridge is usually observed. In every case, the shape of the ridge is asymmetric and can easily be described by the upward flexure of the edge of the lithospheric elastic plate, since transform faults can be defined as vertical planes between two lithospheric plates sliding horizontally one against the other (Sandwell and Schubert 1982; Chen 1988; Wessel and Haxby 1990; Basile and Allemand 2002). The same vertical motion is observed when the two plates define an intra-continental transform faults or a transform continental margin between continental crust and oceanic plate. The EJMfZ is particular; because it was an 1) intra-continental transform zone before the breakup, then 2) became part of a transform margin shortly after the breakup in the southern part of the Vøring Basin. During the progressive displacement of the Jan Mayen Microcontinent, the EJMfZ was locally part of 3) a complex transform margin system involving the Jan Mayen Microcontinent and the oceanic crust. After continuous migration of the Jan Mayen Microcontinent, the EJMfZ started to be finally 4) an active oceanic transform fault then a fault zone. Only the CJMfZ and the WJMfZ are native oceanic faults zones.

Several hypotheses have been proposed to explain the flexure and uplift associated with transform faults. because the topography (or bathymetry) of transform faults appears to be quite uniform, different uplift models can only be used in a specific case. Such a model can explain uplift magnitude in between 500 and 1000 m (without involving any underplating!) and can be explained by several tectonic mechanisms (Fig. 7.9):

- a differential thermal subsidence on either side of the main fault zone (Sandwell and Schubert 1982)
- some shear heating and lateral heat conduction across the transform (Chen 1988)
- erosion and flexural uplift along the fault zone (Basile and Allemand 2002)
- oblique extension or transtension (Clift and Lorenzo 1999; Pockalny et al. 1996)
- lithospheric flow parallel to the transform along the transform margin (Reid 1989)
- twisting movements exerted along the transform fault at the ridge-transform

intersection (Chen 1989).

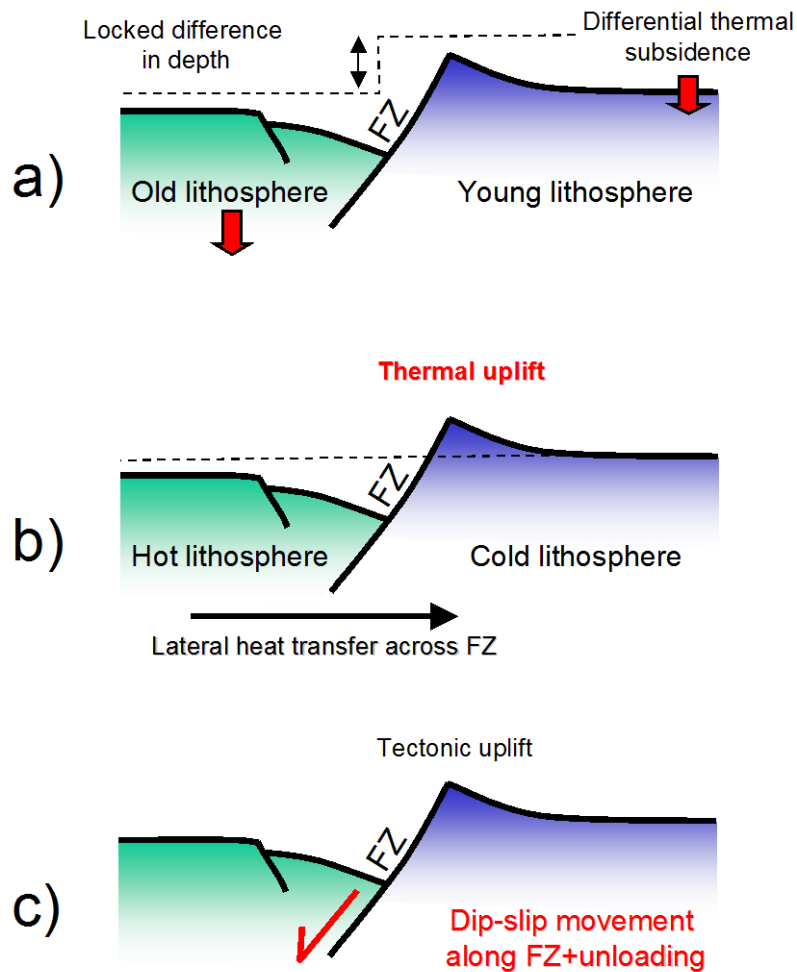


Figure 7.9 Main mechanisms proposed to explain flexural uplift along transform faults: a) differential thermal subsidence across a locked transform faults; b) thermal expansion caused by lateral heat transfer across the transform fault zone; c) tectonic extension or transtension (and induced unloading) oblique to a inclined transform zone. All these models can explain both the current geometry and part of the uplift observed along the Aegir Marginal High (AMH).

7.4 Quantitative analysis

Isostatic uplift due to underplating or overcrusting

We use a simple isostatic calculation to determine the amount of uplift due to the observed deep crust. This assumption neglects flexural effects and then provides the maximum uplift expected after underplating or overcrusting beneath the AMH. When magmatic underplating is added to the crust, uplift of the oceanic surface will occur if the material is less dense than the mantle. For the air-loaded case, the uplift U generated by

emplacement of a melt thickness of H_{melt} is given by $U = H_{\text{melt}}(\rho_m - \rho_{\text{overcrust}}) / \rho_m$. Both ρ_m (Mantle density) and $\rho_{\text{overcrust}}$ are commonly set as constants in the calculation with $\rho_m = 3270 \text{ kg.m}^{-3}$ and $\rho_{\text{overcrust}} = 2900 \text{ kg.m}^{-3}$.

However, during crystallization the initial density of the underplating could be ~10% lower. Assuming a 6 km thick underplating (or overcrusting) isostatic uplift would have been around 1100 m or 679 m if we consider the instantaneous cooling of the melt. This uplift could be less. It does not explain the uplift of ~1500 meters, suggested by the displacement between the EJMFZ valley and the top of the AMH.

Assuming that the deep root controls the uplift, the vertical motion should reach a maximum at the apex of the thickest part of the root. If we consider a NE-SW profile across the AHM and if we consider the mean surface envelope, a main swell ($\lambda = 250 \text{ km}$) seem to have been focus above the EJMFZ, and not above the crustal root, located ~375 km to the north. This observation suggests that underplating (or overcrusting) is not the main process involved in the AHM uplift.

Tectonic uplift due to tectonic flank uplift.

The strong asymmetry of the AMH close to the EJMFZ suggests at least a tectonic component during the uplift of the anomalous bathymetric feature. Assuming simple calculation, we suggest that the shape of the AMH could also be controlled by a flexural flank uplift accommodated by the EJMFZ.

The bathymetric shape of the AMH exhibits prominent asymmetric flanking uplifts; close the EJMFZ (Fig. 7.10). Several driving stresses and thermal-mechanical processes have been proposed to explain the origin of rift flank relief, which can be modeled to infer lithospheric elastic thickness (T_e). The flank uplift of the AMH is probably attributable to flexural upwarping of the lithosphere (Watts 2001). We examine the analytic plate flexure solutions by comparing them to analytic model of footwall flexure at a normal fault. A main border fault can promote decoupling between the hanging wall and footwall, in a two-dimensional elastic plate undergoing extension. The model assumes a strong uplift along the main border fault (EJMFZ), the formation of a deep hanging wall, controlled by the flexure, and a conjugate fault system (broken plate), which is required to accommodate the upward flexure of the plate. If we consider the NE-SW profile, the main fault could represent the EJMFZ and the bathymetric scarp located at distance $x_0 = 60 \text{ km}$ could be the conjugate fault system of the broken plate.

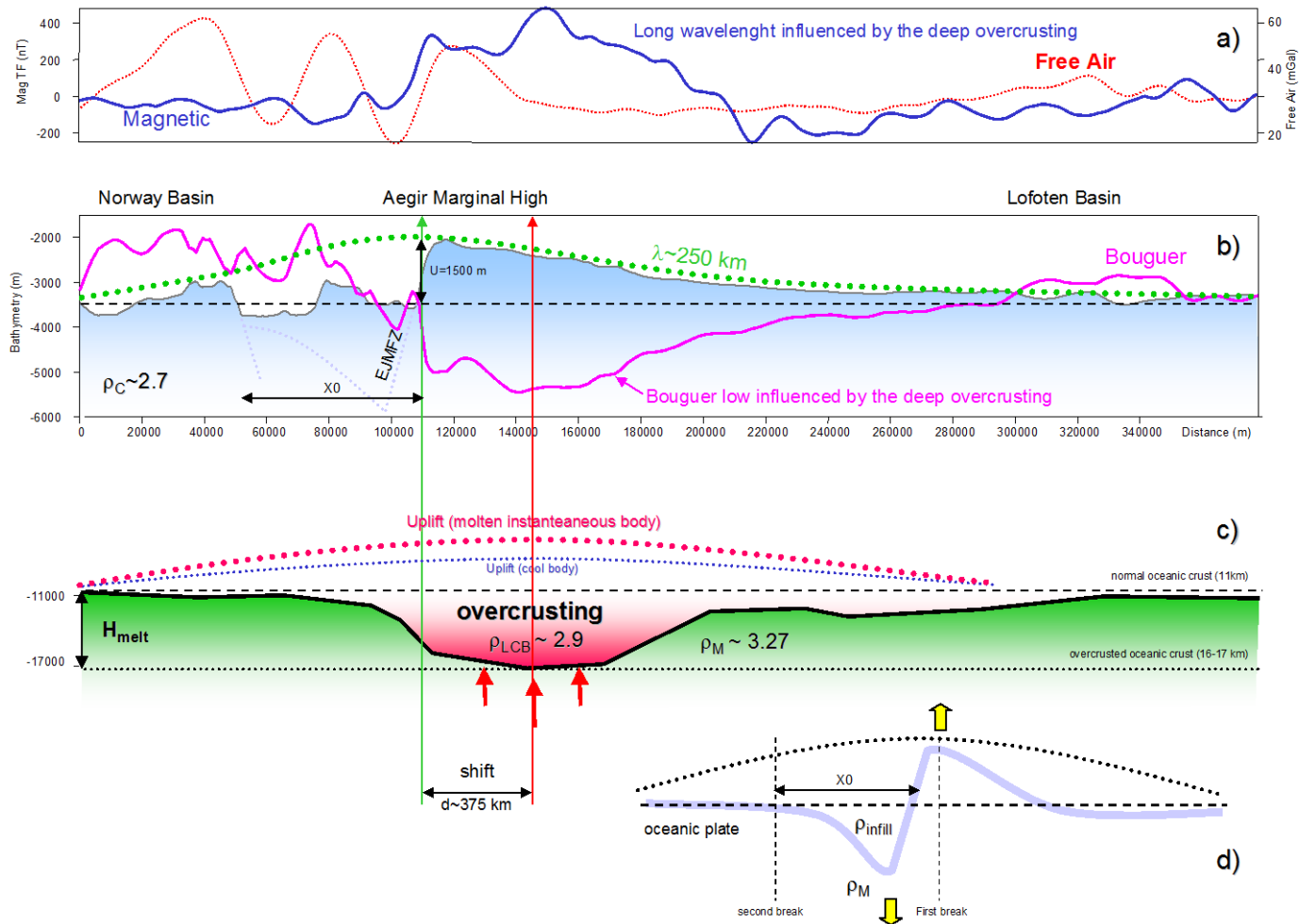


Figure 7.10 a) Free-Air gravity and broad magnetic anomalies across the Aegir Marginal High (AMH). b) NW-SE bathymetric and Bouguer profile across the AMH. The green dot represents the bathymetric envelop and probably the swell due to the AMH uplift. c) The crustal root (overcrusting) beneath the AMH fits the broad Bouguer anomaly and the long-wavelength signature of the magnetic total field but do not explain isostatically the main uplift (1500 m). d) The Bullard's model (Watts, 2001) controlled by the EJMfZ could explain part of the AMH structure.

An analytical solution can be used to investigate the mechanical relations between crustal rheology and flank uplift of this graben (Watts 2001). Assuming the geometric parameter, we can then estimate the elastic thickness of the lithosphere and compare this value with theoretical values of T_e expected for an oceanic lithosphere younger than 55 Ma (North Atlantic breakup). The comparison between calculated and theoretical value should confirm if the flexural flank uplift could be applied for the uplift of the AMH.

Calculating the flexure of a broken elastic plate using the approximation of Bullard (Watts, 2001)

For the T_e estimation we used the following parameters:

$E = 10^{11}$ Pa: Young's modulus

$g = 9,81 \text{ m}\cdot\text{s}^{-2}$: gravity

$\rho_M = 3200 \text{ kg}\cdot\text{m}^{-3}$: mantle density

$\rho_{\text{infill}} = 2300 \text{ kg}\cdot\text{m}^{-3}$: infill density of sediments

The flexure parameter for a broken plate is:

$$\lambda = \sqrt[4]{\frac{3(\rho_{Ml} - \rho_{\text{infill}}) \cdot g}{E \cdot T_e^3}} :$$

Distance from the first break to the location for the second break that occurs where the bending stress is greatest, can be described as a function of λ

$$x_0 = \frac{\pi}{4\lambda} :$$

then

$$\lambda = \sqrt[4]{\frac{3(\rho_{Ml} - \rho_{\text{infill}}) \cdot g}{E \cdot T_e^3}} = \frac{\pi}{4x_0}$$

$$\text{therefore: } \frac{3(\rho_{Ml} - \rho_{\text{infill}}) \cdot g}{E} = \left(\frac{\pi}{4x_0}\right)^4 \cdot T_e^3$$

$$\text{this leads to: } T_e = \sqrt[3]{\frac{3 \cdot 4^3 (\rho_{Ml} - \rho_{\text{infill}}) \cdot g \cdot x_0^4}{E \cdot \pi^4}}$$

The distance of second break can be estimated with $x_0 = 60\text{km} = 6 \cdot 10^4\text{m}$ from bathymetric profile (Fig. 7.10). Assuming this geometry of both the AMH and EJMfZ we obtain a value for the elastic thickness T_e :

$$T_e = \sqrt[3]{\frac{3 \cdot 4^3 (3200 - 2300) \cdot 9.81 \cdot (6 \cdot 10^4)^4}{10^{11} \cdot \pi^4} \left[\frac{\text{kg}}{\text{m}^3} \cdot \frac{\text{m}}{\text{s}^2} \cdot \text{m}^4 \cdot \frac{\text{m}^2}{\text{N}} \right]}$$

$$T_e = \sqrt[3]{\frac{192 \cdot 900 \cdot 9.81 \cdot 1.296 \cdot 10^{19}}{10^{11} \cdot \pi^4} [\text{m}^3]} = \sqrt[3]{2.255438 \cdot 10^{12} [\text{m}^3]} = 13114\text{m} \approx 13\text{km}$$

This value of 13 km can be compared with theoretical values of the T_e predicted for oceanic crust (Fig. 7.11, Watts 2001). This agrees with values predicted for oceanic crust younger than 60 Ma and confirms that the broken plate model is possible according to the reasonable value found for T_e .

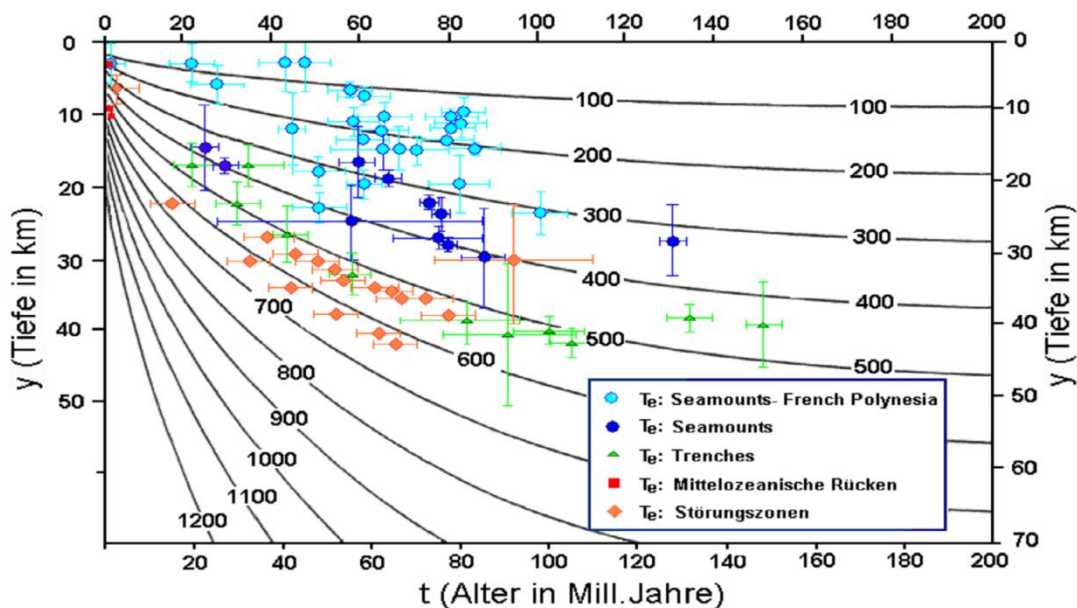


Figure 7.11 Theoretical values of T_e predicted for a cooling oceanic crust (Watts 2001). The elastic thickness is function of the age of the oceanic crust and increases when crust is older.

Flexural flank uplift along the EJMfZ is possible but this mechanism requires a normal stress (extension) along the main border fault. A slight angle between the spreading direction and the EJMfZ is then required to cause the uplift. We point out also that the Aegir Ridge is and was active close to the AMH in late Eocene around C18-C15. Some shear heating and lateral heat conduction between the ridge and the cooling oceanic crust

to the north probably influence the uplift of the AMH as well. After abortion of the Aegir Ridge, around C7 (25 Ma), the cooling of the Aegir Ridge probably enhance the differential subsidence on both side of the EJMF (see Figs 7.9)

To conclude, the uplift of the AMH is probably complex and probably involves several interacting processes, including, faulting, overcrusting, heat transfer and abortion of the Aegir Ridge.

8 TECTONOSTRATIGRAPHIC FRAMEWORK OF THE JMFZ AND COMPARISON AT THE SCALE OF THE ADJACENT MARGIN

Laurent Gernigon

Any attempt to better understand the Cenozoic stratigraphy of the JMFZ margin has to consider the regional tectonic setting. Megasequences development and regional unconformities, previously described tend to reflect major changes in the post-breakup evolution of the Cenozoic oceanic crust. The modification of the tectonic regime, sedimentation patterns along the JMFZ corridor is likely to be a response to regional cinematic events. At the Atlantic margins, plate tectonic processes probably result such changes. Subsidence analyses in the North Atlantic region have previously shown that major episodes of Cenozoic tectonism coincided with reorganisations of tectonic plates through spreading rates and/or directions (Brekke 2000; Mosar et al. 2002; Lundin & Doré 2002; Stoker et al. 2005; Praeg et al. 2005).

By comparing the sedimentary and oceanographic responses to these episodes, the present study provides stratigraphic constraints on the timing of the mains sequences observed in the Lofoten Basin and along the JMFZ corridor. Basically a regional event recorded at the scale of the North Atlantic is likely to be observed along the JMFZ corridor as well. Alternatively, the main sequences and tectonic events observed along the JMFZ can be useful to refine the Cenozoic history of the adjacent basins. Particularly, the effect on compression and sedimentation along the Mid-Norwegian can be better investigated and we plan to see if some relationships exist or not.

8.1 Plate reconstructions

In order to illustrate and summarize the geodynamic history, plate reconstruction models have been carried out. We used published finite rotation parameters summarized in Table 8.1 and rotated the magnetic grid at C21, C13 and C5 level (mid-Eocene/late Eocene, Eocene/Oligocene and intra-Miocene).

Table 8.1 Euler poles used for the plate reconstruction between Greenland, Mid-Norway and the Jan Mayen Microcontinent.

| Plate | Chron (age Ma) | Latitude | Longitude | Angle | References |
|-----------|----------------|----------|-----------|-------|-------------------|
| Greenland | C5 (10) | 67,07 | 138,2 | 2,6 | Unthernehr 1982 |
| Greenland | C13(33.1) | 68,3 | 132.6 | 7,6 | Gaina et al. 2000 |
| Jan Mayen | C13(33.1) | 64,9 | -12,2 | -8 | Lawer et al. 1990 |
| Greenland | C21(47.9) | -53 | -51.67 | -9,29 | Gaina et al. 2000 |
| Jan Mayen | C21(47.7) | 64.3 | -12.7 | -37.3 | Lawer et al. 1990 |

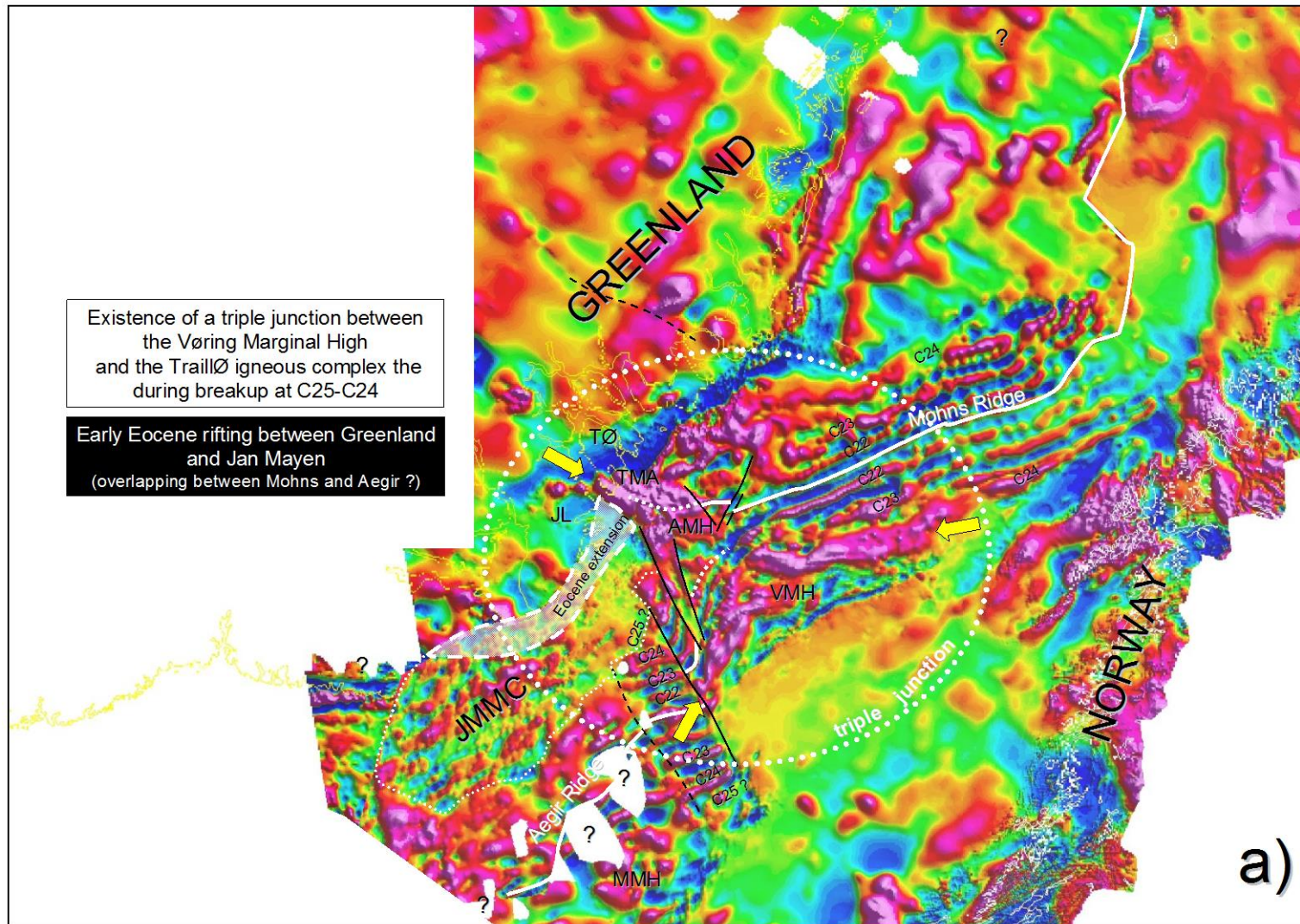


Figure 8.1 Plate reconstruction between Norway, Greenland and the Jan Mayen Microcontinent at C21 (47 Ma-early Eocene). This picture illustrates also a triple junction between the Vøring Marginal High and the TraillØ igneous complex. AMH: Aegir Marginal High; JL: Jameson Land; JMMC: Jan Mayen MC; MMH: Møre Marginal High; TMA: Traill-Vøring igneous complex; TØ: Traill Ø basin; VMH: Vøring Marginal High.

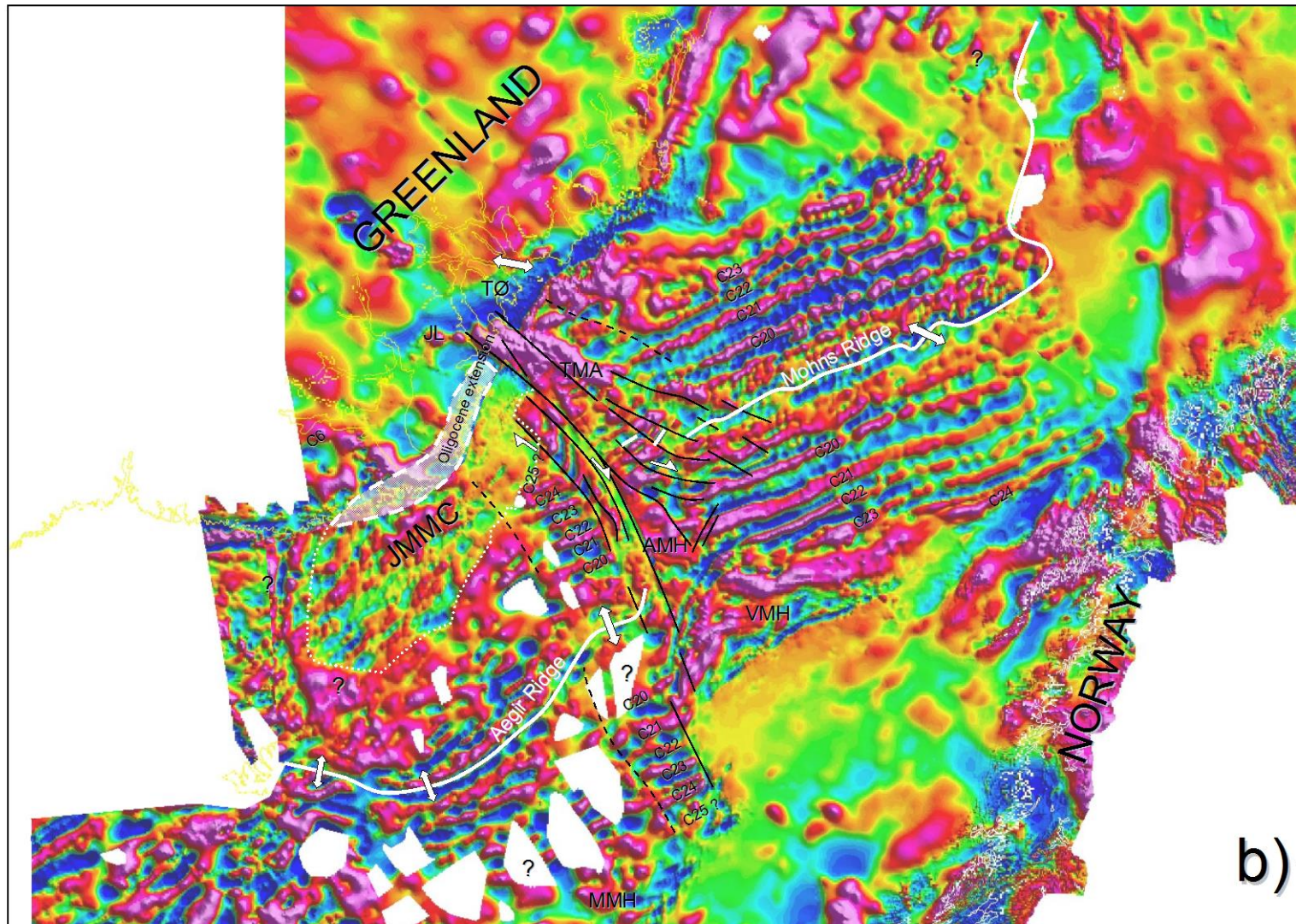


Figure 8.2 Plate reconstruction between Norway, Greenland and the Jan Mayen Microcontinent at C13 (33.3Ma-Eocene/Oligocene boundary). This event coincides with the onset of a major plate reorganization. AMH: Aegir Marginal High; JL: Jameson Land; JMMC: Jan Mayen MC; MMH: Møre Marginal High; TMA: Traill-Vøring igneous complex; TØ: Traill Ø basin; VMH: Vøring Marginal High.

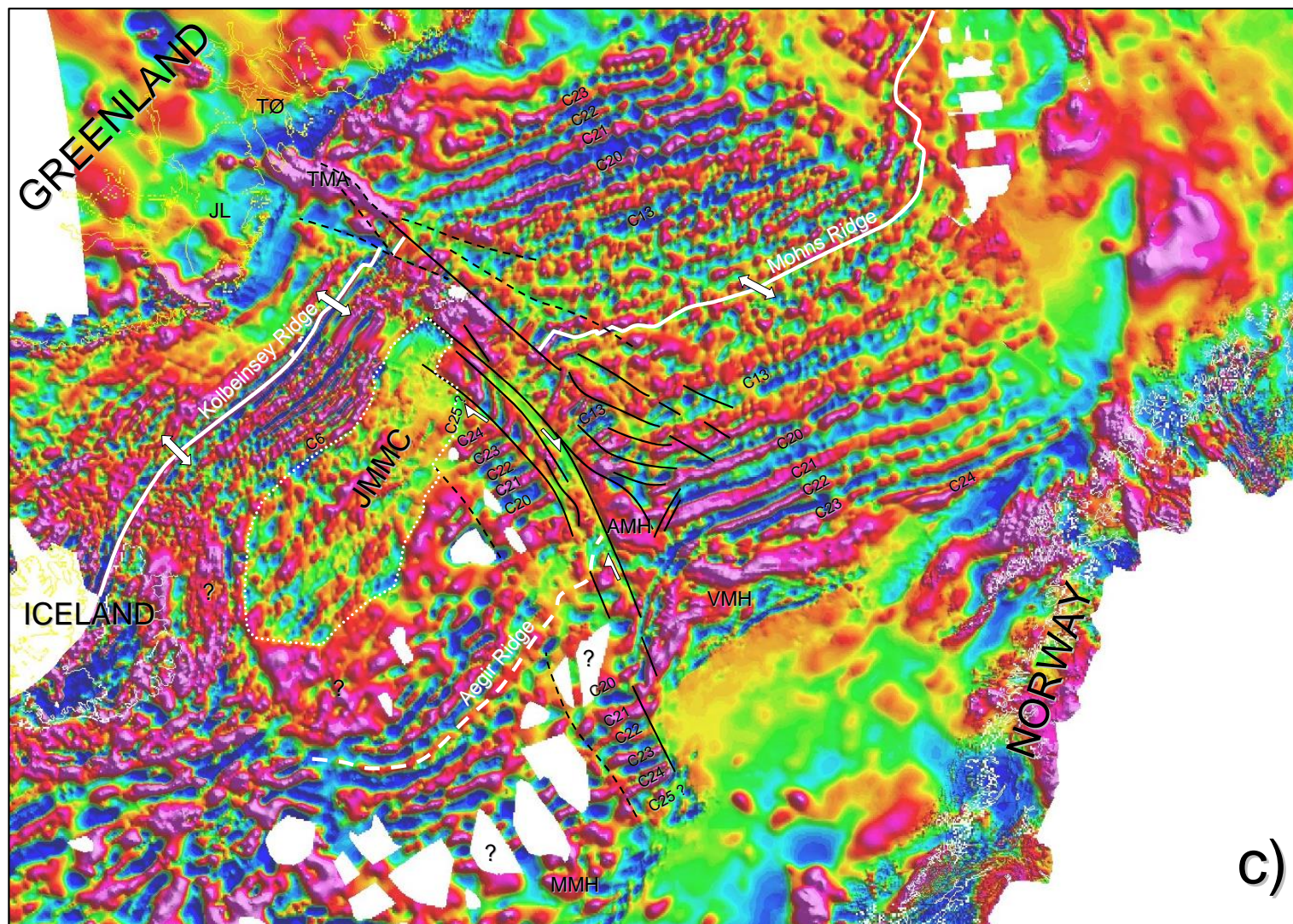


Figure 8.3 Plate reconstruction between Norway, Greenland and the Jan Mayen Microcontinent at C5 (10Ma-late Miocene). AMH: Aegir Marginal High; JL: Jameson Land; JMMC: Jan Mayen MC; MMH: Møre Marginal High; TMA: Trail-Vøring igneous complex; TØ: Trail Ø basin;; VMH: Vøring Marginal High.

8.2 Tectonic evolution from continental extension to seafloor spreading

During the Campanian-Paleocene period, faulting and uplift focus along the outer Vøring Basin, with a complex ridge system (Gjallar-Rån Ridges) described in detail by Gernigon et al., (2003, 2004) (Fig. 8.4). Surprisingly, the Late Cretaceous-Paleocene Ridge system is not so well observed in the Møre margin segment and could be expected along the Jan Mayen Ridge, initially located in the southern prolongation of the Gjallar-Rån Ridges. At this stage, the oceanic JMFZ is not yet formed and the Jan Mayen Microcontinent lies beneath the Gjallar-Rån Ridge system.

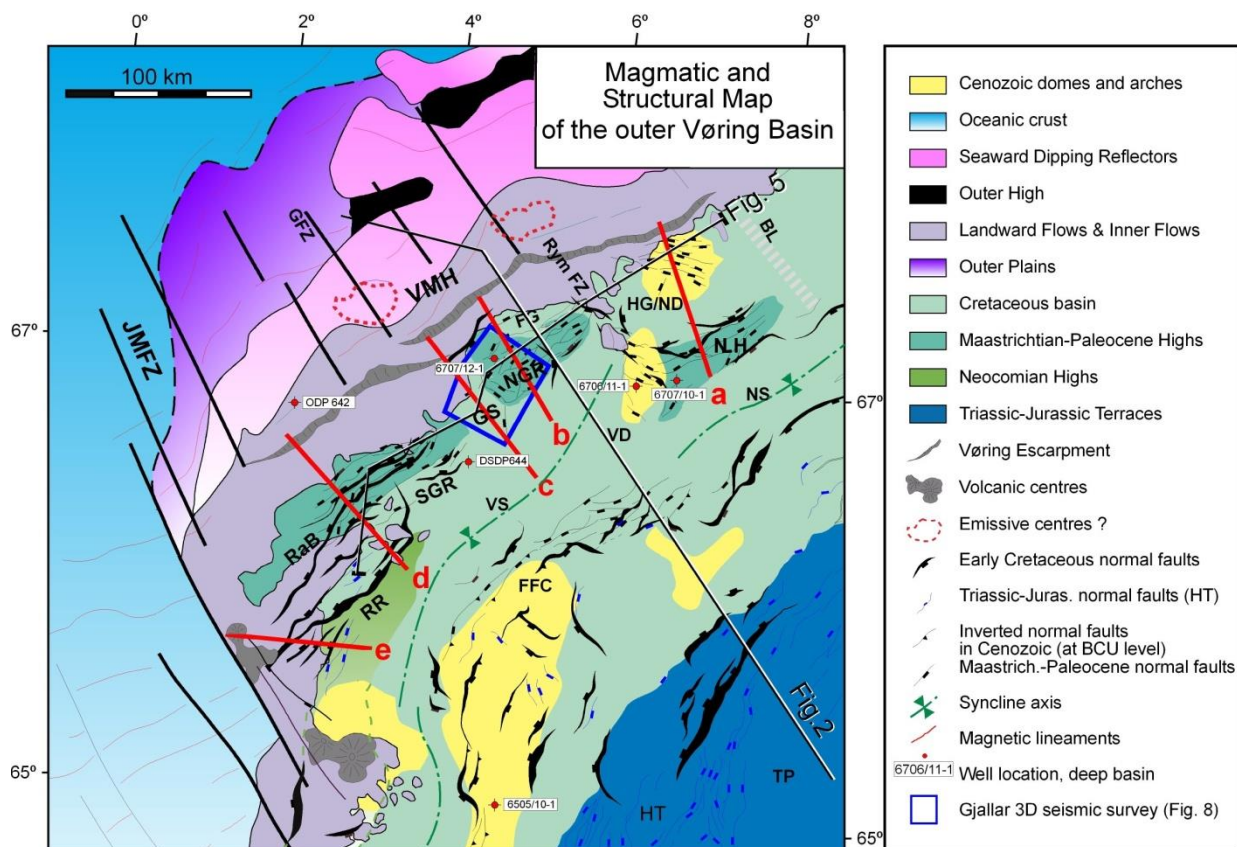


Figure 8.4 Structural map of the outer Vøring Margin (after Gernigon et al., 2003). BL: Bivrost Lineament; FFC: Fles Fault Complex; FG: Fenris Graben; GFZ: Gleipne Fracture zone; GS: Gleipne saddle; HG: Hel Graben; HT: Halten Terrace; JMFZ: Jan Mayen Fracture Zone; ND: Naglfar Dome; NH: Nyk High; NS: Någrind Syncline; NGR: north Gjallar Ridge; RaB: Rån basin; RR: Rån ridge; RFZ: Rym Fault Zone; SGR: south Gjallar Ridge; VS: Vigrid Syncline; VD: Vema Dome; VMH: Vøring Marginal High. Volcanic facies map of the Vøring Marginal high has been modified after Berndt et al. (2001a).

During the late stage of rifting (Latest Maastrichtian-Late Paleocene) extensional strain migrates to the proto-oceanic ridge. It is assumed that a thermal plumbing of the lithosphere induced by a thermal anomaly may have controlled the breakup. Similar

focusing of the deformation related with the onset of magmatism has been observed in the west Greenland Margin (Geoffroy et al. 2001) in relation with a major dike swarm development and the emplacement of an intrusive complex. Thermal erosion allows a lithospheric rupture without necessarily a strong stretching of the lithosphere and may play a role in focusing the deformation (Geoffroy et al. 2001; Gernigon et al. 2006). This model predicts that the initiation of the breakup may be located along the areas mostly affected by the sub-crustal magmatism. In late Paleocene-Early Eocene time (C24), the EJMFZ is part of an active transform margin in the southwestern part of the Vøring Basin. According the magnetic signature, two magnetic anomalies, associated with SDRS formed along the Vøring Marginal High. No SDRS are observed along the transform Vøring margin and are not expected either in the eastern margin of the Jan Mayen Microcontinent.

We will see later that the spreading system during the continental breakup is particular and likely witnesses a triple junction with anomalous magnetic anomaly (Traill Ø magnetic anomaly) observed offshore East Greenland (Figure 8.1).

8.3 Early to mid-Eocene deformation of the AMH and relationship with a probable propagating oceanic rift

During Early to mid-Eocene (C23-C20), oceanic spreading is well established along the Aegir and the Mohns Ridge (Fig. 8.3). The JMFZ started to be formed and accommodated the two spreading systems.

In mid- Eocene time, the magnetic pattern suggests significant faulting and strike-slip deformation across the AMH. According to the magnetic pattern the oceanic (magnetic) basement has been deformed between C21 (48.5 Ma) and C20n (43Ma). The onset of the event roughly coincides to the Lutetian stage (early Eocene). The map on Figure 8.2 shows that the C21 magnetic anomaly is progressively shifted to the north across the AMH. The shift could have been contemporaneous with oceanic accretion since the system was dynamic and still in motion at that time. Displacements of 20 to 50 km are observed and need to be accommodated by dextral strike-slip deformation. These strike-slip corridors are observed on seismic data (Fig. 8.2) and coincide with the main structural elements of the AMH, including the main ridge and the terrace. The magnetic map suggests that the deformation of the AMH magnetic basement already start before the main inversion, which is post-mid. Oligocene.

The block dislocations along the AMH can be explained by the complex geodynamic setting including two different spreading directions suggested by different magnetic patterns on either side of the JMFZ corridor. In the Lofoten Basin, magnetic chrons suggested a NW-SE extension (N°150). South of the AMH, the magnetic chrons between

C23 and C21 suggest a N°100-120 extension. This difference of 50° need to be accommodated and two regional stresses probably interacted along the AMH (Fig. 8.2c).

Other explanation for this dislocation could be the V-shaped bathymetric feature, the so-called Aegir trough, observed between the Vøring Marginal High and the AMH. This V-shaped bathymetric feature coincides also with a V-shaped magnetic anomaly defined at C21 south of the EJMfZ. This magnetic anomaly lies to the south between the chrons C22 and C21 observed to the north of the EJMfZ. This feature can be interpreted as a propagating rift (or propagator) intruding between the Vøring Marginal High and the AMH between C22 and C20r. A propagating system from south to north could have induced the progressive differential displacements observed along the AMH.

On seismic sections, the propagating rift coincides with a graben, active during Eocene times (Fig. 8.3). It is a slightly asymmetric structure and affects the SDRS to the east. The deeper part of the Aegir trough coincides with a narrow and deep graben that represents the propagator axis. Prolongated extension (or reactivation) is observed in this area up to (?) Oligocene.

Several mechanisms have been proposed to explain rift propagation, including concentration of gravity sliding stresses, sudden changes in direction of sea-floor spreading or motion of the ridge in an absolute (hot-spot) reference frame (Hey et al. 1980; 1988; Kleinrock et al. 1997). Higher areas have farther to slide, so gravitational sliding stress is greater there than at lower areas, producing stress concentration at the crack tip. It has also been proposed that rift propagation may be due to relative motion between the spreading plate boundary and the underlying, fixed asthenosphere (Tucholke and Schouten 1988). The progressive changes in the direction of seafloor spreading could explain such a rift propagation but the relationship of this feature with the Aegir Ridge through the EJMfZ is still unclear, due to low magnetic coverage, south of the survey.

A significant clue to the origin of the fast propagators may be found in the gravity data. The propagator correlates with changes from lower to higher gravity anomalies between the Vøring Marginal and the AMH. This implies that some combination of crustal thinning and/or mantle cooling occurred coevally with the initiation and migration of this Aegir propagator. This propagator coincides also with a shallow Moho between the Vøring Marginal High and the AMH. Gravity and Moho variations could be interpreted as episodicity in the amount of magma supplied to the ridge. We infer periods of higher magma supply (corresponding to the gravity lows) to be times when plate separation was more dominated by magmatic intrusion, in contrast to periods of lower magma supply (corresponding to the gravity highs) when most of the separation was taken up by faulting. Thus, the propagator seems to have developed during a transition from more magmatic to less magmatic periods of spreading.

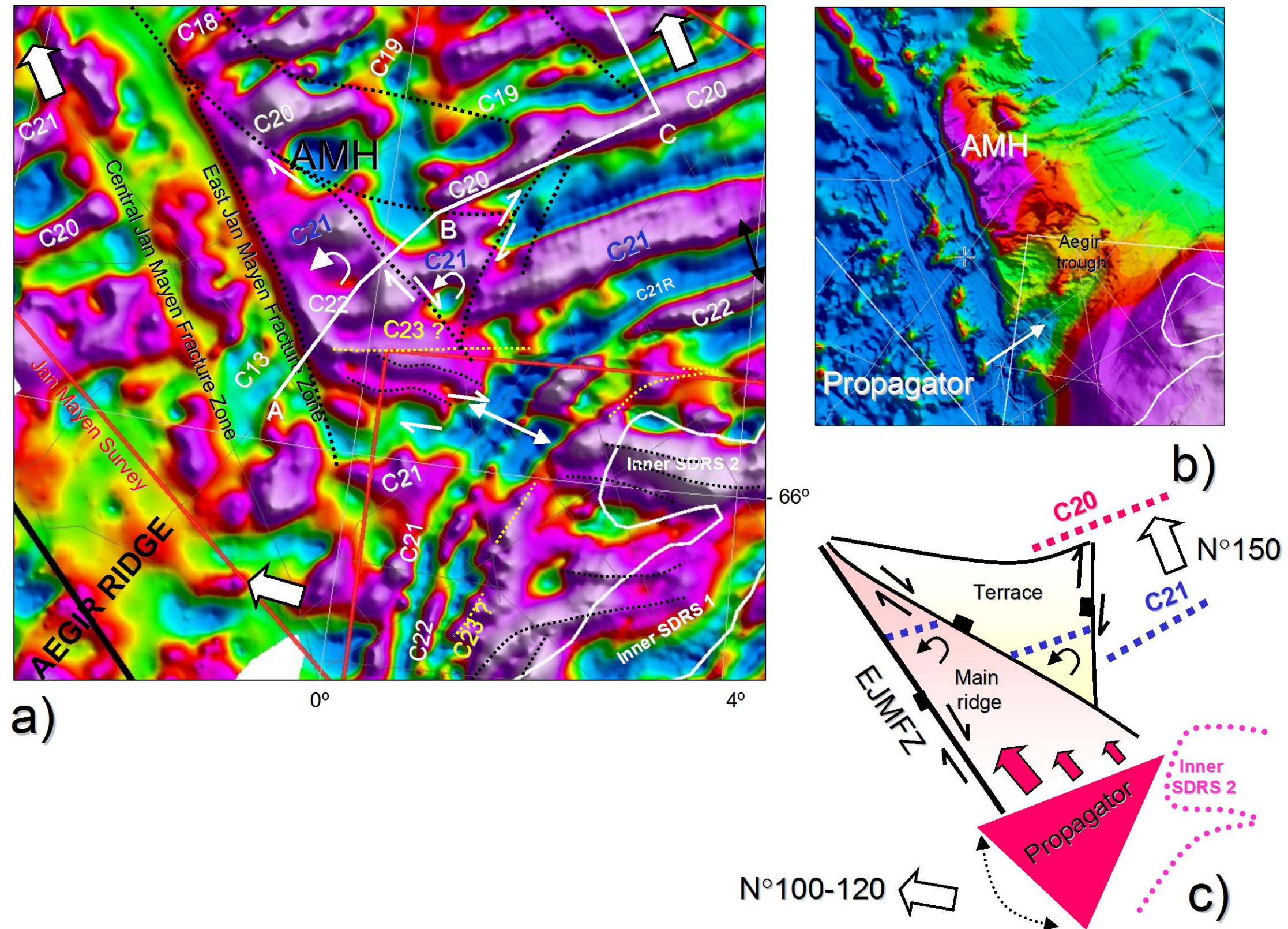


Figure 8.2 a) Magnetic pattern of the oceanic basement around the Aegir Marginal High (AMH). b) High resolution bathymetry between the AMH and the Aegir trough. c) Schematic cartoon that illustrates a possible structural relationship between the Aegir trough and the block dislocation of the AMH. The V-shaped Aegir trough probably represents a propagating oceanic ridge. During the propagation from south to north, lateral oceanic accretion probably induced displacement able to produce the block dislocation of the AMH.

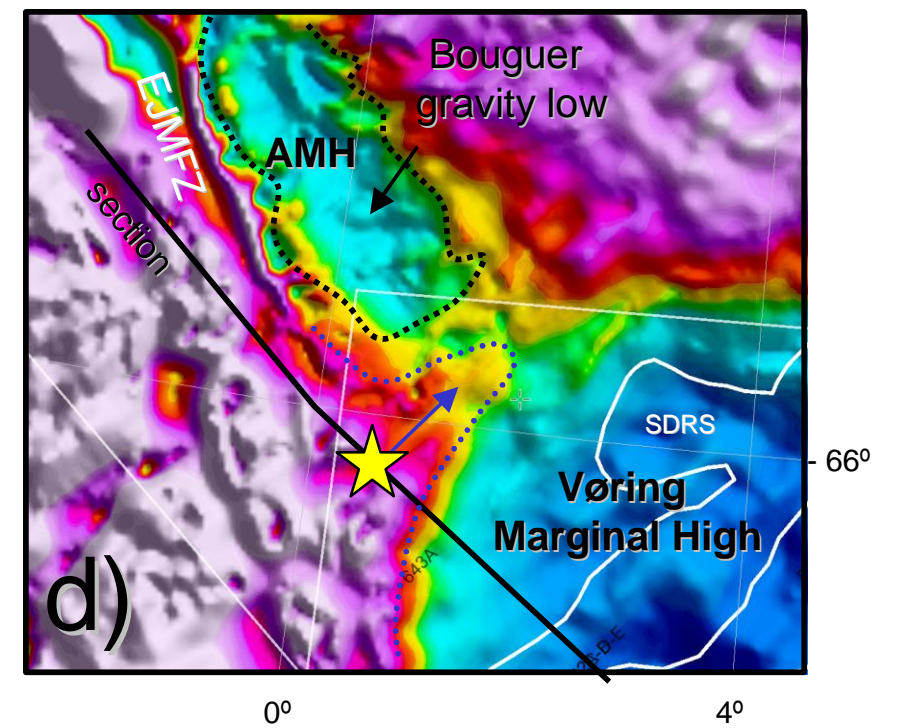
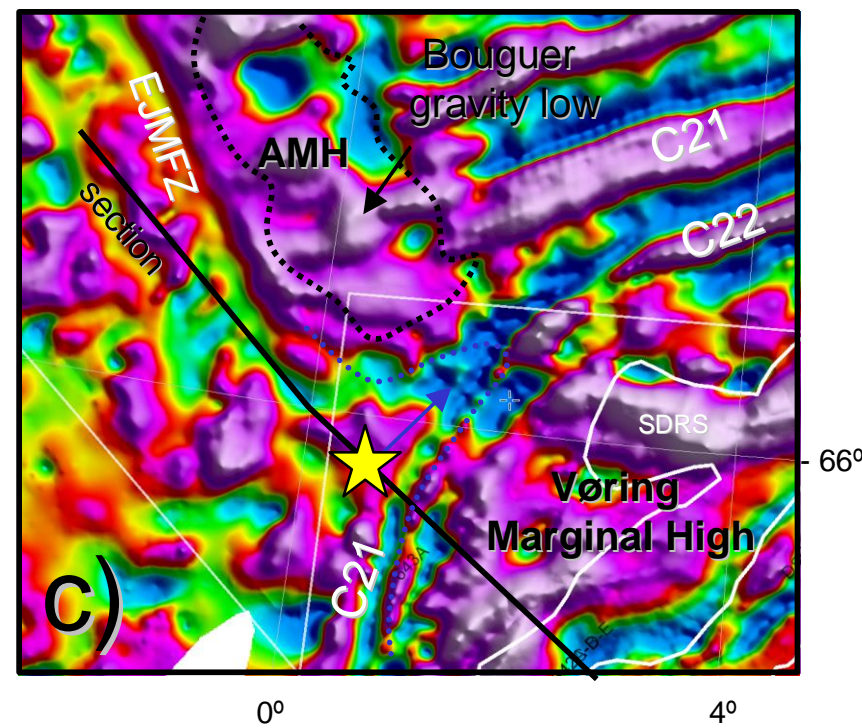
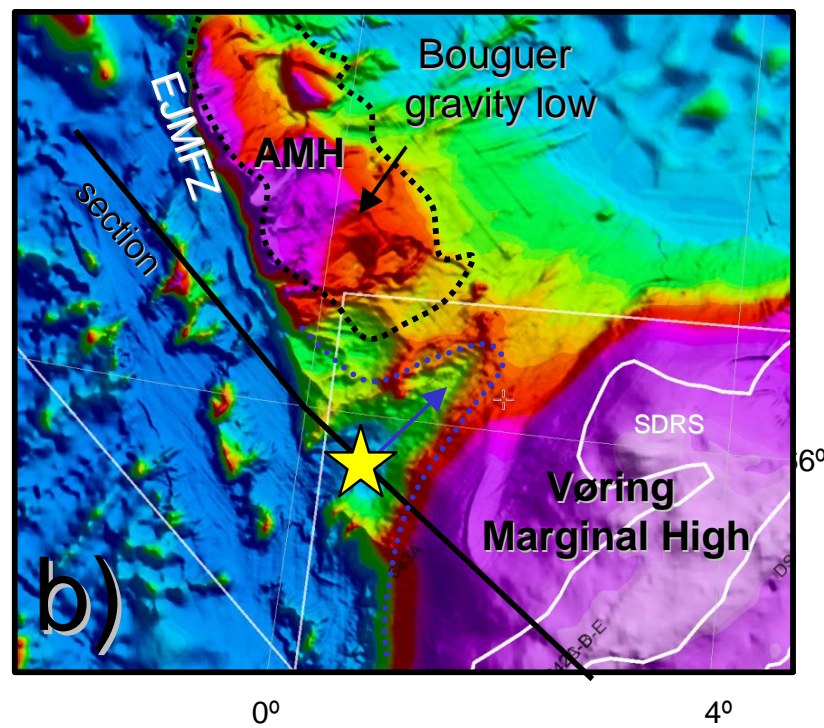
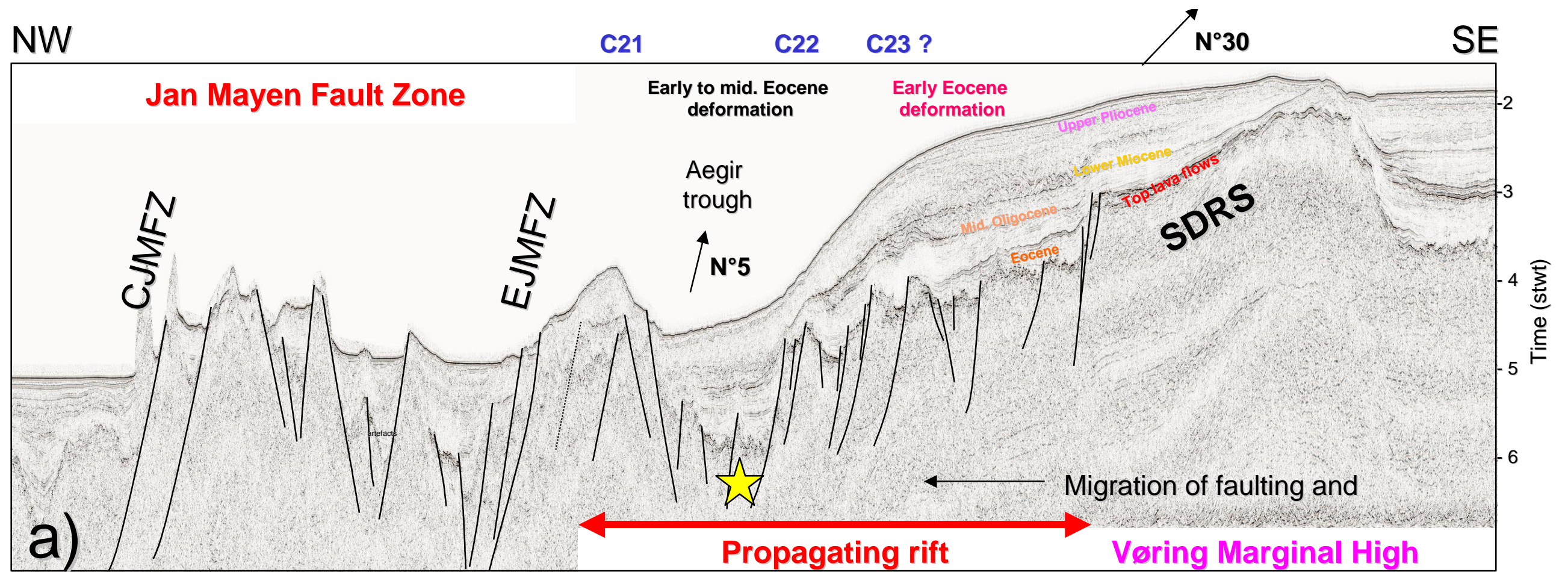


Figure 8.3 a) Seismic transect across the Aegir trough. b) Bathymetry illustrating the V-shaped structure of the Aegir through. c) Magnetic anomalies d) Bouguer gravity anomalies between the Vøring Marginal High and the AMH.

8.4 The late Eocene–early Oligocene

From C20 (43 Ma) to C13 (33.3 Ma), ongoing accretion is still ongoing but the magnetic pattern, north of the EJMFZ) suggests a progressive change of the opening direction (Fig. 8.2 and 8.5). Shifts and faulting of the magnetic anomalies, due to oblique spreading, are already observed at the level of C19 (41.5 Ma) and C18-15 (40-35 Ma) before C13. At this level, significant faulting and dextral dislocation are observed in the northwestern part of the AMH. This area could be defined as a hinge zone between the AMH and the western part of the East JMFZ corridor, also well defined on gravity and bathymetry datasets.

Previous interpretation suggested that a significant counter-clockwise rotation of the opening direction took place in the Norwegian Sea changing from NNW-SSE to NW-SE at C13 (Lundin & Doré 2002). This main event is characterised by a difference in trend between the EJMFZ and CJMFZ and onset of this event was deduced from the eastward termination of the WJMFZ near C13, poorly constrained by the former magnetic dataset. The new survey suggests that the plate reorganisation and oblique spreading initiated earlier after C20 (42 Ma), i.e. 10 Ma before the previous assumption.

At a regional scale, the late Eocene–early Oligocene period witnessed the cessation of seafloor spreading in the Labrador Sea in favor of the NE Atlantic axis (Doré et al. 1999), coeval with the culmination of the Pyrenean orogeny (Knott et al. 1993). These events coincided with rapid differential subsidence in the North Atlantic area, which outstripped sedimentation to drive a rapid deepening, that established the deep-water basins (Stoker et al. 2001).

Anomalous subsidence attributable to a late Eocene to Oligocene episode of rapid (10 Ma), subsidence and sagging, that outstripped sedimentation to drive a km-scale deepening and steepening of the conjugate East Greenland and Rockall margins (Clift 1996). The Rockall Trough and Porcupine Basin subsided to a point that allowed bottom currents to enter the basins from the south as well (McDonnell and Shannon 2001; Stoker et al. 2001, 2005). This regional event may have also affected the Faroe-Shetland and Norwegian margins in the mid-Cenozoic, although this remains unclear due to poor well calibration (Fig. 8.4).

This change in continental margin stratigraphy have been noted on all the Atlantic margins, in the form of late Eocene to early Oligocene shelf to deep-water unconformities, argued by some authors to record eustatic changes in sea level (e.g. Miller et al. 1985; Poag & Ward 1987) but shown by others to record changes in sediment supply and an intensification of deepwater currents linked to tectonic movements (McGinnis et al. 1993).

An upper Eocene Unconformity is traceable north of the Rockall Basin across the Faroe-Shetland and northern North Sea basins to the mid-Norwegian margin (Figs. 8.4. and 8.5). Far from the JMFZ, a similar unconformity corresponding has been correlated from DSDP sites on the southern Irish margin (Goban Spur) (Stoker et al. 2005).

The PM unconformity observed from the Lofoten Basin to the Aegir Marginal High likely coincides with this Early Oligocene regional unconformity.

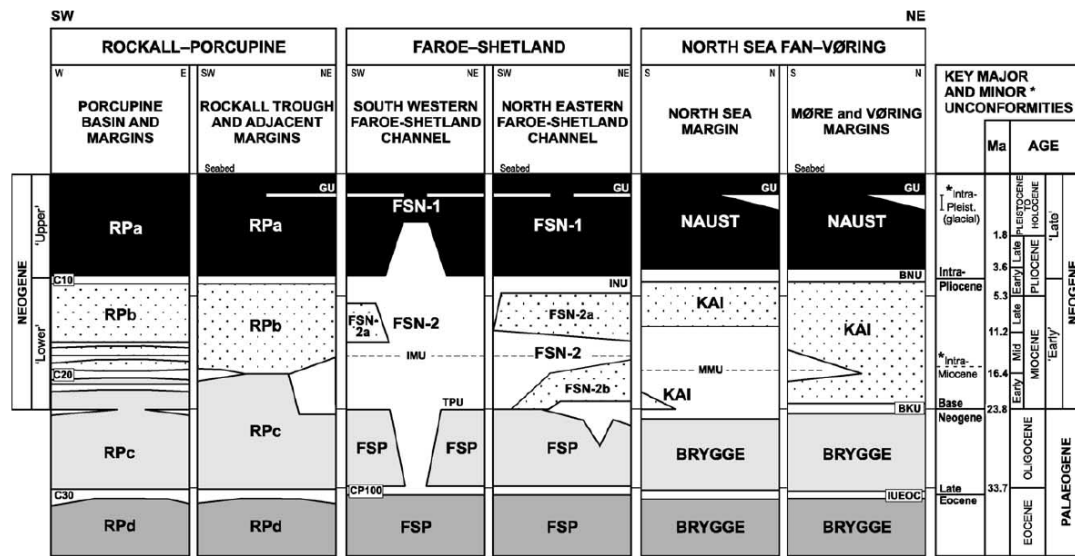


Figure 8.4 Stratigraphy for the upper Palaeogene–Neogene strata on the NW European Atlantic margin (Stoker et al. 2005). The assignment of major and minor unconformities (see text) is based on the correlation of key reflectors from the North Sea Fan–Vøring, Faroes–Shetland and Rockall–Porcupine areas. The two regional unconformities recognized from the Aegir Marginal High to the Lofoten basin (PM and MU) could coincide, respectively with the early Oligocene and the late Oligocene–Early Miocene major and regional unconformities. BNU, base Naust unconformity; INU, intra-Neogene unconformity; BKU, base Kai unconformity; TPU, top Palaeogene unconformity; GU, intra-Pleistocene glacial unconformity; IMU, intra-Miocene unconformity; MMU, mid-Miocene unconformity; IUEOC, intra-upper Eocene unconformity. Timescale after Berggren et al. (1995).

Onset of compressive stress along the Mid-Norwegian margin

During this period, major anticlinal structures on the Mid-Norwegian margin start to form (Fig. 8.5). Major domes lie within the Vøring Basin, and include the Ormen Lange Dome, the Helland–Hansen and Modgunn arches and the Vema and Nalgfar domes. These structures generally trend en echelon between NW–SE trending fracture zones, such as the JMFZ and Norway Basin Fracture Zone. An Eocene–Oligocene growth phase is well documented for the Ormen Lange Dome and the Helland–Hansen Arch, which were reactivated in Miocene along with the development of the remaining structures (Brekke 2000; Lundin & Doré 2002). The most recent work of Gómez and Vergés (2005) suggests however that only the Vema Dome and the Helland-Hansen Arch are likely to initiate in Eocene and Early Oligocene time. This growth phase coincides with the propagating event and the progressive change of seafloor spreading direction in the Lofoten Basin and a genetic correlation could be proposed (Fig. 8.5).

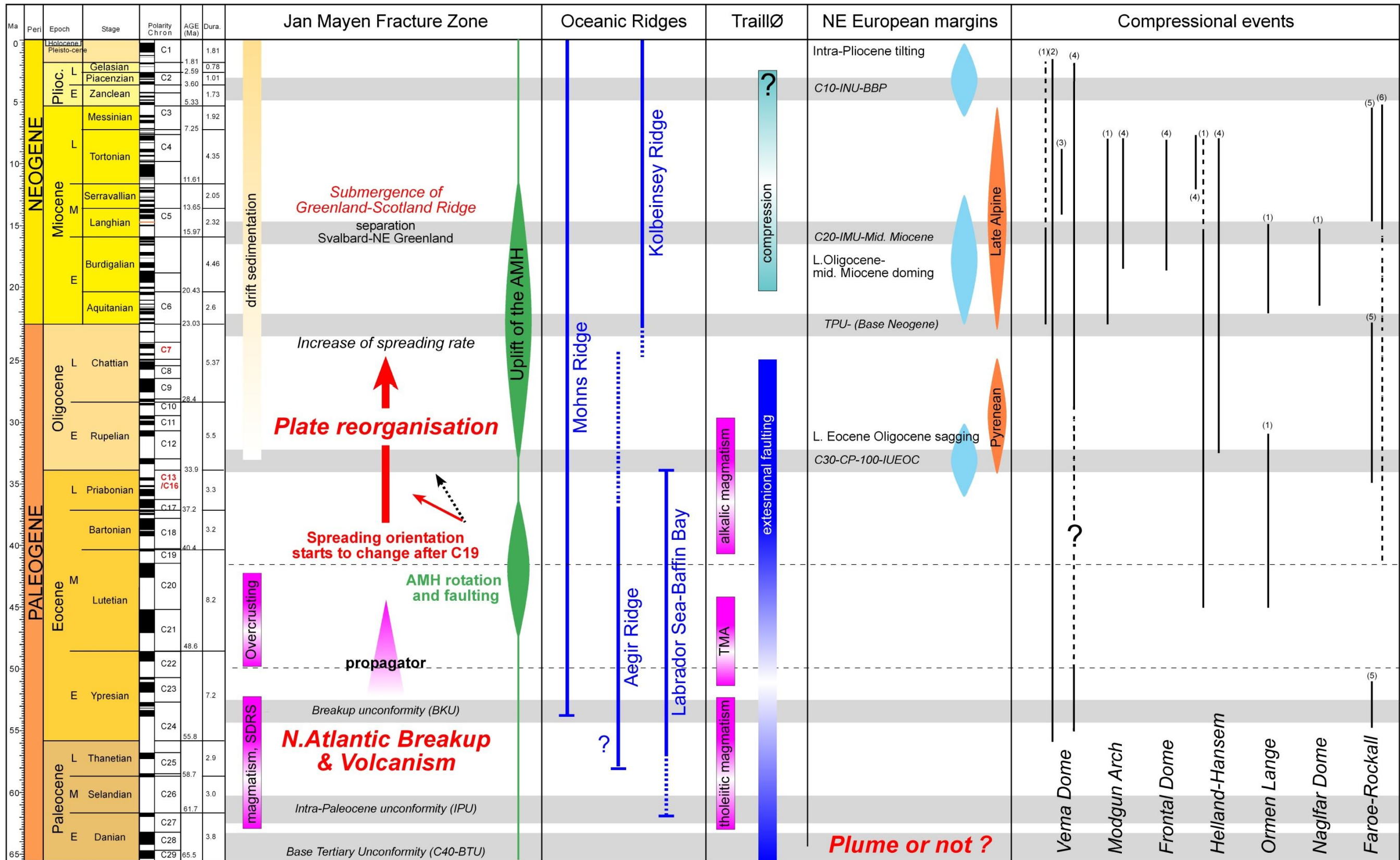


Figure 8.5 Tectonic calendar of Cenozoic geodynamics deduced from the Jan Mayen area. Magmatic and tectonic episodes, onshore Traill Ø, from Price et al. (1997) and Lundin and Doré, (2002). TMO: offshore Traill-Vøring igneous complex (Olesen et al., submitted). Summary of the NW European continental margin megasequences and regional tectonics from Praeg et al. (2005). Compressional events interpretations are from 1) Lundin and Doré, 2002; 2) Våagnes, 1998; 3) Brekke, 2000; 3) Gómez and Vergés, 2005; Boldreel and Anderson, 1993; Ritchie et al., 2003. Time scale from Gradstein et al. (2004).

8.5 Late Oligocene to mid-Miocene

The early to mid-Miocene period included regional changes in plate tectonic motions, including the culmination of the Alpine Orogeny (Knott et al. 1993) (Fig. 8.5). Within the NE Atlantic region, this period witnessed mostly the progressive transfer of spreading from the Aegir Ridge (to the SE) to the Kolbeinsey Ridge (to the NW) between magnetic polarity C13–C7 (3.33–25 Ma, early to late Oligocene) (Figs. 8.2 and 8.3). It results in the separation of Jan Mayen and Greenland sometime between anomalies 7 to 6 interval (latest Oligocene to early-Miocene) (Brekke 2000; Lundin & Doré 2002; Mosar et al. 2002). This regional plate reorganisation was probably accompanied by the onset of inversion structures on the adjacent Norwegian margin (Brekke 2000; Mosar et al. 2002) and probably affects the AMH as well. The main unconformity (MU) may represent this regional cinematic change and we believe that the main phase of inversion and uplift along the AMH, controlled by the change of the regional deviatoric stress direction from NNW-SSE to NW-SE occurred during this period.

At a regional scale, the early to mid-Miocene period of ridge transfer and compressive tectonism brackets the formation of two other major unconformities including the Base Neogene unconformity (Late Oligocene-Early Eocene) and an intra-Miocene (Early to mid-Miocene) unconformity. Locally, the two unconformities merge (Figs 8.4 and 8.5). Submarine erosion of a base Neogene unconformity took place across and north of the Wyville–Thomson Ridge Complex in the Faeroes-Shetland Basin, whereas mid-Miocene surfaces on either side of the ridge record a major expansion of contourite drifts that may be attributed to differential tectonism leading a passageway for deep-water exchange (Stoker et al. 2005). The expansion of the deepwater current system was also approximately coeval with the opening of the Fram Strait between NE Greenland and Svalbard. The Northern Gateway then established was a true deep Arctic–NE Atlantic connection (Eldholm 1990) that certainly affected the corridor and the Lofoten Basin. It can partly explain the different sedimentary facies, seismically observed, above the main unconformity MU.

Compression increases

Most of the authors agree that the main tectonic growth contribution happens between Early to mid-Miocene. Interestingly, the tectonic contribution to the growth of the domes ended or became very small during the Late Miocene (Gómez and Vergés 2005) and do not support any major tectonic or late magmatic event (Fig. 8.5). The late Oligocene to mid-Miocene period marks also the main domes growth in the Mid-Norwegian margin. However, uncertainty has prevailed over the timing of the Miocene growth. According Stoker et al. (2005b), the Helland–Hansen Arch reveals two phases of Miocene contourite deposition along its western flank inferred to reflect a significant mid-Miocene change in the bottom-current circulation system in response to the compressive episode (Hjelstuen et al. 2004).

Stoker et al. (2005b) shows that onlaps onto an existing domal structure of a lower–middle

Miocene elongate mounded contourite sediment drift, has been subsequently tilted during a second phase of inversion, with a relief of at least 500 m. This lower–middle Miocene section is overlapped by less steeply dipping middle–upper Miocene strata. The boundary between the two sediment packages is probably the mid-Miocene unconformity, as recognised by Brekke (2000). This major mid-Miocene growth phase interpretation is slightly later than the early Miocene reactivation/growth of the Ormen Lange, Vema and Naglfar domes proposed by Lundin and Doré (2002). The Mid-Miocene event coincides also with the onset of growth in the Modgunn and Frontal Dome according to Gómez and Vergés (2005).

According to Lundin and Doré (2002), the first development phase of the Ormen Lange dome initiated during Middle Eocene to Early Eocene time (45 to 30 Ma) coincides with the magnetic chrons C21 and C12. This period is tectonically according to the new interpretation of the Jan Mayen Survey and some correlations are expected (Fig. 8.5)

Greenland–Scotland Ridge–Wyville–Thomson Ridge Complex continued to act largely as a barrier to intermediate and deep-water flow through the Oligocene and early Miocene.

9 STRUCTURAL INHERITANCE AND MAGMATISM

Laurent Gernigon

9.1 The JMFZ and its relation to inheritance

The Mid-Norwegian margin is influenced by several boundary zones, which are potentially of great importance for stress transfer, stress perturbation and structural development. Succession of tectonic events during Proterozoic and Caledonian probably influenced the late Paleozoic-Mesozoic development of the margin. In this study, no major NW-SE major faults are directly observed in the continental prolongation of the JMFZ. The JMFZ and the Norwegian Basin Fracture Zone are mostly related to the prolongation of the limits of the Jan Mayen corridor, which is interpreted as a distinct rheological and crustal domain between the Møre and the Vøring Basin. However, lineaments, which controlled the pre-Cretaceous rift system along the corridor, may be related to basement fabrics acting as local stress perturbators. Later, faulting in the trend of the Jan Mayen corridor appears to be initiated during the breakup initiation in Late Paleocene time.

Although the exact impact and age of the pre-existing shear zones can not be precisely determined, Doré et al., (1997) and Fichler et al., (1999) point that the NW-SE offshore trends are likely to represent some crustal lineaments. They are sub-parallel an old NW-SE Proterozoic deep shear zones underlying (?) the Caledonian stacked nappes, mostly NE-SW to NNE-SSW. NW-SE pervasive fabrics in the crust may for example, influence a large volume of rocks and then may define contrasting crustal and even upper mantle domain. The Jan Mayen corridor is assumed to represent such distinct domains. The pre-existing fabrics may inhibit faults and rifting propagation as observed along several small-scale accommodation zone influenced by shear zones (Morley et al. 1999).

In the East Greenland conjugate margin, the JMFZ lies in the trend of the south Traill Ø region (Scott 2000, Skogseid, 2000, Lundin and Doré, 2002). Based on deep crustal investigation, Scindwein and Jokat (1997) stress that this area is an important accommodation zone between different crustal architectures and assume that Mesozoic extension was particularly reduced in southern part of the Kong Oscar Fjord compared to its northern part.

The Jan Mayen corridor is believe to represent a large crustal scale accommodation zone during the stretching of the Mid-Norwegian margin and its Greenlandic conjugate and may be controlled in depth by pervasive NW-SW inherited fabrics.

9.2 Inheritance and magmatism

It is tricky to understand how melt intruded and migrated within the continental crust. However, it is supposed that the repartition of the magmatism is not random. Several observations have suggested that the inheritance may influence the location of magmatism. In the East African Rift system, for example, Cartwright et al. (1992) show that both transfer zones and volcanism are focalised along the trend of inherited shear zones. Across the Namibian continental margin, Bauer et al. (2000) show that volcanic complexes and underlying intracrustal gabbroic intrusions trend along the shear zone existing between a thin crustal Precambrian fold belt and a thick cratonic area. In the British Tertiary Igneous Province, gabbroic chambers that appear to be controlled by old and crustal shear zones, are located 300 km away from the breakup and prebreakup rift axis (Geoffroy et al. 1998).

Along the Jan Mayen corridor breakup related magmatism is present and proved by a porphyritic olivine-nephelinite volcanic plugs dated at 55.7 Ma and drilled 260 km eastward from the proto-oceanic ridge, close to the Norwegian coastline (Bugge et al. 1980). Torske and Prestvik (1991) already suggest a relationship, between Greenland magmatism and the trend of the JMFZ corridor.

The onshore Late Palaeozoic-Mesozoic succession on Traill Ø, in the trend of the current WJMFZ, are well known for being intruded by a large number of basic sills and dikes and huge igneous complexes (Koch & Haller 1971; Noe-Nygaard 1976; Upton 1988; Upton et al. 1995; Price et al. 1997; Lundin & Doré 2002) (Fig. 9.1). Large Tertiary syenite complexes are exposed in eastern Traill Ø, at Kap Parry and at Kap Simpson, in the northern part of Jameson Land (Koch & Haller 1971; Noe-Nygaard 1976, Noble 1988). The Tertiary igneous rocks of Traill Ø form part of a much larger province in East Greenland (Upton 1988). Large volumes of basic intrusions comparable to those exposed on Traill Ø crop out also in Geographical Society Ø. North of Geographical Society Ø, in Hold-with-Hope and Wollaston Forland. Seaward-dipping reflectors, inferred to represent subaerial flood basalts emplaced during the formation of the East Greenland margin, have been identified on seismic reflection profiles across the eastern margin (Coffin & Eldhom 1995). South of Scoreby Sund, even larger volumes of flood basalts are preserved both onshore and offshore (Larsen et al. 1989).

The more recent ^{40}Ar - ^{39}Ar step-heating ages (Price et al. 1997) show that at least two distinct phases of magmatism affected Traill Ø. The limited age data currently available suggest that the earlier phase of magmatism produced:

- 1) Late Paleocene-early Eocene tholeiitic basalts (between 55.8 ± 0.9 and 52.75 Ma) like that erupted simultaneously in Wollaston Forland and Hold-with-Hope, whereas the later phase produced alkalic basalt.
- 2) Late Eocene-early Oligocene alkalic basalt, dykes and the Kap Parry syenite are slightly older than an ^{40}Ar - ^{39}Ar plateau age for a late-stage intrusion in the Myggbukta complex, Hold-

with-Hope (32.7 ± 1.2 Ma; Upton et al. 1995).

Offshore Greenland, the Traill Ø magnetic anomaly, clearly observed until C21 (47 Ma) (Fig. 9.1), probably represents an igneous complex linked with the Traill Ø intrusion (the Traill-Vøring igneous complex, Olesen et al., submitted).

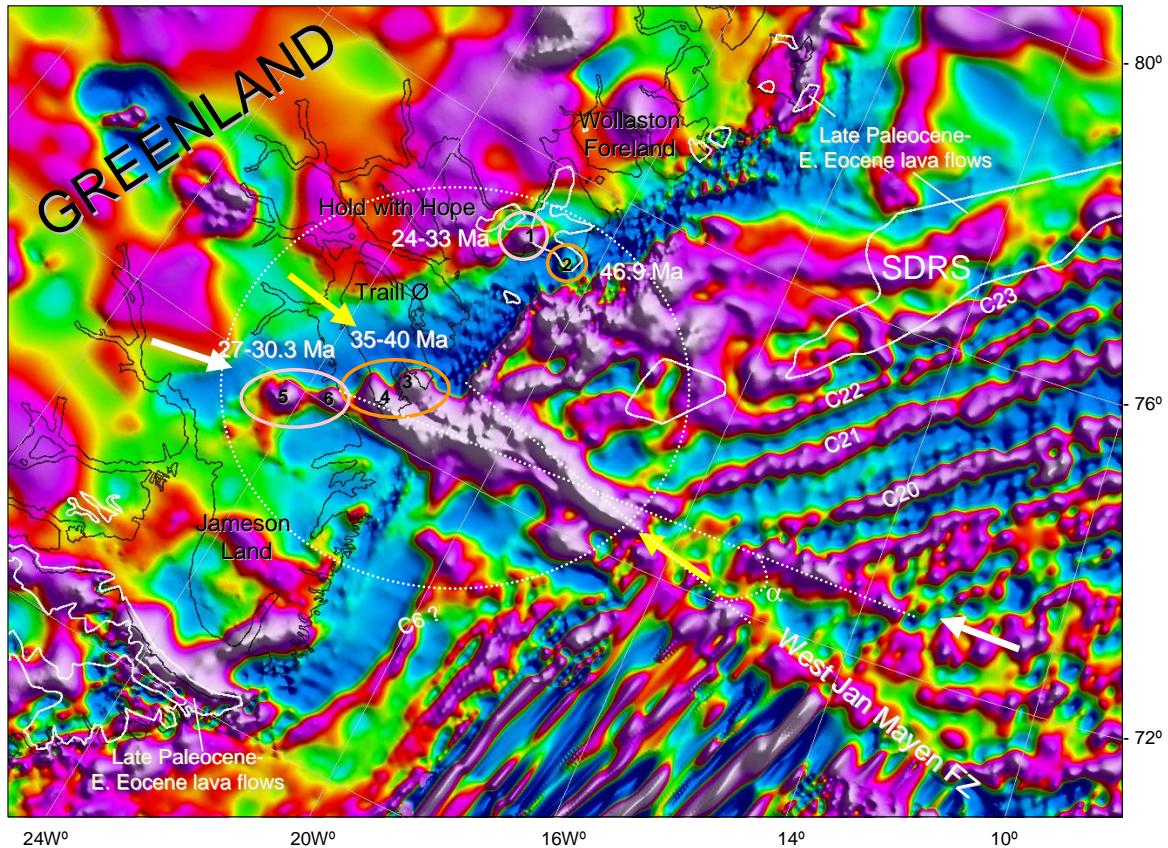


Figure 9.1 The Traill Ø magnetic anomaly and ages of the main onshore intrusions (East Greenland margin). This strong magnetic anomaly observed from the Traill Ø coastline to the C21 likely represents a major igneous complex offshore East Greenland.

Smaller anomalies between C20 and C13 seem to be part of the same trend. Inside the western Traill-Vøring igneous complex, two trends with differences by ($\alpha=10^\circ$) can be observed (NW-SE and NNW-SSE) and probably suggest two discrete magmatic phases (Fig. 9.1).

Between the Traill Ø and the Jameson Land, Oligocene syenites lie in the conjunction of the Traill Ø magnetic anomaly, and the proto-breakup axis (Scott 1998). The Oligocene intrusions are younger than the initiation of seafloor spreading, but may represent some long-lived fusion zone or feeder mantle diapirs probably active during the breakup (Callot et al. 2001). Peacock et al. (2000) also suggested that the same area may represent a deep lateral ramp (a deep transversal shear zone) controlling large relay ramps during both Devonian and Mesozoic extensional episode.

The Jan Mayen corridor may represent a lithospheric weakness zone where magmatic melt may easily be produced or emplaced. Breivik et al. (2004, 2005) suggest that the lithospheric

configuration of the JMFZ corridor favours a Late Miocene underplating of asthenospheric migrating melt sourced from the Iceland mantle plume. We propose that most of the melt could simply be produced by over-accretion of the oceanic crust in Eocene time. Kinematic reconstructions suggest also a continuous magmatic event from the Vøring Marginal High, AMH and the Traill Ø magnetic anomaly on the East Greenland Margin, where Tertiary igneous complexes crop out (Olesen et al. submitted).

We believe that during the breakup the Traill-Vøring igneous complex was part of the Vøring Marginal High, where two similar high anomalies are observed (Figs. 8.1 and 9.2). At this stage, the three branches probably formed a triple junction Ridge-Ridge-Fracture Zone where anomalous magmatism occurred. After breakup, this anomalous magmatism persists in the oceanic domain along the trend of the JMFZ to form the AMH and part of the Traill-Vøring igneous complex (Fig. 8.2 and 8.3). This triple junction scenario is quite similar to the current geodynamic setting observed in the Azores Plateau (Fig. 9.2). Here, anomalous bathymetric highs and thick volcanic plateau are also located at the intersection of the oceanic ridge with the adjacent oceanic fracture zone. A triple junction formed and normal extension along the fracture zone happened as well, probably due to a local mantle upwelling.

Reasons for overaccretion along the JMFZ corridor are not perfectly understood now. However, a relationship with old NW-SE Proterozoics deep shear-zones underlying the Caledonian stacked nappes (Fichler et al. 1999; Doré et al., (1997) could be proposed. These Proterozoic shears zones probably affected the upper mantle. Enhanced magmatism may continue longer than the initial break-up stage if more fertile mantle material (melt prone) lies beneath the oceanic spreading axis ridge and along the trend of the Jan Mayen corridor. More fertile mantle could be related with these pre-existing trends, if they were site of earlier subduction where abundant eclogite is usually expected. Eclogite is the high-pressure form of rocks, and is created when oceanic crust is carried deep into the Earth at subduction zones. Eclogitic rocks in the upper mantle could change the melt solidus of the upper mantle and explain anomalous melt production (Yaxley 2000). This ridge is characterised by anomalous oceanic crust and is almost parallel to the JMFZ. The extent to which subducted crust trapped at shallow levels in the mantle re-homogenizes with its peridotite host is not known. The retention of essentially blocks of crust that are in the order of kilometres in thickness, and complete homogenization with mantle peridotite, represent end-member scenarios. Lower solidus temperatures for the mixture result in enhanced melt productivity at a given temperature.

This model has been proposed to explain the formation of the Greenland-Iceland-Faeroes Ridge to the south (Foulger et al. 2005). Along the Greenland-Faeroes-Iceland Ridge, the problem is however slightly different because the Iceland anomaly (sub-convection, plume?) is certainly involved as well. However, we believe that part of the anomalous magmatic production along such NW-SE trends is likely to be influenced by the old geological history of the North Atlantic.

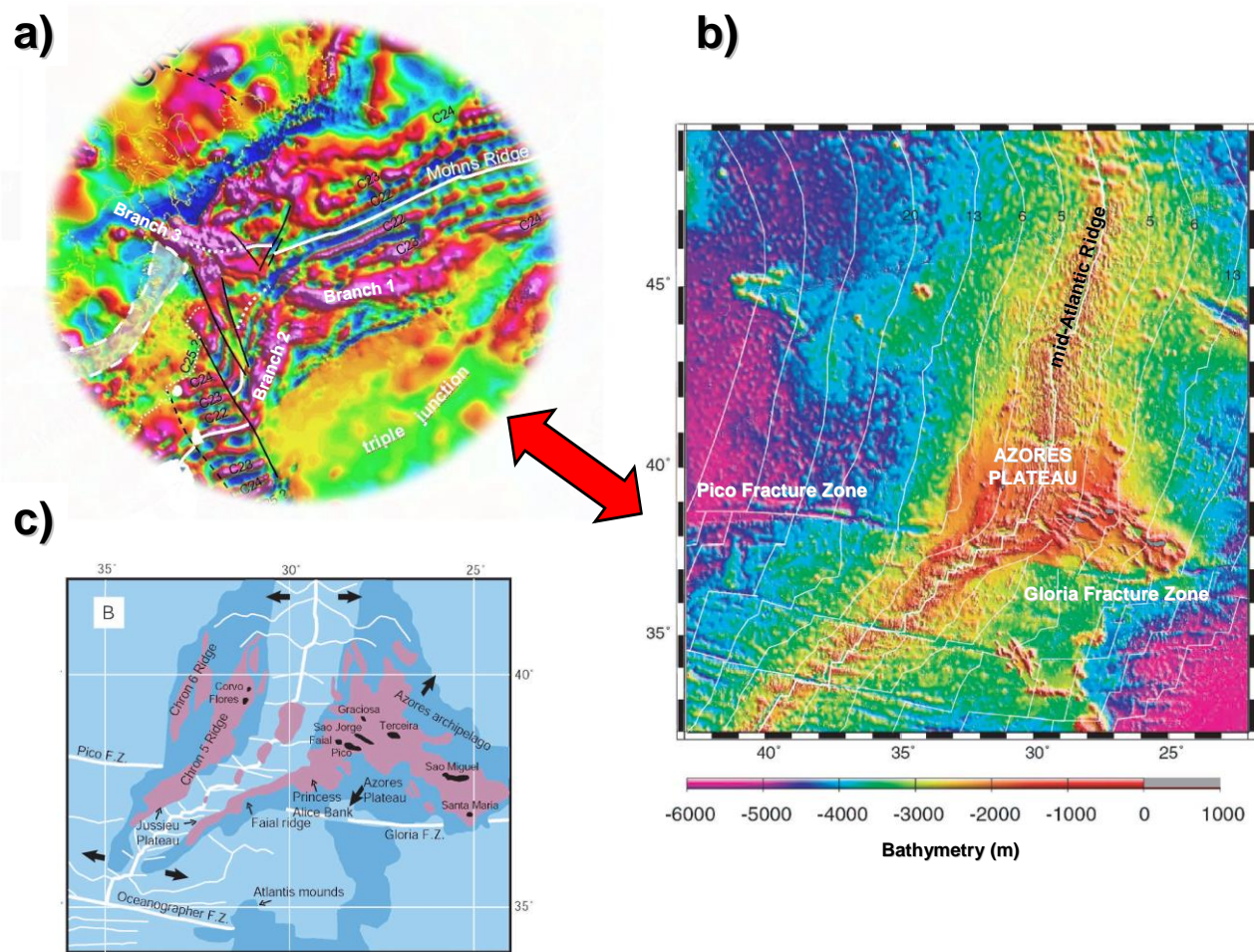


Figure 9.2 a) The Vøring Marginal High-TraillØ triple junction. During late Paelocene-Eocene, the Vøring Marginal High and the Traill Ø magnetic anomaly formed a triple junction R-R-FZ between the spreading ridge and the JMZF. b) This geodynamic setting is quite similar to the Azores triple junction where anomalous magmatic production propagates from the spreading ridge toward the adjacent oceanic fracture zone. c) Note also the southward propagation of the spreading ridge across the Azores Plateau. Figures b and c are from Lagabrielle & Leroy (2005).

10 IMPACT OF DIFFERENTIAL SPREADING RATES ON THE STRUCTURAL EVOLUTION OF THE MID-NORWEGIAN MARGIN

Christophe Pascal

10.1 Rationale

The RAS05 magnetic survey shows that the Jan Mayen Transform Zone was the site of high strain concentrations and heavy deformation during the Cenozoic. The newly acquired data set confirms that contrasting spreading rates prevailed between the Mohns and the Aegir oceanic ridges from Eocene to Oligocene (see also Mosar et al. 2002). This is expected to have resulted in significant dextral shearing along the continental segment (i.e. Jan Mayen Fault Zone, hereafter JMFZ) of the Jan Mayen Transform Zone.

The goal of the present study is to quantify the impact of such dextral motions on the structural evolution of the Norwegian margin. In particular, we aim to test whether dextral strike-slip along the JMFZ could have caused sufficient shortening and can explain the initiation of inversion structures observed in the Vøring Basin. We used finite-element techniques to quantify strain patterns at the Norwegian margin.

10.2 Modelling strategy

For the modelling, we used the commercial finite-element package Ansys. The numerical model involves elasto-plastic rheologies (i.e. Drucker-Prager yield criterion), simulating yielding of rocks, and contact elements describing the behaviour of two blocks sliding against each other along a fault zone (i.e. Mohr-Coulomb criterion). The finite element mesh contains ~6000 triangular and contact elements. Plane stress conditions were assumed. Three main domains are defined according to their rheological parameters (Table 10.1, Fig. 10.1): (1) the oceanic domain assumed to be relatively rigid, (2) the continental domain (i.e. margin) where plastic parameters were selected in order to simulate yielding of weakened crust and (3) the JMFZ, a 50 km wide zone in the model, assumed to be relatively weak too. In particular, Mohr-Coulomb friction was set to 0° along this mature fault zone.

Table 10.1 Modelling parameters.

| | Elasticity | | Drucker-Prager criterion | | | Mohr-Coulomb criterion |
|---------------|---------------------|---------------|--------------------------|--------------------|----------------|------------------------|
| | Young modulus (GPa) | Poisson ratio | Cohesion (MPa) | Friction angle (°) | Flow angle (°) | Friction coefficient |
| ocean | 80 | 0.25 | none | none | none | none |
| margin | 80 | 0.25 | 10 | 30 | 30 | none |
| JMFZ | 80 | 0.25 | 10 | 30 | 30 | 0 |

In order to avoid edge effects, the area of interest was isolated from model boundaries (Fig. 10.1). Bottom and top model boundaries are fixed in the Y direction and the left boundary in the X direction. At the right edge, we applied velocities. In particular, the velocity applied north of the JMFZ was taken 2 mm/yr higher than that applied south of the fault zone. This number was estimated in picking carefully magnetic stripes on the ocean floor. In this preliminary modelling attempt, the previous boundary conditions were applied for a time period of 5 Myr. As a result a dextral offset up to 10 km was simulated along the JMFZ.

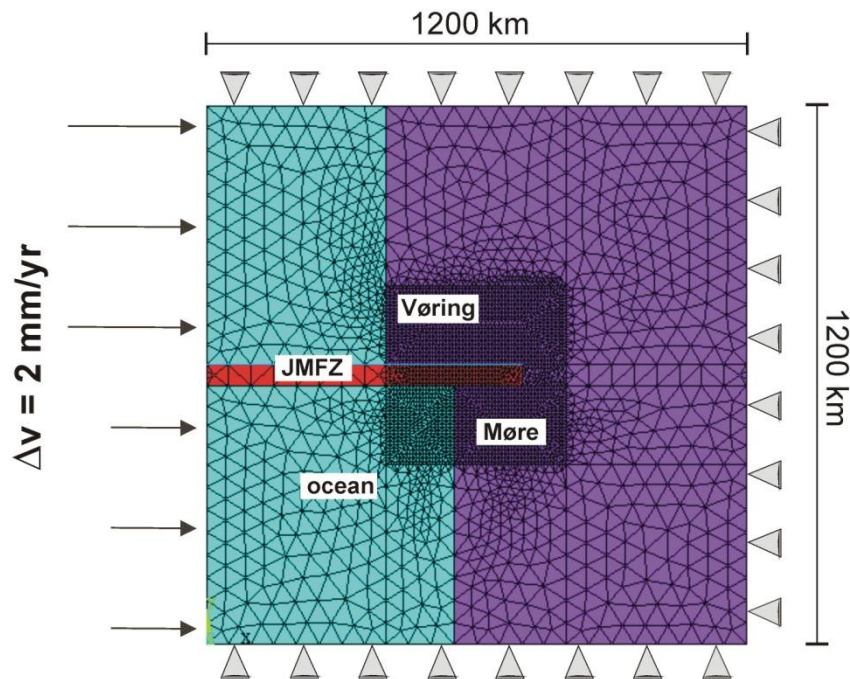


Figure 10.1 Model set-up. The area of interest is a 400 x 400 km square far from model boundaries and depicted by its finer mesh. Contrasting spreading rates (i.e. velocities) are applied between the domains located south and north of the Jan Mayen Fault Zone (JMFZ).

10.3 Results

Fig. 10.2 shows the displacement field parallel to the X-axis (i.e. parallel to the JMFZ) after 5 Myr. In our modelling, no displacement is predicted in the Møre Basin. In the Vøring Basin displacement magnitudes decrease from 10 km at the continent-ocean boundary down to 0 km at the termination of the JMFZ. This simple plot suggests that internal shortening of the Vøring Basin accommodates part of the displacement along the JMFZ.

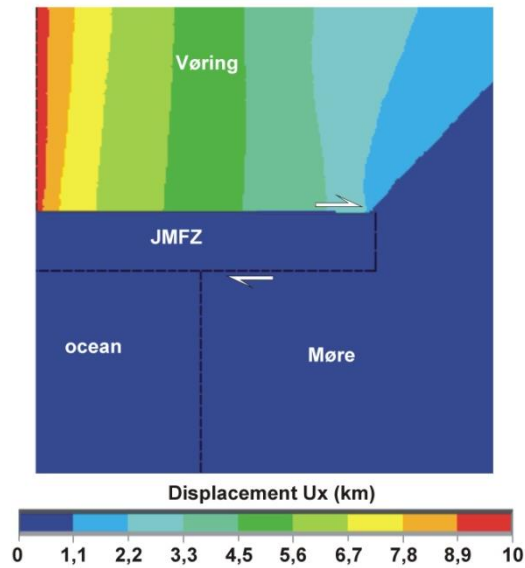


Figure 10.2 Modelled displacement field after 5 Myr (X direction). Note the decrease in displacement along the JMfZ in the Vøring Basin, the effect is due to internal shortening of the block above the MTFC.

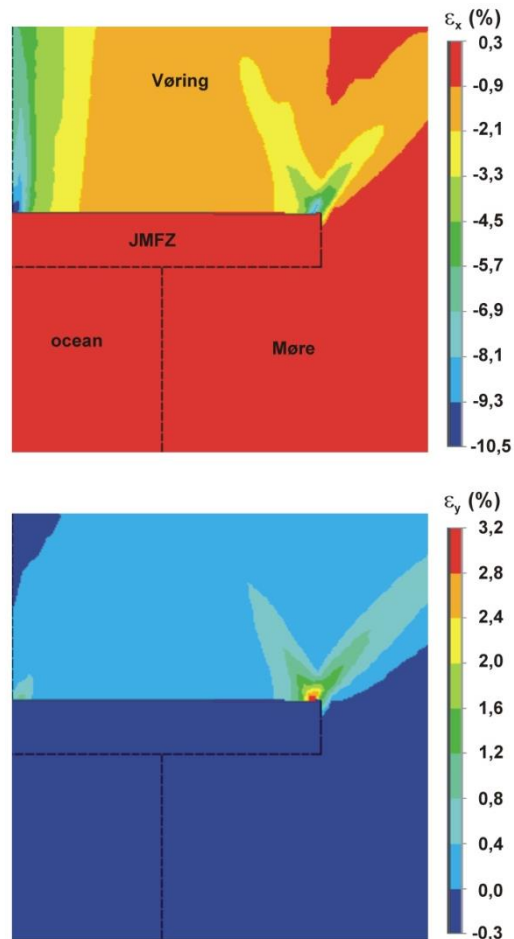


Figure 10.3 Modelled strains after 5 Myr. Negative values are associated to shortening. Note significant strain concentrations at the COB and at the termination of the JMfZ in the Vøring Basin.

Modelled strain patterns are mainly compressive parallel to the JMFZ and, consequently, mainly dilatational perpendicular to it (Fig. 10.3). Strain is insignificant in the Møre Basin whereas it reaches magnitudes up to 10% in the Vøring Basin. Interestingly, maximum shortening is predicted to occur at the continent-ocean boundary and the close to tip of the JMFZ in the Vøring Basin. These areas are characterised by broad zones (i.e. ~50 km wide and 100 to 150 km long) where compressive strains along the X-axis exceed 2%.

10.4 Conclusions and recommendations

Contrasting spreading rates between north of the Jan Mayen Transform Zone (i.e. Mohns Ridge) and south of it (i.e. Aegir Ridge) resulted certainly in dextral strike-slip along the JMFZ, and consequently in dextral offset between the Møre and Vøring basins. On the basis of the new magnetic compilation spreading rates between the two ridge segments appear to differ by ~2 mm/yr for much of the period ranging from continental break up to extinction of the Aegir Ridge. This number can be better constrained by new aeromagnetic surveys of the oceanic floor encompassing the Aegir Ridge, where the data coverage is relatively scarce compared to other areas in the NE Atlantic. This preliminary modelling study suggests that such a minor difference in spreading rates could have led to significant shortening in the Vøring Basin. The present model also explains why we do not observe any significant shortening in the Møre Basin.

However, the present model does not explain why inversion went on in the Vøring Basin after extinction of the Aegir Ridge and initiation of the Kolbeinsey Ridge (i.e. ~20 Ma). A hypothesis that deserves further modelling work is that dextral motion went on along the JMFZ after Late Oligocene times. Probably, the weak Jan Mayen micro-continent damped part of the displacements generated by oceanic accretion at the Kolbeinsey Ridge, resulting in lower motions at the Norwegian margin south of the MTFZ (i.e. Møre Basin). In contrast, displacements originated at the Mohns Ridge are directly transmitted to the Vøring Basin through the rigid oceanic lithosphere. This configuration could also result in dextral strike-slip along the JMFZ in late Cenozoic times.

This preliminary study opens the way to more refined modelling work in the future that will include the testing of the previous hypotheses but also the involvement in the models of relevant key-factors (i.e. pre-existing structure at the Norwegian margin, influence of vertical motions, buoyancy forces, etc).

11 CONCLUSIONS

1. New features have been revealed by the Jan Mayen Aeromagnetic Survey 2005 (JAS-05) and allowed us to significantly refine the tectonic knowledge of the Jan Mayen Fracture Zone (JMFZ). The JMFZ is a complex oceanic corridor affected by episodic phases of anomalous accretion, observed and modelled along the Aegir Marginal High (AMH). The AMH represents an inverted structure, uplifted during late Oligocene-early Miocene time. Cause of this uplift is tectonic and partly related to deep magmatic processes. As a consequence, we believe that the anomalous melt production and crustal thickening observed along the AMH is due to overcrusting formed during the spreading between the Lofoten basin and the AMH. The thickening of the oceanic crust is syn-accretion and is not necessarily related to a Late Miocene underplating (post-accretion), as previously assumed. The magnetic anomaly map shows also evidences of earlier deformation and block rotation linked with a propagator system along the Aegir through. A late Eocene displacement of the magnetic chrons suggests a progressive plate reorganisation leading to a major pulse in Oligocene. The major pulse coincides with two main unconformities seismically observed along the Jan Mayen Corridor (PM and MU) and could explain the main uplift phase of the AMH as well. The magnetic spreading anomalies within the JMFZ show a 50° counter-clockwise rotation revealing a regional compressional phase. The amplitude of the internal anomalies in the eastern part of the JMZF corridor are subdued pointing to a significant alteration of the oceanic crust, possibly associated transport of large quantities of fluids along the 40-50 km wide East and Central JMFZ.

2. We proposed also a new challenging model for the Mid-Norwegian breakup system. Plate reconstruction and our tectonic analysis of the study area, suggest that during the Late Paleocene-Early Eocene breakup between Greenland-Jan Mayen and Norway, a triple junction Ridge-Ridge-Fracture Zone initiated between the Vøring Marginal High and the Traill-Vøring igneous complex, located now partly in the trend of the West Jan Mayen Fracture Zone (WJMFZ). Anomalous melt production started near the Vøring Basin and kept on episodically to the west along the trend of the Jan Mayen corridor. Our interpretation infers also that the north Atlantic breakup probably started earlier at C24R or C25 time south of the EJMFZ.

3. The magnetic modelling shows that most of the magnetic anomalies can be related to sea-floor spreading. Evidence for a secondary influence on the magnetic field is only given for the northernmost line 4 where a vertical superposition of different magnetized bodies is necessary to explain the magnetic anomalies. This particular anomaly may be related to a potential sill intrusion.

4. Spreading rates between the Aegir and Mohns ridges appear on the new magnetic compilation to differ by ~2 mm/yr for much of the period ranging from continental break up to extinction of the Aegir Ridge. The contrasting spreading rates of either side of the Jan

Mayen Transform Zone resulted in dextral strike-slip along the JMFZ, and consequently in dextral offset between the Møre and Vøring basins (initially shifted by an older transfer zone). Preliminary modelling suggests that such a minor difference in spreading rates could have led to significant shortening in the Vøring Basin. The present model also explains why we do not observe any significant shortening in the Møre Basin. This can explain why most of the mid-Norwegian domes are located to the north of the Jan Mayen Lineament.

5. Inversion continued probably in the Vøring Basin in the late Cenozoic because the weak Jan Mayen micro-continent damped part of the displacements generated by oceanic accretion at the Kolbeinsey Ridge, resulting in lower motions at the Norwegian margin south of the MTFZ (i.e. Møre Basin). In contrast, displacements originated at the Mohns Ridge were directly transmitted to the Vøring Basin through the rigid oceanic lithosphere.

12 RECOMMENDATIONS FOR FURTHER WORK

1. We propose to carry out a new aeromagnetic data compilation of the area to the SW of the JAS-05 area to check the earlier proposed fracture zones and to trace the course of the oldest spreading anomalies (20-24/25?) along the conjugate Møre and Jan Mayen margins. Because new hydrocarbons plays concepts in Mid-Norway tend to be constrained to the Paleocene continental deposits (e.g. Ormen Lange), a first order risk parameter in such settings is determining where the boundary between continent and ocean (COB) is located and when the breakup really occurred. New magnetic acquisition in this area is also crucial to really understand the geodynamic evolution of the Norway Basin and to constrain the Jan Mayen Microcontinent evolution, still poorly constrained at the present stage. It is also some interest for 'Law of the Sea' investigations. In the meantime, we propose a reinterpretation and an integrated study of the pre-existing data (gravity, magnetic, refraction and reflection) available along the Jan Mayen Microcontinent

2. The significant improvements in delineating the regional tectonic setting along the Jan Mayen Fracture Zone show that the new aeromagnetic survey was warranted. Considering both these results and the previous results from the Ra 3 Project one may question other proposed fracture zones in the oceanic crust, particularly along the Møre Marginal High and along the western margin of the north and central Barents Sea. The aeromagnetic data on shelf areas of the central North Sea and the southeastern Barents Sea were acquired in early 1970s using Decca and Loran C navigation and should also be replaced by modern high-resolution data. Pre-1980 seismic data are also today regarded as obsolete and are very seldom used for regional interpretations.

ACKNOWLEDGEMENTS

NGU, NPD, Shell and Statoil financed the Jan Mayen Aeromagnetic Survey 2005 (JAS-05). Jaap Mondt and Olav Norvik (Shell), Morten Sand (NPD) and Øyvind Steen (Statoil) gave advice during the project period. NPD provided seismic, bathymetric and aeromagnetic data from the Jan Mayen-Vøring area. Gordon Oakey, Atlantic Geoscience Centre (CGS) in Halifax provided nine aeromagnetic surveys from NRL, NOO and GEUS. Torkild Rasmussen, GEUS gave permission to use the GEUS-79 survey. Carmen Gaina, NGU assisted in defining Euler poles for plate reconstructions. We express our thanks to these companies, institutions and persons.

13 REFERENCES

- Alvestad, E. 1997: Seismic volcanostratigraphy on the Møre margin. *Master thesis, University of Oslo*.
- Andersen, O.B. & Knudsen, P. 1998: Gravity anomalies derived from the ERS-1 satellite altimetry. Kort og Matrikelstyrelsen, DK-2400 Copenhagen NV, Denmark (www.kms.dk).
- Basile, C. & Allemand, P. 2002: Erosion and flexural uplift along transform faults. *Geophysical Journal International* 151, 646-653.
- Bauer, K., Neben, S., Schreckenberger, B., Emmermann, R., Hinz, K., Fechner, N., Gohl, K., Schulze, A., Trumbull, R. & Weber, K. 2000: Deep structure of the Namibian continental margin as derived from integrated geophysical studies. *Journal of Geophysical Research* 105, 25829-25853.
- Berggren, W., Kent, V., Swisher III, C. & Aubry, M. 1995: A revised Cenozoic geochronology and chronostratigraphy. In Berggren, W.A., Kent, V., Aubry, M.P. & Harbenbol (eds) Geochronology, Times Scales and Global Stratigraphic Correlation. *Society for Sedimentary Geology, Special Publications* 54, 129-212
- Berndt, C., Skogly, O.P., Planke, S., Eldholm, O. & Mjelde, R. 2000: High-velocity breakup-related sills in the Vøring Basin, off Norway. *Journal of Geophysical Research* 105, 28.443-28.454.
- Berndt, C., Planke, S., Alvestad, E., Tsikalas, F. & Rasmussen, T. 2001a: Seismic volcanostratigraphy of the Norwegian Margin: constraints on tectonomagmatic break-up processes. *Journal of the Geological Society, London* 158, 413-426.
- Berndt, C., Mjelde, R., Planke, S., Shimamura, H. & Faleide, J. 2001b: Controls on the tectono-magmatic evolution of a volcanic transform margin: the Vøring Transform Margin, NE-Atlantic. *Marine Geophysical Research* 22, 133-152.
- Blakely, R.J. & Simpson, R.W. 1986: Approximating edges of source bodies from magnetic or gravity anomalies. *Geophysics* 51, 1494-1498.
- Blystad, P., Brekke, H., Faereth, R., Larsen, B., Skogseid, J. & Tørudbakken, B. 1995: Structural elements of the Norwegian continental shelf, Part II. The Norwegian Sea Region. *Norwegian Petroleum Directorate Bulletin* 8, 0-45.
- Boldreel, L.O. & Andersen, M.S. 1993: Late Paleocene to Miocene compression in the Faeroe-Rockall area. In Parker J. R. (ed.), *Petroleum Geology of Northwest Europe: Proceedings of the 4th Conference. Geological Society, London*, 1025-1034.
- Bonatti, E. & Seyler, M. 1987: Crustal underplating and evolution in the Red Sea Rift: uplifted gabbro/gneiss complexes on Zabargad and Brothers islands. *Journal of Geophysical Research* 92, 12.803-12.821.
- Breivik, A.B., Verhoef, J. & Faleide, J.I. 1999: Effects of thermal contrasts on gravity modeling at passive margins: results from the western Barents Sea. *Journal of Geophysical Research* 104, 15293-15311.
- Breivik, A. J., Faleide, J. I. & Mjelde, R. 2005; Late Miocene Magmatic Underplating of Oceanic Crust at the Outer Vøring Margin, Norway, Euromargins 2003 OBS Experiment. *Geophysical Research Abstracts* 7, 03646.
- Breivik, A.J., Faleide, J. & Mjelde, R. 2004; Late magmatic underplating of oceanic crust at the outer Vøring margin, Norway, Euromargins 2003 OBS experiments. *Eos Trans. AGU Fall Meeting. Supplement. Abstract V31B-1432*.
- Brekke, H. 2000: The tectonic evolution of the Norwegian Sea continental margin with

- emphasis on the Vøring and Møre basins. In Nøttvedt, A. et al. (eds.) Dynamics of the Norwegian Margin. *Geological Society of London, Special Publications 167*, 327-378.
- Breunig, M., Cremers, A.B., Götze, H.-J., Schmidt, S., Seidemann, R., Shumilov, S. and Siehl, A. 2000: Geological Mapping based on 3D models using an Interoperable GIS. *Geo-Information-Systems. Journal for Spatial Information and Decision Making 13*, 12-18.
- Bugge, T., Prestvik, P. & Rokoengen, K. 1980; Lower Tertiary volcanic rocks off Kristiansund, Mid- Norway. *Marine Geology 35*, 277-286.
- Cartwright, J. 1992: Fundamental crustal lineaments and transverse structural zones in continental rifts. In Mason, R. (ed) Basements Tectonics, 7. *Kluwer, Netherlands*, 209-217.
- Callot, J.P., Grigné, C., Geoffroy, L. & Brun, J.P. 2001: Development of volcanic passive margins: Two-dimensional laboratory models. *Tectonics 20*, 148-159.
- Cande, S.C. & Kent, D.V. 1995: Revised calibration of the geomagnetic polarity timescale for the Late Cretaceous and Cenozoic. *Journal of Geophysical Research 100*, 6093-6095.
- Clift, P. 1996: Temperature anomalies under the Northeast Atlantic rifted volcanic margins. *Earth and Planetary Science Letters 146*, 195-211.
- Chapell, A.R. & Kuszniir, N.J. 2005: Crustal thickness mapping using satellite gravity data: Implications for the formation of the southern Rockall Through. *Geophysical Research Abstracts 7*, 07953.
- Chen, Y. 1989: A mechanical model fro the inside corner uplift at a ridge-transform intersection. *Journal of Geophysical Research 97*, 9275-9282.
- Chen, Y. 1988: Thermal model of oceanic transform faults. *Journal of Geophysical Research 93*, 8839-8851.
- Clift, P. & Lorenzo, J. 1999: Flexural unloading and uplift along the Cote d'Ivoire-Ghana transform margin, equatorial Atlantic. *Journal of Geophysical Research 104*, 25257-25274.
- Coffin, M. & Eldholm, O. 1994: Large igneous provinces: crustal structure, dimensions, and external consequences. *Revue of Geophysics 32*, 1-36.
- Compagnie Générale de Géophysique 1977: Norwegian Petroleum Directorate, Aeromagnetic Survey Jan Mayen Area, Interpretation Report, 23 pp.
- Cox, K. 1993: Continental magmatic underplating. *Royal Society of London Philosophical Transaction A*, 342, 155-166.
- Doré, A., Lundin, E., Jensen, L.N., Birkeland, Ø., Eliassen, P. & Fichler, C. 1999: In Fleet, A. J. & Boldy, S. A. R. (eds) Petroleum Geology of Northwest Europe: Proceedings of the 5th Conference. *Geological Society, London*, 41-61.
- Doré, A.G., Lundin, E., Fischler, C. & Olsen, O. 1997: Patterns of basement structure and reactivation along the NE Atlantic margin. *Journal of the Geological Society, London 154*, 85-92.
- Doré, A. & Lundin, E. 1996: Cenozoic compressional structures on the NE Atlantic margin: nature, origin and potential significance for hydrocarbon exploration. *Petroleum Geosciences 2*, 299-311.
- Ebbing, J., Lundin, E., Olesen, O. & Hansen, E.K 2006: The mid-Norwegian margin: A discussion of crustal lineaments, mafic intrusions, and remnants of the Caledonian root by 3D density modelling and structural interpretation. *Journal of the Geological Society, London 163*, 47-60.
- Eldholm, O., Sundvor, E. & Myhre, A. 1979: Continental margin off Lofoten-Vesterålen, Northern Norway. *Marine Geophysical Researches 4*, 3-35.
- Eldholm, O., Thiede, J. & Taylor, E. et al. (Eds.) 1987: Proceedings Oceanic Drilling Program, Initial Reports 104, College Station, TX (Ocean Drilling Program).

- Eldholm, O., Thiede, J. & Taylor, E. and shipboard scientific party 1987: Summary and preliminary conclusions, ODP leg 104. In Eldholm, O., Thiede, J. & Taylor, E. et al. (eds) Proc. ODP, Initial Reports 104, 751-771.
- Eldholm, O., Tsikalas, F. & Faleide, J.I. 2002: The continental margin off Norway 62-75°N: Palaeogene tectono-magmatic segmentation and sedimentation. In: D. Jolley & B. Bell (eds.). The North Atlantic Igneous Province: stratigraphy, tectonics, volcanic and magmatic processes. *Geological Society London, Special Publications 197*, 39-68.
- Encom 2003: Automag (Modelvision Pro option v5.0), Online Reference Manual pp. 117-153.
- Fichler, C., Rundhovde, E., Olesen, O., Sæther, B.M., Rueslåtten, H., Lundin, E. and Doré, A.G. 1999: Regional tectonic interpretation of image enhanced gravity and magnetic data covering the Mid-Norwegian shelf and adjacent mainland. *Tectonophysics 306*, 183-197.
- Foulger, G., Natland, J. & Anderson, D. 2005: A source for Icelandic magmas in remelted Iapetus crust. *Journal of Volcanology and Geothermal Research 141*, 23-44.
- Gaina, C., Roest, W. & Müller, R. 2002: Late Cretaceous-Cenozoic deformation of northeast Asia. *Earth and Planetary Science Letters 197*, 273-286.
- Gairaud, H., Jacquart, G., Aubertin, F. & Beuzard, P. 1978: The Jan Mayen Ridge synthesis of geological knowledge and new data. *Oceanologica Acta 1*, 335-358.
- Geoffroy, L. 2005: Volcanic passive margins. *Compte-Rendus Geosciences 337*, 1395-1408.
- Geoffroy, L., Gelard, J., Lepvrier, C. & Olivier, P.P. 1998: The coastal flexure of Disko (West Greenland), onshore expression of the 'oblique reflectors'. *Journal of the Geological Society 155*, 463-473.
- Gernigon, L., Lucazeau, F., Brigaud, F., Ringenbach, J.C., S., P. & Le Gall, B. 2006: A moderate melting model for the Vørling margin (Norway) based on structural observations and a thermo-kinematical modeling: Implication for the meaning of the lower crustal bodies. *Tectonophysics 412*, 255-278.
- Gernigon, L., Ringenbach, J.C., Planke, S. & Le Gall, B. 2004: Deep structures and breakup along volcanic rifted margins: Insights from integrated studies along the outer Vøring Basin (Norway). *Marine and Petroleum Geology 21*, 363-372.
- Gernigon, L. 2002: Extension et magmatisme en contexte de marge passive volcanique: Déformation et structure crustale de la marge norvégienne externe (Domaine Nord-Est Atlantique) (Extension and magmatism in a volcanic margin context : deformation and structure of the. *PhD Thesis, " Domaines Océaniques ", IUEM/UBO, Brest. 300 pp.*
- Geosoft 2004: OASIS Montaj v 6.0 Mapping and processing system, The core software platform for working with large volume spatial data. Quick start tutorials. *Geosoft Incorporated*, 258 pp.
- Geosoft 2005a: Montaj Geophysics Levelling System, Processing and Enhancing Geophysicals Data Extension for Oasis montja v6.2. Tutorial and user guide, *Geosoft Incorporated*, 68 pp.
- Geosoft 2005b: Montaj GridKnit, Grid extension for OASIS Montaj v6.1, Tutorial and user guide, *Geosoft Incorporated*, 27 pp.
- Geosoft 2005c: Montaj MAGMAP filtering, 2-D frequency domain processing of potential field data, Extension for Oasis Montaj v6.1. *Geosoft Incorporated*, 66 pp.
- Geosoft 2005d: Montaj grav/mag interpretation, Processing, analysis and visualization system for 3D Inversion of potential field data for Oasis Montaj v6.1, Tutorial and user guide. *Geosoft Incorporated*, 65 pp.
- Gjelsvik, T. 1970: Volcano on Jan Mayen alive again. *Nature*, 228352-352.
- Gómes, M. & Vergés, J. 2005: Quantifying the contribution of tectonic vs. differential compaction in the development of domes along the Mid-Norwegian Atlantic margin.

- Basin Research* 17, 289-310.
- Götze, H.-J. and Lahmeyer, B. 1988: Application of three-dimensional interactive modeling in gravity and magnetics. *Geophysics*, 53(8), 1096-1108.
- Gradstein, F., Ogg, J., and Smith, A., Agterberg, F., Bleeker, W., Cooper, R., Davydov, V., Gibbard, P., Hinnov, L., House, M., Lourens, L., Luterbacher, H., McArthur, J., Melchin, M., Robb, L., Shergold, J., Villeneuve, M., Wardlaw, B. & Ali, J. 2004: A Geologic Time Scale 2004. *Cambridge University Press*, 589 pp.
- Grønlie, G., Chapman, M. & Talwani, M. 1979: Jan Mayen Ridge and Iceland Plateau: Origin and evolution. *Norsk Polarinst Skrifter* 170, 25-47.
- Grunnaleite, I. & Gabrielsen, R. 1995: Structure of the Møre Basin, mid-Norway Continental margin. *Tectonophysics* 252, 221-251.
- Gudlaugsson, S., Grunnarsson, K., Sand, M. & Skogseid, J. 1988: Tectonic and volcanic events at the Jan Mayen Ridge microcontinent. In Morton, A.C. & Parson, L.M. (eds) Early Tertiary Volcanism and the Opening of the NE Atlantic. *Geological Society, Special Publications* 39, 85-86.
- Hagevang, T., Eldholm, O. & Aalstad, I. 1983: Pre-23 magnetic anomalies between Jan Mayen and Greenland-Senja Fracture Zones in the Norwegian Sea. *Marine Geophysical Researches* 5, 345-363.
- Hartz, E.H., Eide, E.A., Andresen, A., Midbøe, P., Hodges, K.V. & Kristiansen, S.N. 2002: $^{40}\text{Ar}/^{39}\text{Ar}$ geochronology and structural analysis: Basin evolution and detrital feedback mechanisms, Hold With Hope region, East Greenland. *Norsk Geologisk Tidsskrift* 82, 341-358.
- Heiskanen, W.A. & Moritz, H. 1967: Physical Geodesy. *W.H. Freeman, San Fransisco*. 364 pp.
- Hjelstuen, B.O., Sejrup, H.P., Haflidason, H., Berg, B. & Bryn, P. 2004: Neogene and Quaternary depositiona environments on the Norwegian continental margin 62-68. *Marine Geology* 213, 257-276.
- Hey, R., Duennebier, F. & W.P., Morgan, J.M. 1980: Propagating rifts on mid-ocean ridges. *Journal of Geophysical Research* 85, 3647-3658.
- Hey, R., Menard, H., Atwater, T. & Cress, D. 1988: Changes in direction of seafloor-spreading revisited. *Journal of Geophysical Research* 93, 2803-2811.
- Havskov, J. & Atakan, K. 1991: Seismicity and volcanism of Jan Mayen Island. *Terra Nova* 3, 517-526.
- Hunt, C., Moskowitz, B.M., Banerje, S.K. 1995: Magnetic properties of rocks and minerals. In Rock Physics and Phase Relations. A Handbook of Physical Constraints. *AGU Reference Shelf* 3, pp. 189-204.
- Imsland, I. 1986: The volcanic eruption on Jan Mayen, January 1985: Interaction between a volcanic island and a fracture zone. *Journal of Volcanology and Geothermal Research* 28, 45-53.
- Johnson, G. & Heezen, B. 1967: The morphology and evolution of the Norwegian-Greenland Sea. *Deep-Sea Research* 14, 755-771.
- Jongepier, K., Rui, J. & Grue, K. 1996: Triassic to Early Cretaceous stratigraphic and structural development of the northeastern Møre Basin margin, off Mid-Norway. *Norsk Geologisk Tidsskrift* 76, 200-216.
- Jung, W.Y. & Vogt, P. 1997: A gravity and magnetic anomaly study of the extinct Aegir Ridge, Norwegian Sea. *Journal of Geophysical Research* 12, 5065-5089.
- Kent, D.V. & Opdyke, N.D. 1978: Paleomagnetism and magnetic properties of igneous rock samples – Leg 38. In Talwani, Udintsev *et al.* (Eds.) Initial reports of the Deep Sea Drilling Project, Supplements to Vol. 38, 39, 40 and 41. *Govt. Printing Office*,

- Washington, D.C., 3-8.
- Kinck, J.J., Husebye, E.S. and Larsson, F.R. 1993: The Moho depth distribution in Fennoscandia and the regional tectonic evolution from Archean to Permian times, *Precambrian Research* 64, 23-51.
- Kleinrock, M., Tucholke, B., Lin, J. & Tivey, M. 1997: Fast rift propagation at slow-spreading ridge. *Geology* 25, 639-642.
- Knott, S., Burchell, M., Jolley, E. & Fraser, A. 1993: Mesozoic to Cenozoic plate reconstructions of the North Atlantic and hydrocarbon plays of the Atlantic margins. In: Parker, J.R (ed) *Petroleum Geology of Northwest Europe: Proceedings of the 4th Conference. Geological Society, London*, 953-974.
- Koch, L. & Haller, J. 1971: Geological map of East Greenland 72-76 N Lat (1:250 000). *Meddelelser om Grønland* 183, 1-26.
- Kodaira, S., Mjelde, R., Gunnarson, K., Shiobara, H. & Shimamura, H. 1998: Structure of the Jan Mayen microcontinent and implications for its evolution. *Geophysical Journal International* 132, 383-400.
- Kuvas, B. & Kodaira, S. 1997: Formation of the Jan Mayen microcontinent: the missing piece in the continental puzzle between the Møre-Vøring Basin. *First Break* 15, 239-247.
- Lagabrielle, Y. & Leroy, S. 2005: Le Visage sous-marin de la Terre: Eléments de géodynamique océanique. Chapitre 10: les Açores. *Commission de la Carte Géologique du Monde (CCGM) and Centre National de la Recherche Scientifique (CNRS). Monography*, 24-25.
- Larsen, L., Watt, W. & Watt, M. 1989: Geology and petrology of the Lower Tertiary plateau basalts of the Scoresby Sund region, East Greenland. *Grønlands Geologiske Undersøgelse Bulletin* 157, 1-164.
- Lawver, L., Muller, R., Sirastava, S. & Roest, W. 1990. The Opening of the Arctic Ocean. In Bleil, U. and Thiede (eds). *Geologic History of the Polar Oceans: Arctic Versus Antarctic. The NATO Symposium (October, 1988), Bremen, West Germany*, 29-62.
- Laxon, S. & McAdoo, D. 1994: Arctic Ocean gravity field derived from ERS-1 satellite altimetry. *Science* 256, 621-624.
- Ludwig, J.W., Nafe, J.E. and Drake, C.L. 1970: Seismic refraction. In: Maxwell, A. (ed.): *The sea*, Vo.4, Wiley, New York.
- Lundin, E. & A.G., D. 2002: Mid-Cenozoic post-breakup deformation in the "passive" margins bordering the Norwegian-Greenland Sea. *Marine and Petroleum Geology* 19, 79-93.
- Lundin, E.R., Rønning, K., Doré, A.G. & Olesen O. 2002: Hel Graben, Vøring Basin, Norway – a possible major cauldron? Abstract, 25th Nordic Geological Winter Meeting, January 6th - 9th, 2002, Reykjavik.
- Lundin, E.R., Doré, A.G. 1997: A tectonic model for the Norwegian passive margin with implications for the NE Atlantic: Early Cretaceous to break-up. *Journal of the Geological Society, London* 154, 545-550.
- McDonnell, A. & Shannon, P. 2001: Comparative Tertiary basin development in the Porcupine and Rockall basins. In Shannon, P.M., Haughton, P.D.W. and Corcoran, D.V. (eds) *The Petroleum Exploration of Ireland's Offshore Basins. Geological Society, London, Special Publications* 188, 323-344.
- McGinnis, J., Driscoll, N., Karner, G., Brumbaugh, W. & Cameron, N. 1993: Flexural response of passive margins to deep-sea erosion and slope retreat: implications for relative sea-level changes. *Geology* 21, 893-896.
- Maclennan, J. & Lovell, B. 2002: Control of regional sea level by surface uplift and subsidence caused by magmatic underplating of Earth's crust. *Geology* 30, 675-678.

- Mathisen, O. 1976: A method for Bouguer reduction with rapid calculation of terrain corrections. *Geographical Survey of Norway geodetic publications 18*, 40 pp.
- Mauring, E. & Kihle, O. 2006: Leveling aerogeophysical data using moving differential median filter. *Geophysics 71*, L5-L11.
- Mauring, E., Smethurst, M.A. & Kihle, O. 1999: Vestfjorden Aeromagnetic Survey 1998. Acquisition and processing report. *NGU Report 99.001*, 23 pp.
- Mauring, E., Beard, L.P., Kihle, O. & Smethurst, M.A. 2002: A comparison of aeromagnetic levelling techniques with an introduction to median levelling. *Geophysical Prospecting 50*, 43-54.
- Mauring, E., Mogaard, J.O. & Olesen, O. 2003: Røst Basin Aeromagnetic Survey 2003 (RAS-03). Ra 3 aeromagnetic compilation. Data acquisition and processing report. *NGU Report 2003.070*, 20 pp.
- Miller, K. & Mountain, G.T., B.E. 1985: Oligocene glacio-eustasy and erosion on the margins of the North Atlantic. *Geology 13*, 10-13.
- Mjelde, R., Kodaira, S., Shimamura, H., Kanazawa, T., Shiobara, H., Berg, E.W. & Riise, O. 1997: Crustal structure of the central part of the Vøring Basin, mid-Norway margin, from ocean bottom seismographs. *Tectonophysics 277*, 235-257.
- Mjelde, R., Digranes, P., Shimamura, H., Shiobara, H., Kodaira, S., Brekke, H., Egebjerg, T., Sørensen, N. & Thorbjørnsen, S. 1998: Crustal structure of the northern part of the Vøring Basin, mid-Norway margin, from wide-angle seismic and gravity data. *Tectonophysics 293*, 175-205.
- Mjelde, R., Shimamura, H., Kanazawa, T., Kodaira, S., Raum T. & Shiobara, H. 2003: Crustal lineaments, distribution of lower crustal intrusives and structural evolution of the Vøring Margin, NE Atlantic; new insight from wide-angle seismic models. *Tectonophysics 369*, 199-218.
- Mjelde, R., Raum, T., Breivik, A., Shimamura, H., Murai, Y., Takanami, T. & Faleide, J.I. 2005: Crustal structure of the Vøring margin, NE Atlantic: a review of geological implications based on recent OBS-data. In Doré, A.G. & Vining, B.A. (eds.) North-West European Petroleum Geology and Global Perspectives: Proceedings of the 6th Conference. *Geological Society, London* 803-813.
- Morgan, W. 1968: Rises, trenches, great faults and crustal blocks. *Journal of Geophysical Research 73*, 1959-1982.
- Morley, C. 1999. How successful are analogue models in addressing the influence of pre-existing fabrics on rift structure. *Journal of Structural Geology 21*, 1267-1274.
- Mosar, J., Lewis, G., & Torsvik, T.H. 2002: North Atlantic sea-floor spreading rates: implications for the Tertiary development of inversion structures of the Norwegian-Greenland Sea, *Journal of the Geological Society of London 159*, 503-515.
- Mutter, J.C., Talwani, M. & Stoffa, P.L. 1984: Evidence for a thick oceanic crust off Norway. *Journal of Geophysical Research 89*, 483-502.
- Naudy, H. 1971: Automatic determination of depth on aeromagnetic profiles. *Geophysics 36*, 5, 717-722.
- Noble, R., Macintyre, R. & Brown, P. 1988: Age constraints on Atlantic evolution: timing of magmatic activity along the E Greenland continental margin. In: Morton, A.C. & Parson, L.M. (eds) Early Tertiary Volcanism and the opening of the NE Atlantic. *Geological Society, London, Special Publications 39*, 201-204.
- Noe-Nygaard, N. 1976: Tertiary igneous rocks between Shannon and Scoresby Sund. In: Escher, A. & Watt, W.S. (eds) Geology of Greenland. *Geological Survey of Greenland, Copenhagen*, 386-402.

- Nordgulen, Ø., Braathen, A., Corfu, F., Osmundsen, P.T. & Husmo, T. 2002: Polyphase kinematics and geochronology of the late-Caledonian Kollstraumen detachment, north-central Norway. *Norsk Geologisk Tidsskrift* 82, 299-316.
- Norges geologiske undersøkelse 1992: Aeromagnetisk anomalikart, Norge M 1:1 mill, Norges geologiske undersøkelse.
- Olesen, O. & Myklebust, R. 1989: LAS-89, Lofoten Aeromagnetic Survey 1989, Interpretation report. *NGU Report 89.168*, 54 pp.
- Olesen, O. & Smethurst, M.A. 1995: NAS-94 Interpretation Report, Part III: Combined interpretation of aeromagnetic and gravity data. *NGU Report 95.040*, 50 pp.
- Olesen, O., Gellein J., Håbrekke H., Kihle O., Skilbrei J. R., & Smethurst M. 1997a: *Magnetic anomaly map Norway and adjacent ocean areas, scale 1:3 million*. Norges geologiske undersøkelse, Trondheim, Norway.
- Olesen, O., Torsvik, T.H., Tveten, E., Zwaan, K.B., Løseth H. & Henningsen, T. 1997b: Basement structure of the continental margin in the Lofoten-Lopphavet area, northern Norway: constraints from potential field data, on-land structural mapping and palaeomagnetic data. *Norsk Geologisk Tidsskrift* 77, 15-33.
- Olesen, O., Lundin, E., Nordgulen, Ø., Osmundsen, P.T., Skilbrei, J.R., Smethurst, M.A., Solli, A., Bugge, T. & Fichler, C. 2002: Bridging the gap between the onshore and offshore geology in Nordland, northern Norway. *Norwegian Journal of Geology* 82, 243-262.
- Olesen, O., Ebbing, J., Skilbrei, J.R., & Lundin, E. 2003: Interpretation of potential field data along the Lofoten continental margin, Part I. NGU Report 2003.070, 68 pp.
- Osmundsen, P.T., Braathen, A., Nordgulen, Ø., Roberts, D., Meyer, G.B. & Eide, E. 2003: The Devonian Nesna shear zone and adjacent gneiss-cored culminations, North-central Norwegian Caledonides. *Journal of the Geological Society of London* 160, 1-14.
- Peacock, D., Price, S., Whitham, A. & Pickles, C. 2000. The World's biggest relay ramp: Hold With Hope, NE Greenland. *Journal of Structural Geology* 22, 843-850.
- Phillips, J.D. 1979: ADEPT: A program to estimate depth to magnetic basement from sampled magnetic profiles. *U.S. Geological Survey (USGS) open-file report 79-367*, 35 pp.
- Planke, S. & Eldholm, O. 1994: Seismic response and construction of seaward dipping wedges of flood basalts: Vøring volcanic margin. *Journal of the Geophysical Research* 99, 9263-9278.
- Planke, S., Skogseid, J. & Eldholm, O. 1991: Crustal structure off Norway, 62° to 70° north. *Tectonophysics* 189, 91-107.
- Poag, C., Ward, L.W. 1987: Cenozoic unconformities and depositional supersequences of North Atlantic margins: testing the Vail model. *Geology* 15, 159-162.
- Praeg, D., Stoker, M., Shannon, P., Ceramicola, S., Hjelstuen, B., Lasberg, J. & Mathiesen, A. 2005: Episodic Cenozoic tectonism and the development of the NW European 'passive' continental margin. *Marine and Petroleum Geology* 22, 1007-1030.
- Pockalny, R., Gente, P. & Buck, R. 1996: Oceanic transverse ridges: a flexural response to fracture-zone normal extension. *Geology* 24, 71-74.
- Price, S., Brodie, J., Whitham, A. & Kent, R. 1997: Mid-Tertiary rifting and magmatism in the Traill Ø region, East Greenland. *Journal of the Geological Society London* 154, 419-434.
- Reid, A.B., Allsop, J.M., Granser, H., Millett, A.J. & Sommerton, I.W. 1990: Magnetic interpretation in three dimensions using Euler deconvolution. *Geophysics* 55, 80-91.
- Ren, S., Skogseid, J. & Eldholm, O. 1998: Late Cretaceous-Paleocene extension on the Vøring Volcanic Margin. *Marine Geophysical Researches* 20, 343-369(27).
- Planke, S., Symonds, P.A., Alvestad, E. & Skogseid, J. 2000: Seismic volcanostratigraphy of

- large-volume basaltic extrusive complexes on rifted margins. *Journal of Geophysical Research* 105, 19335-19351.
- Reid, I. 1989: Effects of lithospheric flow on the formation and evolution of a transform margin. *Earth and Planetary Science Letters* 95, 38-52.
- Reid, A.B., Allsop, J.M., Granser, H., Millett, A.J., Sommerton, I.W. 1990: Magnetic interpretation in three dimensions using Euler deconvolution, *Geophysics* 55, 80-91.
- Roeser, H.A. 1993: Magnetische Messungen auf See. *Deutsche Geoph. Gesellschaft Mittlg.* 2, 11-24.
- Ritchie, J.D., Johnson, H. & Kimbell, G.S. 2003: The nature and age of Cenozoic contractional deformation within the NE Faroe-Shetland Basin. *Marine and Petroleum Geology* 20, 399-409.
- Sandwell, D.T. & Schubert, G. 1982: Lithospheric flexure at fracture zones. *Journal of Geophysical Research* 87, 4657-4667.
- Saunders, A.D., Fitton, J.G., Kerr, A.C., Norry, M.J. & Kent, R.W. 1997: The North Atlantic Igneous Province. In Mahoney, J.J. & Coffin, M.L. (eds). *Large Igneous Provinces*, Geophysical Monograph Series, American Geophysical Union, Washington, DC, 45-93.
- Schlategger, U., H., A., Jamtveit, B., Frank, M., Griffin, W., Gronvold, K., Tronnes, R. & Torsvik, T. 2002: Contamination of OIB by underlying ancient continental lithosphere: U-Pb and Hf isotopes in zircons question EM1 and EM2 mantle components. *Geochimica et Cosmochimica Acta*, 66A673.
- Schlindwein, V. & Jokat, W. 1997: Structure and evolution of the continental crust of northern east Greenland from integrated geophysical studies. *Journal of Geophysical Research* 104, 15227-15245.
- Scott, R., Ramsey, L., Jones, S., Sinclair, S. & Pickles, C. 2005: Development of the Jan Mayen microcontinent by linked propagation and retreat of spreading ridges. In Wandås, B.T.G.; Nystuen, J.P.; Eide, E.; Gradstein, F. (eds). Onshore-Offshore relationships on the North Atlantic Margin. *Norwegian Petroleum Society (NPF)*, 69-82.
- Scott, R. 2000: Mesozoic-Cenozoic Evolution of East Greenland : Implications of a Reinterpreted Continent-Ocean Boundary Location. *Polarforschung*, 68, 83-91.
- Schmidt, S. & Götze, H.-J. 1998: Interactive visualization and modification of 3D models using GIS functions. *Phys. Chem. Earth*, 23(3), 289-296.
- Skogseid, J. & Eldholm, O. 1989: Vøring plateau continental margin: seismic interpretation, stratigraphy and vertical movements. In Eldholm, O., Thiede, J. & Taylor, E & al. (eds). Proceedings of the Ocean Drilling Program, Scientific Results, 104. *Proceedings of the Ocean Drilling Program, Scientific Results, College Station, TX (Ocean Drilling Program)*, 993-1030.
- Skogseid, J. & Eldholm, O. 1987: Early Cenozoic Crust at the Norwegian Continental Margin and the Conjugate Jan Mayen Ridge. *Journal of Geophysical Research* 92, 11471-11491.
- Svellingen, W. & Pedersen, R. 2003: Jan Mayen: a result of ridge-transform-microcontinent interaction. *Geophysical Research Abstracts*, 5.
- Schönharting, G. & Abrahamsen, N. 1989: Paleomagnetism of the volcanic sequence in hole 642E, ODP leg 104, Vøring Plateau, and correlation with early Tertiary basalts in the North Atlantic. In Eldholm, Thiede, Taylor *et al.* (Eds.) Proceedings of the Ocean Drilling Program, Scientific Result 104, College Station, TX, 911-920.
- Simpson, R.W., Jachens, R.C., & Blakely, R.J. 1983: AIRYROOT: A Fortran program for calculating the gravitational attraction of an Airy isostatic root out to 166.7 km. *United*

- States Department of the Interior, Geological Survey, Open-File Report 83-883*, 24 pp.
- Sinton, C.W., Hitchen, K. & Duncan, R.A. 1998: Ar⁴⁰-Ar³⁹ geochronology of silicic and basic volcanic rocks on the margins of the North Atlantic: *Geological Magazine* 135, 161-170.
- Skilbrei, J.R., Håbrekke, H., Olesen, O., Kihle, O., Macnab, R. 1991: Shaded relief aeromagnetic colour map of Norway and the Norwegian-Greenland and Barents seas: Data compilation and examples of interpretation. *NGU Report 91.269*, 15 pp.
- Skilbrei, J.R., Kihle, O., Olesen, O., Gellein, J., Sindre, A., Solheim, D. & Nyland, B. 2000: Gravity anomaly map Norway and adjacent ocean areas, scale 1:3 Million. Geological Survey of Norway, Trondheim.
- Skilbrei, J.R., Olesen, O., Osmundsen, P.T., Kihle, O., Aaro, S. and Fjellanger, E. 2002: A study of basement structures and onshore-offshore correlations in Central Norway. *Norsk Geologisk Tidsskrift* 82, 263-279.
- Skogseid, J., Pedersen, T., and Larsen, V.B. 1992: Vøring Basin: subsidence and tectonic evolution. In Larsen, R.M., Brekke, H. Larsen, B.T. & Talleraas, E. (Eds.) Structural and Tectonic Modelling and its Application to Petroleum Geology. *NPF Special Publication, Elsevier, Amsterdam*, 55-82.
- Smith, W. H. F. & Sandwell, D. T. 1997: Global sea floor topography from satellite altimetry and ship depth soundings. *Science* 277, 1956-1962.
- Stoker, M., Praeg, D., Shannon, P., Hjelstuen, B., Laberg, J., van Weering, T., Sejrup, H. & Evans, D. 2005: Neogene evolution of the Atlantic continental margin of NW Europe (Lofoten Islands to SW Ireland): anything but passive. In Doré, A.G. & Vining, B.A. (eds). North-West European Petroleum Geology and Global Perspectives: Proceedings of the 6th Conference. *Geological Society, London*, 1057-1076.
- Stoker, M.S., Hoult, R., Nilsen, T., Hjelstuen, B.O., Laberg, J.S., P.M., S., Praeg, D., Mathiasen, A., van Weering, T.C.E. & McDonnell, A. 2005b: Sedimentary and oceanographic responses to early Neogene compression on the NW European margin. *Marine and Petroleum Geology* 22, 1031-1044.
- Stoker, M.S., van Weering, T.C.E. & Svaerdborg, T. 2001: A mid- to late Cenozoic tectonostratigraphic framework for the Rockall Trough. In Shannon, P. M. Haughton, P. D. W., & Corcoran, D. V. (eds). The Petroleum Exploration of Ireland's Offshore Basins. *Geological Society, London, Special Publications* 188, 411-438.
- Svela, P.T. 1971: Gravimetriske undersøkelser av Lofoten-Vesterålen området. *Unpublished. Master thesis, University of Bergen*, 131 pp.
- Sykes, L. 1965: Seismicity of the Artic. *Seismological Society of America Bulletin* 55, 501-518.
- Talwani, M. & Udintsev, G.e.a. 1976: Initial Reports of the Deep Sea Drilling Project, Volume 38. *U.S. Government Printing Office, Washington, D.C.* 1256 pp.
- Talwani, Udintsev *et al.* (Eds.) 1978: Initial reports of the Deep Sea Drilling Project, Supplements to Vol. 38, 39, 40 and 41. *U.S. Government Printing Office, Washington, D.C.*
- Thompson, D.T. 1982. EULDPH: A new technique for making computer-assisted depth estimates from magnetic data. *Geophysics* 47, 31-37.
- Torske, T. & Prestvik, T. 1991: Mesozoic detachment faulting between Greenland and Norway: Inferences from Jan Mayen Fracture Zone system and associated alkalic volcanic rocks. *Geology* 19, 481-484.
- Torsvik, T., Mosar, J. & Eide, E. 2001: Cretaceous-Tertiary Geodynamics: a North Atlantic exercise. *Geophysical Journal International* 146, 850-866.
- Tsikalas, F., Faleide, J.I. & Eldholm, O. 2001: Lateral variations in tectono-magmatic style

- along the Lofoten-Vesterålen volcanic margin off Norway. *Marine and Petroleum Geology* 18, 807-832.
- Tsikalas, F., Eldholm, O. & Faleide, J.I. 2002: Early Eocene sea floor spreading and continent-ocean boundary between Gleipne and Senja fracture zones in Norwegian-Greenland Sea. *Marine Geophysical Researches* 23, 247-270.
- Tucholke, B. & Schouten, H. 1988: Kane Fracture Zone. *Marine Geophysical Research* 10, 1-39.
- Unternehrr, P. 1982: Etude structurale et cinématique de la mer de Norvège et du Groenland. Evolution du microcontinent Jan Mayen. *Thèse Université de Brest*, 0-227.
- Våagnes, E., Gabrielsen, R. & Haremo, P. 1998: Late Cretaceous-Cenozoic intraplate contractional deformation at the Norwegian continental shelf: timing, magnitude and regional implications. *Tectonophysics* 300, 29-46.
- Upton, B., Emeleus, C., Rex, D. & Thirlwall, M. 1995: Early Tertiary magmatism in NE Greenland. *Journal of the Geological Society, London* 152, 959-964.
- Upton, B. 1988: History of Tertiary igneous activity in the N Atlantic borderlands. In: Morton, A.C. & Parson, L.M. (eds) Early Tertiary Volcanism and the opening of the North Atlantic. *Geological Society, London, Special Publications*, 39, 429-453.
- Verhoef, J., Roest, W.R., Macnab, R., Arkani-Hamed, J. & Members of the Project Team 1996: Magnetic anomalies of the Arctic and North Atlantic Oceans and adjacent land areas. *Geological Survey of Canada Open File 3125, Parts a and b* (CD-ROM and project report), Geological Survey of Canada, Dartmouth NS.
- Vogt, P.R., Taylor, P., Kovacs, L.C. & Johnson, G.L. 1979: Detailed aeromagnetic investigation of the Arctic Basin. *Journal of Geophysical Research* 84, 1071-1089.
- Vogt, P.R., V. & Perry, R. 1978: Post-rifting accretion of continental margins in the Norwegian-Greenland and Labrador Seas: Morphologic evidence. *EOS Trans. American Geophysical Union*, 59, 1204.
- Vogt, P.R., Johnson, G.L. & Kristjansson, L. 1980: morphology and magnetic anomalies north of Iceland. *Journal of Geophysics* 47, 67-80.
- Vogt, P.R., Bernero, C., Kovacs, L.C. & Taylor, P. 1981: Structure and plate tectonic evolution of the marine Arctic as revealed by aeromagnetism. *Oceanologica Acta No. SP*, 25-40.
- Vogt, D., Ostenso, N. & Johnson, G. 1970: Magnetic and bathymetric data bearing on sea-floor spreading north of Iceland. *Journal of Geophysical Research*, 75, 903-920.
- Watts, A.B. 2001: Isostasy and Flexure of the Lithosphere. *Cambridge University Press*, 458 p.
- White, R. & McKenzie, D. 1989: Magmatism at rift zones: the generation of volcanic continental margins and flood basalts. *Journal of Geophysical Research* 94, 7685-7729.
- Åm, K. 1975: Aeromagnetic basement complex mapping north of latitude 62°N, Norway. *Norsk Geologisk Tidsskrift* 316, 351-374.
- Yaxley, G. 2000: Experimental study of the phase and melting relations of homogeneous basalt+peridotite mixtures and implications for the petrogenesis of flood basalts. *Contributions to Mineralogy and Petrology* 139, 326-338.
- Zobin, V. 1993: The source mechanism of large volcanic earthquakes on Jan Mayen Island. *Volcanology and Seismology* 14, 152-163.

14 FIGURES

Figure 1.1 Bathymetry and topography, Norwegian-Greenland Sea, 100 and 500 m contour intervals. The red frame shows the JAS-05 survey area.

Figure 1.2 The Navajo PA31 LN-NPZ operated by Blom Geomatics was hired by TGS NOPEC for the data acquisition.

Figure 2.1 Diagram from the Tromsø Geophysical Observatory (<http://www.tgo.uit.no/aix>) showing the magnetic disturbances in Tromsø during the time period 1987-2005. The JAS-05 survey was carried out during August and September 2005, a period with intermediate to high geomagnetic activity.

Figure 2.2 Example of statistical levelling (Geosoft 2005a) of line 170 in the JAS-05 survey. 'Outliers' of intersection differences have been removed manually from the lines.

Figure 2.3 JAS-05 flight pattern.

Figure 2.4 Total magnetic field of the JAS-05 survey referred to DGRF-05. The contour interval is 50 nT.

Figure 2.5 Gaussian 20 km high-pass filtered magnetic field.

Figure 2.6 Compilation of magnetic surveys in the NE Atlantic area. The sub-grids from the 35 aeromagnetic surveys listed in Table 2.1 are produced from original profile data. The marine magnetic survey (pale blue), Fairey surveys to the west of Shetland (olive green lines) and the GEUS-survey on mainland Greenland (GEUS-74) are adapted from the Verhoef et al. (1996) Gammaa5 compilation and added to the regional data-set.

Figure 2.7 Compilation of aeromagnetic surveys in the Norwegian-Greenland Sea (subset of NE Atlantic compilation in Fig. 2.4)..

Figure 2.8 Compilation of gravity surveys in the NE Atlantic (Skilbrei et al. 2000).

Figure 2.9 Magnetic compilation of the NE Atlantic. Total magnetic field referred to DGRF.

Figure 2.10 Magnetic compilation of the Norwegian-Greenland Sea. Total magnetic field referred to DGRF.

Figure 2.12 Free air gravity at sea and Bouguer gravity on land in the Greenland-Norwegian Sea area (Skilbrei et al. 2000). The contour interval is 10mGal. The red frame shows the JAS-05 area.

Figure 2.13 Residual gravity after isostatic correction of Bouguer gravity data from the Greenland and Norwegian Seas and adjacent areas. The isostatic correction has been calculated applying the AIRYROOT algorithm (Simpson et al. 1983) to the topography/bathymetry in Fig. 1.1 (rock density 2670 kg/m³ on land, 2200 kg/m³ at sea and a crust/mantle density contrast of 300 kg/m³). The contour interval is 10mGal. The red frame shows the JAS-05 area.

Figure 2.14 Seismic database for the interpretation of the JAS-05 data. The OBS and reflection seismic data have been provided by Breivik et al. (2004) and NPD, respectively. The information from the Deep Sea Drilling Project is adapted from Talwani et al. (1978).

Figure 3.1 Bathymetry of the Norwegian-Greenland Sea and location of the Jan Mayen survey area.

Figure 3.2 Picture of the active Beerenberg volcano, northern Jan Mayen during its eruption in 1985 (<http://www.jan-mayen.no/>). The Beerenberg has erupted six times between 1732 and 1985. All of these eruptions were on flank vents and produced lava flows and scoria cones. The most recent eruptions were in 1970, 1973, and 1985.

Figure 3.3 Interpreted line-drawings of seismic reflection profiles across the Jan Mayen Ridge and the Jan Mayen Basin (Kuvaas & Kodaira 1997). SDW=Seaward dipping wedge (referred as SDRS in our report). The sediments lying above JA are Miocene or younger in age: The sediments below JA are Oligocene or older. Rocks below Horizon O have not been drilled but may represent Palaeozoic to Mesozoic faulted Ridges. Red sequences represent volcanic rocks. Reflectors F in the western Jan Mayen Margin masks the underlying structures and is interpreted as Early Miocene lava flows. Note also that crustal extension occurs during Eocene?-Oligocene time in the western part of the Jan Mayen Ridge.

Figure 3.4 Regional bathymetric transects between the main spreading systems located on both side of the JMFZ corridor. Blue curves represent the magnetic anomalies with the interpreted magnetic chrons from C24 to the current or extinct spreading Ridges. The oceanic crust

between Norwegian and Greenland Seas can be subdivided into four domains: 1) The Mohns Ridge spreading system along the Greenland Basin and the Lofoten Basin and 2) the aborted Aegir Ridge spreading system, situated west of the Møre Margin and delimited to the west by 3) the Jan Mayen Microcontinent. The microcontinent separates 4) the currently active Kolbeinsey Ridge from the extinct Aegir Ridge. A ridge jump between Aegir Ridge and the Kolbeinsey Ridge occurred progressively between C13 (33.3 Ma) and C6-C7(20-25 Ma).

Figure 4.1 The study area: Total magnetic field anomaly and the location of the three interpreted transects. The orange line denote the location of OBS lines in and adjacent to the study area (Mjelde et al. 2005 and references therein).

Figure 4.2 Source depth of Located Euler deconvolution for $SI=-1$ (dyke). The deep solutions are mainly located in areas with clear observable magnetic reversals, pointing to a source at the boundary between inverse and normal polarised magnetic domains. The solutions have been limited to solutions with a horizontal and vertical uncertainty less than 15 %.

Figure 4.3 Gridded source depth Located Euler deconvolution for $SI=-1$ (dyke). The depth map is based on the source depth solutions in Fig. 4.2.

Figure 4.4 Free-air anomaly of the Jan Mayen Survey area.

Figure 4.5 Bouguer anomaly of the Jan Mayen Survey area. For the Bouguer plate reduction a density of 2.200 Mg/m^3 has been used.

Figure 4.6 Bathymetry (IBCAO) and profile location.

Figure 4.7 Density structure along Line 1. The upper panels show the modelled and observed Free-air and Bouguer anomaly. The lower panel shows the density model (densities in Mg/m^3) and the depth-converted shallow seismic interpretation.

Figure 4.8 Magnetic model along Line 1. a) The upper panels shows the modelled induced and observed total magnetic field anomaly. The lower panel shows magnetic susceptibilities in 10^{-5} SI . Below the drawn depth to Curie temperature the model is featuring non-magnetic material. b) The upper panels shows the modelled induced + remanent and observed total magnetic field anomaly. The modelled field is generated by the geometry and Q -ratios shown in the lower panel and the susceptibilities shown in (a). Arrows next to the magnetic properties indicate the directions of induced and remanent magnetisation. In addition shown are the located Euler-depth solutions (red-crosses).

Figure 4.9 Density structure along Line 2. a) The upper panels show the modelled and observed free-air and the lower panel the density structure (densities in Mg/m^3). b) The upper panels show the modelled and observed free-air and the lower panel the same density structure as in (a) and the colour-coded OBS velocity model by Breivik et al. (2005) as an overlay.

Figure 4.10 Magnetic model along Line 2. a) The upper panels shows the modelled induced and observed total magnetic field anomaly. The lower panel shows magnetic susceptibilities in 10^{-5} SI . Below the drawn depth to Curie temperature the model is featuring non-magnetic material. b) The upper panels shows the modelled induced + remanent and observed total magnetic field anomaly. The modelled field is generated by the geometry and Q -ratios shown in the lower panel and the susceptibilities shown in (a). Arrows next to the magnetic properties indicate the directions of induced and remanent magnetisation.

Figure 4.11 Density structure along the Cross-line 3. The upper panels show the observed magnetic anomaly, and the central ones the modelled and observed free-air and Bouguer anomaly. Lower panel shows density structure (densities in Mg/m^3) and depth-converted shallow seismic interpretation.

Figure 4.12 Density structure along Line 4. The upper panels show the modelled and observed Free-air and Bouguer anomaly. The lower panel shows the density model (densities in Mg/m^3) and the coloured lines refer to the OBS model L2-96 (Mjelde et al. 2003).

Figure 4.13 Magnetic model along Line 4. a) The upper panels shows the modelled induced and observed total magnetic field anomaly. The lower panel shows the magnetic part of the model with magnetic susceptibilities in 10^{-5} SI . b) The upper panels shows the modelled induced + remanent and observed total magnetic field anomaly. The modelled field is generated by the geometry and Q -ratios shown in the lower panel and the susceptibilities

shown in (a). Arrows next to the magnetic properties indicate the directions of induced and remanent magnetisation.

Figure 5.1 Schematic diagram illustrating the concepts of transform fault and fracture zone in the strict sense.

Figure 5.2 Bathymetric and gravity transects (isostatic anomalies) along the whole Jan Mayen Fracture Zone. CJMFZ: Central Jan Mayen Fracture Zone; EJMfZ: East Jan Mayen Fracture Zone; WJMfZ: West Jan Mayen Fracture Zone. The transects illustrate the complex physiography of JMFZ corridor divided in two main segments (West JMFZ corridor and East JMFZ corridor) at the level of Jan Mayen. The aeromagnetic survey covers most of the East JMFZ corridor). Inside the East JMFZ corridor, both symmetric or asymmetric bathymetric feature can be observed and suggest lateral sub-segmentation of the corridor.

Figure 5.3 Longitudinal transect across the Jan Mayen Fault Zone Corridor (location A-B) on previous map (Fig. 5.2). Interpolated gravity (Free-Air and Bouguer anomalies) and interpreted magnetic profiles along the bathymetry illustrate the complexity of the corridor. Yellow triangles indicate the intersection with the previous profiles.

Figure 5.4 Map of gridded bathymetry along the East JMFZ corridor, constructed using high-resolution ship-track and satellite-derived data set. The main fracture zones and magnetic anomalies have been re-interpreted using a systematic comparison between bathymetry, gravity, magnetic patterns and available seismic data. The white frame represents the location of the Jan Mayen aeromagnetic survey located between the Jan Mayen Ridge (to the west) and the Vøring Marginal High (to the east). Note that the Norway Basin is deeper than the Lofoten Basin. The JMFZ corridor delimits these two subsiding oceanic domain. Across the Norway Basin, the Aegir Ridge represents a fossil-spreading axis. Close to the Jan Mayen Island, the Mohns Ridge is still active. NW-SE elongated troughs and elongated ridges characterise CJMFZ, EJMfZ and WJMfZ. North of the EJMfZ, the Aegir Marginal High (AMH) represents a broad and anomalous bathymetric high. This bathymetric feature is atypical and shallower than surrounding areas. Dashed curved represent the Bouguer lows.

Figure 5.5 Map of terrain slope along the East JMFZ corridor. The map is overlain with fault zones and magnetic anomalies. The slope has been calculated at any bathymetric grid node on the surface. Terrain slope is reported in percentage from zero (horizontal) to 90 (vertical). For a particular point on the surface, the terrain slope is based on the direction of steepest descent or ascent at that point. This means that across the surface, the gradient direction can change. This filter was extremely useful to constrain the fault pattern. This map illustrates also the asymmetry or asymmetry of the main structures identified along the survey area. Red circles represent the seismicity recorded by USGS in this area between 1973 and 2005. Only the northern part of the Jan Mayen Island is extremely active now.

Figure 5.6 Map of gridded Free-Air anomalies along the East JMFZ corridor overlain with fault zones and magnetic anomalies. The anomalies show trends and structure resembling those of bathymetry, although short-wavelength gravity features are subdued. The map is overlain with magnetic anomalies and faults zones. Note that the EJMfZ is characterized by lower free air anomalies compared to the WJMfZ.

Figure 5.7 High-resolution bathymetry between the Vøring Marginal High and the Aegir Marginal High (AMH). The Aegir trough (AT) represents a V-shaped bathymetric low and a bathymetric hinge between the two shallow highs.

Figure 5.8 Magnetic anomaly map (Gridded magnetic anomalies) along the East JMFZ corridor overlain with the identified and interpreted magnetic anomalies (C24 to C1) between the Lofoten Basin and the Norway Basin. The main fracture zones have been re-interpreted using a systematic comparison between bathymetry, gravity, magnetic patterns and seismic data.

Figure 5.9 Magnetic and bathymetric profiles along the Jan Mayen survey. The main magnetic chrons have been interpreted. CJMFZ: Central Jan Mayen Fracture Zone; EJMfZ: East Jan Mayen Fracture Zone; WJMfZ: West Jan Mayen Fracture Zone.

Figure 6.1 a) General bathymetry of the Mid-Norwegian margin and b) detail of the magnetic map between the Vøring Marginal High (VMH) and the Aegir Marginal High (AMH). The broad high positive anomalies along the VMH coincide with the main SDRS wedges. There is no clear identifiable magnetic chrons along the two distinct branches. However, some EW-oriented magnetic lineaments are observed and could suggest a link between the SDRS and the AMH. AMH: Aegir Marginal High; MMH: Møre Marginal High; VMH: Vøring Marginal High. Outline of the Inner SDRS and Outer SDRS (white contours) and the limit of the Inner Lava flows are from Berndt et al. (2001a).

Figure 6.2 Seismic transect AA' across the Vøring Marginal High, combined with gravity and magnetic signatures. The transect crosscut the two high-amplitude magnetic branches observed along the volcanic plateau. Two Inner SDRS (1 and 2) represent wedge-shaped units interpreted as lava piles emplaced during the breakup. Intra-wedges reflections are fairly weak, discontinuous with a divergent-arcuate pattern. The top basalt is characterised by strong amplitude reflections. Small angular unconformities suggest syn-volcanism growth of the SDRS. Unclear magnetic trends may represent "real C24" anomalies or dike swarms. Two Inner SDRS wedges can be observed and may reflect an overlapping spreading system along the Vøring Marginal High.

Figure 6.3 Seismic transect BB' from the Norway Basin to the Lofoten Basin. The seismic line crosses the Vøring Marginal High, the Inner SDRS 2 and the Outer SDRS observed near the C23 magnetic anomalies. The Inner SDRS are characterised by the highest magnetic anomalies. Some strong reflections and small plugs between the Vøring Marginal High and the Lofoten Basin suggest some kind of post-breakup (may be?) volcanic mound and sills. Alternatively, it could represent the syn-breakup Outer High defined by Planke et al. (2001). Note also the thick sedimentary section (contourite drift) overlying the volcanic plateau. This kind of drift sedimentation could explain the thick sedimentary section atypically observed on top of the AMH, located in the trend of the structure illustrated above. Arrows indicates the different orientations of the magnetic trends.

Figure 6.4 From rift to breakup-evolution of the volcanic margin and formation of the main volcano-stratigraphic sequences. (modified after Planke et al. 2000). The geometry of the wedge is not only controlled by lava flows loading but could also be controlled by the structure of the underlying necking system, controlled by the distribution of magmatic underplating. OLCB: Oceanic high velocity lower crustal body.

Figure 6.5 Magnetic pattern (gridded anomalies) near the Jan Mayen microcontinent. At the northeastern margin, the "SDRS" are surprisingly located before the C24B. However, SDRS are not observed at the conjugate margin, between the East Jan Mayen Fracture Zone and the Norway Fracture Zone according Berndt et al. (2001). In this part of the Jan Mayen, all wedges are not necessarily volcanic features but could also represent the southern prolongation of the Rån Ridge located to the north before the opening of the Norway Basin. Positive anomaly before C24B probably represents C25 anomalies. This suggests an early phase of breakup in Thanethian time. Same observation has been made in the Norwegian part by Gernigon, (2002).

Figure 7.1 Composite seismic transect from the Aegir Marginal High (AMH) to the Lofoten Basin. Section A-B illustrates the main ridge bounded to the west by the East Jan Mayen Fracture Zone (EJMFZ). Section B-C illustrates the transition between the AMH and the Lofoten Basin. This transition is characterised by an intermediate terrace, clearly defined by the main unconformity MU (yellow curve). Section CD represents the oceanic crust accreted between Chrons C20n (43 Ma) and C12n (31 Ma), underlined by the magnetic total field anomalies. C13n marks the Eocene-Oligocene transition according to the geomagnetic polarity time scale of Cande and Kent (1995). Two main sedimentary units (Unit I and Unit II) are defined (see text for description). Unit II pinch-out the northern flanks of the AMH, at the terrace level. Units II and I are divided by the major erosional unconformity (MU) assumed to be Late Oligocene (?) to intra-Miocene in age. This significant seismic unconformity, overlaying the C12 anomaly, formed during the inversion of the AMH, which represents a former Eocene-Oligocene depocentre uplifted

during Late Oligocene (?)– Miocene time.

Figure 7.2 a) Depth-converted seismic transect from the Aegir Marginal High (AMH) to the Lofoten Basin. The main ridge is bounded to the southwest by the East Jan Mayen Fracture Zone (EJMFZ) and probably by the prolongation of the West Jan Mayen Fracture Zone (WJMFZ) to the northeast. MU represent the major erosional unconformity (MU) assumed to be Late Oligocene (?) to intra-Miocene in age. PM is the prominent marker (Late Eocene-mid-Oligocene?). The dotted red curve represents the Bouguer anomalies along the transect, and the blue dotted curve the magnetic signature. This depth profile has been used to constrain the gravity modelling along the AMH and Lofoten Basin (see Potential field modelling chapter). b) Location of the seismic line draped on the Bouguer anomaly map. The figure shows clearly that AMH coincides with a gravity low, which is not observed in the western part of the West JMFZ corridor, covered by the Jan Mayen survey.

Figure 7.3 Details of the seismic interpretation on the eastern flank of a major oceanic horst situated close to the transition between Eocene and Oligocene (the C13n magnetic chron). This example illustrates the main seismic units (Units I and II) and their sub-sequences (I-A, I-B, II-A, II-B). MU represents the main unconformity between Unit I and Unit II and PM represents the prominent marker and unconformity between sub-sequences I-A and I-B. After C13, sediments between the top oceanic basement (Early Oligocene in age) is obviously post-early Oligocene. The growth wedge observed to the east of the C12 oceanic horst represents probably a late Oligocene (?)–Early Miocene sequence. Onlaps suggest that the growing wedge has been formed during the inversion of the underlying Unit I.

Figure 7.4 Details of the seismic interpretation on the northern part of the AMH. This example illustrates the seismic sequences and the relationships with the main faults. This section suggests a long-live period of fault activity. Comparison with magnetic data suggests dextral transtension between C19 (41.5 Ma) and C13 (33.3 ma). Faulting probably started before the main inversion between Unit I-A and II-B. A forced folding feature can be observed in Unit II-B and suggests late reactivation (Miocene) and rotation of pre-existing hanging-wall. Deep wedges suggest faulting during Late Eocene time as well.

Figure 7.5 Map of Bouguer anomalies along the East JMFZ corridor overlain with fault zones and magnetic anomalies. This map reflects the crustal anomalies along the East JMFZ corridor. The Aegir Marginal High represents a clear gravity low (green color) compared to the surrounding oceanic domain (red-purple).

Figure 7.6 Map of isostatically corrected Bouguer anomalies along the East JMFZ corridor overlain with the identified and interpreted magnetic anomalies. Isostatic residual gravity anomaly maps are produced by subtracting long-wavelength anomalies, produced by masses deep within the crust or mantle, from the Bouguer anomaly map. Isostatic residual gravity anomaly maps therefore reveal more clearly than Bouguer anomaly maps the density distributions within the upper crust.

Figure 7.7 Ocean Bottom Seismometer (OBS) velocity transect across the Vøring Marginal High and across the Aegir Marginal High (AMH) to the west (from Brevik et al. 2004, 2005, Euromargins experiment 2003). A thick anomalous crust is observed underneath the AMH. The thickening is similar in size with the lower crustal body (LCB), lying underneath the Vøring Marginal High and is generally interpreted as mafic underplating formed during the breakup and of the Norwegian–Greenland Sea. The V-shaped Aegir Through coincides with a shallow Moho between the two highs. COT: continent-ocean transition.

Figure 7.8 Two hypotheses to explain the anomalous thick crust beneath the Aegir Marginal High (AMH). a) A late Miocene magmatic underplating added to the preexisting oceanic crust (underplating model from Brevik et al. 2004, 2005). b) anomalous melt production generated during the oceanic accretion of the AMH in Eocene (overcrusting model, proposed by NGU). P: Aegir through propagating system. AMH: Aegir Marginal High; VMH: Vøring Marginal High.

Figure 7.9 Main mechanisms proposed to explain flexural uplift along transform faults: a) differential

thermal subsidence across a locked transform faults; b) thermal expansion caused by lateral heat transfer across the transform fault zone; c) tectonic extension or transtension (and induced unloading) oblique to a inclined transform zone. All these models can explain both the current geometry and part of the uplift observed along the Aegir Marginal High (AMH).

Figure 7.10 a) Free-Air gravity and broad magnetic anomalies across the Aegir Marginal High (AMH). b) NW-SE bathymetric and Bouguer profile across the AMH. The green dot represents the bathymetric envelop and probably the swell due to the AMH uplift. c) The crustal root (overcrusting) beneath the AMH fits the broad Bouguer anomaly and the long-wavelength signature of the magnetic total field but do not explain isostatically the main uplift (1500 m). d) The Bullard's model (Watts, 2001) controlled by the EJMFCZ could explain part of the AMH structure.

Figure 7.11 Theoretical values of T_e predicted for a cooling oceanic crust (Watts 2001). The elastic thickness is function of the age of the oceanic crust and increases when crust is older.

Figure 8.1 Plate reconstruction between Norway, Greenland and the Jan Mayen Microcontinent at C21 (47 Ma-early Eocene). This picture illustrates also a triple junction between the Vøring Marginal High and the TraillØ igneous complexe. AMH: Aegir Marginal High; JL: Jameson Land; JMMC: Jan Mayen MC; MMH: Møre Marginal High; TMA: Traill-Vøring igneous complex; TØ: Traill Ø basin; VMH: Vøring Marginal High.

Figure 8.2 Plate reconstruction between Norway, Greenland and the Jan Mayen Microcontinent at C13 (33.3Ma-EoceneOligocene boundary). This event coincide with the onset of a major plate reorganization. AMH: Aegir Marginal High; JL: Jameson Land; JMMC: Jan Mayen MC; MMH: Møre Marginal High; TMA: Traill-Vøring igneous complex; TØ: Traill Ø basin; VMH: Vøring Marginal High.

Figure 8.3 Plate reconstruction between Norway, Greenland and the Jan Mayen Microcontinent at C5 (10Ma-late Miocene). AMH: Aegir Marginal High; JL: Jameson Land; JMMC: Jan Mayen MC; MMH: Møre Marginal High; TMA: Traill-Vøring igneous complex; TØ: Traill Ø basin; VMH: Vøring Marginal High.

Figure 8.4 Structural map of the outer Vøring Margin (after Gernigon et al., 2003). BL: Bivrost Lineament; FFC: Fles Fault Complex; FG: Fenris Graben; GFZ: Gleipne Fracture zone; GS: Gleipne saddle; HG: Hel Graben; HT: Halten Terrace; JMFZ: Jan Mayen Fracture Zone; ND: Naglfar Dome; NH: Nyk High; NS: Någrind Syncline; NGR: north Gjallar Ridge; RaB: Rån basin; RR: Rån ridge; RFZ: Rym Fault Zone; SGR: south Gjallar Ridge; VS: Vigrid Syncline; VD: Vema Dome; VMH: Vøring Marginal High. Volcanic facies map of the Vøring Marginal high has been modified after Berndt et al. (2001a).

Figure 8.2 a) Magnetic pattern of the oceanic basement around the Aegir Marginal High (AMH). b) High resolution bathymetry between the AMH and the Aegir trough. c) Schematic cartoon that illustrates a possible structural relationship between the Aegir trough and the block dislocation of the AMH. The V-shaped Aegir trough probably represents a propagating oceanic ridge. During the propagation from south to north, lateral oceanic accretion probably induced displacement able to produce the block dislocation of the AMH.

Figure 8.3 a) Seismic transect across the Aegir trough. b) Bathymetry illustrating the V-shaped structure of the Aegir through. c) Magnetic anomalies d) Bouguer gravity anomalies between the Vøring Marginal High and the AMH.

Figure 8.4 Stratigraphy for the upper Palaeogene–Neogene strata on the NW European Atlantic margin (Stoker et al. 2005). The assignment of major and minor unconformities (see text) is based on the correlation of key reflectors from the North Sea Fan–Vøring, Faroes–Shetland and Rockall–Porcupine areas. The two regional unconformities recognized from the Aegir Marginal High to the Lofoten basin (PM and MU) could coincide, respectively with the early Oligocene and the late Oligocene–Early Miocene major and regional unconformities. BNU, base Naust unconformity; INU, intra-Neogene unconformity; BKU, base Kai unconformity; TPU, top Palaeogene unconformity; GU, intra-Pleistocene glacial unconformity; IMU, intra-Miocene unconformity; MMU, mid-Miocene unconformity; IUEOC, intra-upper Eocene unconformity. Timescale after Berggren et al. (1995).

- Figure 8.5 Tectonic calendar of Cenozoic geodynamics deduced from the Jan Mayen area. Magmatic and tectonic episodes, onshore Traill Ø, from Price et al. (1997) and Lundin and Doré, (2002). TMO: offshore Traill-Vøring igneous complex (Olesen et al., submitted). Summary of the NW European continental margin megasequences and regional tectonics from Praeg et al. (2005). Compressional events interpretations are from 1) Lundin and Doré, 2002; 2) Vågnes, 1998; 3) Brekke, 2000; 3) Gómez and Vergés, 2005; Boldreel and Anderson, 1993; Ritchie et al., 2003. Time scale from Gradstein et al. (2004).
- Figure 9.1 The Traill Ø magnetic anomaly and ages of the main onshore intrusions (East Greenland margin). This strong magnetic anomaly observed from the TraillØ coastline to the C21 likely represents a major igneous complex offshore East Greenland.
- Figure 9.2 a) The Vøring Marginal High-TraillØ triple junction. During late Paelocene-Eocene, the Vøring Marginal High and the Traill Ø magnetic anomaly formed a triple junction R-R-FZ between the spreading ridge and the JMFZ. b) This geodynamic setting is quite similar to the Azores triple junction where anomalous magmatic production propagates from the spreading ridge toward the adjacent oceanic fracture zone. c) Note also the southward propagation of the spreading ridge across the Azores Plateau. Figures b and c are from Lagabrielle & Leroy (2005).
- Figure 10.1 Model set-up. The area of interest is a 400 x 400 km square far from model boundaries and depicted by its finer mesh. Contrasting spreading rates (i.e. velocities) are applied between the domains located south and north of the Jan Mayen Fault Zone (JMFZ).
- Figure 10.2 Modelled displacement field after 5 Myr (X direction). Note the decrease in displacement along the JMFZ in the Vøring Basin, the effect is due to internal shortening of the block above the MTFC.
- Figure 10.3 Modelled strains after 5 Myr. Negative values are associated to shortening. Note significant strain concentrations at the COB and at the termination of the JMFZ in the Vøring Basin.
- Table 2.1. Offshore aeromagnetic surveys compiled for the present study (Figs. 2.6, 2.7, 2.9 & 2.10 Maps 1 & . CGG - Compagnie Générale de Géophysique; GEUS – Geological Survey of Denmark and Greenland; NOO - Naval Oceanographic Office; NGU – Geological Survey of Norway; NPD – Norwegian Petroleum Directorate; NRL - Naval Research Laboratory
- Table 2.2. Magnetic properties of igneous rocks from drilling in the Vøring area within the Deep Sea Drilling Project (DSDP) and Ocean Drilling Program (ODP) in 1974 and 1985, respectively (¹Kent & Opdyke 1978, ²Eldholm et al. 1987). The ODP susceptibility data are claimed to be cgs-units, but they are most likely in SI-units, because a corresponding magnetite content of 30-40 % in the volcanics is highly unlikely. A log diagram of the 642E well in Schönharting & Abrahamsen (1989) supports this conclusion.
- Table 4.1 Densities for structures in the 2.5D models. The water density is used in modelling the Free-Air/Bouguer anomaly, respectively.
- Table 8.1 Euler poles used for the plate reconstruction between Greenland, Mid-Norway and the Jan Mayen Microcontinent.
- Table 10.1 Modelling parameters.

15 TABLES

Table 2.1. Offshore aeromagnetic surveys compiled for the present study (Figs. 2.6, 2.7, 2.9 & 2.10 Maps 1 & . CGG - Compagnie Générale de Géophysique; GEUS – Geological Survey of Denmark and Greenland; NOO - Naval Oceanographic Office; NGU – Geological Survey of Norway; NPD – Norwegian Petroleum Directorate; NRL - Naval Research Laboratory

Table 2.2. Magnetic properties of igneous rocks from drilling in the Vøring area within the Deep Sea Drilling Project (DSDP) and Ocean Drilling Program (ODP) in 1974 and 1985, respectively (¹Kent & Opdyke 1978, ²Eldholm et al. 1987). The ODP susceptibility data are claimed to be cgs-units, but they are most likely in SI-units, because a corresponding magnetite content of 30-40 % in the volcanics is highly unlikely. A log diagram of the 642E well in Schönharting & Abrahamsen (1989) supports this conclusion.

Table 4.1 Densities for structures in the 2.5D models. The water density is used in modelling the Free-Air/Bouguer anomaly, respectively.

Table 8.1 Euler poles used for the plate reconstruction between Greenland, Mid-Norway and the Jan Mayen Microcontinent.

Table10.1 Modelling parameters.

16 APPENDIX A, TECHNICAL REPORT JAN MAYEN AEROMAGNETIC SURVEY 2005 (JAS-05)

By Johannes Hauge, TGS-NOPEC Geophysical Company

16.1 INTRODUCTION

TGS Nopec Geophysical Company (TGS) was awarded a contract on the acquisition of 33,000 line kilometres of fixed-wing airborne magnetic data on behalf of NGU.

TGS commenced test flights with calibration of instruments at Torp (Sandefjord) on 1. August 2005. Mobilisation to the site at Jan Mayen and start of survey operations began on 3. August 2005. Productive flying was completed on 3. October and final products were delivered 11. October 2005.

16.2 SURVEY AREA

The survey area was southeast of Jan Mayen in the Norwegian-Greenland Sea. The southeasterly extreme of the survey area lies at approximately 8° 25' east by 68° 48' north whilst the north-westerly extreme of the survey area lies at approximately 7° 40' west by 71° 18' north. The crew was based on Jan Mayen.

The following coordinates define the survey area.

Survey Boundary Coordinates

| | X | Y | LONG | LAT |
|---|-----------|------------|-------------|-------------|
| 1 | 120060.36 | 7944472.71 | -7.40.00.00 | 71.18.00.00 |
| 2 | 718361.71 | 7641693.83 | 8.25.00.00 | 68.48.00.00 |
| 3 | 679816.25 | 7595720.08 | 7.23.00.00 | 68.25.00.00 |
| 4 | 385087.95 | 7591931.72 | 0.12.00.00 | 68.25.00.00 |
| 5 | 380091.64 | 7441470.80 | 0.14.30.00 | 67.04.00.00 |
| 6 | 80070.18 | 7730272.74 | -7.43.00.00 | 69.21.00.00 |

Geodetic parameters:

| | |
|--------------|-------------|
| Projection | UTM zone 31 |
| Lat0 | 0 |
| Lon0 | 3 |
| Scale Factor | 0.9996 |
| Datum | WGS84 |

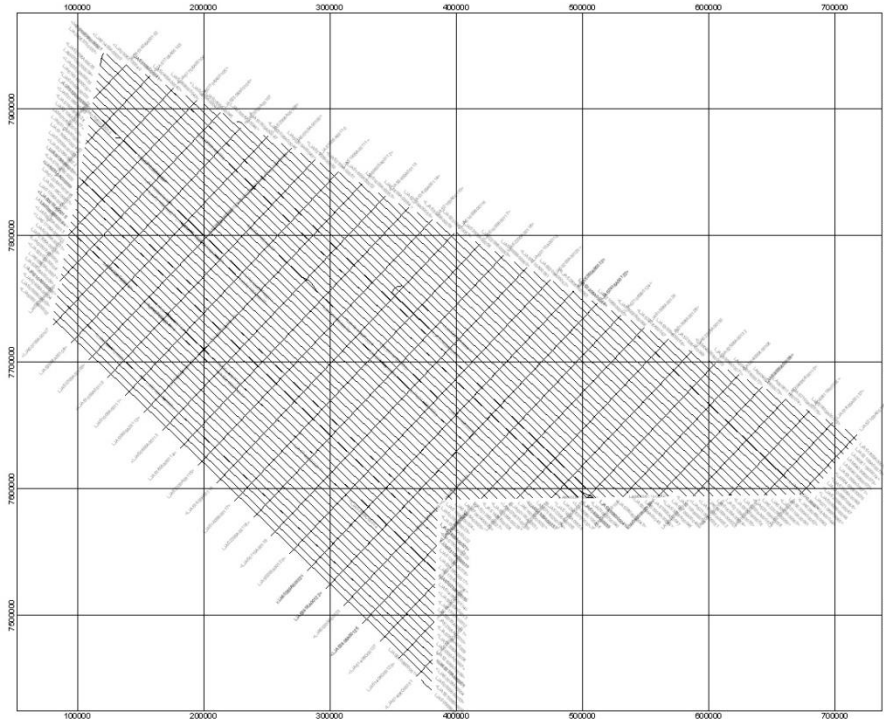


Figure 1. JAS-05 survey outline and flight path

16.3 PERSONNEL

- | | |
|-------------------------------------|---|
| • Project Manager | Jørn B. Christiansen |
| • Field Project Manager | Johannes Hauge |
| • Pilots | Jon Wold, Tobias Ødegaard, John Aalborg and John Wiese |
| • Field Geophysicist/Data Processor | Johannes Hauge and Lasse Christiansen |
| • Office Data processor/QC control | Sergej Usov and Reidun Myklebust |
| • Airborne Operator | Anders Vegstein |

16.4 SURVEY DETAILS

The following summary details the essence of the geophysical survey program:

- | | |
|-----------------------------------|---|
| • Survey area | JAS-05 |
| • Base of operation: | Jan Mayen and Bodø |
| • Traverse line spacing and trend | 5,000 m at 314 / 134° |
| • Tie line spacing and trend | 20,000 m at 134 / 44° |
| • Flying height | 230 metres |
| • Speed | 140 knots/h |
| • Total line kilometres | 33,000 line kilometres |
| • Data recorded | Total field magnetic intensity, Barometric, radar altitude, and positional data |

Data sampling

- | | |
|-------------------------|-----------------------|
| • Magnetic | < 8 metres (0.1 sec). |
| • Magnetic base station | 1 second intervals. |
| • Altimeters | < 8 metres (0.1 sec). |

- GPS Position < 80 metres (1.0 sec).

16.5 EQUIPMENT

The following equipment was used for the survey:

Aircraft: Piper Navajo PA31 LN-NPZ (Registration: LN-NPZ)

Engines: 2 x 6 cyl. 310 BHP turbo charged

Seats: 8 (3-4 in survey mode, incl. pilots)

Nacelle kit fuel tanks (920 liter), extra fuel tank behind engines.

Vortex Generator Kit to increase max take-off weight and stability.

Replaced all control wires to ORION/Electra anti-magnetic spec.

Contra-weights replaced with Antimagnetic Iron weights.

Aft. bulk-head replaced for extra strength.

Stringers mounted under aft. fuselage for extra strength/less vibrations.

Rivets replaced and added for non magnetic and extra strength/less vibrations.

Special silver coated coax cables mounted for all sensors and antennas.

Performance

Accelerate/Stop distance MTOW: 610 m.

Normal take off distance over 50 feet MTOW: 520 m

Cruising speed: 170 knots/h

Survey Speed: 120-140 knots/h

Max altitude: 23,000 feet Survey altitude: down to 300 feet

Capacity

Fuel: 1120litres

Max take-off weight: 3104 kg

Range: Survey 9h45min. + 45min. res.

Range: Ferry 8h15min. + 45min. res.

Range: 1,400 nautical miles

Two sensors (back stingers) layout are used for normal aeromagnetic operations.

Technical Specifications

Flag: Norwegian

CAA modification approvals: LSTA Transport Canada (Canada) Luftfartsverket (Norway)

Length: 10.8 m

Wingspan: 13.5 m

Sensor distance from fuselage: Upper rear: 2.2 m, Lower rear: 2.5 m

Sensor distance from wings: Left: 1.80 m, Right: 1.80 m

Sensor separation 1.54m

Aircraft Operator Certificate: Commercial License no. CAA-N 004 for civil aviation and passenger transport

Safety

Important elements: Two pilot operation

Twin engine

25-hour maintenance interval

Documented HSE system

Full compliance with all regulatory requirements. Fully equipped for IFR

Magnetometers: Geometrics G-822A Cesium Vapor, installed in tail stinger.

Sensors: 2 Cesium sensors

Compensator: RMS AADC-II magnetometer compensation system with TFM 100G2-1E 3-axis Fluxgate magnetometer.

Compensation mag sensor: RMS AADC-II

Recording: RMS Instruments. DGR-33 recording system and chart recorder.

Base station magnetometer: Geometrics G822 A high sensitivity with digital recording.

Acquisition system: RMS DGR33A, real time compensation. 0.1 Hz

Flight path tracking: Digital into RMS DGR33A

Navigation: Flight guidance: Tracker, Real time flight guidance system.

GPS systems: Ashtech Z-surveyor 12 channels GPS Receiver

Altimeter: KING KRA 405 radar altimeter.

Accuracy: 0.25%.

Resolution: 1 foot.

35A circuits for geophysical equipment and navigation equipment.

HF radio installed for long distance operation.

Integrated Iridium satellite telephone.

Barometer: AIR DB2B Intellisensor barometric altimeter.

Resolution: 1 foot

Processing platform: Windows PC, Dell Latitude D810, Oasis Montaj Geosoft ver. 6.0.

16.6 REFLIGHT SPECIFICATIONS

The crews maintained the following tolerances:

Diurnal: If the earth's magnetic activity exceeded 10 nT when measured from a linear chord of 10 minutes a re-flight was undertaken.

16.7 CALIBRATIONS

A series of pre survey tests were undertaken, before starting acquisition of data for the Jan Mayen Aeromagnetic Survey. These tests and calibrations were conducted in the period 1-6. August and conform to survey specifications.

The following tests and calibrations were undertaken:

- Figure of Merit
- Magnetic Heading
- Base Station Noise Test

All of these checks conform to or exceed the tender specifications. Further checks, tests and calibrations were undertaken also during the survey.

Figure of merit (FOM)

A test was carried on 1. August and repeated on 6. August 2005. The tests were carried out in areas of low magnetic gradient at an altitude of >1,000 meters. Data were collected from a series of lines consisting of 10 degrees rolls, 5 degrees pitches and 5 degrees yaws, over a period of 4 to 5 seconds, in the same direction as the survey flight and tie lines. The Figure of Merit (FOM) for the aircraft was then calculated by summing the peak-to-peak amplitudes of the magnetic responses. Both tests are well within the specified FOM of 2.0 nT

Magnetic heading (clover leaf test)

This test shows how FOM test reported above compensates for the Bias.

The test was flown at the same altitude as the FOM test because the absence of high magnetic gradients is important for a successful performance of the test.

Base station noise test

The test base magnetic logging took place on 6. August 2005.

Noise level was 0.117 nT defined as a standard deviation.

Conclusion

All of the tests and checks conformed to, or exceeded the specifications in the tender document. Detailed description of the tests was given in JAS05 Start-up Report presented in Appendix B.

16.8 REFLIGHTS

A line list with comments and classification of magnetic diurnals can be seen in Table 1.

16.9 PROCESSING FLOW - IN FIELD DATA PROCESSING & QUALITY CONTROL

Geosoft Oasis Montaj and customised software packages were used to produce corrected flight path and contour plots of the data for verification purposes.

Data recovery

- Separation of acquired data on a line-by-line basis
- Verification of all digital data acquired on the most recent flight
- Verification of all GPS data
- Merging of the data from the flight into the "master" survey data base
- Computation/plotting/storage of the results of all daily checks and tests
- Quality control of all acquired data and tests and tabulation of all instances of marginal or out-of-tolerance data
- Daily reports of line kilometers completed to Company.
- The Project Manager maintained a daily diary of events, which formed the basis of a weekly report.

QC procedures

The extracted field tape information was uploaded to the Geosoft Oasis data base structure. During the upload process various report files were generated, detailing statistics for each flight line and each flight, namely:

- Minimum, maximum, average and standard deviation values of the magnetic data.
- Minimum, maximum, average and standard deviation values of the linear tracking altimeter data.

All of the above information was plotted graphically to verify the system's performance as well as to monitor the veracity of the data. Oasis Airborne QC was used to verify that data was within specification. Fourth difference was used to monitor noise on the magnetic.

Base Magnetic Data

Base station information was downloaded from remote logger to the field PC.

A Geosoft Oasis magnetic base station look up table was then generated.

No analogue records were produced. Time synchronised diurnal was imported to the Oasis database and interpolated to 0.15 interval for on-screen plots, together airborne mag. Oasis QC Toolkit was used to flag out of specification diurnal for further considerations.

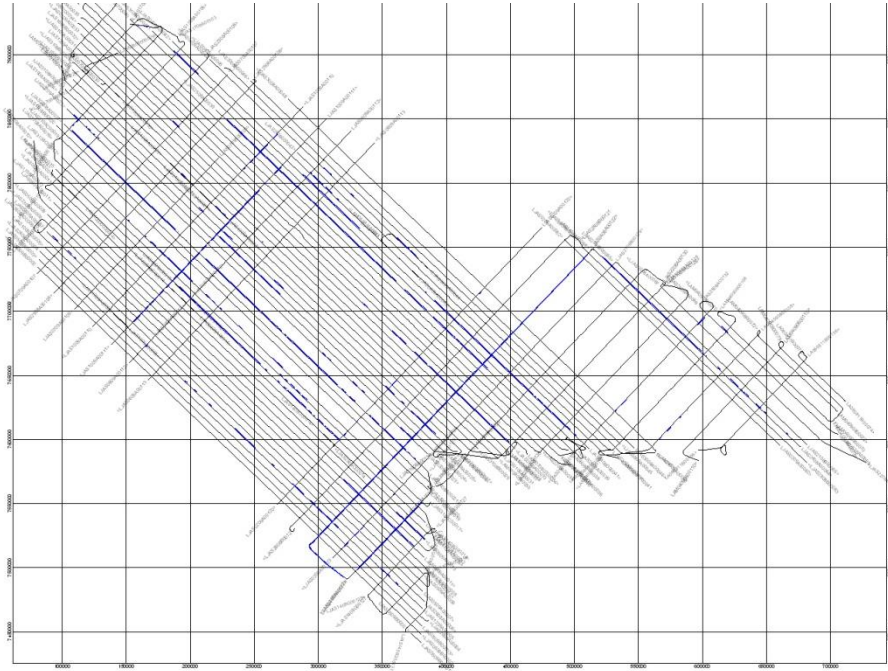


Figure 2. Magnetic profiles influenced by diurnal variation $> 10 \text{ nT}/10 \text{ min.}$ are shown in blue color.

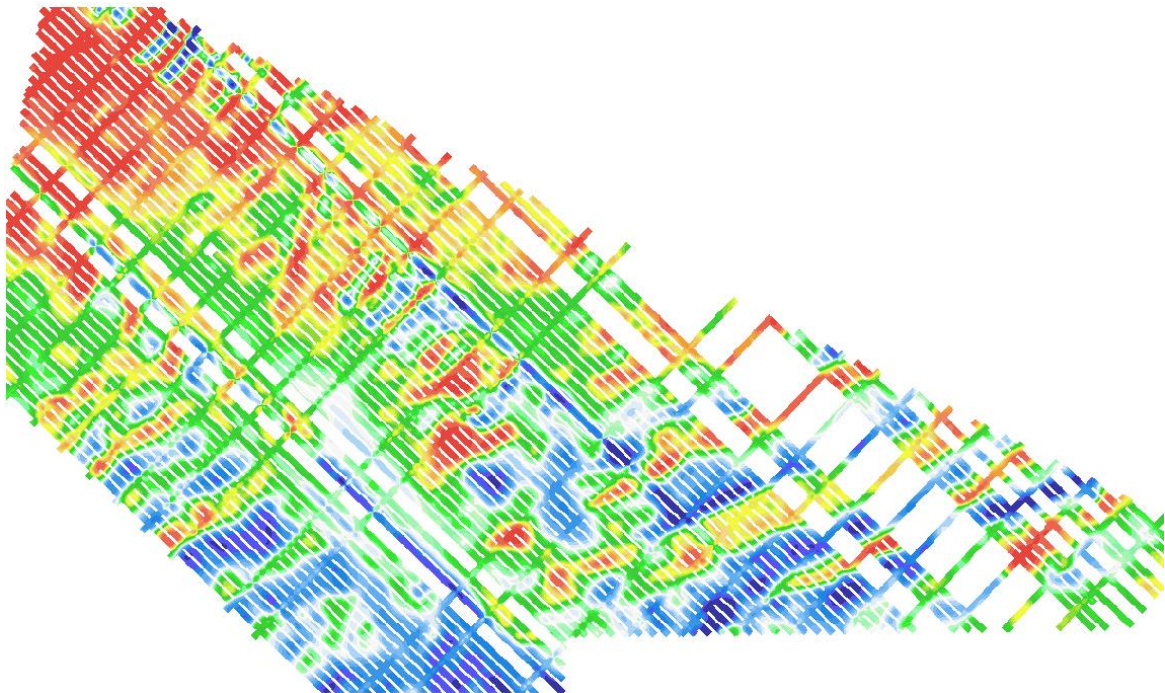



Figure 3. Profiles influenced by magnetic disturbance are easily seen on the grid (example of unprocessed total field flights 1-42)

Magnetic Reference Stations

Magnetic data from the following reference stations have been utilized in the QC control and daily survey planning <http://geo.phys.uit.no/geomag.html> (Figure 2.):

- Leknes

- Tromsø
- Bjørnøya



**Geomagnetic data from
Tromsø Geophysical Observatory
Faculty of Science
University of Tromsø, Norway**

Magnetograms and Information based on 'near - realtime' files:

- Latest available [Magnetograms](#) from NAL-BJN-TRO-LEK-DOB-KAR
- Latest available [Magnetograms](#) from LYB-SOR-AND-ROR-SOL
- Stacked [D](#) or [H](#) or [V](#)
- [Activity index](#) for the previous 30 days. (Tromsø)
- [Plot 2-3 months old data](#) (Large GIF's)
- Realtime K-indices for [LYB / TRO / DOM](#)
- Realtime .gif's may also be downloaded via ftp from here:
 - <ftp://geo.phys.uit.no/data/gifs>

Magnetograms and Information based on 10 sec. resolution archive files:

- Data [coverage](#)
- [Timing](#) information!
- [Plot archive data](#) (.GIF)
- [List archive data](#) (ASCII)
- [Stackplot of archive data](#)
- [Statistical distribution](#) NAL / TRO / DOB
- [K-indices](#) NAL / LYB / TRO / DOB
- [Activity index](#) for Tromsø 1987 -> Today
- [Daily mean values](#) (all day) from 1986 -> today

Diverse Information:

- [Rules of the road](#)
- Site [MAP](#) & Info Page
- Statistics, [downloads & requests](#).
- About our [Instruments](#)
- Saba's '[Geomagnetic Information](#)' pages

From november 2. 2005, DHZ will be called DHV.
Declination [deg.], Horizontal & Vertical intensity [nT.]

Online Logger information:

| | | | | | |
|----------------------------|---------------------|-----------------------------|---------------------|--------------------------|---------------------|
| Ny Ålesund | NAL | Longyarbyen | LYB | Bjørnøya | BJN |
| Tromsø | TRO | Andenes | AND | Dombås | DOB |
| Karmøy | KAR | Leknes | LEK | Solund | SOL |
| | | Rørvik | ROR | Sørøya | SOR |

[\[Home\]](#)

Figure 4. Geomagnetic Data available from Tromsø Geophysical Observatory

Additional geomagnetic services have been provided by the Tromsø Geophysical Observatory (TGO):

- Geomagnetic forecast on weekly basis, updated every 3 days
- Digital daily readings with calculations of magnetic gradients during 5 and 10 min. intervals

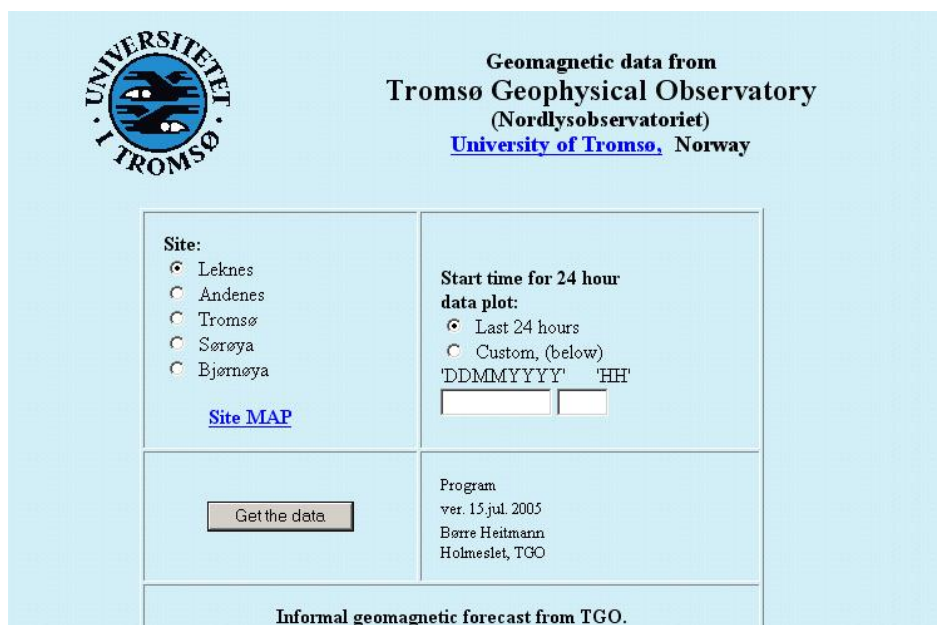


Figure 5. Geomagnetic Forecast from TGO

Characteristics of the magnetic field during the survey period:

| Period | Geomagnetic forecast | Magnetic field |
|---------------------|--|--|
| 5. – 10. Aug. | Solar activity without having caused any significant disturbance | Mainly quiet or unsettled, minor storms can not be excluded |
| 11. –19. Aug. | Quiet or unsettled | Mainly quiet with unsettled sections 16. and 17. Aug. |
| 18. –23. Aug. | High speed solar wind. Moderate flare occurred 22. Aug. | Quiet 18. – 20. Aug. Active / unsettled 21. - 22. Quiet 23. Aug. |
| 24. – 25. Aug. | Storm quenced by northwards IMF (Interplanetary Mag Field) | Storm on 24. unsettled on 25. Aug. |
| 26. Aug. – 1. Sept. | The storm period is over | Quiet |
| 2. – 9. Sept. | | Unsettled or active |
| 10. –16. Sept. | | Unsettled or active with minor storms |
| 18. Sept – 3. Oct. | | Mainly quiet |

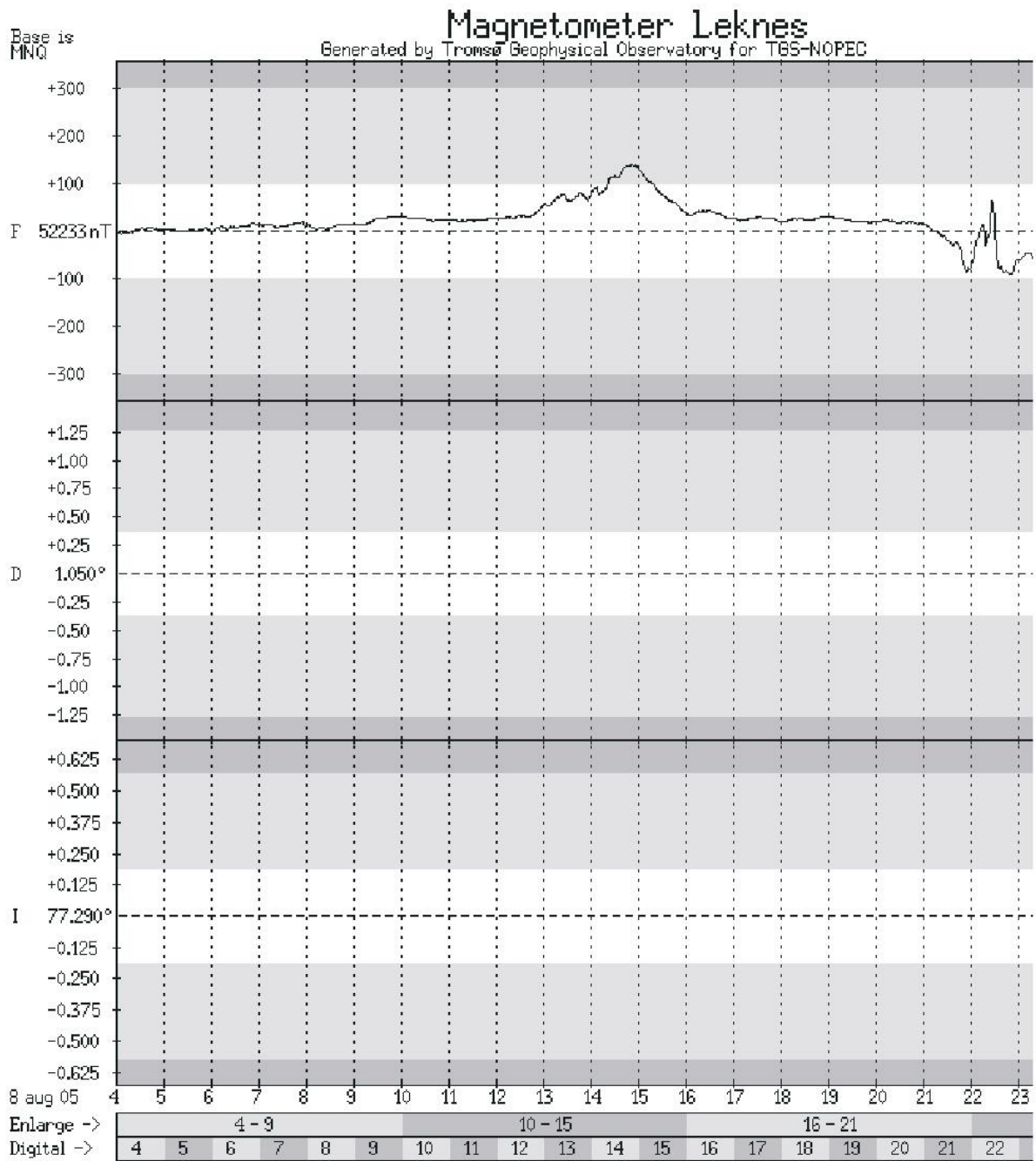


Figure 6. Magnetic Data from Leknes 8. Aug. 2005. Unsettled period 13:00 – 15:00.

Table 1. Magnetic data from Leknes. Diurnal variations during 5 min. (F-F05) and 10 min. (F-F10) intervals. total field (FFFFF), and deviation from quiet field.

Magnetometer Leknes
Base is: MNQ

| DD/MM/YYYY | HH:MM | F-F05 | F-F10 | FFFFF | Deviation from quiet field (Field value - quiet value) | | |
|------------|-------|-------|-------|-------|---|-------|------|
| | | | | | D.DD | I.II | FFFF |
| 08/08/2005 | 15:00 | -7 | -8 | 52363 | -0.09 | -0.00 | 119 |
| 08/08/2005 | 15:01 | -10 | -10 | 52362 | -0.09 | -0.00 | 118 |
| 08/08/2005 | 15:02 | -10 | -12 | 52361 | -0.08 | 0.00 | 117 |
| 08/08/2005 | 15:03 | -9 | -11 | 52360 | -0.08 | 0.00 | 116 |
| 08/08/2005 | 15:04 | -8 | -12 | 52358 | -0.08 | 0.00 | 114 |
| 08/08/2005 | 15:05 | -8 | -15 | 52355 | -0.08 | 0.00 | 111 |
| 08/08/2005 | 15:06 | -9 | -19 | 52353 | -0.08 | 0.00 | 109 |
| 08/08/2005 | 15:07 | -12 | -22 | 52349 | -0.09 | -0.00 | 105 |
| 08/08/2005 | 15:08 | -12 | -21 | 52348 | -0.09 | -0.00 | 104 |
| 08/08/2005 | 15:09 | -13 | -21 | 52345 | -0.09 | 0.00 | 101 |
| 08/08/2005 | 15:10 | -12 | -20 | 52343 | -0.10 | 0.00 | 99 |
| 08/08/2005 | 15:11 | -13 | -22 | 52340 | -0.10 | 0.00 | 96 |
| 08/08/2005 | 15:12 | -11 | -23 | 52338 | -0.10 | 0.00 | 94 |
| 08/08/2005 | 15:13 | -11 | -23 | 52337 | -0.09 | 0.01 | 93 |
| 08/08/2005 | 15:14 | -9 | -22 | 52336 | -0.09 | 0.01 | 92 |
| 08/08/2005 | 15:15 | -7 | -19 | 52336 | -0.08 | 0.01 | 92 |
| 08/08/2005 | 15:16 | -4 | -17 | 52336 | -0.08 | 0.01 | 92 |
| 08/08/2005 | 15:17 | -5 | -16 | 52333 | -0.08 | 0.01 | 89 |
| 08/08/2005 | 15:18 | -4 | -15 | 52333 | -0.08 | 0.02 | 89 |
| 08/08/2005 | 15:19 | -4 | -13 | 52332 | -0.08 | 0.02 | 88 |
| 08/08/2005 | 15:20 | -8 | -15 | 52328 | -0.08 | 0.02 | 84 |
| 08/08/2005 | 15:21 | -11 | -15 | 52325 | -0.08 | 0.01 | 81 |
| 08/08/2005 | 15:22 | -9 | -14 | 52324 | -0.08 | 0.01 | 80 |
| 08/08/2005 | 15:23 | -12 | -16 | 52321 | -0.08 | 0.01 | 77 |
| 08/08/2005 | 15:24 | -14 | -18 | 52318 | -0.08 | 0.01 | 74 |
| 08/08/2005 | 15:25 | -12 | -20 | 52316 | -0.08 | 0.01 | 72 |
| 08/08/2005 | 15:26 | -10 | -21 | 52315 | -0.08 | 0.01 | 71 |
| 08/08/2005 | 15:27 | -11 | -20 | 52313 | -0.08 | 0.01 | 69 |
| 08/08/2005 | 15:28 | -10 | -22 | 52311 | -0.09 | 0.01 | 67 |
| 08/08/2005 | 15:29 | -8 | -22 | 52310 | -0.09 | 0.01 | 66 |
| 08/08/2005 | 15:30 | -7 | -19 | 52309 | -0.09 | 0.01 | 65 |
| 08/08/2005 | 15:31 | -7 | -17 | 52308 | -0.09 | 0.01 | 64 |
| 08/08/2005 | 15:32 | -6 | -17 | 52307 | -0.08 | 0.01 | 63 |
| 08/08/2005 | 15:33 | -5 | -15 | 52306 | -0.08 | 0.01 | 62 |
| 08/08/2005 | 15:34 | -5 | -13 | 52305 | -0.08 | 0.01 | 61 |
| 08/08/2005 | 15:35 | -5 | -12 | 52304 | -0.09 | 0.01 | 60 |
| 08/08/2005 | 15:36 | -6 | -13 | 52302 | -0.09 | 0.01 | 58 |
| 08/08/2005 | 15:37 | -6 | -12 | 52301 | -0.08 | 0.00 | 57 |
| 08/08/2005 | 15:38 | -7 | -12 | 52299 | -0.08 | 0.00 | 55 |
| 08/08/2005 | 15:39 | -7 | -12 | 52298 | -0.08 | 0.00 | 54 |
| 08/08/2005 | 15:40 | -8 | -13 | 52296 | -0.08 | 0.00 | 52 |
| 08/08/2005 | 15:41 | -7 | -13 | 52295 | -0.08 | 0.00 | 51 |
| 08/08/2005 | 15:42 | -6 | -12 | 52295 | -0.08 | 0.00 | 51 |
| 08/08/2005 | 15:43 | -4 | -11 | 52295 | -0.08 | 0.01 | 51 |
| 08/08/2005 | 15:44 | -4 | -11 | 52294 | -0.07 | 0.01 | 50 |
| 08/08/2005 | 15:45 | -3 | -11 | 52293 | -0.08 | 0.01 | 49 |
| 08/08/2005 | 15:46 | -2 | -9 | 52293 | -0.08 | 0.01 | 49 |
| 08/08/2005 | 15:47 | -2 | -8 | 52293 | -0.07 | 0.01 | 49 |
| 08/08/2005 | 15:48 | -5 | -9 | 52290 | -0.07 | 0.01 | 46 |
| 08/08/2005 | 15:49 | -5 | -9 | 52289 | -0.08 | 0.01 | 45 |
| 08/08/2005 | 15:50 | -6 | -9 | 52287 | -0.07 | 0.01 | 43 |
| 08/08/2005 | 15:51 | -8 | -10 | 52285 | -0.08 | 0.00 | 41 |
| 08/08/2005 | 15:52 | -10 | -12 | 52283 | -0.08 | 0.00 | 39 |
| 08/08/2005 | 15:53 | -9 | -14 | 52281 | -0.08 | 0.00 | 37 |
| 08/08/2005 | 15:54 | -10 | -15 | 52279 | -0.08 | -0.00 | 35 |
| 08/08/2005 | 15:55 | -11 | -17 | 52276 | -0.08 | -0.00 | 32 |
| 08/08/2005 | 15:56 | -9 | -17 | 52276 | -0.08 | -0.00 | 32 |
| 08/08/2005 | 15:57 | -8 | -18 | 52275 | -0.08 | -0.00 | 31 |
| 08/08/2005 | 15:58 | -7 | -16 | 52274 | -0.09 | -0.00 | 30 |
| 08/08/2005 | 15:59 | -7 | -17 | 52272 | -0.09 | -0.00 | 28 |

16.10 DELIVERABLES

Pre-Survey Report: Delivered 15. August 2005. Delayed due to bad weather at Jan Mayen.

Weekly Reports: Summaries from the weekly reports can be seen in Appendix C in the JAS-05 Archive CD.

| Weekly Report no. | Date | Number of flights | Total kms flown |
|-------------------|-----------|-------------------|-----------------|
| 1 | 17. Aug. | 11 | 6495.81 |
| 2 | 21. Aug. | 13 | 9440.675 |
| 3 | 29. Aug. | 22 | 15034.046 |
| 4 | 5. Sept. | 31 | 21873.123 |
| 5 | 12. Sept. | 37 | 26238.067 |
| 6 | 19. Sept. | 43 | 28526.912 |
| 7 | 29. Sept. | 48 | 30936.524 |
| 8 | 3. Oct. | 54 | 32561.864 |

QC-controlled data was delivered as Geosoft Database (GDB format) with following columns:

| | |
|----------|---|
| Linename | Survey line names |
| Time | Time based fiducial index |
| Lat | Latitude in decimal degrees |
| Lon | Longitude in decimal degrees |
| Day | Day number from the year start |
| Time2 | Time in seconds |
| Alt1 | Radar height(m) |
| Alt2 | GPS height (m) |
| Alt3 | Radar height (mV) to be multiplied by -80 to get meters |
| Gx | |
| Gy | Fluxgate magnetometer X;Y;Z channels |
| Gz | |
| MAGU1 | |
| MAGU2 | Uncompensated Total Magnetic Intensity from 2 sensors |
| MAGC1 | |
| MAGC2 | Compensated TMI |
| SAT | Number of satellites |
| PDOP | PDOP value |
| X | UTE (m) |
| Y | UTN(m) |
| Dist | Distance from the line start |
| Timedh | Time in decimal hours |
| Bmag | Basemag data from Jan Mayen |
| Leknes | Basemag data from Leknes geophysical observatory |

17 APPENDIX B START-UP REPORT, AUGUST 2005, JAN MAYEN AEROMAGNETIC SURVEY

By Johannes Hauge, TGS-NOPEC Geophysical Company

Mobilisation, test results

- Figure of Merit Test
- Clover Leaf Test
- Base Station

The test flight took place on 6 August 2005 prior to the survey start.

Figure 1 shows the flight path recovery of the test flight.

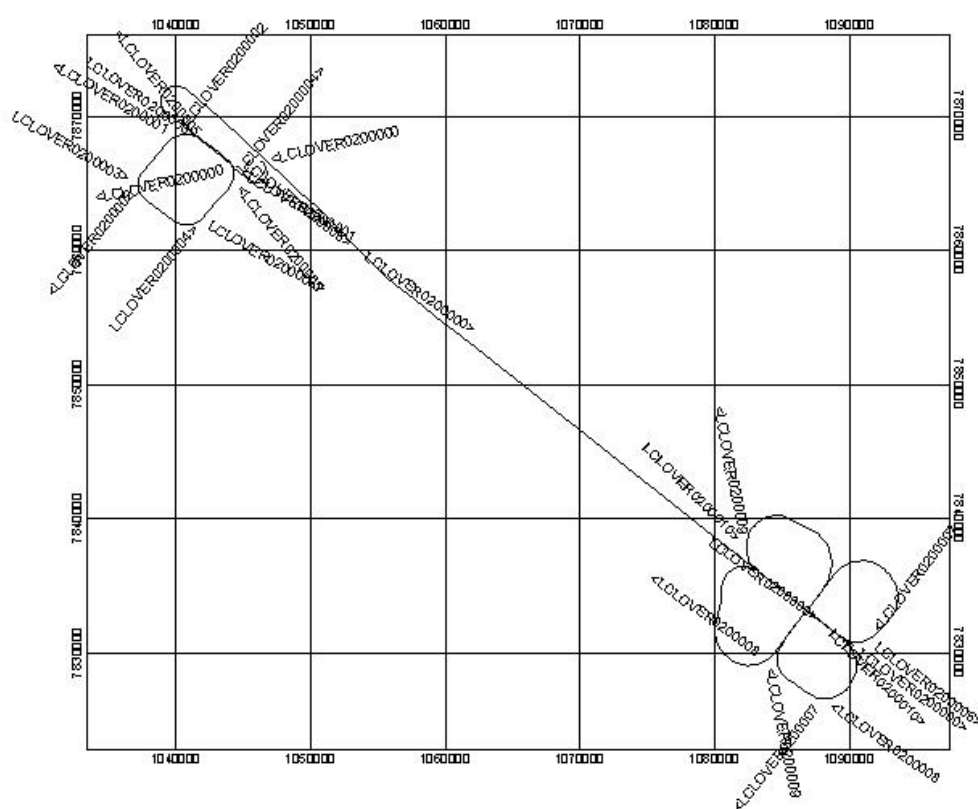


Figure 1 Flight path of test lines.

Figure of Merit Test

Aircraft calibration (FOM) tests were carried out 6th August.

The purpose of the test is to verify if the compensation system eliminates the aircraft generated magnetic noise.

The flight was performed at altitudes about 1000 meters, as there are less high frequency external disturbances at this level.

Totally 7 calibrations were performed in order to have several solutions to choose from.

The following solution was used during the survey:

| Date | Std.dev. uncomp (nT) | Std.dev. comp (nT) | Improvement ratio |
|----------|-------------------------|-----------------------|-------------------|
| 06.08.05 | 0.28 | 0.032 | 8.7 |

A rule of thumb is that the compensated standard deviation should be multiplied by $12 \cdot \text{SQRT}(2)$ to approximate the Figure Of Merit (FOM)

After testing the analogue charts and digital data were inspected, and it was conducted that very good compensation was obtained for all headings meaning FOM in the order of magnitude 2 or better ($0.03 \cdot 12 \cdot 1.41 = 0.507$).

Fig. 10.2 shows the high pass filtered magnetic residual measured during the calibration box flight and allows us to estimate the amplitudes caused by roll/pitch/yaw manoeuvres. It is clear that the compensated HP value oscillates within ± 0.1 nT or better

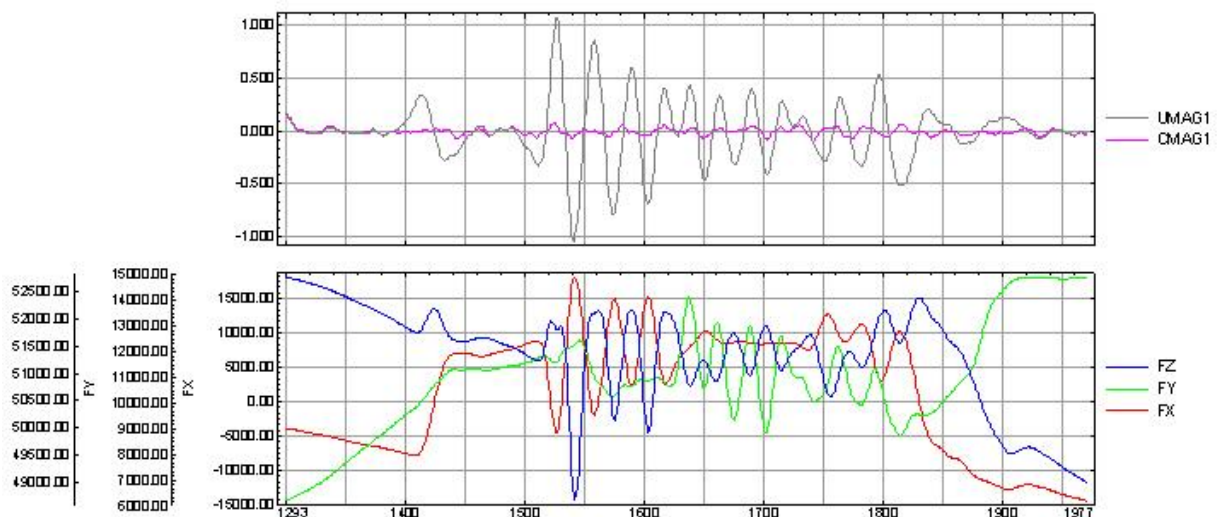


Figure 2 High pass 500 m magnetic residuals before and after compensation and fluxgate measurements reflecting airplane manoeuvres.

Magnetic Heading (Clover Leaf test)

Clover leaf test was performed on the 6th August after the FOM test. The flight path of the test is shown in Fig. 10.3. Purpose of the test was to acquire magnetic values on 4 different headings over the same point. This test shows how FOM test reported above compensates for the Bias.

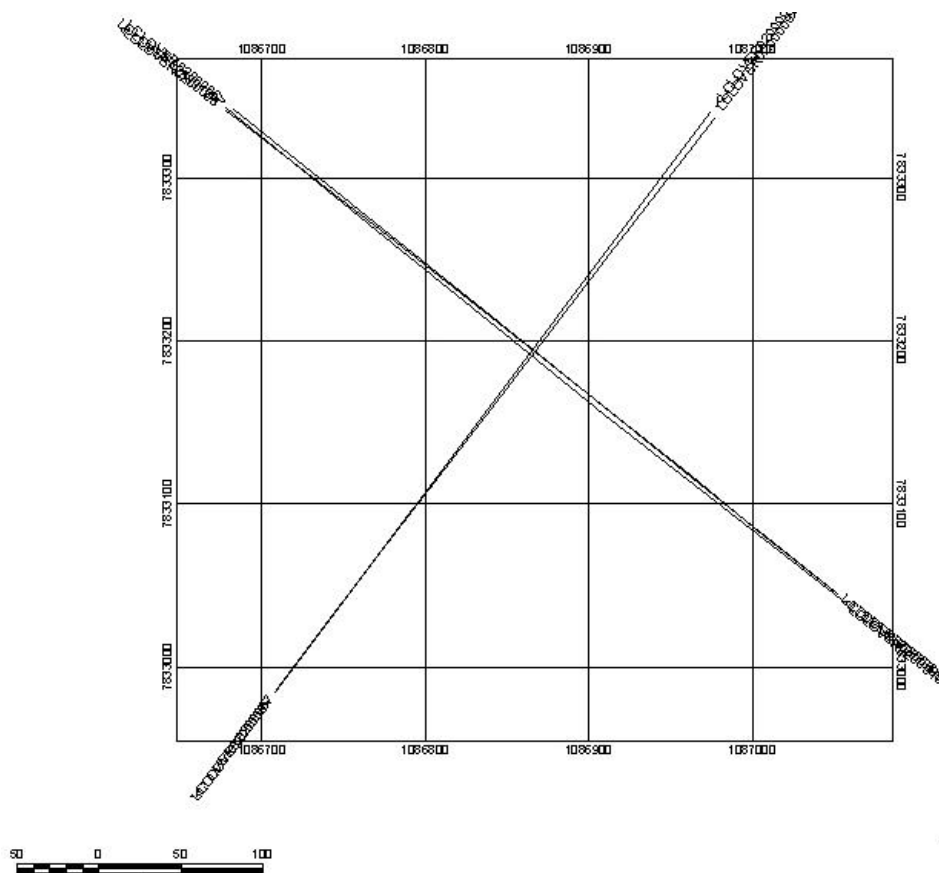


Figure 3 The flight path of clover leaf test.

The test was flown at the same altitude as the FOM test because the absence of high magnetic gradients is important for a successful performance of the test.

The intensities of total magnetic field for the crossing point are shown below 1.

| Line N | TMI | Direction |
|--------|---------|-----------|
| 6 | 53513.8 | SE |
| 7 | 53503.5 | SW |
| 8 | 53499.0 | NW |
| 9 | 53505.8 | NE |

Base Station

A magnetic base station has been established at 75m distance from the building where the accommodation and the office of the field crew were located. This area was almost free from cultural noise.

The test base magnetic logging took place on 6 August 2005.

Noise level was 0.117 nT defined as a standard deviation.